Universidad de Granada

Facultad de Ciencias

Collider Signatures of a Non-Standard Higgs Sector

Thesis submitted by Mikael Rodríguez Chala
for the degree of Doctor of Philosophy

2014

Departamento de Física Teórica y del Cosmos

Editor: Editorial de la Universidad de Granada
Autor: Mikael Rodríguez Chala
D.L.: GR 2097-2014
ISBN: 978-84-9083-125-0

Universidad de Granada

Facultad de Ciencias

Señales de un sector de Higgs no estándar en colisionadores

Tesis presentada por Mikael Rodríguez Chala
para obtener el grado de Doctor en Física y Ciencias del Espacio

2014

Departamento de Física Teórica y del Cosmos

El doctorando Mikael Rodríguez Chala y los directores de la tesis D. Francisco del Águila Giménez, catedrático de Universidad, y D. José Santiago Pérez, profesor titular de Universidad,

GARANTIZAMOS: al firmar esta tesis doctoral, *Collider Signatures of a Non-Standard Higgs Sector* (*Señales de un sector de Higgs no estándar en colisionadores*), que el trabajo ha sido realizado por el doctorando bajo la dirección de los directores de la tesis. Y hasta donde nuestro conocimiento alcanza, en la realización del trabajo se han respetado los derechos de otros autores a ser citados, cuando se han utilizado sus resultados o publicaciones, así como que el doctorando ha disfrutado de una estancia en el extranjero, durante un periodo de tres meses, en la División Teórica de la Organización Europea para la Investigación Nuclear (CERN).

Granada, a 5 de mayo de 2014.

Fdo: Francisco del Águila Giménez José Santiago Pérez

Agradecimientos

No hay estudio alguno que haya podido llevarse a buen puerto con la modesta capacidad para el trabajo de un solo individuo, sin la inestimable ayuda de quienes, de una u otra forma, han colaborado en su quehacer diario. Esta tesis no es diferente. Espero que estas líneas sirvan para enaltecer a quienes la han hecho posible.

Quisiera empezar recordando a quienes han contribuido más directamente al desarrollo de este trabajo, mis directores Paco del Águila y José Santiago. Con ellos he tenido la fortuna de aprender más física que en ningún otro momento de mi vida. Han sabido tratarme mucho más como amigo y colaborador que como estudiante. Han sabido administrar mis arrebatos de físico joven con un tacto del que solo con el tiempo he podido darme cuenta. Me han hecho sentir como un privilegiado. No tengo palabras para transmitir lo afortunado que he sido de haber podido trabajar con ellos. Ni tengo palabras para expresar mi admiración por las capacidades intelectuales de que disfrutan, fuera de toda órbita de lo normal. Por su capacidad de trabajo y su habilidad para *hacer las cosas bien*. Si hay algo en lo que no acertaron, en todo caso, es con aquello de que *también habría momentos malos*, :).

Quisiera recordar también a todos aquellos con quienes he colaborado en mi actividad investigadora. A Adrián Carmona, con quien he tenido la oportunidad de publicar buena parte de mis artículos, y la fortuna de coincidir en Granada durante su etapa de doctorando, y más tarde en París, Varsovia, Zurich y Orsay. A José Wudka y a Arcadi Santamaria, a quien agradezco asimismo que me recomendara para la obtención de una plaza de *postdoc*. A Anupama Atre, quien además se tomó la molestia de ayudarme tanto como requerí en los inicios de mi doctorado. A Roberto Barceló, Manel Masip y Jorge de Blas, con quienes espero colaborar muchas más veces en mi futura etapa investigadora. A Gilad Perez, Mojtaba Mohammadi Najafabadi y Sara Khatibi, con

quienes tuve además la oportunidad de compartir mi segunda estancia en el CERN. A Adam Falkowski, a quien me gustaría igualmente dar las gracias por haberse molestado en escribir cuantas cartas de recomendación necesité para el *postdoc*. A Christophe Grojean, a Rafael Cerezo y a Javier Martínez Lizana, con quienes me siento en deuda por haber comenzado unos proyectos que, tristemente, quedaron en agua de borrajas.

No puedo olvidar tampoco a todos aquellos a los que he podido dirigirme para desentrañar algunas de mis innumerables dudas, ya tuvieran que ver estas con la física, con las matemáticas, con la informática con el inglés o con las clases. A Manuel Pérez-Victoria, Mar Bastero Gil, José Ignacio Illana, Fernando Cornet y Elvira Gámiz. A mis compañeros de despacho, Pablo Guaza, Olaf Kittel y Javier Martínez Lizana. Habida cuenta de sus extraordinarias facultades, enfrentarse a un doctorado con ellos en el despacho es muchísimo más fácil. Al grupo de LIP, Juan Pedro Araque, Nuno Castro, Antonio Onofre y Miguel Fiolhais, con quienes cerré además, en mi primera estancia en el CERN, gran parte de la brecha típica de quien termina la carrera sin saber qué es exactamente un Monte Carlo. A Jordi Hidalgo, por haber tenido ahí siempre el *script*, el programa, la documentación o lo que fuere que anduviese buscando en el justo momento. Y a la *enana Esperanza*, quien además se ha tomado la molestia de leer esta tesis y corregir buena parte de mi mediocre castellano y gran parte de mi nefasto inglés.

Mención especial me merecen aquellos con quienes he tenido la gigantesca suerte de iniciarme en la investigación. Javier Merí y Miguel Martín, que se prestaron, allá por mi segundo año de carrera, a perder un poco de su tiempo para introducirme las primeras ideas de lo que es investigar... en matemáticas. Y a Patrick Meessen y Bert Janssen. Durante el tiempo que duraron mis becas de iniciación a la investigación en Granada, y durante mi estancia en el IFT en Madrid al final de mi carrera, me enseñaron los fundamentos de la relatividad general, de la supergravedad y las nociones elementales de la teoría de cuerdas. Todos ellos me trataron como cualquier estudiante hubiera *deseado*. Se ve que la suerte de poder colaborar con personas excepcionales me ha acompañado desde el primer momento. Me es difícil explicar cuán agradecido les estoy por ello.

Asimismo, no puedo sino acordarme de todas esas personas con quienes he hecho buenas migas en mis múltiples escapadas a escuelas, congresos y estancias de investigación. Al grupo de LIP, a quienes acompañé durante dos maravillosas semanas en

Sudáfrica. A Daniel Cámpora, con quien lo he pasado en grande en mis tres visitas al CERN. A Víctor Martín Lozano, con quien he tenido el placer de coincidir en Bilbao, Barcelona y Granada. A James Ferrando, quien me ha echado una mano cuando lo he necesitado desde que nos conociéramos en Valencia. A mis geniales amigos y compañeros de Cargèse, Juan González Fraile, Joan Elías Miró, Juan Herrero García, Bogna Kubik, Iftah Galon, Andrea Lami y Miguel Villaplana. Con la mayoría de ellos he podido organizar posteriormente varios viajes *off the record*. A Alice Donati, con quien también he tenido el placer de compartir una semana inolvidable en Barcelona, por el módico precio de un bol roto y un *don't like* en Airbnb, :). No puedo olvidarme tampoco de Roberto Barceló y de Alberto Aparici, y de mis fantásticos compañeros de despacho en la Divisón Teórica del CERN, Christine Hartmann y Ahmad Zein Assi. He de aludir, asimismo, a quienes me han dado cobijo, más allá de las necesidades que cualquier persona podría precisar, en mis múltiples viajes al extranjero: a mis tíos y a mis primas en Ginebra y en Lyon, a Adrián y a Nicolasa.

Por supuesto, me he de referir también a mis maravillosos compañeros de carrera y amigos excepcionales, con quienes he compartido los mejores años de mi vida. Desde los tiempos del picante, la nata y los chupitos. A Jordi, Migue, Frenando, Germi, Juanpe, Isi, Laura, Benja, María del Mar, Leo, Rafa, Javi, Paquito, Álvaro, Javivi, Emilio, Lourdes y Jope. Y a las incorporaciones más tardías: Germán, Alice, Ben, Adriano y los demás compañeros *del otro despacho*: Laura, Bruno, Mariano, Alberto y Patri.

No quisiera terminar sin destacar a todos los *mondongos* con quienes he convivido en el día a día, con quienes he disfrutado de la amistad en su máxima expresión. Desde siempre y para siempre jamás. A Albertoto, a Brian, a Davi, A Frenando, a Jonasan, a Jordi, a Josef, a Jospi, a Juan Marrón y a Peri. Porque *juntos hemos crecido, juntos hemos envejecido, pero nunca madurado, :)*. A buen seguro pocos llegarán a disfrutar del privilegio de rodearse de unas personas tan excepcionales en tantísimos sentidos.

Por último, quisiera recordar a mi familia. A la de Priego, a la de Granada, a la de Francia y a la de Córdoba. Y en particular a mis padres. Por haber decidido, con un acierto inigualable, cuando yo aún no podía hacerlo, sentando así las bases para que pudiera ser lo que soy hoy. Y también a mi amiga, compañera y *saquito de nervios*, Esperanza López Centella. En particular porque hayamos podido resistir los embates de las horas y modos de trabajo que se requieren para acabar una tesis doctoral.

A mi hermano.

Por enseñarme, en su excepcional capacidad para administrar el dinero, que dos más ocho es igual a cinco más cinco.

¡Qué cabronazo, :)!

Contents

Chapter 1

Introduction

The time in which this thesis has been developed is, without any doubt, one of the most interesting of the last years. Indeed, at the beginning of this work, the Higgs boson was just a well-motivated theoretical hypothesis [1]. Three years later, after its discovery at CERN in July 2013, the Higgs boson is a well-established experimental fact. Furthermore, the measurements of its couplings to the heaviest particles are, within the (still large) error bars, compatible with the Standard Model predictions. This observation completes a process of decades of theoretical work and experimental searches, which has led to the likely most precise and ambitious scientific theory. However, the Standard Model can not give an answer to some fundamental questions. Why is the Higgs boson, an elementary scalar particle, so light? The mass of the elementary scalars is not protected by any symmetry within the Standard Model. Thus, any new physics at some scale Λ coupling to such a scalar (and we know there is new physics related to gravity) gives order Λ corrections to its mass. (This is roughly speaking the *hierarchy problem.*)

Why are fermion masses so different? For instance, the mass of the heaviest fermion, the top quark, is more than five orders of magnitude larger than the mass of the up quark. And why are neutrinos massive? Within the Standard Model, only left-handed

[1] It is true that there were strong theoretical evidences and precision measurements to suggest that the Higgs boson had to be discovered later or before. But it is also true that, in the years previous to the LHC starting, different Higgsless models were proposed [1, 2]. Later, in the light of the first LHC data —coming all of them with negative results—, new similar works also appeared (see for instance [3]).

neutrinos are present. Right-handed neutrinos are singlets and hence do not interact with any other particle within the Standard Model. Hence, mass terms for the neutrinos can not be constructed. All these questions suggest that there is physics beyond the Standard Model, at some scale Λ, giving solutions to these challenges. The main goal of this thesis is the study of some of these solutions and their consequences.

In order to study the properties of still unknown physics, one can adopt two approaches, depending on whether Λ is larger enough than the energy scale of the allowed experiments or rather it is of the same order. In the first case, the heavy physics can be integrated out, giving rise to an expansion in terms of effective operators. The coefficients of these operators, if they can be measured, can give indirect information over the properties of the new particles. If, instead, the scale of new physics is accessible to the experiments, then the new particles can be directly produced and studied. At the LHC era, and inasmuch as there are strong theoretical arguments to think there is new physics at the TeV scale, we adopt this second approach. The main part of this thesis is based on the articles published in [4–9] and, at a lesser extent, in [10, 11] (we also refer to the proceedings published in [12–15]). In [16] we adopt an effective field theory approach, and hence it is not part of this thesis.

The three-stage scheme we have just outlined, *problem-solution-consequences*, configures the structure of this text. We have tried to make this presentation as much self-contained as possible. For this purpose, we assume that the fundamentals of quantum field theory and group theory are well known. In more or less detail, the rest of contents are then constructed out of this base. Thus, in Chapter 2, we describe the Standard Model of particle physics. In particular, the Higgs sector and their associated problems [2]. There we briefly introduce some models that can alleviate these difficulties: composite Higgs models and scalar lepton number violating models. They both contain new heavy particles that can be produced in accelerators like the LHC. Accordingly, the subsequent sections are devoted to the study of the collider phenomenology of these non-standard Higgs sectors.

Nevertheless, we can not bring this work to a successful conclusion without the

[2]The questions we have formulated previously suggest that some of the main problems that affect the Standard Model are related to the mass of the particles. And hence with the Higgs sector. This is however not surprising inasmuch as the scalar sector is the experimentally less known sector of the theory.

computational and statistical tools that a study with this scope requires. Thereby, and for the sake of self-content, Chapter 3 is devoted to the fundamentals of phenomenological and experimental particle physics research: basic concepts of accelerators and detectors, Monte Carlo simulation, data analysis and statistics.

In Chapter 4 we study the phenomenology of the minimal composite Higgs model, which is based on the coset $SO(5)/SO(4)$ and thus contains the same number of degrees of freedom as the Standard Model scalar sector. In a first step we introduce the theoretical aspects of this model. In particular, we discuss the concept of *degree of compositeness*, that allows us to guide the subsequent study. Roughly speaking, the degree of compositeness of a particle gives a measure of its interaction with the composite sector —in which the Higgs boson is assumed to live—. As we will see, heavier particles are naturally more composite than lighter particles (although under some conditions light particles can be also sizably composite). This observation allows us to study three different cases of the minimal composite Higgs model phenomenology. First, the one in which the top quark is rather composite. Second, the case in which the bottom quark is also composite. And finally the one in which even the light quarks are composite. This chapter ends with the brief introduction and discussion of a non-minimal composite Higgs model, based on a composite sector with global symmetry group $SO(7)$, spontaneously broken to G_2. We will see that the scalar content of this model is enlarged, and the new degrees of freedom can modify the decay of the Higgs boson into diphotons.

Finally, in Chapter 5, we consider the phenomenology of extended Higgs sectors that allow the neutrino masses to be Majorana, and then contain lepton number violating scalars. For that purpose, we classify these fields using an effective field theory approach. Then, using appropriate current ATLAS and CMS analyses we set the first bounds on lepton number violation in the scalar sector. At the end of this chapter, we describe how to measure the quantum numbers of the corresponding scalar fields if they were detected in a second phase of the LHC running.

This thesis concludes in Chapter 6. In the Appendices we present additional information: explicit expressions of the $SU(2)$ generators for different representations in Appendix A, the mathematics of non-linear sigma models (essentially the definition of the Maurer-Cartan one-form) in Appendix B, the group theory of the $SO(5)/SO(4)$ breaking pattern in Appendix C and the group theory of $SO(7)/G_2$ in Appendix D.

Introducción

El periodo de la física de partículas que le ha tocado vivir al desarrollo de esta tesis es, sin duda alguna, uno de los más apasionantes de los últimos años. En efecto, al comenzar el trabajo que ha dado lugar al grueso de este texto, el bosón de Higgs no era más que una hipótesis teórica bien motivada [3]. Tres años después, tras el descrubimiento del mismo en julio de 2013 en el CERN, la existencia del bosón de Higgs es un hecho experimental. Más aún, las medidas de los acoplamientos del bosón de Higgs a las partículas más masivas son compatibles, en sus (todavía grandes) márgenes de error, con el modelo estándar. Se cierra así un proceso de décadas de desarrollo teórico y búsqueda experimental, que ha derivado en la que es, posiblemente, la teoría científica más precisa y ambiciosa. Sin embargo, el modelo estándar no es capaz de responder algunas preguntas fundamentales. ¿Por qué el bosón de Higgs, entendido como una partícula escalar elemental, tiene una masa tan pequeña? No hay ninguna simetría que proteja las masas de los escalares fundamentales. Si a cierta escala Λ hay física que acople a estos (y sabemos que a la escala de Planck tiene que haber física relacionada con el campo gravitatorio), la masa de estos escalares recibe correcciones de orden Λ (este es, *grosso modo*, el famoso problema de las jerarquías).

¿Por qué las masas de los fermiones son tan dispares? Por ejemplo, la masa del fermión más pesado, el quark *top*, es más de cinco órdenes de magnitud mayor que la masa del quark *up*. ¿Y por qué los neutrinos son masivos? El modelo estándar solo contiene neutrinos levógiros Los neutrinos dextrógiros son singletes y, por tanto,

[3] Es cierto que existían fuertes evidencias teóricas y medidas de precisión que sugerían que el bosón de Higgs tendría que ser descubierto tarde o temprano. Pero no lo es menos que, en los años previos a la construcción del LHC, se propusieron diferentes modelos que no incluían el bosón de Higgs [1, 2]. Más tarde, y a la luz de los datos arrojados por el LHC en sus primeras colisiones –todos ellos con resultados negativos—, también aparecieron trabajos de estas características (véase por ejemplo [3]).

no interaccionan con el resto de partículas del modelo estándar. En consecuencia, no pueden escribirse términos de masa para los neutrinos. Todas estas cuestiones sugieren que hay física más allá del modelo estándar, a cierta escala Λ, capaz de ofrecer soluciones a estas anomalías. El objetivo principal de esta tesis es estudiar algunas de estas soluciones y sus consecuencias fenomenológicas.

Para estudiar las propiedades de esta física aún no conocida se pueden tomar dos grandes caminos, dependiendo de si Λ es suficientemente mayor que la escala de energía de los experimentos a los que tenemos acceso, o si por el contrario es del mismo orden. En el primer caso, la física pesada puede integrarse, dando lugar a un desarrollo en operadores efectivos. Los coeficientes de estos operadores, si pueden medirse, nos proporcionan información indirecta sobre las propiedades de las nuevas partículas. Si, en cambio, la nueva física se sitúa en escalas de energía accesibles a los experimentos, entonces las nuevas partículas pesadas pueden producirse y estudiarse en estos directamente. En la era del LHC, y habida cuenta de que sobran argumentos teóricos para pensar que hay física nueva a la escala del TeV, es este segundo enfoque el que aquí adoptamos. El grueso de la tesis se basa en los artículos publicados en [4–9] y, en menor medida, [10, 11] (véanse también las siguientes contribuciones a congresos: [12–15]). En [16] adoptamos el segundo enfoque y, por tanto, no forma parte de esta tesis.

El esquema en tres etapas que hemos esbozado aquí, *problema-solución-consecuencias*, es el que determina la estructura de este texto. Se ha intentado que la exposición del mismo sea lo más *autocontenida* posible. A tal efecto, se asume que los fundamentos de la teoría cuántica de campos y de la teoría de grupos son conocidos. El resto de los contenidos se explican pues, en mayor o menor detalle, partiendo de esta base. Así, en el capítulo 2 se describe el modelo estándar. Discutimos, en particular, el sector de Higgs y las dificultades que trae consigo [4]. Allí introducimos brevemente los modelos que pueden sortear estas dificultades: modelos en los que el bosón Higgs es una partícula compuesta y modelos con escalares que no conservan el número leptónico. Estos contienen nuevas partículas pesadas que pueden ser producidas en aceleradores como el LHC. El desarrollo posterior de la tesis, en consecuencia, se dedica a estudiar la

[4]Las preguntas que nos hemos formulado anteriormente sugieren que algunos de los problemas más importantes que encierra el modelo estándar están relacionados con las masas de las partículas. Y, por lo tanto, con el sector de Higgs. Lo que no es de extrañar, por cuanto el sector escalar es la parcela de la teoría menos explorada experimentalmente.

fenomenología en colisionadores de estas extensiones del sector de Higgs. Este trabajo, no obstante, no podría llevarse a buen puerto sin las herramientas computacionales y estadísticas que requiere un estudio de esta envergadura. Por ello, y con vistas a mantener un planteamiento *autocontenido*, se dedica el capítulo 3 a los fundamentos de la investigación fenomenológica y experimental en física de altas energías: elementos básicos de los aceleradores y los detectores, simuladores Monte Carlo, conceptos elementales del análisis de datos y teoría estadística.

En el capítulo 4 estudiamos la fenomenología del mínimo modelo de Higgs compuesto, que se basa en el *coset* $SO(5)/SO(4)$ y, en consecuencia, presenta el mismo número de grados de libertad que el sector escalar del modelo estándar. En una primera parte se introducen los desarrollos teóricos. En particular, se introduce el concepto de *grado de composición*, que sirve de guía para el estudio posterior. A grandes rasgos, el grado de composición de una partícula cuantifica el grado de interacción de esta con las partículas del sector compuesto —al que se asume que pertenece el Higgs—. Como veremos, las partículas más pesadas tienen, de forma natural, un mayor grado de composición (aunque bajo ciertas condiciones las partículas ligeras pueden ser también compuestas). Esta observación nos permite estudiar tres casos distintos de la fenomenología de estos modelos: aquel en que el quark *top* es muy compuesto, aquel en que lo es el *bottom* y, por último, el caso de partículas ligeras muy compuestas. El capítulo termina con el desarrollo de un modelo de Higgs compuesto basado en un sector fuerte cuya simetría global $SO(7)$ se rompe espontáneamente a G_2. Veremos que los nuevos grados de libertad que surgen en este modelo pueden modificar la desintegracin del bosón de Higgs en fotones.

Finalmente, en el capítulo 5, nos preguntamos si es posible observar en el LHC bosones escalares que no conserven el número leptónico. Para ello, clasificamos estos campos desde un enfoque efectivo. Utilizando análisis actuales de ATLAS y CMS, establecemos las primeras cotas a la violación de número leptónico en el sector escalar. Al final del capítulo, describimos cómo determinar los números cuánticos de estos campos si, finalmente, son detectados. La tesis finaliza con las conclusiones del capítulo 6. En los apéndices A, B, C y D proporcionamos información auxiliar: expresiones concretas de los generadores de $SU(2)$, las bases matemáticas de los modelos sigma no lineales, la estructura de $SO(5)/SO(4)$ y la de $SO(7)/G_2$ respectivamente.

Acronyms

$0\nu\beta\beta$ Neutrinoless double beta decay

BR Branching ratio

C.L. Confidence level

c.m.e. Center of mass energy

CHM Composite Higgs model

CKM Cabbibo-Kobayashi-Maskawa

DM Dark matter

EW Electroweak

EWPD Electroweak precision data

EWSB Electroweak symmetry breaking

FCCC Flavor changing charged currents

FCNC Flavor changing neutral currents

GF Gluon fusion

LH Left handed

LN Lepton number

LNV Lepton number violation

LO Leading order

MC Monte Carlo

MFV Minimal flavor violation

NGB Nambu-Goldstone boson

NLO Next-to-leading order

NP New physics

PDF Parton-distribution function

pNGB pseudo Nambu-Goldstone boson

QCD Quantum Chromodynamics

QED Quantum Electrodynamics

RH Right handed

SILH Strongly-interacting light Higgs

SM Standard Model

UV Ultraviolet

VBF Vector-boson fusion

VBHF Vector boson Higgs fusion

VEV Vacuum expectation value

WIMP Weak-interacting massive particle

Chapter 2

The Standard Model of particle physics

The Standard Model (SM) is our current description of the elementary particles and their interactions (due to its different nature, we do not consider the gravitational force in what follows). It is a quantum gauge field theory based on the gauge group $SU(3)_c \times SU(2)_L \times U(1)_Y$, whose matter content (i.e., fields with spin 1/2) is given by three replicas of each field in Table 2.1. The $SU(3)_c$ component of the SM gauge group is known as the *color group*, and its associated force is called the *strong force*. The theory of strong interactions is known as *Quantum Chromodynamics (QCD)*. Similarly, the $SU(2)_L \times U(1)_Y$ group is called the *electroweak (EW) group* and its associated interaction the *EW interaction*. Besides, the $U(1)_Y$ charge is known as the *hypercharge*. Those fermionic fields carrying color are called *quarks*, and comprise the left-handed (LH) $q_L = (u_L, d_L)^T$ fields as well as the right-handed (RH) u_R and d_R (and their heavier replicas, $(c_L, s_L)^T$, c_R, s_R, $(t_L, b_L)^T$, t_R and b_R) [1]. And those fields that are not charged under the color group, the LH $L_L = (\nu_{eL}, e_L)^T$ and the RH e_R, are called *leptons*. Their respective heavier partners, namely $(\nu_{\mu L}, \mu_L)^T$, μ_R, $(\nu_{\tau L}, \tau_L)^T$ and τ_R are of course also leptons [2]. Note that the RH fields are uncharged under the EW gauge group, so that

[1] Hereafter, the LH and RH u, c and t fields are generically known as the *up quarks*, being c and t specifically named *charm* and *top* quarks. Analogously, the LH and RH d, s and b fields are generically known as the *down quarks*, while s and b are specifically called *strange* and *bottom* quarks.

[2] In the following, we refer to the light e and μ leptons by ℓ, while l stands either for e, μ or τ.

Field	*Spin*	$SU(3)_c$ irrep	$SU(2)_L$ irrep	$U(1)_Y$ charge
$q_L = (u_L, d_L)^T$	1/2	**3**	**2**	1/6
u_R	1/2	**3**	1	2/3
d_R	1/2	**3**	1	−1/3
$L_L = (\nu_L, l_L)^T$	1/2	1	**2**	−1/2
l_R	1/2	1	1	−1
ν_R	1/2	1	1	0
g_μ^a	1	**8**	1	0
W_μ^I	1	0	**3**	0
B_μ	1	1	1	0
ϕ	0	0	**2**	1/2

Table 2.1: SM field content. The RH neutrino is shown in gray because it is not assumed to exist in the SM, for it transforms trivially under the SM gauge group and thus does not interact with any other particle. Fermionic antiparticles (carrying complex-conjugated charges) are not explicitly shown.

the parity symmetry is explicitly and maximally broken by the EW interaction. It is also worth noting that the RH neutrino transforms trivially under the SM gauge group, and hence does not interact with any other field in the theory. Thus, it is assumed not to be part of the SM. Nonetheless, SM extensions with heavy RH neutrinos have been considered in the literature and we refer to them later in this section.

The theory contains also 12 gauge bosons (i.e., fields with spin 1) transforming in the adjoint representation of the SM gauge group. Eight of them are called *gluons (g)*, g_μ^a with $a = 1, 2, ..., 8$, and represent the force carriers of the strong interaction. The remaining four gauge bosons, W_μ^I with $I = 1, 2, 3$ and B_μ, are the mediators of the EW interaction and correspond to the $SU(2)_L$ and $U(1)_Y$ groups respectively. The dynamics of these fields is determined in terms of a lagrangian, whose structure is completely fixed by the principle of gauge invariance, together with the requirement of renormalizability. Finally, there is a last piece that allows the SM gauge group, $SU(3)_c \times SU(2)_L \times U(1)_Y$, to be spontaneously broken to $SU(3)_c \times U(1)_Q$, where $U(1)_Q$ is the electromagnetic group, whose associated interaction is known as *Quantum Electrodynamics (QED)*. This is achieved by the vacuum expectation value (VEV) of an uncolored scalar EW doublet, ϕ, with hypercharge 1/2. After EW symmetry breaking (EWSB), three of the scalar fields in ϕ are *eaten* by the EW gauge bosons, which then become massive.

The SM has been developed throughout the second half of the 20th century, as a collaborative effort of scientists around the world. The SM in its current form in a single report was first presented by John Iliopoulos. From the theoretical point of view, the first step towards the construction of the SM was given by Sheldon Glashow with the development of the theory of the EW interactions in 1961 [17] (what earned him the Nobel Prize in 1979). After that, the discovery of the Higgs mechanism by Peter Higgs [18], Robert Brout and François Englert [19] (Higgs and Englert shared the Nobel Prize in 2013 by this contribution) allowed Steven Weinberg [20] and Abdus Salam to bring the SM in its modern form, after incorporating the Higgs mechanism in Glashow's theory in 1967, and win the Nobel Prize in 1979 too. The theory of the strong interactions, to which many contributed (it is worth mentioning Murray Gell-Mann [21] and George Zweig [22] by the prediction of the quarks), acquired its modern form around mid 70s. From the experimental point of view, many of the particles were already known before the development of the SM. That is the case of the electron/positron (1897/1932), the photon (in early 1900), the muon (1936) or the electron and muon neutrinos (1956 and 1962 respectively). The light quarks (discovered in 1968) [23, 24], the tau (1975) [25], the bottom (1977) [26], the gluon (1978) [27, 28], the EW gauge bosons (1983) [29, 30], the top quark (1995) [31, 32], the tau neutrino (2000) [33] and the Higgs boson (2012) [34, 35] instead were predicted, and subsequently discovered at SLAC, the SLAC-LBL group, the Fermilab E288 experiment (at Tevatron), the TASSO Collaboration (at PETRA, DESY), the UA1 and UA2 collaborations (at CERN), the CDF and DO Collaborations (at Tevatron, Fermilab), the DONUT Collaboration and the ATLAS and CMS collaborations (at CERN) respectively.

Martin Lewis Perl, Leon M. Lederman, Carlo Rubbia and Simon van der Meer were awarded with the Nobel Prize for their contributions.

Thus, up to the date, the SM has been tested by an impressive amount of data, leading to a robust and huge agreement between theory and experiments. However, the recent discovery of the Higgs boson, implies that the scalar sector is only starting to be probed, and thus deviations from the SM predictions in the Higgs sector can be expected to appear in the next years. Indeed, as we discuss in Section 2.3, there are significant arguments to think that the minimal scalar sector of the SM is not adequate to describe the full phenomenology of elementary particles. In this text we mainly

focus on fine-tuning problems (related to the Higgs mass and the puzzling hierarchy in the quark masses) and the well-established evidence of neutrino masses. Hence, in the following we describe in detail the gauge interactions of the SM fermions and gauge bosons in Section 2.1. In Section 2.2 we introduce the scalar sector of the SM, hence completing the mathematical formulation of the SM, and discuss the interplay between theory and experiments. In Section 2.3 we argue that, although most of the experiments developed so far are in extremely good agreement with the SM, there are theoretical questions (mainly fine-tuning problems) as well as experimental evidences (like neutrino masses) that can not be accommodated in the SM. Given that, contrary to the other particles and interactions, the scalar sector has been only poorly tested, we argue that the SM Higgs sector has to be necessarily modified in order to explain these observations. Thus, in Section 2.4 we briefly introduce extensions of the scalar sector that are discussed in detail in the next chapters.

2.1 Gauge symmetry and interactions

The interactions among the fermions, mediated by the gauge bosons, are described by the most general renormalizable gauge invariant lagrangian, given by:

$$\begin{aligned}\mathcal{L}_{SM} = &-\frac{1}{4}G^a_{\mu\nu}G^{\mu\nu}_a - \frac{1}{4}W^I_{\mu\nu}W^{\mu\nu}_I - \frac{1}{4}B_{\mu\nu}B^{\mu\nu} \\ &+ i\overline{q_{Li}}\not{D}q_{Li} + i\overline{u_{Ri}}\not{D}u_{Ri} + i\overline{d_{R,i}}\not{D}d_{Ri} + i\overline{L_{Li}}\not{D}L_{Li} + i\overline{l_{Ri}}\not{D}l_{Ri},\end{aligned} \tag{2.1}$$

where i is used to label the different families. The different strength tensors are given by $G^a_{\mu\nu} = \partial_\mu g^a_\nu - \partial_\nu g^a_\mu - g_s f^a_{bc} g^b_\mu g^c_\nu$, $W^I_{\mu\nu} = \partial_\mu W^I_\nu - \partial_\nu W^I_\mu - g\epsilon^I_{JK} W^J_\mu W^K_\nu$, $B_{\mu\nu} = \partial_\mu B_\nu - \partial_\nu B_\mu$, f_{abc} and the totally antisymmetric ϵ_{IJK} are the group structure constants of $SU(3)_c$ and $SU(2)_L$ respectively. $\not{D} \equiv \gamma^\mu D_\mu$, and the convention for the covariant derivative acting over an arbitrary field φ that we use is given by

$$D_\mu\varphi = \left(\partial_\mu + ig_s\frac{\lambda_a}{2}g^a_\mu + igT_I W^I_\mu + ig'Y B_\mu\right)\varphi, \tag{2.2}$$

what can be also written as

$$D_\mu\varphi = \left[\partial_\mu + ig_s\frac{\lambda_a}{2}g^a_\mu + \frac{ig}{\sqrt{2}}\left(T^+W^+_\mu + T^-W^-_\mu\right) + \frac{ig}{c_W}\left(T_3 - s^2_W Q\right)Z_\mu + ieQA_\mu\right]\varphi \tag{2.3}$$

if we define $T^{\pm} = T_1 \pm iT_2$ and $W^{\pm} = (W^1_\mu \mp iW^2_\mu)/\sqrt{2}$. T_I are the generators of $SU(2)$, whose explicit expression depends on the exact representation the field φ transforms in. In Appendix A one can find different examples, that are extensively used in Chapter 5. λ_a stand for the Gell-Mann matrices (which should be set to zero for leptons). Y stands for the hypercharge, Z_μ and A_μ are defined as

$$A_\mu = c_W B_\mu + s_W W^3_\mu, \quad Z_\mu = c_W W^3_\mu - s_W B_\mu, \tag{2.4}$$

$Q \equiv T_3 + Y$ and s_W (c_W) is the sine (cosine) of the Weinberg angle θ_W, given by $\tan\theta_W = g'/g$. In addition, $e \equiv g s_W = g c_W$. It is clear that the strong interaction does not break parity, because both the LH and RH components of the same fermion transform identically under $SU(3)$. Hence we say that the strong force is *vector like*. Concerning the EW interactions, we can see that any two fermions ψ and ψ' in the same doublet, $(\psi, \psi')^T$, interact through the interchange of a W boson according to the following equation:

$$-\frac{g}{2\sqrt{2}}\left[\overline{\psi}\gamma^\mu(1-\gamma^5)\psi' W^+_\mu + \overline{\psi'}\gamma^\mu(1-\gamma^5)\psi W^-_\mu\right]. \tag{2.5}$$

It is apparent from this equation that parity is maximally broken in EW charged interactions. Analogously, we have the following neutral interactions for each fermion ψ:

$$e\overline{\psi}\gamma^\mu\psi A_\mu + \frac{g}{2c_W}\overline{\psi}\gamma^\mu\left(2Qs^2_W - T_3 + T_3\gamma^5\right)\psi Z_\mu, \tag{2.6}$$

where now T_3 (the third component of the *isospin*) stands only for the ψ LH component. Thus, the interactions mediated by A_μ are vector like while those mediated by Z_μ break also parity. Hence, A_μ can be identified with the photon (γ), Q with the electromagnetic charge and $e = \sqrt{4\pi\alpha}$ (being α the fine-structure constant). The only remaining requirement is the introduction of masses, that are explicitly forbidden by the gauge symmetry, by means of the Higgs mechanism.

2.2 The Higgs sector

The spontaneous breaking of the gauge $SU(3)_c \times SU(2)_L \times U(1)_Y$ symmetry is achieved in the SM in a minimal way, by introducing the uncolored Higgs doublet $\phi = (\phi^+, \phi^0)^T$

with hypercharge $Y = 1/2$. Thus, the most general lagrangian involving the Higgs and the rest of the SM particles reads

$$\begin{aligned}\mathcal{L}_S = &(D_\mu\phi)^\dagger(D^\mu\phi) - \mu_h^2\phi^\dagger\phi - \lambda_h(\phi^\dagger\phi)^2 \\ &- \left[y^u_{ij}\overline{q_{Li}}\tilde{\phi}u_{Rj} + y^d_{ij}\overline{q_{Li}}\phi d_{Rj} + y^l_{ij}\overline{L_{Li}}\phi l_{Rj} + \text{h.c.}\right],\end{aligned} \tag{2.7}$$

where $\tilde{\phi}$ stands for $\tilde{\phi} = i\sigma_2\phi^*$, being σ_2 the second Pauli matrix (Appendix A). $\tilde{\phi}$ transforms also as a doublet but with hypercharge $Y = -1/2$. The first line in the last equation contains the Higgs interactions with the gauge bosons and the Higgs self-interactions (the potential). The second line, known as the *Yukawa sector*, contains the couplings of the Higgs doublet to the fermions. This potential allows the Higgs doublet to get a VEV in its neutral component if $\mu_h^2 < 0$, so that in the unitary gauge we obtain

$$\phi = \frac{1}{\sqrt{2}}\begin{pmatrix}0\\ h+v\end{pmatrix}, \qquad \text{with } v = \sqrt{\frac{-\mu_h^2}{\lambda_h}}, \tag{2.8}$$

being $h \equiv \sqrt{2}\text{Re}(\phi^0)$ the only physical degree of freedom in the scalar sector. Once h takes the VEV v, the EW symmetry $SU(2)_L \times U(1)_Y$ is broken to $U(1)_Q$, the electromagnetic group generated by $T_3 + Y$. After EWSB, the term $(D_\mu\phi)^\dagger(D^\mu\phi)$ in equation 2.7 reduces to

$$(D_\mu\phi)^\dagger(D^\mu\phi) = \frac{1}{2}\partial_\mu h\partial^\mu h + \frac{g^2}{4}\left(v^2 + 2vh + h^2\right)\left(W^+_\mu W^{\mu\,-} + \frac{1}{2c_W^2}Z_\mu Z^\mu\right). \tag{2.9}$$

Thus, we see the W and Z bosons acquire a mass given by $m_W = 1/2gv$ and $m_Z = m_W/c_W$ respectively. Analogously, the Yukawa setor reduces, after EWSB, to the following lagrangian:

$$-\frac{v}{\sqrt{2}}\left(1 + \frac{h}{v}\right)\left(y^u_{ij}\overline{u^i_L}u^j_R + y^d_{ij}\overline{d^i_L}d^j_R + y^l_{ij}\overline{l^i_L}l^j_R + \text{h.c.}\right). \tag{2.10}$$

This equation presents mixing terms between the different SM fermions. In order to get the physical fields, the matrices $y^{u,d,l}$ (whose components are $y^{u,d,l}_{ij}$) have to be diagonalized. This can be done by means of two unitary matrices $\mathcal{U}^{u,d,l}_L$ and $\mathcal{U}^{u,d,l}_R$ for each sector (u, d and l) satisfying $(\mathcal{U}^u_L)^\dagger y^u \mathcal{U}^u_R = \text{diag}(y_u, y_c, y_t)$; $(\mathcal{U}^d_L)^\dagger y^d \mathcal{U}^d_R = \text{diag}(y_d, y_s, y_b)$

	u	d	c	s	t	b	e	μ	τ	W	Z	h
Mass	0.002	0.005	1.3	0.009	173	4.2	0.0005	0.1	1.8	80.4	91.2	126

Table 2.2: Approximate mass (in GeV) of the massive SM particles. The photon (γ), the gluon (g) and the neutrinos (ν) are massless.

and $(\mathcal{U}_L^l)^\dagger y^l \mathcal{U}_R^l = \text{diag}(y_e, y_\mu, y_\tau)$, where $y_{u,d,l}$ are real positive values. Thus, the masses of any SM fermion ψ is then given by $m_\psi = v y_\psi/\sqrt{2}$ (note, however, that the absence of RH neutrinos implies that neutrinos are massless in the SM). Hence, the larger its Yukawa coupling the larger the mass of the fermion. The masses of all the SM particles have been measured with relatively good accuracy. The masses of the SM massive particles are shown in Table 2.2. The rotations above introduce flavor-changing charged currents (FCCCs), so that equation 2.5 reads in the physical basis (i.e., after EWSB) [3]

$$-\frac{g}{2\sqrt{2}}\left\{\left[\overline{u^i}\gamma^\mu(1-\gamma^5)V_{ij}d^j + \overline{\nu^i}\gamma^\mu(1-\gamma^5)l^j\right]W_\mu^+ + \text{h.c.}\right\}, \tag{2.11}$$

where $V = (\mathcal{U}_L^u)^\dagger \mathcal{U}_L^d$ is the Cabbibo-Kobayashi-Maskawa (CKM) matrix. Finally, the EWSB mechanism also provides a mass to the physical Higgs boson h. This is given by $m_h = \sqrt{2\lambda_h}v$. The interactions between the Higgs boson and the rest of the SM particles allow h to be produced and decay in different ways. Among the production mechanisms, gluon fusion (GF) and vector-boson fusion (VBF) are the main ones. Concerning the decays, the Higgs boson mainly decays into $b\bar{b}$ (although the top quark is the fermion with the largest Yukawa coupling —and hence the largest mass—, the Higgs boson is not allowed to decay into on-shell $t\bar{t}$ because m_h is smaller than twice m_t) and, in a lower rate, $W^\pm W^{\mp *}$ (W^* representing an off-shell W), gg, $\tau^+\tau^-$, $c\bar{c}$, ZZ (with one off-shell Z^*), $\gamma\gamma$ and $Z\gamma$.

Finally, let us comment that the global symmetry of the SM is larger than just the gauge symmetry. Indeed, there is an accidental global symmetry left, given by the group $U(1)_B \times U(1)_{L_e} \times U(1)_{L_\mu} \times U(1)_{L_\tau}$, being $U(1)_B$ the baryon number symmetry group and $U(1)_{L_{e,\mu,\tau}}$ the e, μ, τ lepton number (LN) symmetry groups. The charge of all the quark

[3] Flavor-changing neutral currents (FCNCs) are however not introduced. Note also that, due to the absence of RH neutrinos in the SM, FCCCs do not occur in the lepton sector.

fields under $U(1)_B$ is $B = 1/3$ while the rest of the particles are singlets. Similarly, the first, second and third families of leptons transform with charge $L_{e,\mu,\tau} = 1$ under $U(1)_{L_e}$, $U(1)_{L_\mu}$ and $U(1)_{L_\tau}$ respectively. The total LN is defined to be $L = L_e + L_\mu + L_\tau$. Although both B and L are accidentally conserved at the tree level in the SM, at the quantum level they are anomalous and then violated, but not their difference $B - L$.

Regarding only the purely scalar lagrangian (i.e., *switching off* the gauge and Yukawa interactions), there is another important transformation, known as the *custodial symmetry*. Under the custodial symmetry, the real components of the Higgs doublet ϕ, that is, $\vec{\phi} = (\phi_1, \phi_2, \phi_3, \phi_4)^T$, transform in the vector representation of $SO(4) \simeq SU(2) \times SU(2)$, where the first $SU(2)$ is exactly the EW gauge symmetry group $SU(2)_L$ [4]. The custodial symmetry is explicitly broken by the gauging of $U(1)_Y$ and the difference between the top and bottom Yukawa couplings [5], and spontaneously broken to $SU(2)_{L+R} \simeq SO(3)_V$ after EWSB. This symmetry is responsible for the tree-level relation $\rho \equiv m_W^2/(m_Z^2 c_W^2) = 1$. Quantum corrections make ρ slightly increase, setting it in very good agreement with the experimental measurement: $1.0004^{+0.0003}_{-0.0004}$ at the 95% confidence level (C.L.).

2.3 Problems of a minimal sector

The SM of elementary particles has been tested with an impressive level of detail. Not only all the predicted particles have been discovered, but their interactions have been probed with a very good accuracy in a large number of experiments, being in very good agreement with the theoretical predictions. The main experimental tests of the SM come from low-energy scattering data, precision CP, P and flavor experiments (LEP and SLAC), e^+e^- scattering above the Z pole up to energies around 200 GeV (LEP2), $p\bar{p}$ collisions at 1.96 TeV of center of mass energy (c.m.e.) (Tevatron) and pp collisions at 7 and 8 TeV of c.m.e. (LHC). The theoretical predictions have been computed up to (at least) the one-loop accuracy. A global EW fit to different observables, as reported in reference [36], is shown in Table 2.3. On another front, the interactions in the scalar sector are now only starting to be probed in both ATLAS and CMS

[4] Hereafter we write the custodial symmetry group as $SU(2)_L \times SU(2)_R$.

[5] The different c and s Yukawa couplings, as well as the difference between the u and d Yukawa couplings also break the custodial symmetry, but this breaking is suppressed by their small values.

Parameter	*Input value*	*Free in the fit*	*Fit result*
m_h [GeV]	125.7 ± 0.4	yes	125.7 ± 0.4
m_W [GeV]	80.385 ± 0.015	-	80.367 ± 0.007
Γ_W [GeV]	2.085 ± 0.042	-	2.091 ± 0.001
m_Z [GeV]	91.1875 ± 0.0021	yes	91.1878 ± 0.0021
Γ_Z [GeV]	2.4952 ± 0.0023	-	2.4954 ± 0.0014
$\sigma^0_{\rm had}$ [nb]	41.540 ± 0.037	-	41.479 ± 0.014
R^0_ℓ	20.767 ± 0.025	-	20.740 ± 0.017
$A^{0,\ell}_{FB}$	0.0171 ± 0.0010	-	0.01627 ± 0.0002
A_ℓ	0.1499 ± 0.0018	-	$0.1473^{+0.0006}_{-0.0008}$
$\sin^2\theta_{\rm eff}(\mathcal{Q}_{\rm FB}$	0.2324 ± 0.0012	-	$0.23148^{+0.00011}_{-00007}$
A_c	0.670 ± 0.027	-	$0.6680^{+0.00025}_{-0.00038}$
A_b	0.923 ± 0.020	-	$0.93464^{+0.00004}_{-0.00007}$
$A^{0,c}_{\rm FB}$	0.0707 ± 0.0035	-	$0.0739^{+0.0003}_{-0.0005}$
$A^{0,b}_{\rm FB}$	0.0992 ± 0.0016	-	$0.1032^{+0.0004}_{-0.0006}$
R^0_c	0.1721 ± 0.0030	-	0.17223 ± 0.00006
R^0_b	0.21629 ± 0.00066	-	0.21474 ± 0.00003
$\overline{m_c}$ [GeV]	$1.27^{+0.07}_{-0.11}$	yes	$1.27^{+0.07}_{-0.11}$
$\overline{m_b}$ [GeV]	$4.20^{+0.17}_{-0.07}$	yes	$4.20^{+0.17}_{-0.07}$
m_t [GeV]	173.19 ± 0.94	yes	173.52 ± 0.88
$\Delta\alpha^{(5)}_{\rm had}(m^2_Z) \cdot 10^{-5}$	2757 ± 10	yes	2755 ± 11
$\alpha_s(m^2_Z)$	-	yes	0.1191 ± 0.0028
$\delta_{\rm th} m_W$ [GeV]	$[-4, 4]_{\rm theo}$	yes	4
$\delta_{\rm th} \sin^2\theta^\ell_{\rm eff} \cdot 10^{-5}$	$[-4.7, 4.7]_{\rm theo}$	yes	-1.4

Table 2.3: Input values and fit results for the observables and parameters of the global EW fit. The first and second columns list, respectively, the observables/parameters used in the fit, and their experimental values or phenomenological estimates. The subscript *theo* labels theoretical error ranges. The third column indicates whether a parameter is floating in the fit, and the fourth column quotes the results of the fit including all experimental data. This table is provided by the `GFitter` group in reference [36].

experiments. For instance, the measurements of Higgs signal strengths μ (defined as the ratio between the measured cross section and the SM one) in different channels can

Channel	*Signal strength* (ATLAS)	*Signal strength* (CMS)
$h \to \gamma\gamma$	$\mu = 1.57^{+0.33}_{-0.28}$	0.72 ± 0.27
$h \to ZZ^* \to \ell^+\ell^-\ell^+\ell^-$	$\mu = 1.44^{+0.40}_{-0.35}$	0.93 ± 0.27
$h \to WW^* \to \ell^+\nu\ell^-\overline{\nu}$	$\mu = 1.00^{+0.32}_{-0.29}$	0.72 ± 0.19
$W, Z\, h \to b\bar{b}$	$\mu = 0.2^{+0.7}_{-0.2}$	1.0 ± 0.5
$h \to \tau^+\tau^-$	$\mu = 1.4^{+0.5}_{-0.4}$	0.78 ± 0.27

Table 2.4: The measured signal strengths for the Higgs boson, normalized to the SM expectations. The ATLAS results have been taken from reference [37] and the corresponding ones for CMS from [38–42] (CMS).

be found in reference [37] (for ATLAS) and references [38–42] (for CMS). We summarize in Table 2.3 the main results, in units of the SM ($\mu = 1$). The combined signal strength for ATLAS is given by $\mu = 1.30^{+0.18}_{-0.17}$ [37]. Although errors are still large, the results are in quite good agreement with the SM expectations; large deviations coming mainly from $h \to \gamma\gamma$. We discuss this channel in more detail in Section 4.8.

Concerning the accidental global symmetries, one may then wonder if they are also exactly realized in Nature, as predicted by the SM (up to non-perturbative effects). If broken, they are only very tinily violated. In fact, if the proton decays, B number would be broken, but we know that the proton mean life is extremely long $\tau_p > 2.1 \times 10^{29}$ yr at 90% C.L. [43]. The observed B asymmetry of the universe is also quite small $\eta \sim 10^{-10}$ [43], as it is the B number violation required to explain it if this is actually its origin. Similarly, LN is only very tinily broken if it is not exact. The only low-energy process which might provide conclusive evidence of LN violation (LNV), neutrinoless double beta decay ($0\nu\beta\beta$), has not been undoubtedly observed $\tau_{\frac{1}{2}}(^{76}\mathrm{Ge} \to {}^{76}\mathrm{Se} + 2e^-) > 1.9 \times 10^{25}$ yr at 90% C.L. [43]. Besides, if the B asymmetry is due to leptogenesis [44] and hence to LNV, its amount at low energy should be rather small, too. Hence, in summary, the field content of the SM, together with the gauge symmetry principle based on $SU(3)_c \times SU(2)_L \times U(1)_Y$, describe extremely well most of the physics of elementary particles.

However, there are still theoretical and experimental facts that can not be accommodated within the SM, all of them being related to the Higgs sector (of course, the SM does not explain either gravitation, the cosmological evidence of dark matter (DM) or

inflation, but these observations have a different nature, and thereby we do not refer to them in detail throughout this text). This observation should not be surprising, insomuch as the experimental evidence of the Higgs sector is very recent, and thus the scalar sector is the one from which we have less experimental data. Indeed, regarding the lagrangian in equation 2.7, we observe that —laying aside the kinetic lagrangian— there are either theoretical or phenomenological problems associated to every term. Thus, it is well known that the mass of an elementary scalar (μ_h in our case) is quadratically sensitive to every scale it couples too, giving rise to a *hierarchy problem*. Also, the running of the quartic term $\lambda_h(\phi^\dagger\phi)^2$ shows that the Higgs potential can develop an instability at large field values [45, 46]. Concerning the Yukawa sector, two observations are worth to point out: the puzzling hierarchy between the different fermion masses and the fact that neutrinos have a mass. All these remarks suggest that the SM is not a complete theory, and new degrees of freedom have to be added at energies above the EW scale, in order to overcome these difficulties. In what follows we describe in more detail the hierarchy problem and the intriguing quark masses, as well as the well-established evidence of massive neutrinos. Then we assert that extended Higgs sectors (by *extended Higgs sectors* we mean either extending the SM Higgs sector with new scalar degrees of freedom, or by means of new interactions) provide appealing solutions to these questions. In particular, composite Higgs models (CHMs) can alleviate the hierarchy problem as well as naturally achieve the hierarchy in the quark spectrum. On another front, neutrino masses can be elegantly explained by the *see-saw* mechanism [6].

2.4 Extended Higgs sectors

In the next sections we briefly introduce CHMs and *see-saw* models. The first can naturally arrange both the hierarchy problem and the puzzling quark mass hierarchy. *see-saw* models can accommodate massive neutrinos in a natural way. Let us start describing these problems in a deeper level of detail.

The hierarchy problem comes from the observation that masses of elementary scalars are not stable under radiative corrections. Hence, in general, the Higgs mass is quadrat-

[6]Note that, although we do not consider the instability problem in the SM [46], this can be also stabilized extending the scalar sector. For example, introducing a heavy scalar singlet with a large VEV, as first shown in [45].

ically sensitive to radiative corrections due to new particles. For example, let us assume that some new massive fermion Ψ, with mass M_Ψ, couples via Yukawa terms to the Higgs doublet with Yukawa coupling Y_Ψ. In such a case, radiative corrections due to loops of Ψ modify the Higgs mass term μ_h, such correction being [47]

$$\delta\mu_h \propto \frac{Y_\Psi}{16\pi^2} M_\Psi^2. \tag{2.12}$$

Similar expressions can be found for other scenarios (for instance: if Ψ is not a fermion but a boson or if Ψ only interacts with the Higgs boson by means of gauge interactions (see reference [47] for details). Hence, if M_Ψ is much larger than the EW scale, the correction $\delta\mu_h$ can be huge. In that case, an incredibly large fine-tuning in the parameters of the theory is required to keep the mass of the Higgs boson at its measured value $m_h \sim 126$ GeV. As a matter of fact, new particles are expected at the Planck scale, $\Lambda_P \sim 10^{19}$ GeV. Thus, unless some new symmetry is enforced to protect the Higgs boson mass (as it stands in SUSY [7]), the SM alone becomes an unnaturally fine-tuned theory (note that similar problems do not affect to SM elementary fermions and bosons which, contrary to the Higgs scalar, acquire their mass via the EWSB mechanism). This can be solved if the Higgs boson is a bound state rather than an elementary scalar.

On another front we have the large differences between the masses of the different fermions (see Table 2.2). In particular, there are more than six orders of magnitude between the top quark mass ($m_t \sim 173$ GeV) and the electron mass ($m_e \sim 0.5$ MeV). Even in the same family the splitting can be very large. For example, $m_t - m_b > 100$ GeV. These unnatural differences can not be explained by the SM, and hence they suggest that the SM has to be enlarged with new physics (NP). But of most importance is the fact that, contrary to what several experiments have definitely well established, neutrinos are massless within the SM [8]. The reason is that LH neutrinos do not have

[7] In (unbroken) SUSY, each fermion (boson) has a scalar (fermionic) superpartner that couples with identical strength to the Higgs boson. Thus, any loop of fermions is accompanied by a loop of bosons. Due to the different sign in fermions and boson loops, these contributions cancel exactly.

[8] Neutrino experiments, mainly solar [48–53], atmospheric [54, 55], reactor [56–59] and accelerator [60–62], have provided compelling evidences for oscillations of neutrinos. By *neutrinos oscillations* we mean that, if a neutrino with a given flavor i is produced in some process, at a large enough distance L from the source the probability to find a neutrino of a different flavor j is not zero. This quantum mechanical effect can not occur if neutrinos are massless. For a large review on this we refer to [43].

their RH counterparts. In addition, Majorana mass terms $m_\nu \overline{\nu_L^c} \nu_L$ violate explicitly gauge symmetry and thus can neither be written at the tree level nor be produced at any order in perturbation theory. As a result, LN is also accidentally conserved. Note that this conserved quantity does not come directly from gauge symmetry, but as a combination of both gauge symmetry and renormalizability. Indeed, at the effective level we can construct the Weinberg operator $\mathcal{O}^{(5)} = (\overline{L_L^c}\tilde{\phi}^*)(\tilde{\phi}^\dagger L_L)$. This operator is compatible with the gauge symmetry while does not conserve LN, and in fact gives a Majorana mass to the neutrinos after EWSB [9]. Hence, if we consider neutrinos to be Majorana (see Footnote 9), the question is whether the scalar sector is also responsible for neutrino masses, and then of LNV, and if can be tested at the LHC. That is to say: whether signals of LNV scalars can be found at the LHC. This is precisely what we answer in Section 5. There we classify, using an EFT approach, the scalar fields with LNV interactions that can be potentially observed at the LHC, and bound this NP using current ATLAS and CMS analyses. Among the models that can fulfill our EFT approach, the *see-saw* model of type II is the most famous one. In fact, the ATLAS and CMS analyses that we use in Section 5 proposed to probe this model. In Section 2.4.2 we briefly introduce the *see-saw* model of type II.

2.4.1 Composite Higgs models

CHMs [63–65] provide a compelling solution to the hierarchy problem. The Higgs boson arises as a bound state of a new strongly-interacting sector, with a global symmetry group G spontaneously broken to $H \subset G$. Thus, its mass is protected by its finite size. The Higgs boson is assumed to be a pseudo Nambu-Goldstone boson (pNGB) of the global symmetry breaking pattern, and hence if the NP scale f is around the TeV, the Higgs boson mass can be naturally at the EW scale.

Two ways are usually considered to achieve the explicit breaking of G: gauging only the SM gauge subgroup of H and mixing linearly the composite resonances with the

[9] One can of course also try to extend the SM with the neutrinos RH counterparts, ν_R, in order to give neutrinos a mass through the Higgs mechanism as for the rest of the SM Dirac fermions. In such a case, however, the LNV gauge invariant term $M\overline{\nu_R^c}\nu_R$ is present, and thus neutrinos are still Majorana unless some NP is invoked to make LN an exact symmetry. At any rate, the observation of non-vanishing neutrino masses necessarily requires NP. Either to explain why LN is an exact symmetry and neutrinos are Dirac, or to achieve Majorana masses and thus LNV. We only consider this last case in this text.

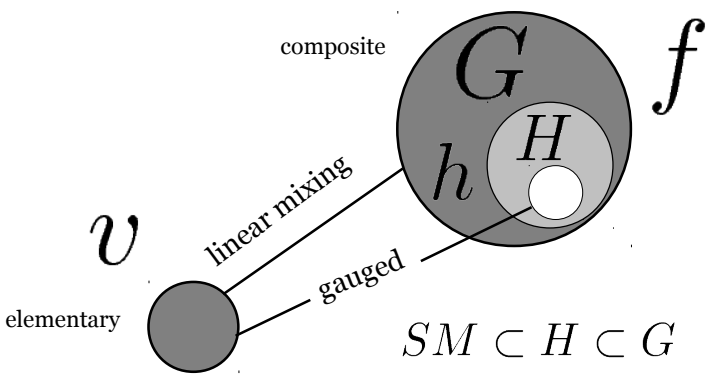

Figure 2.1: Pictorial description of CHMs. A new composite and strong sector, with approximate global symmetry group G is spontaneously broken to H. It couples to the elementary particles via linear mixings, while the Higgs remains fully composite.

elementary SM fields. As a consequence, the physical fields are admixtures of composite and elementary states (partial compositeness [66]). This point implies that the larger the mixing, the larger the interaction of an elementary field with the strong sector —in particular with the Higgs boson, which is fully composite— and thus its mass. Therefore, flavor can be naturally accommodated in this framework. Contrary to what happens in the SM, the Higgs potential is dynamically generated.

This scenario can be pictorially shown as in Figure 2.4.1: two sectors, one elementary and the other new strongly coupled, mix linearly. The dynamics of the composite Higgs boson at low energy is described by a non-linear sigma model, and thus non-linear interactions parametrized by the scale f appear. In this sense, the scalar sector is non-minimal. The couplings of the Higgs boson to the SM particles become hence modified at order $\xi \sim v^2/f^2$. If ξ is close to zero then the Higgs couplings are SM-like. In addition, new heavier particles (the ones the elementary SM fermions linearly couple to, together with their partners filling full representations of G) are also present. Although EW precision data (EWPD) typically require these resonances to be beyond the reach of current analyses [67–69], we will see in Chapter 4 that more ingenious searches can actually probe the new strong sector even with the data of the first LHC run. In particular, in Sections 4.5, 4.6 and 4.7 in that chapter we see that new color-octet resonances can be more efficiently searched for through their decay into a massive fermion resonance and a SM quark, due to the very distinctive kinematics.

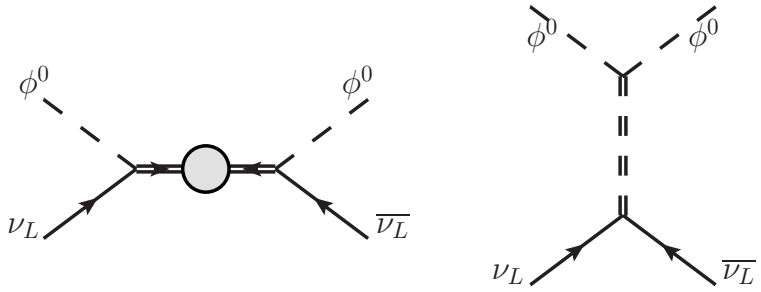

Figure 2.2: LNV interactions in the *see-saw models* of type I and III (left) and II (right). In the *see-saw* model of type I (III) LNV is mediated by new singlets (triplets with $Y = 1$) fermionic resonances. In the *see-saw* model of type II this is achieved through the addition of a new scalar triplet with $Y = 1$. The heavy fields are denoted with a double line. The gray big dot represents a (LNV) mass insertion. After EWSB, the field ϕ_0 takes a VEV and these diagrams generate a Majorana mass term for the neutrinos.

2.4.2 Seesaw model

The *see-saw* models of type I, II and III allow the neutrinos to get Majorana masses at the tree level [10] extending the SM with heavy fermionic SM singlets [75–79], a heavy scalar $SU(2)_L$ triplet with $Y = 1$ [80–85] and heavy fermionic $SU(2)_L$ triplets with $Y = 0$ [86, 87] respectively. As we assume that NP is likely related to the Higgs sector, and we in fact extend *see-saw* of type II searches to generic LNV scalar interactions, let us consider here this second model. We only describe the basic features that are needed for further discussions in Chapter 5. For more details see for instance reference [88]. In the *see-saw* of type II, the SM scalar sector is accompanied by an $SU(2)_L$ triplet with $Y = 1$ that we denote $\Delta = (\Delta^{++}, \Delta^{+}, \Delta^{0})^T$. As we will see in Chapter 5, Δ can interact with the leptons through the operator $\mathcal{O}_\Delta = y_\Delta(\overline{\tilde{L}_L}\tau^a L_L)M^\Delta_{ab}\Delta^b + \text{h.c.}$, where $a, b = 1, 0, -1$, M^Δ is a 3 times 3 matrix with entries equal to 1 for $a + b = 0$ and zero in other case. τ^a are the Pauli matrices in the spherical basis, $A^{+1} = -\frac{1}{\sqrt{2}}(A_1 - iA_2)$, $A^0 = A_3$, $A^{-1} = \frac{1}{\sqrt{2}}(A_1 + iA_2)$, times the Clebsch-Gordan coefficients $\mathrm{C}^{1\times1\to0}_{a,-a}$, up to a global factor and sign: $\tau^{\pm1} = \pm(\sigma_1 \mp i\sigma_2)/2$, $\tau^0 = \sigma_3/\sqrt{2}$. And $\tilde{L}_L = i\sigma_2 L^c_L$. Abusing of notation, we also call Δ to the traceless matrix $\Delta = [(\Delta^+/\sqrt{2}, \Delta^{++}), (\Delta^0, -\ Delta^+/\sqrt{2})]$. In this way, the lagrangian involving the SM gauge and Higgs bosons and the new field can be

[10] More elaborated models give rise to radiatively-generated Majorana masses. See for instance references [70–74].

written as

$$\mathcal{L} = (D_\mu \Delta)^\dagger D^\mu \Delta + m_\Delta^2 \mathrm{tr}(\Delta^\dagger \Delta) + \lambda_1 (\phi^\dagger \phi)\mathrm{tr}(\Delta^\dagger \Delta) + \lambda_2 [\mathrm{tr}(\Delta^\dagger \Delta)]^2 \\ + \lambda_3 \mathrm{det}(\Delta^\dagger \Delta) + \lambda_4 (\phi^\dagger \Delta \Delta^\dagger \phi) + \left[\frac{1}{\sqrt{2}} \mu (\phi^T i\sigma_2 \Delta \phi) + \mathrm{h.c.} \right]. \tag{2.13}$$

The first term in equation 2.13 stands for the kinetic term of the triplet and the rest of the equation represent the new scalar lagrangian. In this model, the EW scale $v \sim 246$ GeV does not coincide with $v_\phi = \langle \phi^0 \rangle$ but rather $v = \sqrt{v_\phi^2 + v_\Delta^2/2}$ being $v_\Delta \propto \mu v_\phi^2$. v_Δ gives neutrinos a Majorana (and hence LNV) mass once it is inserted in the operator $\mathcal{O}_\Delta$. Thus, in order to break LN both y_Δ and μ have to be non-vanishing. v_Δ breaks also the custodial symmetry, and thus has to be small to fulfill the constraints on the ρ parameter. Besides, the tiny neutrino masses, together with a natural value of y_Δ, also require v_Δ to be small. The addition of Δ to the SM implies that we have five physical scalar degrees of freedom instead of only one. Among these, we find three neutral scalars, two singly-charged scalars $\Delta^\pm_{\mathrm{phys}}$ given by

$$\Delta^\pm_{\mathrm{phys}} = -\sin\beta \Delta^\pm + \cos\beta \phi^\pm, \qquad \text{with} \quad \tan\beta = \frac{\sqrt{2} v_\Delta}{v}, \tag{2.14}$$

and, of most importance for this work, two doubly-charged scalars $\Delta^{\pm\pm}$ that can decay into same sign leptons trough the operator $\mathcal{O}_\Delta$ (if y_Δ is non-vanishing) and into same-sign W bosons trough $(D_\mu \Delta)^\dagger D^\mu \Delta$ (if μ —and hence v_Δ— is non-vanishing). Thus, $\Delta^{\pm\pm}$ can decay into $l^\pm l^\pm$ and $W^\pm W^\pm$ if, and only if, LN is violated [11]. Otherwise, if they only decay into two leptons with the same leptonic charge, the LN would be well-defined and different from zero by 2 units, while if they only decay into a pair of gauge bosons, their LN would be preserved and equal to 0.

Although current ALTAS [89] and CMS [90] searches proposed to probed the *see-saw* model of type II only consider leptonic decays (and hence do not provide LNV bounds), we see in Chapter 5 that LNV scalar interactions can be also tested with current analyses.

[11] Note that $\Delta^{\pm\pm}$ can also decay into their singly-charged partners $\Delta^\pm_{\mathrm{phys}}$ and a W boson if there is a large enough splitting between the mass of the doubly-charged scalar and the mass of the singly-charged one. We discuss this point in detail in Section 5.

Chapter 3

Collider phenomenology and Monte Carlo simulations

In the previous chapter we have presented the SM of particle physics. We have remarked that, although most of the phenomenology of elementary particles is in very good agreement with the SM predictions, there are a few open questions that can not be accommodated within this framework. We have argued that extending the scalar sector of the SM can provide good explanations to the observed deviations. In the following we want to test whether these non-standard Higgs sectors are reliable or not.

The common prediction of these models are new particles that can be produced at colliders. The signals of these particles at the detectors are the distinctive traces that have to be compared with the theoretical predictions [91]. However, the understanding of both the production of these particles and the traces of their subsequent decays on the detectors require a huge amount of computation. This is mainly due to the large number of involved Feynman diagrams [92], the radiation and hadronization [1] of colored particles and the precise description of detector effects. Hence, in order to address this work, computational tools, mainly Monte Carlo (MC) simulators, are unavoidable. At the most basic level, a MC generator is a program which produces particle physics events with the same probability as they (would) occur in nature. In other words: it

[1] Quarks and gluons can be found only within hadrons, either baryons -made of three quarks- or mesons -made of one quark and one anti-quark-, except the top quark, whose mean lifetime ($\sim 10^{-25}$ s) is so small that is decays before hadronization [43]. This phenomenon is known as *confinement*.

is a virtual collider. We describe the fundamentals of MC simulation in Section 3.3. But first we describe the general features of the collider and detectors where the NP we want to test takes place: the LHC and the ATLAS and CMS experiments. This is discussed in Sections 3.1 and 3.2, and it is mainly based on reference [93].

3.1 The Large Hadron Collider

The LHC [94–96] is a proton-proton collider located at CERN laboratory, near Geneva (Switzerland). With a c.m.e. of $\sqrt{s} = 8$ TeV, it has become the world's largest and highest-energy particle accelerator. The LHC is designed to give an answer to some of the most relevant questions in high-energy physics: the origin of mass, the hierarchy problem, the DM observation, the mystery of antimatter and the origin of our Universe among others. The LHC is a circular accelerator with 26 km of circumference, installed at an average depth of 100 meters. At the end of 2010, the LHC began colliding protons at $\sqrt{s} = 900$ GeV and, for the first time, at $\sqrt{s} = 2.36$ TeV, exceeding the c.m.e. of Tevatron. On March 30, 2010 the LHC achieved collisions at $\sqrt{s} = 7$ TeV, launching a new era in particle physics. Since April 2012 until today a luminosity of around 20 fb^{-1} of collisions at $\sqrt{s} = 8$ TeV has been recorded, and the operations for a running at $\sqrt{s} = 14$ TeV just started.

The beams of protons collide at four interaction points, where ATLAS, CMS, ALICE and LHC-B detectors are placed. The first two are generic purpose detectors, appropriate to study the physics we discuss in this work.

The production of high-energy proton beams requires a complex injection and acceleration chain. Protons are obtained from hydrogen atoms, then produced in bunches and injected in the linear accelerator LINAC. After this step protons have an energy of 50 MeV. Afterwards, they are injected in the PSB synchrotron, reaching an energy of 1 GeV. These protons are then accelerated up to 26 GeV in the PS synchrotron and are further accelerated to 450 GeV in the SPS one. Finally, the two counter-rotating beams are injected in the main ring (LHC) where they reach a maximum (so far) energy of 4 TeV. The proton bunches circle the ring inside vacuum pipes, guided by superconducting magnets. There are thousands of magnets directing the beams around the accelerator: 1232 dipole magnets keeping the particles in their orbits, placed in the curved sections of the LHC; and 392 quadrupole magnets focusing the beams, located

proton beam energy	7 TeV
number of particles per bunch	1.15×10^{11}
number of bunches	2808
bunch spacing	25 ns
circulating beam current	0.582 A
stored energy per beam	362 MJ
mean bunch length	7.55 cm
mean beam diameter (ATLAS and CMS)	16.7 μm
peak luminosity (ATLAS and CMS)	$10^{34}\text{cm}^{-2}\text{s}^{-1}$

Table 3.1: Summary of relevant parameters for the LHC collisions (extracted from [93] and [97]).

in the straights ones. For a 8 TeV c.m.e., the dipoles have to work at a temperature of 1.9 K (using superfluid helium for cooling), providing a 8.4 T magnetic field and a current flow of 11.7 kA. The beams are accelerated and kept at a constant energy with superconducting radiofrequency cavities. The LHC uses eight radiofrequency cavities per beam. These cavities are operated at 4.5 K. At $\sqrt{s} = 14$ TeV, the LHC will be able to reach a luminosity of 10^{34} $\text{cm}^{-2}\text{s}^{-1}$ when working under nominal conditions. This would give an integrated luminosity of about 100 fb^{-1} per year (in ATLAS or CMS). Under these operating conditions, each proton beam has 2808 bunches, being the number of particles per bunch of around 1.15×10^{11}. Table 3.1 summarizes the relevant LHC parameters.

3.2 General Features of detectors

The ATLAS [98, 99] and CMS [100] are the two general-purpose detectors placed at the LHC. Although they differ in the details, the general features we describe here are shared by these two experiments.

For its interest in this work, we describe briefly the coordinate system in this kind of detectors. This is represented in Figure 3.1 left. The nominal interaction point is defined as the origin of the coordinate system, while the z-axis is placed along the beam direction, and the xy plane is transverse to this. The positive x-axis is defined as pointing from the interaction point to the centre of the LHC ring, and the positive y-axis is defined as pointing upwards. The azimuthal angle φ is measured around the beam axis

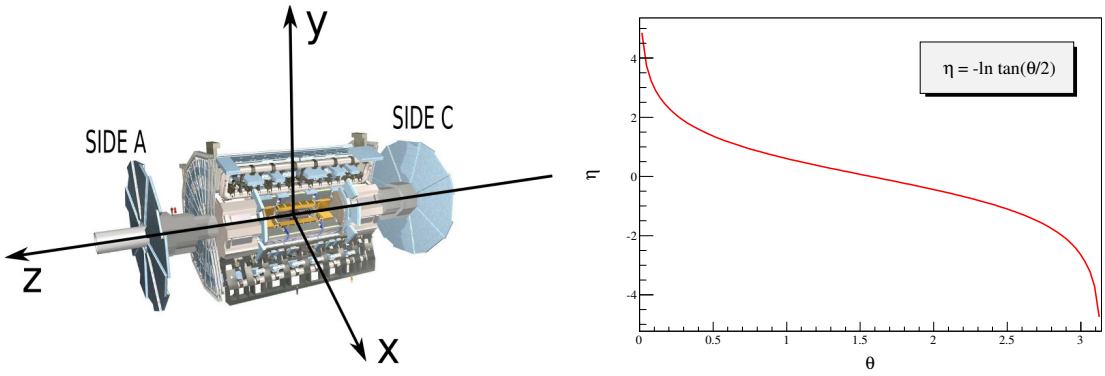

Figure 3.1: Left: General-purpose detector coordinate system (figure extracted from [93]). The positive x-axis is defined as pointing from the interaction point to the center of the LHC ring and the positive y-axis is defined as pointing upwards. The side-A of the detector is defined as that with positive z and side-C is that with negative z. The azimuthal angle φ is measured around the beam axis (with $\varphi = 0$ corresponding to the x-axis), and the polar angle θ is the angle from the beam axis. Right: Pseudorapidity as a function of the polar angle. As angle increases from zero, pseudorapidity decreases from infinity.

(with $\varphi = 0$ corresponding to the x-axis), and the polar angle θ is the angle measured from the beam axis (z-axis). The *pseudorapidity* is defined as $\eta = -\log\tan(\theta/2)$ and it is represented in Figure 3.1 right [2]. The distance ΔR in the pseudorapidity-azimuthal angle space is defined as $\Delta R = \sqrt{\Delta\eta^2 + \Delta\varphi^2}$. In the following, we also define the momentum of any particle in the transverse plane to be $p_T = \sqrt{p_x^2 + p_y^2}$, where p_x and p_y are the components of its momentum in the x and y directions respectively. Also, its transverse energy is defined to be $E_T = \sqrt{p_T^2 + m^2}$, being m the particle mass. E_x and E_y are defined analogously.

Inside the detectors, the trajectories of charged particles are bent by magnetic fields, and their radius of curvature is used to calculate their momentum: the higher the kinetic energy, the shallower the curvature. Other important parts of a detector are calorimeters for measuring the energy of particles (both charged and uncharged). Combining

[2] One can also define the *rapidity* $y = 1/2\log[(E - p_z)/(E + p_z)]$, where p_z and E represent the momentum in the z direction and the total energy respectively. For massless (or ultra-relativistic) particles, $y = \eta$.

the information from the different layers of the detector, it is possible to determine the type of particle which has left each trace. Indeed, electrons are very light and therefore lose their energy quickly in the electromagnetic calorimeter, while charged hadrons penetrate further through the layers of the detector. Photons themselves leave no trace, but in the electronic calorimeter each photon converts into one electron and one positron, the energies of which are then measured. The energy of neutral hadrons is also measured indirectly: they transfer their energy to charged hadrons, and these ones are then detected. Muons are the only particles that reach (and are detected by) the outermost layers of the detector. And neutrinos do not interact with the detectors, and so they manifest as missing energy. Thus, it is clear that only electrons (or positrons), photons, muons and hadrons can be distinguished.

Besides, hadrons are grouped into jets, in order to be related to parton quarks [3]. Thus, what a jet exactly is depends on the algorithm we use [101]. Roughly speaking, there are mainly two kind of algorithms: *cone* and *clustering* based algorithms. At the most basic level, cone algorithms work in three steps: *(i)* some hadron with p_T (or E_T) above certain threshold is used as the seed of the algorithm. *(ii)* a cone of fixed radius R is constructed around this particle, and all the objects inside the cone are merged. *(iii)* step *(ii)* is iterated until the cone becomes stable (by *stable* we mean that the cone points in the direction of the total momentum of their constituents). *(iv)* this cone is considered a *proto-jet*. *(v)* steps *(i)* to *(iv)* are done with every different seed. After this process, proto-jets can overlap, what has to be resolved with further algorithms (split-merging procedures [102]). With slight differences, IC and SISCone [102] among other algorithms work in this way. However, cone algorithms are commonly not *infrared* and/or *collinear* safe. That means that the algorithms usually provide different jets if they are applied over a colored particle or over the system formed by this particle and its soft emissions or collinear splitting. Accordingly cluster algorithms (that are infrared and collinear safe by construction), such as the k_t [103, 104] and the anti-k_t [105] algorithms are typically used. These procedures usually start defining a distance d_{ij} between any two hadrons i and j, and a distance d_{iB} between any hadron i and the beam. Then one finds the smallest of all the distances: if this corresponds to any d_{ij}

[3]Note that, due to radiation and fragmentation, a same final state quark can lead to a large amount of hadronds.

then i and j are recombined. Otherwise (i.e., if the smallest distance is some d_{iB}) i is called a jet and removed from the list of objects. After that the distances are recalculated and the procedure is repeated until no objects are left. The definition of d_{ij} and d_{iB} depend on the momenta $p_{i,j}$ of the particles involved, and are given by the equations

$$d_{ij} = min(p_{ti}^{2x}, p_{tj}^{2x})\frac{\Delta_{ij}^2}{R^2}, \qquad d_{iB} = p_{ti}^{2x}, \tag{3.1}$$

being $\Delta_{ij}^2 = (y_i - y_j)^2 + (\varphi_i - \varphi_j)^2$ and R and arbitrary parameter. What makes the difference between different algorithms is the value of x. Thus, for instance, $x = 1$ stands for the k_t algorithm and $x = -1$ for the anti-k_t. It is worth noting that, at the experimental level, jets produced by b quarks can be distinguished from other jets [4]. This is called *b-tagging*.

Finally, transverse missing energy, that we call E_T^{miss} hereafter, can be measured for the transverse energy in the initial state is known to be zero: $(E_T^{miss})^2 = (\sum_i E_x^i)^2 + (\sum_i E_y^i)^2$ where the sums extends over all the objects i. This fact does not apply to missing energy in the z direction, as this is governed by the parton-distribution functions (PDFs) of the partons inside the initial protons.

3.3 Monte Carlo simulations

We have mentioned that MC generators are mandatory to properly make predictions at colliders. The work with MC tools commonly comes in three different steps. First, we should get the resulting particles after the pp collisions (depending on the collider, we can of course have different initial states: e^+e^- (LEP), $p\overline{p}$ (Tevatron), etc.). This is the so-called *partonic level*, where NP lies, and which is of course model dependent. This step is usually given by perturbative calculations. However, these calculations describe final states in terms of quarks, gluons, leptons and photons, while experiments observe the signatures of mesons, baryons, leptons and photons in the detector apparatus. So, we need tools in order to provide the connection between these two pictures. This connection lies in the two final steps. In the second one, we should describe the evolution (including the subsequent radiation) of these partons before forming bound states: mesons and baryons. This evolution starts at hard interaction scale described in the

[4] Although this also applies to different flavors, the efficiencies are much smaller.

first step, and ends at the hadronization scale, where the last step takes place. The physics behind these steps is well known, since it relies mainly on QCD, being then model independent. However, matrix elements involving $q \to qg$ (or $g \to gg$) are strongly enhanced when the final state particles are close in the phase space [5]:

$$\frac{1}{(p_q + p_g)^2} \simeq \frac{1}{2E_q E_g(1 - \cos\theta).} \tag{3.2}$$

Hence, we see that we have both soft (due to low energies) and collinear (due to small θ) divergences. In this case, the integration over the phase space becomes a very hard task and the description based on matrix elements is no longer satisfactory. Furthermore, this step usually involves too many particles, and for this reason its implementation is computationally very expensive. The common practice in order to avoid this problem is describing the evolution of partons in the step two with an approximate algorithm. This *parton shower* algorithm has to complement the evolution in terms of matrix calculations. Matrix calculations are the appropriate description of well separated partons, i.e., away from collinear region. Matrix calculations also provide a good of description of interference effects and spin correlations, and are implemented in many software packages, although not all of them use the same approach. For instance, `MadGraph/MadEvent` and `Sherpa` [106] use Feynman diagrams and helicity amplitudes, while `ALPGEN` [107] and `HELAC` [108] use recursion relations (S-matrix [109]/Dyson-Schwinger [110–112]). On the other hand, parton showering describe successive QCD bremsstrahlung emissions, using the soft/collinear emission approximation. In this approximation, collinear emissions factorize and can be easily iterated [113]. This is of course the leading contribution, but we should keep in mind that as the energy grows and the angle of emission becomes larger, the MC prediction based on parton showering is less accurate. In order to avoid this problem, we need to compute (exactly) as many as possible real emission diagrams before starting the shower. Several software packages implement the parton showering. `PYTHIA` [114], `HERWIG` [115] and `ISAJET` [116] are some examples of them. They use different variables in the parametrization of the parton evolution: p_T^2 is used by `PYTHIA` and `ISAJET`, and $E^2\theta^2$ by `HERWIG`. The main differences between the matrix elements

[5] Here p_q (E_q) and p_g (E_g) stand for the momenta (energy) of the final quark and gluons in the final state respectively. θ represents the angle of each momentum with respect to the incoming direction.

Matrix elements	*Parton showering*
✓ Fixed order calculation	✓ Resums large logs
✓ Computationally expensive	✓ Computationally cheap
✓ Limited number of particles	✓ No limit particle multiplicity
✓ Hard and well-separated partons	✓ Collinear and/or soft partons
✓ Quantum interference correct	✓ Partial quantum interference
✓ Multi-jet description	✓ Hadronization/detector simulation

Table 3.2: Main differences between matrix elements computations and parton showering.

and the parton showering approaches are shown in Table 3.2. So, we see that the two approaches are complementary, and are necessary in high-precision studies of multi-jets processes. However, although they work almost in well separated regions of phase space, they can overlap in some events. Thus, we need to avoid this double-counting in order to get correct results, and this is the idea behind *matching*: using matrix element description for well separated jets, and parton showers for collinear jets [117]. In this way, we can combine the two descriptions without double counting. We would also like to get a smooth transition between the two phase space regions, as well as a small or even null dependence from precise cut-off and the largest multiplicity sample. So far, there are mainly two solutions: the CKKW [118, 119] matching and the MLM [120] matching. For its interest in this work we restrict here to the last one. The MLM procedure is implemented in both `MadEvent` and `ALPGEN`. According to MLM, the hadrons produced in the showering routine (e.g. `PYTHIA` or `HERWIG`) are matched to the partons obtained from the matrix element calculation. For this purpose, a jet clustering algorithm (so far, IC or k_t have been investigated) is applied to the final-state particles. The event is kept if each hard parton in the event can be matched to a jet, based on a distance in $\eta - \varphi$ space. Otherwise it is rejected. The parton-level configuration for the samples is generated for a particular number of hard jets (*exclusive sample*). Only for the sample with the highest jet multiplicity, extra jets which do not match to hard partons are allowed to be present after the showering is performed (*inclusive sample*). Events with extra jets from parton shower are kept if extra jets are softer than matrix elements jets. Although the parameters used for the clustering and the matching are somewhat arbitrary, usually the cuts with respect to the separation and minimum momentum

applied at parton level are used.

The last step in the chain simulation is the simulation of the detector. After this step, we should get the detector response to the interaction of leptons, photons and hadrons. The transverse momentum of the neutrinos (and, if they exist, other weakly interacting particles) can also be reconstructed, because of conservation of transverse momentum in proton-proton collisions. Two widely used simulators are `PGS` [121] and `Delphes` [122]. Every generic-purpose simulator provides the following features: realistic simulation taking into account subdetector extensions, types, segmentations and resolutions; a tracker in a solenoidal magnetic field; calorimeters with electromagnetic and hadronic sections; a muon system; trigger simulation and, of course, a human-readable output, like `LHEF` [123] of even a `ROOT` [124] file directly.

In this text, unless otherwise explicitly stated, `MadGraph v4` [125] is used for the generation of parton level signal events and `ALPGEN v2.13` [107] is used for the generation of background events [6], with the default parameters; linked both to `PYTHIA v6` [114] for initial and final state radiation, parton showering and hadronization, matched via the MLM method [120]. `Delphes v1.9` [122] is used for detector simulation. Regarding the latter we use a tuned version of the standard ATLAS card that results in an very good agreement with published experimental results [126]. The main changes are: the tracking efficiency is updated to 95; the isolation criteria is changed to $\Delta R = 0.4$ and the b-tagging efficiency is set to 0.7. Also we use the CTEQ6L1 [127] PDFs and the default values of the renormalization and factorization scales. In addition, the anti-k_t algorithm implemented in `Fastjet v3` [128] with $R = 0.4$ is assumed to be used unless otherwise stated for jet definition, and the b-tagging fake-rate is conservatively set to 1/100 for light jets and 1/10 for c-jets. Jets j are required to have $|\eta_j| < 5$, and light leptons (e and μ), that we call ℓ instead of l (that is used also for τ), are required to have $|\eta_\ell| < 2.5$. They are also required to be isolated from any jet by demanding $\Delta R(\ell, j) > 0.4$. Missing transverse energy is denoted as E_T^{miss}.

3.4 Statistical tools: limits and sensitivity reach

Particle physics experiments usually involve cross section measurements, through the counting of events in different regions of the available phase space, or observables con-

[6] What *signal* and *backgrounds* events exactly mean is defined in the next section.

structed out of them (such as asymmetries).

As of today, the SM has revealed itself as an excellent description of the real *data*, so that NP manifests as departures from the SM *background*. However, given its quantum-mechanical nature, the background can fluctuate. Hence, the question is how we can discriminate between random background fluctuations and actual departures (signals). We would like to address two main goals: *(i)* given a signal prediction determine whether it is or not compatible (at some C.L.) with the observed data; and *(ii)* giving a data departing from the SM background predictions, quantify how statistically significant this fluctuation is.

Concerning point *(i)*, let us consider an N-bin experiment (where each bin is typically the number of events in a particular phase-space region). We make use of the CL_s method [129] for the calculation of exclusion limits, which constructs the statistic defined by

$$Q = \prod_i \frac{(s_i + b_i)^{\tilde{n}_i} e^{-(s_i+b_i)}}{b_i^{\tilde{n}_i} e^{-b_i}} = e^{-\sum_i s_i} \prod_i \left[1 + \frac{s_i}{b_i}\right]^{\tilde{n}_i} , \tag{3.3}$$

where b_i and s_i are the number of predicted background events and of expected signal events for the bin i, respectively, while $\tilde{n}_i$ is the Poisson-distributed variable with mean s_i+b_i (b_i) for the signal+background (background-only) hypothesis. Q is then a random variable distributed according to some density function $P_{s+b}(Q)$ (resp. $P_b(Q)$) in the signal+background (resp. background-only) hypothesis. The confidence estimators

$$\mathrm{CL}_{s+b} = 1 - \int_{Q_{obs}}^{\infty} P_{s+b}(Q)\, dQ \quad \text{and} \quad \mathrm{CL}_b = 1 - \int_{Q_{obs}}^{\infty} P_b(Q)\, dQ \tag{3.4}$$

are then defined integrating the corresponding density functions up to Q_{obs}, which is the value of for $\tilde{n}_i$ equal to the number of observed events n_i. In what is called the CL_{s+b} method, one carries out a statistically test based only on the CL_{s+b} variable. In such a case, a signal is said to be excluded at the 95% C.L. if $\mathrm{CL}_{s+b} < 1 - 0.95 = 0.05$.

However, it is well known that, when the signal is small, and hence the functions P_b and P_{s+b} are strongly overlapped, the CL_{s+b} method can exclude signal levels which are not statistically significant. In order to avoid this problem, the parameter space regions excluded at the 95 % C.L. can be obtained requiring that $\mathrm{CL}_s \equiv \mathrm{CL}_{s+b}/\mathrm{CL}_b \leq 0.05$.

The signals excluded by CL_s are thus equivalent to those excluded by CL_{s+b} in the limit of large s.

It is also worth noting that either Q or $\log Q$ can be used as statistic, although the latter is more convenient for calculating CL_s if there is only one bin (counting experiment). Indeed, in that case

$$Q = e^{-s}\left(1+\frac{s}{b}\right)^{\tilde{n}} \Rightarrow \log Q = -s + \tilde{n}\left(1+\frac{s}{b}\right). \tag{3.5}$$

Hence, $\log Q$ is distributed as $\tilde{n}$ up to a scale factor and a shift. But none of them changes the ratio of areas defining CL_s, being then easier to use the $\tilde{n}$ distribution as statistic. This result implies, in particular, that the number of signal events that are excluded in a one-bin experiment when zero events are expected and zero events are observed is $s \simeq 2.996$. That means, in any case, that no model can be excluded if it does not predict more than 3 events.

If we consider multi-bin analyses, the MC estimation of the Q distributions has to be performed. As a matter of fact, this can be carried out using the `TLimit` class of `ROOT`, which contains all the required routines.

In what respects to point *(ii)*, we briefly comment the case of a single background component (we refer to [130] for multi-bins examples and further details). In such a case, if s is the number of predicted signal events and b stands for the number of predicted background events, the sensitivity $\mathcal{S}(s,b)$ that is used in this text reads [7]

$$\mathcal{S}(s,b) = \sqrt{2\left[(s+b)\log\left(1+\frac{s}{b}\right) - s\right]} \tag{3.6}$$

A discovery is claimed when $\mathcal{S}(s,b) = 5$. As explained in reference [130], when this equation is used to predict the sensitivity reach of a future collider experiment by means of MC simulations, one important remark is mandatory: this equation can be only used if the number of generated events (both for signal and background) is much larger than the number of expected events in such a experiment. Otherwise, the limited statistic has to be taken into account. We return to this point in Section 4.6, where we consider the effects of limited statistics using `SigCalc` [130].

[7] In reference [130] the limit $s \ll b$ is proved to give the widely used expression $\mathcal{S}(s,b) \sim s/\sqrt{b}$.

Chapter 4

Composite Higgs models

CHMs, which were introduced for the first time by Georgi and Kaplan in [63, 64], are an appealing solution to the hierarchy problem, in which the Higgs boson is assumed to be a bound state of some new strongly interacting sector instead of an elementary scalar. In order to explain its low mass, it is further required to be the pNGB of a spontaneously broken global symmetry $G \to H$ in the strong sector, in analogy to the chiral symmetry breaking in QCD [1]. The low-energy theory description of the Higgs sector is thus described by a non-linear sigma model. The phenomenological implications of the CHM solution include: (i) deviations in the SM couplings introduced by the non-linear interactions in the scalar sector; and (ii) the presence of new fermionic and vector resonances mixing with the elementary SM particles, whose experimental observation depends largely on the SM fermions they mostly couple to. Thus, in the following sections, we discuss the general details of CHMs in Section 4.1 and introduce the low-energy theory description of the Higgs sector in terms of non-linear interactions in the Coleman-Weinberg-Wess-Zumino (CCWZ) formalism in Section 4.2. In Section 4.3 we describe the fermionic resonances of the strong sector and their mixing with the SM particles in the partial compositeness setting. We then discuss in detail the minimal realization of a phenomenologically viable CHM, based on the breaking of

[1] Other strongly-interacting scenarios include technicolor theories [131–133] and little Higgs models [134, 135]. In the first case, the EW symmetry is already broken by the strong sector, and thus no Higgs is necessary at all. In the second case, although a Higgs boson is also present in the NGB spectrum, only its mass (and not the corresponding quartic coupling) is radiatively generated, in contrast to CHMs in which the whole potential is generated at the loop level.

$SO(5) \to SO(4)$, in Section 4.4. This introduction is mostly based on references [136–138]. The text which is properly speaking part of the work done in this thesis is presented in Sections 4.5, 4.6, 4.7 and 4.8. In Sections 4.5, 4.6 and 4.7 we study the collider signatures of the new fermionic resonances depending on whether they mainly couple to the top, bottom or light quarks, respectively. We also discuss their interplay with other vector resonances and their impact on indirect observables (such as asymmetries). We then argue that the study of non-minimal CHMs is timely, and introduce finally in Section 4.8 an extended CHM based on the breaking of $SO(7) \to G_2$. We study its algebraic structure in detail and its phenomenological implications at the LHC.

4.1 General idea

CHMs provide an elegant solution to the hierarchy problem assuming the Higgs is a composite state. In this way, its finite size protects its mass, which is not sensitive to radiative corrections above the compositeness scale f_π. However, the lack of evidence of NP up to near the TeV scale [139] implies $f_\pi \sim$ TeV, while the mass of the Higgs boson is known to be well around ~ 125 GeV. In order to reconcile these two observations we consider the Higgs boson to be a pNGB of the strong sector, dynamically generated by the spontaneous breaking $G \to H$ of an approximate global continuous symmetry G. Thereby, the Higgs boson mass is naturally small while the NP stays at the TeV scale. Given the appropriate description of nature provided by the SM, G and H are typically required to fulfill the following properties: (i) both G and H contain the SM group $SU(3)_c \times SU(2)_L \times SU(2)_R$, where the custodial symmetry has been included in order to protect the $\rho \sim 1$ parameter; (ii) the NGBs of G/H contain at least an uncolored bidoublet of the SM group, acting then as the Higgs degrees of freedom; (iii) all the SM fermions can be embedded in representations of G. This last requirement implies that the elementary SM fermions can mix with fermionic resonances in the strong sector without breaking the SM gauge symmetry. In the following, given that we will not consider colored scalars, we assume breaking patterns of the form $G \times SU(3)_c \to H \times SU(3)_c$ and forget the $SU(3)_c$ components. Several coset structures fulfill this setup, from the minimal CHM (MCHM) [2] based on the coset $SO(5)/SO(4)$

[2]It is minimal in the sense that only four degrees of freedom, that will be identified with the Higgs doublet, arise as pNGBs. The CHM based on the coset $SU(3)/SU(2) \times U(1)$ provides also a minimal

described in Section 4.4 to extended ones like the $SO(7)/G_2$ of Section 4.8.

On another front, the global symmetry group G is explicitly broken in two ways: (i) by the gauging of $SU(3)_c \times SU(2)_L \times U(1)_Y \in H$ and (ii) by the linear couplings of the SM fermions to the fermionic resonances in the strong sector. In the first case, the loops of gauge bosons propagate the breaking of the global symmetry —for those NGBs whose generators do not commute with the generators T_{SM} of the SM— and thus generate an effective potential. The rest of the generators, that is, the T_a of G satisfying the relation $[T_a, T_{SM}] = 0$ are uncharged under the SM symmetry and, as a consequence, their associated NGBs do not interact with the gauge bosons. The group constructed out of these operators is actually the largest subgroup of G that contains $SU(3)_c \times SU(2)_L \times U(1)_Y$ as an ideal. Thereby, the gauging of the SM group explicitly breaks G to this group. However, as firstly shown by Witten [140], the radiative contribution from gauge fields generate a potential whose VEV tends to be aligned in the direction that preserves the gauge symmetry. In the second case, the symmetry breaking comes from the fact that SM fermions do not transform in complete representations of G, and thus the symmetry is explicitly reduced to the SM gauge group. Loops of fermions thus induce an effective potential which can give rise to a non-trivial EW VEV. For this reason, hereafter we only consider the fermion contribution to the effective potential, although gauge contributions are relevant if one wants to perform detailed calculations.

The mixing of heavier resonances with SM fermions is also responsible for the Yukawa interactions. As we discuss in Section 4.3, the physical degrees of freedom are admixtures of elementary and composite states, according to the so called *partial compositeness* setup. The Higgs boson, however, remains completely composite, and the fermion masses arise after EWSB.

4.2 The CCWZ formalism

In order to describe the dynamics of the low-energy states of a CHM, the NGBs are parametrized as fields φ_a taking values in the coset space G/H. An effective lagrangian can be constructed out of these fields applying the CCWZ [141, 142] formalism. This

Higgs sector but, unlike $SO(5)/SO(4)$, does not respect custodial symmetry and thus does not hold point (i) of the discussion above.

method starts considering the Maurer-Cartan one-form of the global symmetry group G (see Appendix B for further details) reduced to the coset space. That is,

$$\omega_\mu = -iU^\dagger \partial_\mu U, \quad U = e^{-i\Pi/f_\pi}, \quad \text{with} \quad \Pi = \sum \varphi_a C^a, \tag{4.1}$$

where C^a represent the broken generators. f_π has been introduced to normalize the dimensions inside the exponential. As stressed in Appendix B, ω can be decomposed in its components along the broken and unbroken generators. These components are usually called perpendicular (d_μ) and parallel (E_μ) projections respectively, and allow us to write $-iU^\dagger \partial_\mu U = d_\mu + E_\mu$. The CCWZ formalism states that the lagrangian describing the dynamics of the NGB associated to G/H, at the level of two derivatives, is given by

$$\mathcal{L} = \frac{f_\pi^2}{4} \mathrm{tr}(d_\mu d^\mu). \tag{4.2}$$

f_π is thus an arbitrary energy scale that can be shifted if the generators are normalized in a different way, or if the fields φ_a are redefined. In any case, the limit $f_\pi \to \infty$ represents the point in which the underlying NP decouple.

A last comment is in order. If we want to consider gauge theories, in which some subgroup of H is gauged, we only need to make the replacement $\partial_\mu \to D_\mu$ in the definition of ω in equation 4.1, where D_μ is the covariant derivative of the SM gauge group. We apply this formalism to the case of $SO(5)/SO(4)$ in Section 4.4.

4.3 Partial compositeness

The global symmetry of the strong sector in CHMs is explicitly broken by the coupling of the elementary fermions ψ to some composite operators $\mathcal{O}(x)$, but this is also the mechanism in which fermions acquire a mass in CHMs. The question is which composite operators the elementary fermions couple to. Several attempts to give an answer to this question have been proposed. For instance, inspired in technicolor theories [131–133], one could start proposing a *bilinear* coupling between elementary and composite operators, $\sim \Delta_\psi \bar{\psi}\psi\mathcal{O}(x)$. However, it has been shown that this mechanism either introduce again the hierarchy problem or large FCNC (if one wants to generate large enough fermions masses), but they can not be avoided at the same time. Thus, an alternative mechanism consists of coupling *linearly* [66] the elementary fermions to

the composite sector, $\sim \Delta_\psi \bar{\psi}\mathcal{O}(x) + \text{h.c.}$ In such a case, FCNC can be suppressed without reintroducing ultraviolet (UV) instabilities and, in addition, provides a natural explanation of the hierarchies in the fermion sector (except of course for the neutrinos), through the renormalization-group evolution of the Δ_ψ couplings.

As a consequence of these linear couplings, we find another interesting feature, called *partial compositeness*, which stands for the following property. At energies below the scale of compositeness, the operator $\mathcal{O}(x)$ can excite a tower of massive fermionic composite states ξ_n, i.e., $\langle 0|\mathcal{O}(x)|\xi_n\rangle = m_n$, so that linear couplings induce mass mixing between the composite states and the elementary fermions: $\mathcal{L}_{mix} = \sum m_n(\bar{\psi}\xi_n + \text{h.c.})$. This mass mixing means that the physical states before EWSB are an admixture of elementary and heavy states (thus the name *partial compositeness*) in CHMs. As a first approximation, the low-energy phenomenology of these models can be studied if we consider a truncation of each tower of composite fermions to the first resonance, neglecting the rest of the heavy states. As an example, we consider for simplicity the case of only one vector-like resonance ξ and a chiral LH elementary fermion ψ_L, whose lagrangian in the elementary/composite basis reads

$$\mathcal{L} = i\overline{\psi_L}\not{\partial}\psi_L + \bar{\xi}(i\not{\partial} - M)\xi + \Delta_\psi(\overline{\psi_L}\xi_R + \text{h.c.}). \tag{4.3}$$

Neither ξ nor ψ_L are mass eigenstates, due to the mixing term. Hence, in order to obtain the physical states we have to take the rotation given by $\psi_L \to \cos\phi_L\ \psi_L + \sin\phi_L\ \xi_L$ and $\xi_L \to -\sin\phi_L\ \psi_L + \cos\phi_L\ \xi_L$, where ϕ_L is the rotation angle and its value is given in terms of the previous parameters by $\tan\phi_L \sim \Delta_\psi/M$. The resulting lagrangian after this rotation is expressed as

$$\mathcal{L} = i\overline{\psi_L}\not{\partial}\psi_L + \bar{\xi}\left(i - \frac{M}{\cos\phi_L}\right)\xi. \tag{4.4}$$

We see that the elementary fermion remains massless (before EWSB), due to the conservation of the fermionic index [3]. In a more complete model, before the rotation, only ξ couples to the Higgs sector though proto-Yukawa interactions, for the Higgs boson is

[3] Charged fermions Dirac masses mix LH fields with RH fields. The fermion content we started with was two LH fields and one RH field, thus, after rotation we are left with a single LH field that has to be massless.

fully composite. After diagonalization ψ_L also interacts with the Higgs boson, so that after EWSB it gets a mass. Thus, concerning the value of ϕ_L, several comments are worth to emphasize: (*i*) the larger the value of ϕ_L, the more composite a SM particle is (the SM yukawa is typically given by $y \sim Y_* \sin\phi_L \cos\phi_R$ once we consider also RH fermions, where Y_* stands for the yukawa among composites). (*ii*) heavier particles (after EWSB) couple stronger to the Higgs and therefore are more composite, what means that $\sin\phi_L$ (the *degree of compositeness*) is large, while light particles are more elementary [4]. Thus, it is expected that heavier fermions like the top and bottom quarks play a main role in the phenomenology.

4.4 The minimal composite Higgs model

The MCHM [143] is based on the symmetry breaking pattern $SO(5)/SO(4)$. The group theory of $SO(5)$ and its maximal $SO(4)$ custodial subgroup can be found in Appendix C. The coset space has dimension four, and thus four scalar degrees of freedom appear in the NGB spectrum, with the same quantum numbers as the SM Higgs boson. In the following, we first discuss in Section 4.4.1 the scalar sector (both gauge and Yukawa interactions) of the MCHM, and in particular we show how the interactions with the elementary particles become modified with respect to their SM values, and compare with the recent measurements performed at the LHC. We then implement in Section 4.4.2 the partial compositeness formalism, and derive the quantum numbers of the fermionic resonances and their interactions with the SM quark fields. In the MCHM we just embed the SM fields in the **5** representation of the whole group, because this is the smallest representation that can be used to protect the $Z\bar{b}_L b_L$ coupling [144]. In the literature, this scenario is referred to MCHM5 [144]. Nonetheless, other representations, like the **4**, the **10** and the **14**, have been also considered [143–148]. In Section 4.4.3 we derive the Coleman-Weinberg potential [149, 150] induced by loops of SM particles, giving rise to the mass and quartic terms in the Higgs potential, and comment on the interplay between the Higgs mass and the presence of light resonances in the spectrum. Finally, in Section 4.4.4 we argue for the presence of colored-vector resonances in the MCHM and

[4] This fact guarantees the absence of flavor violating processes in the light generations, because these are suppressed by the small mixing angles. These can be large, however, if some flavor symmetry is forced on the strong sector, like in the scenario that we consider in Section 4.7.

describe their interactions with the SM fields and the fermionic resonances. We then briefly discuss the approximations that are taken in order to study the phenomenology of composite tops, bottoms or light quarks.

4.4.1 Scalar sector

The scalar sector of the MCHM contains four degrees of freedom that we call ϕ_a. The dynamics of ϕ_a is well described by the perpendicular component d_μ of the Maurer-Cartan one-form as commented in Section 4.2. In order to project d_μ into the coset space as required by the CCWZ formalism, we can take a vacuum Σ_0 that is killed only by the $SO(4)$ subgroup generators T^a. That is, $T^a\Sigma_0 = 0$ while $C^a\Sigma_0 \neq 0$. According to the matrices presented in Appendix C, this vacuum can be trivially chosen to be $\Sigma_0 = (0,0,0,0,1)^T$. In this way, the non-linear sigma model lagrangian $\mathcal{L} = 1/4\, f_\pi^2\, \mathrm{tr}(d_\mu d^\mu)$ can be also computed as

$$\mathcal{L} = \frac{f^2}{2}\left(D_\mu \Sigma\right)^\dagger D^\mu \Sigma, \quad \text{with } \Sigma = U\Sigma_0, \tag{4.5}$$

where we have defined $f = \sqrt{2} f_\pi$ in order to simplify the following equations. The explicit expression for Σ is hence given by:

$$\Sigma = \frac{\sin\left(|\phi|/f\right)}{|\phi|}\left[\phi_1,\, \phi_2,\, \phi_3,\, \phi_4,\, |\phi| \cot\left(\frac{|\phi|}{f}\right)\right]^T, \quad |\phi| = \sqrt{\phi_1^2 + \phi_2^2 + \phi_3^2 + \phi_4^2}. \tag{4.6}$$

In the unitary gauge, three of the NGBs are eaten by the gauge bosons. In such a gauge, we can impose the physical Higgs h to be completely aligned in the ϕ_3 direction without loss of generality. In that case, $h = \phi_3 = |\phi|$ and

$$\Sigma^T = \left[0,\, 0,\, \sin\left(\frac{h}{f}\right),\, 0,\, \cos\left(\frac{h}{f}\right)\right]. \tag{4.7}$$

According to the conventions we are using in this text, the covariant derivative acts on Σ as

$$D_\mu \Sigma = \left(\partial_\mu + igT_I W_\mu^I + ig' Y B_\mu\right)\Sigma \tag{4.8}$$

$$= \left[\partial_\mu + \frac{ig}{\sqrt{2}}(T^+ W_\mu^+ + T^- W_\mu^-) + \frac{ig}{c_W}(T_3 - s_W^2 Q) Z_\mu + ieQA_\mu\right]\Sigma, \tag{4.9}$$

where now the matrices are the five-dimensional matrices of Appendix C generating the SM subgroup of $SO(5)$. Therefore, the term $(D_\mu\Sigma)^\dagger D^\mu\Sigma$ in equation 4.5 is given by

$$\begin{aligned}(D_\mu\Sigma)^\dagger D^\mu\Sigma =&(\partial_\mu\Sigma)^\dagger\partial^\mu\Sigma + \Sigma^\dagger\left\{\frac{g^2}{2}\left(T^+W_\mu^+ + T^-W_\mu^-\right)^2\right.\\ &\left.+\frac{g^2}{c_W^2}\left[(T_3 - s_W^2Q)Z_\mu\right]^2 + e^2Q^2A_\mu A^\mu\right\}\Sigma\\ =&\frac{1}{f^2}\left(\partial_\mu h\right)^2 + \frac{g^2}{2}\sin^2\left(\frac{h}{f}\right)W_\mu^+W^{\mu-} + \frac{g^2}{4c_W^2}\sin^2\left(\frac{h}{f}\right)Z_\mu Z^\mu. \end{aligned} \tag{4.10}$$

Thus,

$$\mathcal{L} = \frac{1}{2}\partial_\mu h\partial^\mu h + \frac{g^2}{4}f^2\sin^2\left(\frac{h}{f}\right)W_\mu^+W^{\mu-} + \frac{g^2}{8c_W^2}f^2\sin^2\left(\frac{h}{f}\right)Z_\mu Z^\mu. \tag{4.11}$$

Up to this point, the Higgs boson h is an exact NGB, described by a kinetic term and a set of non-linear interactions to the gauge bosons. As it was previously discussed, the interactions with the gauge bosons generate a potential and then a mass, but they tend to align the VEV in the unbroken direction. However, the couplings to the fermion sector can generate a non-trivial VEV $\langle h\rangle$. If we expand the previous lagrangian to second order in h after symmetry breaking, we get

$$\mathcal{L} = \frac{1}{2}\partial_\mu h\partial^\mu h + \frac{g^2}{4}\left[v^2 + 2v\sqrt{1-\xi}h + (1-2\xi)h^2\right]\left[W_\mu^+W^{\mu-} + \frac{1}{2c_W^2}Z_\mu Z^\mu\right]$$

where we have defined

$$v = f\sin\left(\frac{\langle h\rangle}{f}\right), \quad \text{and } \xi = \frac{v^2}{f^2}. \tag{4.12}$$

$v \sim 246$ GeV fixes the EW scale, while ξ is called the *degree of compositeness*. Note that, in this framework, the Higgs VEV $\langle h\rangle$ does not coincide with v. We see that the tensor structures of the hVV and $hhVV$ interactions (where V stands for any SM gauge boson) are identical to the SM ones, but the couplings differ by deviations of order $\mathcal{O}(\xi)$. Indeed, in the limit $\xi = 0$, i.e., in the limit in which the scale of NP, f, is large enough, we recover the SM Higgs lagrangian. The NP coming from the composite sector decouples.

In order to analyze the Higgs interactions with the fermions, the $SO(5)$ group has

to be extended to $SO(5) \times U(1)_X$. Otherwise, the elementary quarks and leptons can not be embedded in representations of the global symmetry [5]. Given that $U(1)_X$ is not broken, Σ is not charged under this group and the previous computations are not affected.

The full description of the Yukawa lagrangian requires the introduction of the composite partners according to the partial compositeness language, and are in fact worked out in detail in the next section. However, if we are only interested in the lowest-mass degrees of freedom we can decouple the heavy masses m_Q (that is, $m_Q \gg \Lambda$ being Λ any other relevant scale). This is useful, for instance, if we only want to know the SM corrections to the Yukawa sector coming from non-linear effects. In that case, we only need to introduce, for each fermion family, four new multiplets of $SO(5)$, that we call $Q_L^{2/3}, Q_L^{-1/3}, U_R$ and D_R. The SM up ($u_{L,R}$) and down ($d_{L,R}$) fields are embedded in these multiplets in the following way (see Appendix C):

$$Q_L^{2/3} = \frac{1}{\sqrt{2}}\begin{pmatrix} d_L,\, -id_L,\, u_L,\, iu_L,\, 0 \end{pmatrix}^T, \quad U_R = \frac{1}{\sqrt{2}}\begin{pmatrix} 0,\, 0,\, 0,\, 0,\, \sqrt{2}u_R \end{pmatrix}^T,$$
$$Q_L^{-1/3} = -\frac{1}{\sqrt{2}}\begin{pmatrix} u_L,\, iu_L,\, -d_L,\, id_L,\, 0 \end{pmatrix}^T, \quad D_R = \frac{1}{\sqrt{2}}\begin{pmatrix} 0,\, 0,\, 0,\, 0,\, \sqrt{2}d_R \end{pmatrix}^T. \quad (4.13)$$

The superscript in Q_L denotes the charge under $U(1)_X$, while U_R and D_R have charges $X = 2/3$ and $X = -1/3$ respectively. The hypercharges $Y = T_R^3 + X$ of the quark fields are thus correctly reproduced in this embedding. The Yukawa lagrangian is then given by the following equation (note that we are ignoring family mixings):

$$\begin{aligned} \mathcal{L}_Y &= f\left[-y_u(\overline{U_R}\Sigma)(\Sigma^T Q_L^{2/3}) - y_d(\overline{D_R}\Sigma)(\Sigma^T Q_L^{-1/3})\right] + \text{h.c.} \\ &= -\frac{f}{\sqrt{2}}\sin\left(\frac{h}{f}\right)\cos\left(\frac{h}{f}\right)\left(y_u\overline{u_L}u_R + y_d\,\overline{d_L}d_R + \text{h.c.}\right). \end{aligned} \quad (4.14)$$

Again, after EWSB, $h \to h + \langle h \rangle$, and we obtain, up to factors of order $\mathcal{O}(h^2/f^2)$ [6], the

[5] If we were not introducing an extra $U(1)_X$ group, the hypercharge would be given by the T_3 generator of $SU(2)_R$. However, the five-plets in $SO(5)$ (see Appendix C for more details) only decompose under this T_3 in representations of charge +1/2 and -1/2, so that fermions with hypercharges different from these values are not allowed.

[6] Higher-order terms produce effective tree-level interactions with two Higgs bosons and two

following lagrangian:

$$\begin{aligned}\mathcal{L}_Y &= -\frac{v}{\sqrt{2}}\left[\sqrt{1-\xi}+(1-2\xi)\frac{h}{v}\right]\left(y_u\overline{u_L}u_R+y_d\overline{d_L}d_R+\text{h.c.}\right)\\ &= \left[1+\left(\frac{1-2\xi}{\sqrt{1-\xi}}\right)\frac{h}{v}\right]\left(m_u\overline{u_L}u_R+m_d\overline{d_L}d_R\right).\end{aligned} \tag{4.15}$$

Of course, we recover the SM again in the limit $\xi = 0$. Thus, the ratios of the tree level couplings of the Higgs to two SM particles to the corresponding SM coupling are given by

$$R_{hVV} = \sqrt{1-\xi} \quad \text{and} \quad R_{hff} = \frac{1-2\xi}{\sqrt{1-\xi}}, \tag{4.16}$$

where V and f stand for any EW gauge boson and SM fermion, respectively. Thereby, the Higgs production cross section in the GF channel receives a suppression proportional to R^2_{hff} while that in the VBF channel becomes multiplied by R^2_{hVV}. Analogously [151, 152], the different decay widths scale with the corresponding couplings squared except for the $h \to \gamma\gamma$ channel that reads

$$\Gamma(h\to\gamma\gamma) = \frac{(R_{hff}I_\gamma + R_{hVV}J_\gamma)^2}{(I_\gamma+J_\gamma)^2}\Gamma^{\text{SM}}(h\to\gamma\gamma), \tag{4.17}$$

where the functions I_γ and J_γ read

$$I_\gamma = -\frac{8}{3}x_t[1+(1-x_t)f(x_t)], \quad J_\gamma = 2+3x_W[1-(2-x_W)f(x_W)], \tag{4.18}$$

with $x_t = 4m_t^2/m_h^2$, $x_W = 4m_W^2/m_h^2$ and

$$f(x) = \begin{cases} \arcsin[1/\sqrt{x}]^2, & x \geq 1, \\ -\frac{1}{4}\left[\log\frac{1+\sqrt{1-x}}{1-\sqrt{1-x}} - \mathrm{i}\pi\right]^2, & x < 1. \end{cases} \tag{4.19}$$

The $h \to \gamma Z$ is also modified in a similar way, with different loop functions. We do not give the explicit result as it is not used in the following. The above equations completely determine all the relevant properties of the Higgs due to its pNGB nature

---

fermions. These interactions are important as they give rise to strong double-Higgs production in CHMs. We come back to this point in Section 4.7.

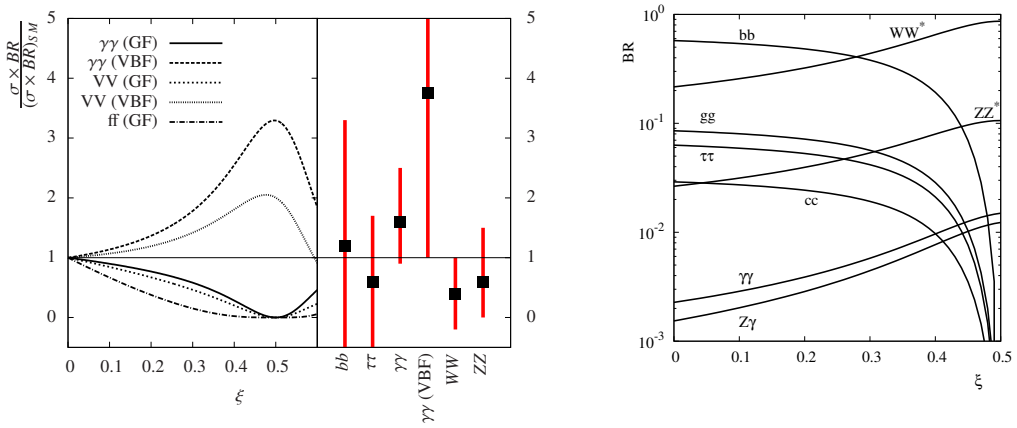

Figure 4.1: Left: Higgs production cross section (separated in GF and VBF) times BR into different channels in units of the corresponding SM process, and best fit value for the same observable obtained by the CMS Collaboration. Right: BRs of a composite Higgs of mass 125 GeV as a function of the degree of compositeness in logarithmic scale.

The Higgs becomes SM-like in the limit $\xi = 0$. As an example, we show in Fig. 4.1 the Higgs production cross section times branching ratio (BR) into different channels in units of the corresponding SM cross section as a function of ξ. For comparison we also show the best fit values for these cross sections as reported by CMS in [153].

4.4.2 Fermionic resonances

Up to this point, we have considered decoupled fermionic resonances, to study the effects of non-linear scalar interactions in the SM fermions. However, fermionic resonances are naturally light (as we will comment below), and thus their dynamics has to be included in the theory. In order to do that, we use the language of partial compositeness. We introduce vector-like fermions which have quantum numbers such that they can mix linearly with the SM fermions embedded in the representations given in equation 4.13. We introduce composite fermions transforming as complete $\mathbf{5}_{2/3}$ and $\mathbf{5}_{-1/3}$ under $SO(5) \times U(1)_X$. The composite multiplets for one family can be written as

$$\psi_U = \frac{1}{\sqrt{2}}\left(D - U_{5/3},\ -i(D + U_{5/3}),\ U + U_{2/3},\ i(U - U_{2/3}),\ \sqrt{2}\tilde{U}\right)^T, \tag{4.20}$$

$$\psi_D = \frac{1}{\sqrt{2}}\left(D_{-4/3} - U',\ -i(D_{-4/3} + U'),\ D_{-1/3} + D',\ i(D_{-1/3} - D'),\ \sqrt{2}\tilde{D}\right)^T,$$

where the subscripts indicate the electromagnetic charge of the corresponding fields, and U', D' and $\tilde{D}$ have $Q = 2/3$, $Q = -1/3$ and $Q = -1/3$ respectively. The lagrangian for the fermionic fields and the Higgs then reads:

$$\begin{aligned}\mathcal{L} = &\frac{i}{2}\left(\overline{Q_L^{2/3}}\not{D}Q_L^{2/3} + \overline{Q_L^{-1/3}}\not{D}Q_L^{-1/3}\right) + \sum_{\psi=U_R,D_R,\psi_U,\psi_D} i\overline{\psi}\not{D}\psi \\ &+ \frac{f^2}{4}\left(D_\mu\Sigma\right)^\dagger D^\mu\Sigma - \sum_{\psi=\psi_U,\psi_D}\left[Y_\psi f(\overline{\psi}\Sigma)(\Sigma^T\psi) + M_\psi\overline{\psi}\psi\right] \\ &- \left(\Delta_{L1}\overline{\psi_U}Q_L^{2/3} + \Delta_{L2}\overline{\psi_D}Q_L^{-1/3} + \Delta_{uR}\overline{U_R}\psi_U + \Delta_{dR}\overline{D_R}\psi_D + \text{h.c.}\right).\end{aligned} \tag{4.21}$$

The first line contains the kinetic terms of both the elementary and composite states. In the second line, we have the lagrangian of equation (4.11), the proto-yukawa interactions and the vector-like mass terms, parametrized by the constants $Y_{U(D)}$ and $M_{U(D)}$ respectively. The third line contains the mixing terms breaking the full global $SO(5)$ symmetry according to the partial compositeness setup.

We should diagonalize the mixing matrices to obtain the physical states. However, the fact that the SM LH doublet mixes with two different sectors through Δ_{L1} and Δ_{L2}, complicates the expressions for the corresponding rotations, which can be only obtained numerically or if some approximation is used. We will elaborate on this in Sections 4.5, 4.6 and 4.7.

4.4.3 The Coleman-Weinberg potential

The linear coupling of elementary fermions to the composites, parametrized by the terms $\Delta_{L1}, \Delta_{L2}, \Delta_{uR}$ and Δ_{dR} in equation 4.21, breaks explicitly the global symmetry of the strong sector. The loops of fermions hence generate an effective potential that, in particular, provides a mass to the scalar particles, so that they are no longer NGBs but pNGBs. In order to study this radiatively induced potential, let us consider the lagrangian in equation (4.21) in the unitary gauge. We only keep the u-like contribution, since this represents also the top quark which, as commented in Section 4.3, plays the main role because of its large interaction with the strong sector [7]. If we work in

[7]Note also that heavy partners do not break the global symmetry, so that they do not need to be introduced in the potential computations.

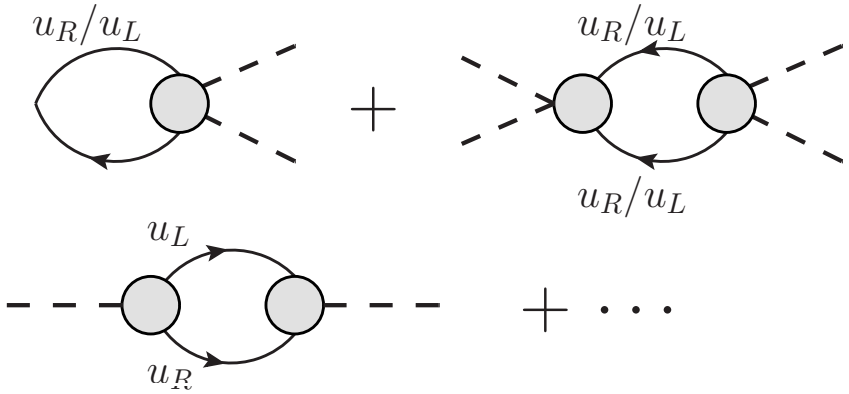

Figure 4.2: $u_{L/R}$ one-loop contribution to the effective Coleman-Weinberg potential for the Higgs boson. Diagrams in the top panel stand for the contribution with only u_R or only u_L. Diagrams in the bottom panel involve both u_L and u_R (note that in order to close the loop we need two vertex, and thus the square in the Higgs potential).

momentum space, the relevant lagrangian is then given by

$$\mathcal{L}_{eff} = \overline{u_L}\not{p}\left[\Pi_0^q(p^2) + \frac{1}{2}\sin^2\left(\frac{h}{f}\right)\Pi_1^q(p^2)\right]u_L + \overline{u_R}\not{p}\left[\Pi_0^u(p^2) + \frac{1}{2}\sin^2\left(\frac{h}{f}\right)\Pi_1^u(p^2)\right]u_R + \frac{1}{\sqrt{2}}M_1^u(p^2)\sin\left(\frac{h}{f}\right)\cos\left(\frac{h}{f}\right)\overline{u_L}u_R + \text{h.c.} \tag{4.22}$$

Π_i^j and M_1^u are form factors and are related to the free parameters in equation (4.21), and p stands for the transfered momentum. The loop contribution to the Higgs effective potential can be evaluated through the Coleman-Weinberg equation [149, 150]:

$$V(h) = -2N_c\int\frac{d^4p}{(2\pi)^2)}\log\left(\det\frac{\partial^2\mathcal{L}_{eff}}{\partial\overline{\psi}_i\psi_j}\right), \tag{4.23}$$

where N_c is the number of colors, and ψ_i can be either u_L or u_R. Up to Higgs-independent term we find

$$V(h) = -2N_c\int\frac{d^4p}{(2\pi)^2)}\left\{\log\left[1+\frac{1}{2}\sin^2\left(\frac{h}{f}\right)\frac{\Pi_1^q}{\Pi_0^q}\right] + \log\left[1+\frac{1}{2}\sin^2\left(\frac{h}{f}\right)\frac{\Pi_1^u}{\Pi_0^u}\right] + \log\left[1-\frac{1}{2}\sin^2\left(\frac{h}{f}\right)\cos^2\left(\frac{h}{f}\right)\frac{(M_1^u)^2}{p^2\left[\Pi_0^q+\Pi_1^q\sin\left(h/f\right)/2\right]\left[\Pi_0^q+\Pi_1^q\sin\left(h/f\right)/2\right]}\right]\right\}. \tag{4.24}$$

The first two contributions come from diagrams involving only u_L or u_R (top panel of Figure 4.4.3) [8], while the last contribution comes from diagrams involving both u_L and u_R. It is usually assumed that the integrals involved in the previous calculation converge, and that we can expand the logarithms so that

$$V(h) \simeq (\alpha - \beta)\sin^2\left(\frac{h}{f}\right) + \beta\sin^4\left(\frac{h}{f}\right), \tag{4.25}$$

with

$$\alpha = -N_c \int \frac{d^4p}{(2\pi)^4}\left(\frac{\Pi_1^q}{\Pi_0^q} + \frac{\Pi_1^u}{\Pi_0^u}\right), \quad \beta = N_c \int \frac{d^4p}{(2\pi)^4}\left[\frac{(M_1^u)^2}{p^2\Pi_0^q\Pi_0^u}\right]. \tag{4.26}$$

The actual values of these integral determine whether $V(h)$ can generate or not a reasonable VEV. The form factors can be explicitly calculated in theories with extra dimensions [68], or by means of Weinberg sum rules [146, 154, 155] in the large N_c limit [156, 157] (otherwise they are free parameters to be constrained by the experiments). It turns out that, when explicitly computed, they relate the Higgs mass to the mass of the composite resonances. These relations, together with the observation of a light Higgs and naturalness arguments, prefer lighter fermion resonances for the third generation [146, 155, 158, 159]. We will keep this in mind although we will not enter in more details in the following.

4.4.4 Vector resonances

In addition to heavy fermions, vector resonances can be also present in the spectrum of CHMs. In particular, the implementation of partial compositeness in the quark sector requires the fermionic composites to transform as triplets of the $SU(3)_c$ gauge group. Hence, the presence of spin-1 color octet resonances is mandatory in this framework, as they arise from the tensor product of spin-1/2 color triplets, given that $\mathbf{3} \times \mathbf{3} = 1 + \mathbf{8}$ for $SU(3)_c$. They can then mix with the SM elementary gluon in a similar way to that described in Section 4.3 (as the ρ-photon mixing in QCD). The lagrangian describing the dynamics of both the elementary (written with superscript e) and the composite (superscript c) gluons contains the elementary and composite kinetic terms:

[8] Contributions coming from gauge bosons, that tend to align the VEV and hence will not be discussed here (see Section 4.1), provide a term similar to this one.

$-1/2\,\mathrm{tr}\big(G^e_{\mu\nu}G^{e\,\mu\nu}\big)$ and $-1/2\,\mathrm{tr}\big(G^c_{\mu\nu}G^{c\,\mu\nu}\big)$ respectively, and a mixing term given by [9]

$$\mathcal{L}_{mix} = \frac{1}{2}\left(\frac{g_e M_{G^c}}{g_c}\right)^2 (G^e_\mu)^2 + \frac{1}{2}M^2_{G^c}(G^c_\mu)^2 + \frac{1}{2}\frac{g_e}{g_c}M^2_{G^c}G^c_\mu G^{e\,\mu}, \tag{4.27}$$

where g_e and g_c stand for the strong couplings in the elementary and composite sectors respectively. This lagrangian can be diagonalized by means of the following rotation: $G^e_\mu \to \cos\theta\, G^e_\mu + \sin\theta\, G^c_\mu$ and $G^c_\mu \to -\sin\theta\, G^e_\mu + \cos\theta\, G^c_\mu$, where $\tan\theta = g_e/g_c$. The physical massless gluon, that we will still call g remains massless, while the physical heavy gluon, G, has a non-vanishing mass. The SM strong gauge coupling is given by $g_s = g_e\cos\theta = g_c\sin\theta$.

The relevant part of the lagrangian that is used in the following adds the heavy gluon contribution to the lagrangian of equation 4.21, together with the potential obtained in the last section. If we consider up to renormalizable interactions (see references [161–163] for a discussion of the non-linear Higgs couplings effects), the full lagrangian can be written as

$$\begin{aligned}
\mathcal{L} = &-\frac{1}{2}\,\mathrm{tr}\big(G^e_{\mu\nu}G^{e\,\mu\nu}\big) + \frac{1}{2}\left(\frac{g_e M_{G^c}}{g_c}\right)^2 (G^e_\mu)^2 + \overline{q_L} i\not{D} q_L + \overline{u_R} i\not{D} u_R + \overline{d_R} i\not{D} d_R \\
&- \frac{1}{2}\mathrm{tr}\big(G^c_{\mu\nu}G^{c\,\mu\nu}\big) + \frac{1}{2}M^2_{G^c}(G^c_\mu)^2 + \frac{1}{2}\mathrm{tr}\big(D_\mu\mathcal{H}^\dagger D^\mu\mathcal{H}\big) - V(\mathcal{H}^\dagger\mathcal{H}) \\
&+ \mathrm{tr}\left[\overline{\mathcal{Q}}\left(i\not{D} - g_c\not{G}^c - M_{\mathcal{Q}}\right)\mathcal{Q}\right] + \overline{\tilde{U}}\left(i\not{D} - g_c\not{G}^c - M_{\mathcal{Q}}\right)\tilde{U} \\
&+ \mathrm{tr}\left[\overline{\mathcal{Q}'}\left(i\not{D} - g_c\not{G}^c - M_{\mathcal{Q}'}\right)\mathcal{Q}'\right] + \overline{\tilde{D}}\left(i\not{D} - g_c\not{G}^c - M_{\mathcal{Q}'}\right)\tilde{D} \\
&- \left[Y_U\mathrm{tr}\big(\overline{\mathcal{Q}}\mathcal{H}\big)\tilde{U} + Y_D\mathrm{tr}\big(\overline{\mathcal{Q}'}\mathcal{H}\big)\tilde{D} + \Delta_{L1}\overline{q_L}\,(U,D)^T + \Delta_{L2}\overline{q_L}\,(U',D')^T\right. \\
&\left.+ \Delta_{uR}\overline{u_R}\tilde{U} + \Delta_{dR}\overline{d_R}\tilde{D} + \mathrm{h.c.}\right],
\end{aligned} \tag{4.28}$$

where we have defined the scalar bidoublet $\mathcal{H}$, and the fermionic bidoublets $\mathcal{Q}$ and $\mathcal{Q}'$, in the following way:

$$\mathcal{H} = \begin{pmatrix} \phi_0^\dagger & \phi^+ \\ -\phi^- & \phi_0 \end{pmatrix}, \quad \mathcal{Q} = \begin{pmatrix} U & U_{5/3} \\ D & U_{2/3} \end{pmatrix}, \quad \mathcal{Q}' = \begin{pmatrix} D_{-1/3} & U' \\ D_{-4/3} & D' \end{pmatrix}. \tag{4.29}$$

[9] This mixing term can be seen to be equivalent to that obtained from the Hidden Local Symmetry method [160].

Resonance	T_L^3	T_R^3	X	$Y = T_R^3 + X$	$Q = Y + T_L^3$
U	1/2	-1/2	2/3	1/6	2/3
$U_{5/3}$	1/2	1/2	2/3	7/6	5/3
D	-1/2	-1/2	2/3	1/6	-1/3
$U_{2/3}$	-1/2	1/2	2/3	7/6	2/3
$D_{-1/3}$	1/2	-1/2	-1/3	-5/6	-1/3
U'	1/2	1/2	-1/3	1/6	2/3
$D_{-4/3}$	-1/2	-1/2	-1/3	-5/6	-4/3
D'	-1/2	1/2	-1/3	1/6	-1/3
$\tilde{U}$	0	0	2/3	2/3	2/3
$\tilde{D}$	0	0	-1/3	-1/3	-1/3

Table 4.1: T_L^3, T_R^3, X, hypercharge and electric charge quantum numbers of the different fermionic resonances involved in the lagrangian of equation 4.28.

We also define $M_{\mathcal{Q}} \equiv M_U$ and $M_{\mathcal{Q}'} \equiv M_D$. Thus, up to higher-order corrections, the physics of the composites appears to be equivalent to a theory of two singlet vector-like quarks, $\tilde{U}$ and $\tilde{D}$, two vector-like bidoublets, $\mathcal{Q}$ and $\mathcal{Q}'$, and a color octet vector field conveniently coupled to the SM elementary fields. Note again that none of these fields (excepting the fully composite Higgs) are mass eigenstates.

This model has been first proposed in [164], where the phenomenology of the heavy quarks and gluon and their interactions with the gauge bosons is studied in very detail. In Sections 4.5, 4.6 and 4.7 we adopt different limits of this lagrangian in order to study separate aspects of the resonances phenomenology, but with emphasis on Higgs-related channels.

4.5 Composite top

According to our framework, the top quark is highly motivated to have a large degree of compositeness, given that, under the assumption of an anarchic composite sector, heavier particles mix more strongly with the composite resonances. Thus, under the anarchic assumption, we mainly expect the phenomenology of top partners (heavy resonances with the quantum numbers of the top) to be relevant in a first run of experiments at the LHC. Top partners decay to a top (or bottom) quark plus a SM gauge or Higgs boson as depicted in the left panel of Figure 4.3, although they can be

Figure 4.3: Left: Decay of a heavy quark into a SM quark and the Higgs boson. Right: Decay of a heavy gluon into a SM quark and its heavy partner.

produced in several and very different ways. For instance, as heavy quark partners are charged under $SU(3)_c$, they can be pair produced through QCD interactions, so that this mechanism is essentially model independent [165, 166]. An alternative channel has been considered in [167, 168]. It consists of EW single production of new vector-like quarks with subsequent decay into the Higgs and a SM quark. This channel is more model dependent as the production cross section depends on unknown EW couplings of the heavy quark. In this section, instead, we consider the production of heavy quarks through the decay of the heavy gluon into a heavy-light topology, as represented in the right panel of Figure 4.3. This channel, as we discuss below, is dominant in a wide region of the parameter space if the heavy gluon mass is not large enough to open the final state made of two heavy partners.

In order to study the constraints on the model we are dealing with, as well as the collider implications it has, we first need to properly define the degrees of freedom and parameter space region that are actually relevant for our study. These are apparent once we go from the elementary/composite basis to the physical one. As we mentioned previously, we need either to proceed numerically or to adopt any well-motivated approximation, as the presence of Δ_{L1} and Δ_{L2} makes this diagonalization non-trivial. In this case, we decide to take the limit $\Delta_{L2} \ll M$, with M any of the dimensionful parameters in the lagrangian of equation 4.28. This limit is well motivated by the fact that corrections to the $Z\overline{b_L}b_L$ coupling scale like Δ_{L2}^2 and experimental bounds on this coupling therefore imply that $\Delta_{L2} \ll M$ [164] [10]. Furthermore, the bottom quark mass is also propor-

[10] Actually, in the limit $\Delta_{L2} = 0$ we are effectively decoupling the heavy resonances in the $\mathbf{5}_{-1/3}$ representation from the LH quark sector, so that it only couples to the representation $\mathbf{5}_{2/3}$. This representation, however, has the desirable feature that the the $Z\overline{b_L}b_L$ vertex does not receive tree-level corrections, provided that a discrete symmetry P_{LR} exchanging the $SU(2)_L$ and $SU(2)_R$ factors is

tional to Δ_{L2} and we can relate the absence of large corrections to the $Z\overline{b_L}b_L$ vertex with the fact that $m_b \ll m_t$. Finally, the choice $\Delta_{L2} \ll \Delta_{L1}$ is radiatively stable [144]. This assumption has two other implications for our approach: (i) the bottom sector, characterized by the quark bidoublet $\mathcal{Q}'$ decouples from our study [11]; and (ii) analytical expressions for the rotation matrices can be obtained. Thus, under this approximation, and before EWSB, the model is described in terms of two vector-like quark doublets, that we call $Q_{1/6} = (T, B)^T$ and $Q_{7/6} = (T_{5/3}, T_{2/3})^T$, with hypercharges 1/6 and 7/6 respectively, one singlet, $\tilde{T}$, with $Y = 2/3$ and a heavy gluon G. The degree of compositeness of the quarks $q_L = (t_L, b_L)^T$, t_R, b_R and the SM gluon is then given in terms of the free parameters of equation 4.28 ($g_e, g_c, M_{G^c}, M_{\mathcal{Q}}, M_{\mathcal{Q}'}, Y_T, Y_B, \Delta_{L1}, \Delta_{L2}, \Delta_{tR}, \Delta_{bR}$), respectively, by the expressions

$$\tan\phi_{qL} = \frac{\Delta_{L1}}{M_{\mathcal{Q}}} \quad \tan\phi_{tR} = \frac{\Delta_{tR}}{M_{\mathcal{Q}}}, \quad \tan\phi_{bR} = \frac{\Delta_{bR}}{M_{\mathcal{Q}'}}, \quad \tan\theta_s = \frac{g_e}{g_c}. \tag{4.30}$$

The masses of the physical states then read:

$$\begin{aligned} M_{Q_{1/6}} =& \frac{M_{\mathcal{Q}}}{\cos\phi_{qL}}, \quad M_{Q_{7/6}} = M_{\mathcal{Q}}, \quad M_{\tilde{T}} = \frac{M_{\mathcal{Q}}}{\cos\phi_{tR}}, \quad M_G = \frac{M_{G^c}}{\cos\theta_s} \\ m_t \simeq& \frac{v}{\sqrt{2}} Y_T \sin\phi_{qL} \sin(\phi_{tR}), \quad m_b \simeq \frac{v}{\sqrt{2}} Y_B \sin\phi_2 \sin\phi_{bR}, \end{aligned} \tag{4.31}$$

where $\sin\phi_2 = \Delta_{L2}\cos\phi_{qL}/M_{\mathcal{Q}'}$. If we take $Y_* \equiv Y_U = Y_D$ and $M_G = 2M_{\tilde{T}}$ we have to deal only we the following set of free parameters: $g_{*3} \equiv g_c$, M_G, $s_{tR} \equiv \sin\phi_{tR}$ and $s_2 \equiv \sin\phi_2$. The requirement $M_G = 2M_{\tilde{T}}$ is enforced to restrict ourselves to the region of parameter space in which the decay of G into two massive fermionic resonances is kinematically suppressed, given that when this decay mode opens up, the width of G is of the order of the mass itself and talking about resonances stops making sense. Indeed, the coupling of the massive gluon G to the SM fermions $\psi = q_L, t_R$ or b_R is given by

$$g_{G\psi\psi} = g_s \left(\sin^2\phi_\psi \cot\theta_s - \cos^2\phi_\psi \tan\theta_s\right), \tag{4.32}$$

enforced [144].

[11] The EW singlet $\tilde{B}$, with charge $Q = -1/3$, can be also disregarded in the processes that we study in this section, given that, although it can be produced in association with b_R, this process is not relevant in the region of the parameter space we are interested in.

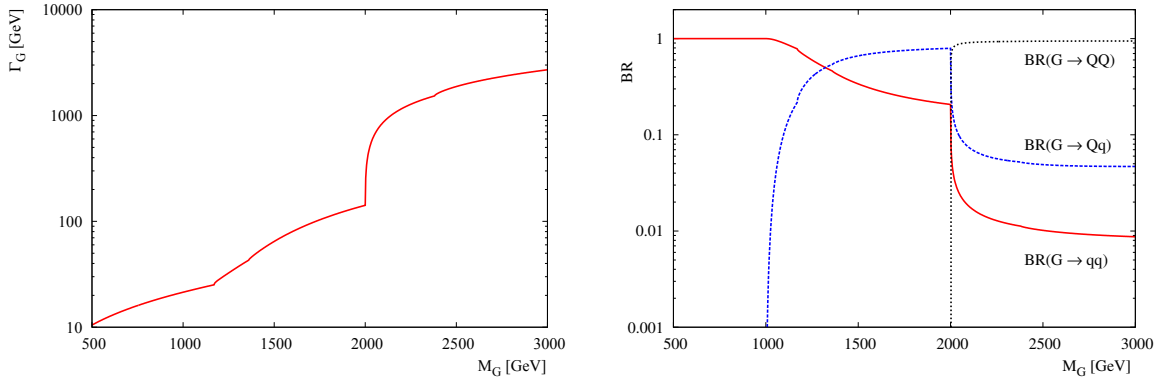

Figure 4.4: Left: Massive gluon width as a function of its mass for $M_{\tilde{T}} = 1$ TeV, $s_{tR} = 0.6$, $s_2 = 0.1$ and $g_{*3} = Y_* = 3$. Right: Massive gluon BR in two SM quarks (labeled qq), one SM and one heavy quark (Qq) and two heavy quarks (QQ), respectively.

while the coupling of G to one SM fermion and one composite resonance, and the couping to two fermionic resonances are given respectively by

$$g_{G\psi\Psi} = g_s \frac{\sin\phi_\psi \cos\phi_\psi}{\sin\theta_s \cos\theta_s}, \quad g_{G\Psi\Psi} = g_s(\cos^2\phi_\Psi \cot\theta_s - \sin^2\phi_\Psi \tan\theta_s), \tag{4.33}$$

where the relevant combinations of $\psi\Psi$ are $t_L T_L$, $b_L B_L$ and $t_R \tilde{T}_R$, and where $\phi_\Psi = \phi_{qL}, \phi_{qL}, \phi_{tR}$ for T, B and $\tilde{T}$ respectively [12]. Thus, for a strongly coupled sector ($g_{*3} \gg 1$), $\cot\theta_s \gg 1$ and the heavy resonances are strongly coupled to the heavy gluon (except for maximally composite SM fermions). For instance, for the choice $M_{\tilde{T}} = 1$ TeV, $s_{tR} = 0.6$, $s_2 = 0.1$ and $g_{*3} = Y_* = 3$, we obtain the G decay widths and BRs of Figure 4.4.

In the following, we fix $Y_* = 3$ and $s_2 = 0.1$, and vary the parameters g_{*3}, M_G and s_{tR}, although we also give results for a benchmark model defined by $g_{*3} = 3$ and $s_{tR} = 0.6$. The model constraints in terms of these parameters are given in Section 4.5.1, while the LHC implications for the current and futures runs are discussed in Section 4.5.2.

[12] Other quarks present in the spectrum couple in pairs to G with a similar structure but different values of the couplings. These couplings are nevertheless irrelevant for the process we are interested in. See [144] for details.

4.5.1 Constraints

The constraints to the model we are dealing with come mainly from three different kind of searches. (*i*) *Dijet searches.* Indeed, the heavy gluon G couples to pairs of jets (this is in fact the main production mechanism we consider in pp collisions) [13]. In this case, dijet production can impose stringent constraints in the model. A very detailed study of the implication of dijet searches on contact interactions is reported in [169]. Their analysis considers the experimental results reported in [170], that correspond to an integrated luminosity of 2.2 fb^{-1}. Denoting the coupling of the first generation SM quarks to the massive gluon by

$$G_\mu^A \Big[g_{q_L} \bar{q}_L \gamma^\mu T^A q_L + g_{u_R} \bar{u}_R \gamma^\mu T^A u_R + g_{d_R} \bar{d}_R \gamma^\mu T^A d_R], \tag{4.34}$$

we get the following effective Lagrangian after integration of the massive gluon, in the basis of [169]:

$$\mathcal{L} = \frac{c_{uu}^{(1)}}{M^2}\mathcal{O}_{uu}^{(1)} + \frac{c_{dd}^{(1)}}{M^2}\mathcal{O}_{dd}^{(1)} + \frac{c_{ud}^{(8)}}{M^2}\mathcal{O}_{ud}^{(8)} + \frac{c_{qq}^{(8)}}{M^2}\mathcal{O}_{qq}^{(8)} + \frac{c_{qu}^{(8)}}{M^2}\mathcal{O}_{qu}^{(8)} + \frac{c_{qd}^{(8)}}{M^2}\mathcal{O}_{qd}^{(8)}, \tag{4.35}$$

where the different coefficients read

$$c_{uu}^{(1)} = -\frac{g_{u_R}^2}{6}, \quad c_{dd}^{(1)} = -\frac{g_{d_R}^2}{6}, \quad c_{ud}^{(8)} = -g_{u_R} g_{d_R}, \tag{4.36}$$

$$c_{qq}^{(8)} = -\frac{g_{q_L}^2}{2}, \quad c_{qu}^{(8)} = -g_{q_L} g_{u_R}, \quad c_{qd}^{(8)} = -g_{q_L} g_{d_R}. \tag{4.37}$$

The results of [169] can be directly applied to these coefficients to obtain the corresponding bound on M_G. Besides, direct dijet resonance searches can also constrain our model. We have simulated dijet signals in our model and compared the results after cuts with the bounds on simplified gaussian resonances reported in [171]. The corresponding limits are included in our final results in Section 4.5.2.

(*ii*) $t\bar{t}$ *searches.* In models of strong EWSB with a composite top, new vector resonances and in particular heavy gluons decay most of the time in $t\bar{t}$ pairs, which has

[13] Note that, although we are considering that light quarks have a negligible degree of compositeness, they couple to G^e, which is partially composite and then the coupling is propagated to G. This can be also seen from equation 4.32 if we set $\phi_\psi = 0$.

been traditionally considered the golden discovery mode of such new particles. If the top is not fully composite (as in the case we are considering), if other quarks can be as composite as the top (as we will see in Sections 4.6 and 4.7), or if new decay channels involving fermion composite states are open, the BR into $t\bar{t}$ can substantially change. At any rate, this production mechanism is always present and current limits [172–174] set non-negligible bounds. We include the constraints resulting from these searches in our general analysis in Section 4.5.2.

(*iii*) *Higgs searches.* In one hand, we should consider the implications that current Higgs measurements have on CHMs. These have been studied in detail in [151, 152] and in more general extensions in [175–178]. The result is that, for $m_h = 125$ GeV, the region $0 \leq \xi \lesssim 0.4$ is allowed. As a consequence, we use $\xi = 0.2$ as a benchmark value in this section. Effects of variations in this parameter can be easily obtained rescaling the number of signal events by the ratio of Higgs BR in the corresponding channel for the different values of ξ, what is displayed in the right panel of Figure 4.1. On the other hand, let us point out that searches of $ht\bar{t}$, which is the final state we consider in the next section (resulting from the production of $pp \to G \to \bar{T}t(T\bar{t})$ and the subsequent decay of $T(\bar{t}) \to t(\bar{t})h$), do not exclude significant regions of the parameter space of the model, quite the contrary. Indeed, the last searches on $ht\bar{t}$ performed by both ATLAS and CMS [179, 180] suggest a (still not significant enough) small excess of events over the SM background. In fact, our studied production mechanism has been proposed as a possible explanation of this phenomena, and has been considered by CMS as a guideline for future analyses [181].

4.5.2 Collider signatures

The new Higgs production mechanism we want to study consists of single production of new vector-like quarks (together with a SM quark) mediated by the exchange of a heavy color octet vector boson. The vector-like quark then decays into the composite Higgs and a SM quark. Sample diagrams of this production mechanism are shown in Figure 4.5. The t-channel diagram on the right panel of the figure is actually not relevant in this scenario, for first generation SM quarks are assumed to be completely elementary. The final state is then $ht\bar{t}$. The corresponding cross sections depend on the coupling of G to the SM quarks, to qQ and also on the BRs of the heavy quarks into a SM quark and the Higgs. The relevant such BRs are, in the limit of large masses [164],

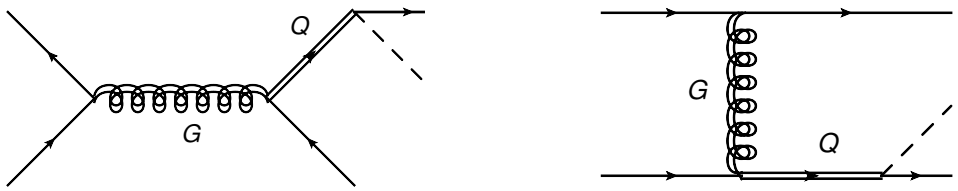

Figure 4.5: Sample diagrams for the new Higgs production mechanism. The t-channel exchange on the right is only relevant for composite u or d quarks.

BR($T \to th$) ≈ 0.5, BR($\tilde{T} \to th$) ≈ 0.25, while other channels do not result in a Higgs boson in the final state. We show in Figure 4.6 the production cross section times BR for the $ht\bar{t}$ channel in the benchmark model. In the following we propose a dedicated analyses for this channel. We consider three different configurations for the LHC parameters, namely 5 fb^{-1} integrated luminosity at $\sqrt{s} = 7$ TeV (LHC7), 20 fb^{-1} integrated luminosity at $\sqrt{s} = 8$ TeV (LHC8) and 100 fb^{-1} integrated luminosity at $\sqrt{s} = 14$ TeV (LHC14). The range of masses probed with the first two configurations (that we call the *low-energy phase*) is quite different from the one probed by the *high-energy phase* (the third option). Thus, the analyses are also different depending on the phase. In particular, as we describe below, the analysis in the high-energy phase benefits from using boosted techniques. In these analyses the anti-k_t algorithm with $R = 0.7$ is used for jets, and $p_T(j) > 30$ GeV is required. Isolated charged leptons (e or μ) are considered when $p_T(\ell) > 20$ GeV. We use as discriminating variable as the scalar sum

$$S_T \equiv \sum_{j=1}^{n_j} p_T(j) + \sum_{\ell=1}^{n_\ell} p_T(\ell) + E_T^{miss}, \tag{4.38}$$

where $n_{j,\ell}$ is the relevant number of jets or leptons (ordered according to their p_T), which depends on the analysis and is specified later on. We list in Table 4.2 the leading-order (LO) cross sections for the main backgrounds and two sample points in parameter space for our benchmark model. For the low energy phase ($\sqrt{s} = 7$ or 8 TeV), the mass range that can be probed at the LHC is relatively low. This means that the decay products are not extremely boosted. Thus, traditional analyses are more efficient probing this region of parameter space than analyses that use boosted techniques. Also, since we

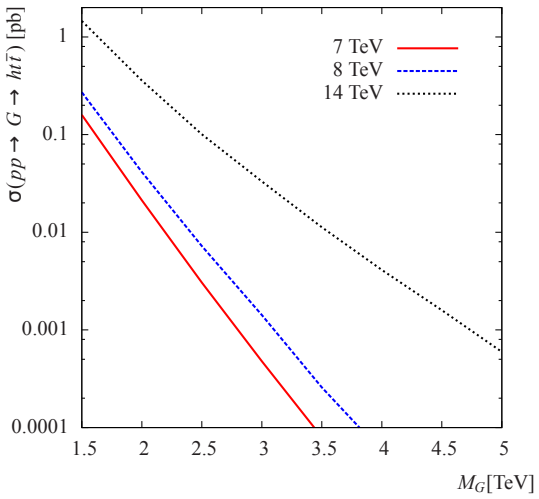

Figure 4.6: $ht\bar{t}$ production cross section in the benchmark CHM mediated by a color octet vector resonance with decay into a fermionic resonance and a top quark.

have the leptonic top decays to trigger on, we can afford to use the main Higgs decay channel, namely $b\bar{b}$, with $\mathrm{BR}(h \to b\bar{b}) = 0.48$. We are therefore interested in the process $pp \to G \to T\bar{t} + \bar{T}t \to ht\bar{t} \to 4b + 2j + \ell + E_T^{miss}$. The main backgrounds are $t\bar{t}$ and $t\bar{t}b\bar{b}$. In order to reduce the number of background events to manageable values we impose the following initial cuts. (i) at least four jets j, of which at least three must be tagged as b-jets; (ii) at least one isolated charged lepton ℓ; (iii) a cut on S_T (in this case we have $n_j = 4$ and $n_\ell = 1$) that depends on the test M_G we are considering: $S_T > 0.9,\ 1.1,\ 1.5$ TeV for $M_G = 1.5,\ 2,\ 2.5$ TeV.

We show in the left panel of Table 4.3, the efficiencies of the different cuts for the main backgrounds and our signal for our benchmark model with $M_G = 2$ TeV. The global efficiencies for the signal and relevant backgrounds are reported, as a function of M_G, in the right panel of the table.

In the high-energy phase, $\sqrt{s} = 14$ TeV, larger masses can be probed. In this case the decay products of the heavy gluon and quarks are highly boosted and one can benefit from the use of boosted techniques. In this study we use a very simple technique, based on fat jet invariant masses. Clearly there is room for improvement if more sophisticated tools are used. Hence, we propose the following set of cuts for this phase: (i) at least three jets j, with a minimum of two b tags; (ii) at least one isolated charged lepton ℓ; (iii) all jets are then ordered according to their invariant

Process	LHC7 σ [pb]	LHC8 σ [pb]	LHC14 σ [pb]
$M_G = 2$ TeV	0.029	0.058	0.39
$M_G = 3$ TeV	0.00061	0.0018	0.046
$t\bar{t} + 0 - 4j$ (semileptonic+leptonic)	48	70	297
$t\bar{t}b\bar{b}$	0.09	0.15	0.85
$Z_{ll}/\gamma_{ll} + 1 - 4j$	531	641	1423
$W_{l\nu}W + 0 - 2j$	15	23	49
$W_{l\nu} + 1 - 2j$ ($p_T > 150$ GeV)	–	–	85
$W_{l\nu} + 1 - 4j$	5133	6489	–

Table 4.2: LO cross sections for the signal and main backgrounds for different values of the LHC energy. $l = e, \mu, \tau$ have been considered in both semileptonic and leptonic decays. The corresponding BR are included in the calculation of the cross section (when the decays -leptonic or semileptonic- are explicitly stated).

cut	$\epsilon_{M_G=2\text{ TeV}}$	$\epsilon_{t\bar{t}}$	$\epsilon_{t\bar{t}b\bar{b}}$
$n_j \geq 4$	77.31	52.16	91.85
$n_\ell \geq 1$	66.86	63.02	42.84
$n_b \geq 3$	35.31	2.64	33.08
S_T	75.01	0.12	1.20
Total	13.69	0.00108	0.156

M_G [TeV]	ϵ_s	$\epsilon_{t\bar{t}}$	$\epsilon_{t\bar{t}b\bar{b}}$
1.5	15.8	0.00652	0.514
2.0	13.69	0.00108	0.156
2.5	9.67	0.000292	0.0174
3.0	9.14	0.000292	0.0174

Table 4.3: Left panel: Cut by cut efficiencies for the signal and main backgrounds for the $ht\bar{t}$ analysis in the low-energy phase for a sample point (benchmark model with $M_G = 2$ TeV). Right panel: Global efficiencies for the signal and relevant backgrounds as a function of M_G. All efficiencies are reported as percent.

mass and the first two jets are required to have invariant masses close to the top and Higgs mass, respectively, $|m_{j_1} - m_t| \leq 40$ GeV and $|m_{j_2} - m_h| \leq 40$ GeV (here $j_{1,2}$ are the jets with the largest and second largest invariant masses); (*iv*) a cut on S_T (in this case we have $n_j = 3$ and $n_\ell = 1$) that depends on the test M_G we are considering: $S_T > 1.2,\ 1.5,\ 1.7,\ 2$ TeV for $M_G = 2,\ 2.5,\ 3, \geq 3.5$ TeV. The results of these cuts on the main backgrounds and the signal are reported in Table 4.4. In the left panel we

cut	$\epsilon_{M_G=3\ \text{TeV}}$	$\epsilon_{t\bar{t}}$	$\epsilon_{t\bar{t}b\bar{b}}$
$n_j \geq 3$	98.03	85.46	98.88
$n_\ell \geq 1$	75.24	61.08	45.16
$n_b \geq 2$	64.38	29.49	68.50
$m_{j_1} \sim m_t$	58.08	0.22	1.70
$m_{j_2} \sim m_h$	72.70	15.36	31.72
S_T	90.07	10.24	18.10
Total	18.06	0.00054	0.0298

M_G [TeV]	ϵ_s	$\epsilon_{t\bar{t}}$	$\epsilon_{t\bar{t}b\bar{b}}$
2.0	11.74	0.00265	0.1021
2.5	15.61	0.00095	0.0518
3.0	18.06	0.00054	0.0298
3.5	17.74	0.00027	0.0188
4	19.08	0.00027	0.0188
4.5	19.40	0.00027	0.0188

Table 4.4: Left panel: Cut by cut efficiencies for the signal and main backgrounds for the $ht\bar{t}$ analysis in the high-energy phase for a sample point (benchmark model with $M_G = 3$ TeV). Right panel: Global efficiencies for the signal and relevant backgrounds as a function of M_G. All efficiencies are reported as percent.

report cut by cut efficiencies for a sample signal point (benchmark model with $M_G = 3$ TeV) whereas in the right panel we report the global efficiencies as a function of M_G.

With all this information, we now proceed to report our results as a function of the most relevant input parameters. We found that the discovery limits or exclusion bounds are not very sensitive to the composite Yukawa couplings Y_*, but the main sensitivity is to the composite coupling of the heavy gluons, g_{*3}, and the degree of compositeness of the t_R, parametrized by s_{tR}. In all cases we show our results in the form of contour plots of the required luminosity for a $5\,\sigma$ discovery, defined as $\mathcal{S}(s,b) = 5$, and we also show contours of the luminosity required for the expected 95% exclusion bound (see Section 3.4 for the pertinent definitions). Our main results are shown in Figure 4.7 [14].

Several comments are worth to emphasize: (i) using the 2011 run, masses up to $M_G \approx 1.9 - 1.6$ TeV can be discovered in the region allowed by current constraints for $g_{*3} \gtrsim 4-5$. Exclusion bounds in the $M_G \sim 2.2-1.9$ TeV can be reached for $g_{*3} \sim 3-5$. These results assume $s_{tR} \sim 0.5 - 0.7$, outside this range the reach decreases as shown in the left column of Figure 4.7. The plot corresponding to this energy is not shown as

[14]Note that, because we are imposing the SM light quarks to be fully elementary, the bounds from dijet contact interactions depend only on g_{*3}. In particular, for the benchmark value $g_{*3} = 3$ they imply a constant bound $M_G \geq 2.5$ TeV. This bound decreases as g_{*3} increases. For instance it becomes $M_G \geq 1.5$ TeV for $g_{*3} \approx 4.6$.

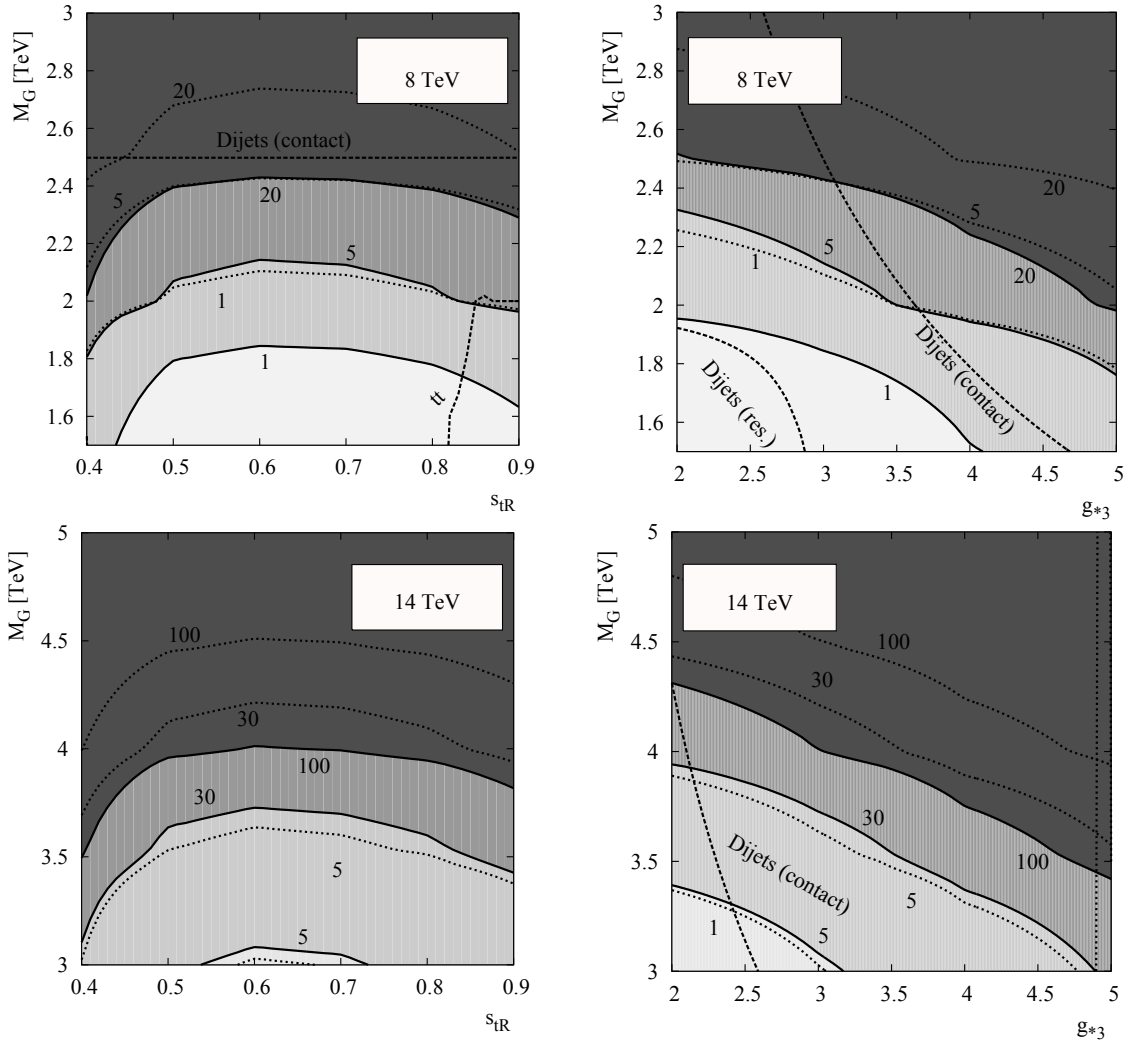

Figure 4.7: Contours of required luminosity for a 5σ discovery (bands and solid lines) and 95% exclusion limits (dotted lines) as a function of s_{tR} and M_G (left column) and g_{*3} and M_G (right column) for $\sqrt{s} = 8$ and 14 TeV (first and second row, respectively) in the $ht\bar{t}$ channel. Current bounds are shown with dashed lines (the area below the dashed lines is excluded).

it is quite similar to the one at $\sqrt{s} = 8$ TeV, only with the numbers reduced to match the results we have described. (*ii*) the 2012 run with 20 fb^{-1} at $\sqrt{s} = 8$ TeV can lead to a discovery in the region $M_G \sim 2.5 - 2$ TeV (and a similar exclusion with just 5 fb^{-1}) for $g_{*3} \sim 3 - 5$. Exclusion bounds in the $M_G \sim 2.8 - 2.4$ TeV region can be set, for $g_{*3} \sim 2.5 - 5$, with the same luminosity. (*iii*) data with $\sqrt{s} = 14$ TeV can probe a

much larger region of parameter space. Values up to $M_G \sim 4.3$ TeV can be discovered with 100 fb^{-1} and bounds up to 4.8 TeV can be set with the same luminosity.

If we consider composite bottoms or light quarks, the phenomenology can be drastically different. We explore these scenarios in the next sections.

4.6 Composite bottom

In this section we reveal the implications that the fact of a composite bottom quark has at the LHC. In this case, we do not make use of the explicit approximate expressions obtained in the limit $\Delta_{L2} \ll \Delta_{L1}$, but we use the top and bottom quark masses to (numerically) fix the values of Δ_{L1} and Δ_{L2} in terms of the remaining parameters of the model. We have checked that, in all the cases we consider, the hierarchy $\Delta_{L2}/\Delta_{L1} \ll 1$ is preserved. Now, we have to add $s_{bR} \equiv \sin\phi_{bR}$ to the list of free parameters. Concerning the fermionic spectrum, it has to be pointed out that $\tilde{B}$ as well as $\mathcal{Q}'$ do play an important role in this case. We also decide to set $M_{\mathcal{Q}} = M_{\mathcal{Q}'} \equiv M_F$ [15]. $Y_* = 3$ is still assumed. Thus, for each value of $s_{tR} \equiv \sin\phi_{tR}$, s_{bR} and M_F the fermion spectrum is then completely fixed.

Under these assumptions, the lightest new fermion is almost always a charge -1/3 quark that decays, with 100% BR, into hb. Let us call this fermion B_h. B_h turns out to be a combination of $\tilde{B}$ and $B^+ \equiv (B' + B_{-1/3})/\sqrt{2}$. B^+ is thus a symmetric combination of quarks with third component of isospin $T^3_L = \pm 1/2$, so that in absence of any further mixing, it has the decay pattern $\mathrm{BR}(B^+ \to hb) = 1$. Hence, B_h inherits its large decay to hb from B^+. In the left panel of Figure 4.8 we show the mass of the lightest charge 2/3 (solid horizontal lines) and charge -1/3 (dashed line) new quarks as a function of s_{bR} and for two different values of s_{tR}, corresponding to a midly ($s_{tR} = 0.6$) and very strongly ($s_{tR} = 0.95$) composite t_R, respectively. We assume $M_F = 1.5$ TeV (which corresponds to the mass of the charge 5/3 and charge -4/3 new quarks). The dots in the figure represent the mass of the charge -1/3 new quark that decays predominantly (with 100% BR for the parameters of the plot) into hb. This always agrees with the lightest one (still, if $M_{\mathcal{Q}'} < M_{\mathcal{Q}}$ as suggested by naturalness arguments [146, 155, 158, 159],

[15] Note the difference with respect to the mass conditions in the last section. There we were fixing the masses of the different quarks after mixing with the elementary fermions. Now we are fixing the masses before mixing (and of course before EWSB).

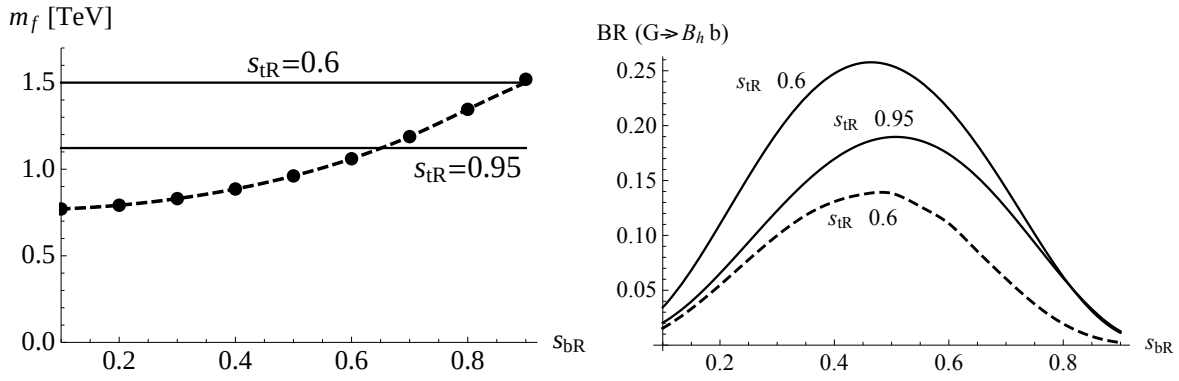

Figure 4.8: Left: Mass of the lightest charge 2/3 (solid) and $-1/3$ (dashed) quark as a function of s_{bR} and for different values of s_{tR}. The dots correspond to the mass of B_h (see text). Right: BR of the heavy gluon into $B_h\bar{b} + \bar{B}_h b$ as a function of s_{bR} and for different values of s_{tR}. We have fixed $M_G = 2.5$ TeV, $g_c = 3$ and the mass of the fermion resonances are fixed so that the lightest new fermion has a mass $M_G/2$.

there is a relatively light charge -1/3 quark with a 100% BR into hb [7]).

Let us now turn our attention to the only two remaining parameters in the model, namely M_G and g_c. Again, in order to avoid too large a width for the heavy gluon we choose its mass so that pair production of top and bottom partners is kinematically forbidden. Thus, we fix the mass of the heavy gluon to have twice the mass of the lightest new heavy fermion after EWSB [16]. Once M_G is fixed, all the phenomenological implications of the model can be worked out. We show in the right panel of Figure 4.8 the BR of the heavy gluon into $B_h\bar{b}+\overline{B_h}b$ as a function of s_{bR} for different values of s_{tR}. We fix $M_G = 2.5$ TeV and $g_c = 3$ in this figure. The bell-like shape of the figure arises from the fact that the coupling between the heavy gluon and $b_R B_h$ is proportional to $s_{bR}c_{bR}$, (analogously to equation 4.33) where $c_{bR} \equiv \cos\phi_{bR}$.

Hence we see that the heavy gluon has a sizably BR into $B_h\bar{b}+\overline{B_h}b$ for a wide range of values of s_{bR}. Thus, similarly to the case of composite top quark, single production of B_h via the s-channel exchange of G results in an $hb\bar{b}$ final state with a significant production cross section. We show in Figure 4.9 the $hb\bar{b}$ production cross section as a function of the heavy gluon mass. This production cross section is sizable but not large

[16] In practice what we do is to choose a value for M_G and fix the value of M_F that makes the mass of the lightest new fermion $M_G/2$.

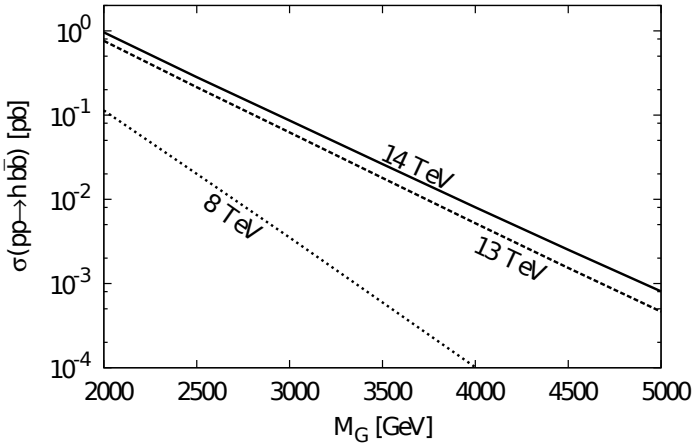

Figure 4.9: $hb\bar{b}$ production cross section with $g_c = 3$, as a function of M_G. M_F has been chosen such that the lightest fermionic resonance has a mass $M_G/2$.

enough to allow us to use the cleaner $h \to \gamma\gamma,\ ZZ^*$ decay channels. Among the two leading decay channels, the $h \to b\bar{b}$ is the most promising one. The main reasons are the large number of b quarks in the final state, which is a very powerful discriminator against the background, together with very special kinematics inherited from the large masses of G and B_h. As we now show, the latter ensures a clean trigger and a very simple reconstruction algorithm.

The process we are interested in is therefore

$$pp \to G \to B_h\bar{b} + \bar{B}_h b \to hb\bar{b} \to 4b. \tag{4.39}$$

Due to the large masses we can probe at the LHC, all four b quarks in the final state are very hard. We show in Figure 4.10 (left) the p_T distribution of the four b quarks at the partonic level, for a heavy gluon mass $M_G = 2.5$ TeV, together with the p_T distribution of the hardest b quark for the irreducible QCD background (distributions are normalized to unit area). All four b-jets are quite hard with the p_T of the two leading jets well above 300 and 200 GeV, respectively. This allows for a very clean trigger of the signal events and also for the possibility of hard cuts on the p_T of the leading b-jets, an important ingredient to bring the irreducible background down to manageable levels. Again, one important feature is that, due to the relatively large mass of B_h, the Higgs

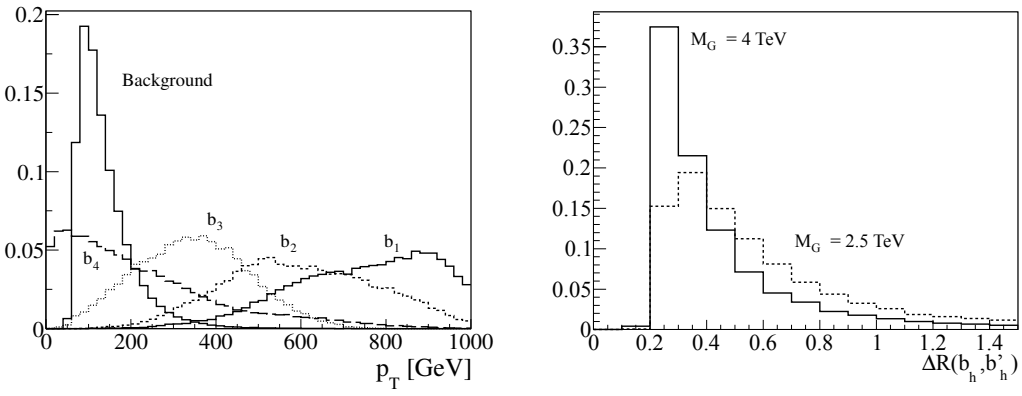

Figure 4.10: Left: Parton level p_T distribution of the four b quarks in the signal (denoted in decreasing order of p_T by $b_{1,2,3,4}$) and of the hardest b quark in the irreducible background. Right: ΔR separation between the two b-quarks from the Higgs decay at the partonic level for two different values of the heavy gluon mass. All distributions are normalized to unit area.

boson tends to be quite boosted and its decay products relatively aligned. We show in Figure 4.10 (right) the ΔR separation between the two b-quarks that reconstruct the Higgs, at the partonic level, for two different values of M_G (recall that we have $M_{B_h} = M_G/2$). We find that less than 35% of the events have $\Delta R < 0.4$ for $M_G = 2.5$ TeV. This number goes up to 60% for $M_G = 4$ TeV. Thus, it is clear that, once more, for larger heavy gluon masses the use of boosted techniques is likely to enhance the sensitivity. However, we decide to restrict ourselves to traditional techniques because the use of one less b-tag forces us to consider new background processes that are difficult to estimate with other means than data-driven methods.

In the analysis we propose, jets and charged leptons ℓ are defined to have $p_T > 20$ GeV. We consider two different configurations for the LHC parameters: $\sqrt{s} = 8$ TeV with $\mathcal{L}_{int} = 20$ fb^{-1} (LHC8) and $\sqrt{s} = 14$ TeV with $\mathcal{L}_{int} = 100$ fb^{-1} (LHC14). Before discussing the phenomenological implications of the proposed analyses, let us consider the bounds that current LHC searches can impose on our signal.

4.6.1 Constraints

As we have discussed in the previous scenario, dijet searches impose severe constraints on our model, and these are again included in the final results in Section 4.6.2. In

addition, other current searches, not specifically aimed at this model, can be somewhat sensitive to the signal we are considering. Among them, the most important ones are searches with many b-quarks in the final state, typically motivated by SUSY models [182–185]. In particular, searches for $hb\bar{b}$ production in SUSY models and searches for multi-b final states in association with E_T^{miss} are the most sensitive ones. Let us discuss them in turn.

Searches for $hb\bar{b}$ (or hb) in SUSY look for events with three or more relatively hard b-jets in the final state and try to reconstruct the Higgs from the two leading b-jets. The expected p_T distribution of the signal in SUSY models is much softer than in our model (see Figure 4.10 left) and therefore the focus is in a highly background populated region in which our signal gets easily diluted. This fact, combined with the small luminosity collected up to the date, make these searches not very sensitive to our model, although a very simple extension of the analysis with harder cuts on the p_T of the b-tagged jets would make them a very sensitive probe of CHMs.

Searches for multi-b final states in association with E_T^{miss}, on the other hand, look for signatures with many b-jets in the final state, with a large value of H_T (scalar sum of all the b-jets p_T) and a sizable amount of E_T^{miss}. Due to the large energy of the final state particles in our model, the fake E_T^{miss} is non-negligible and these searches are sensitive to our model. It is interesting to note that analyses in which sophisticated observables are used to avoid contamination from fake E_T^{miss} (like α_T in [186]) kill our signal together with the multi-jet background. However, other analyses in which the rejection of fake E_T^{miss} is less sophisticated impose some constraints on the parameter space of the model in our current scenario. We have used reference [187] that analyzes the full 8 TeV LHC data and show in next section that, although this search imposes some constraints on the model, our modified analysis in which the E_T^{miss} requirement is replaced for a more stringent requirement in terms of the p_T of the different b-jets, leads to a much better reach. This is an example of a very simple modification of current analyses that could maximize the number of models the searches are sensitive to.

4.6.2 Collider signatures

In order to design the analyses, we have to figure out which backgrounds can overwhelm the signal we are dealing with. The main one comes from the irreducible QCD production of four b-jets, given that other purely hadronic backgrounds are suppressed by

the small b-tagging fake-rate (see Section 3.3) and hence can be neglected. The same happens to other SM processes in which at least one isolated lepton is produced (we do impose a lepton veto to reduce these to negligible levels). Thus, the only background we have to consider is the irreducible one. Still, the cross section of this QCD background is so large that we are forced to generate events in the phase space region defined by $p_T^b > 50$ GeV and $\Delta R(b,b) > 0.3$, since otherwise we are not able to generate a large enough sample. The cross section in this region of the parameter space is ~ 12 pb. In order to ensure enough statistics we generate a number of events corresponding to a luminosity of ~ 1 ab^{-1}. In light of the results of next-to-leading order (NLO) studies [188, 189] we assume that the shape of the p_T distributions is well described by our LO calculations but the total cross section must be corrected with a K-factor that we conservatively set to 1.5.

In order to bring the irreducible background down to manageable levels, we impose the following set of cuts [17]: (i) at least four b-tagged jets are required; (ii) zero isolated light leptons ℓ; (iii) the p_T of each of the b-tagged jets has to be larger than 50 (60) GeV; (iv) the p_T of the hardest jet is required to be larger than 200 (300) GeV; (v) the p_T of the second hardest jet has to be higher than 100 (200) GeV; (vi) $|m_{b_h b'_h} - m_h| \leq 30$ GeV, where we denote b_h and b'_h the two b-jets that better reconstruct the Higgs. After this, we impose a final cut, (vii) the invariant mass of the four leading b-jets (that is used as the discriminating variable) is required to be close to the test mass of the heavy gluon: $M_G - 1000$ GeV $< m_{4b} < M_G + 500$ GeV. The efficiencies of the different cuts for the signal (with $M_G = 2.5$ TeV) and the irreducible background are given in Table 4.5. The relatively low efficiency for the signal of the N_b cut is due to the fraction of boosted events.

We show in Figure 4.11 (left) the invariant mass of the four leading b-jets, after the cuts we impose, for the signal and irreducible background. The figure shows that this observable is clearly a discriminating variable, with a distinct peak around the mass of the heavy gluon. Cutting on a window around the test mass, the background is reduced to negligible levels. Once we reconstruct the heavy gluon mass, we can reconstruct the heavy bottom by taking the invariant mass of the two b-tagged jets that best reconstruct

[17] The parenthesis indicate that the corresponding cut applies only for LHC14. Otherwise, the cut is set for both LHC8 and LHC14.

8 TeV	N_b	N_ℓ	p_T^b	$p_T^{b_1}$	$p_T^{b_2}$	$\lvert m_{bb} - m_h \rvert$	$m(4b)$
Signal	16	99	68	99	99	56	89
Background	17	99	10	13	89	46	0.7
14 TeV							
Signal	16	99	59	98	98	59	92
Background	20	99	12	7.6	63	36	11

Table 4.5: Cut by cut efficiencies (in percent) for the signal with $g_c = 3$ and $M_G = 2.5$ TeV for two different c.m.e, and the irreducible $b\bar{b}b\bar{b}$ background. The slightly low efficiency in N_b for the signal is consequence of the boosted regime.

the Higgs mass (b_h and b'_h) and the leading one among the remaining b-jets (denoted b_{lead}). It can be checked that the peak in this distribution around the heavy bottom mass is narrower than the one obtained with other combinations of b-jets, for the values of M_G and M_{B_h} that we consider. An example of this is shown in the right panel of Figure 4.11.

With all this information, we can report on the expected bounds and discovery reach at the LHC. Our main result, summarized in Figure 4.12, shows the expected 95% C.L. upper limit on the $hb\bar{b}$ production cross section as a function of the heavy gluon mass. We overlay the cross sections for several points in parameter space for our model that allow us to compute the corresponding bounds on M_G. The results for the LHC8 are shown in the left panel of the figure in which we also show the corresponding bound from current searches on multi-b plus E_T^{miss} final states. As we see, our modified analysis can improve the current limits (using the same data) by more than an order of magnitude in cross section and by almost 1 TeV in the reach of the heavy gluon mass up to ~ 3 TeV for the benchmark model (defined with $g_c = 3$). The expected bound for the LHC14, together with several different scenarios for this model (i.e., different values of s_{bR} and g_c) is shown in the right panel of the figure. In this case 100 fb^{-1} of integrated luminosity allow us to probe masses in the $4 - 5$ TeV region for the heavy gluon, depending on the parameters. The sensitivity of the LHC8 and LHC14 to different parameters in the model is shown in Figures 4.13 and 4.14 respectively, in which we give the sensitivity that can be reached, as a function of s_{bR} (left) and g_c

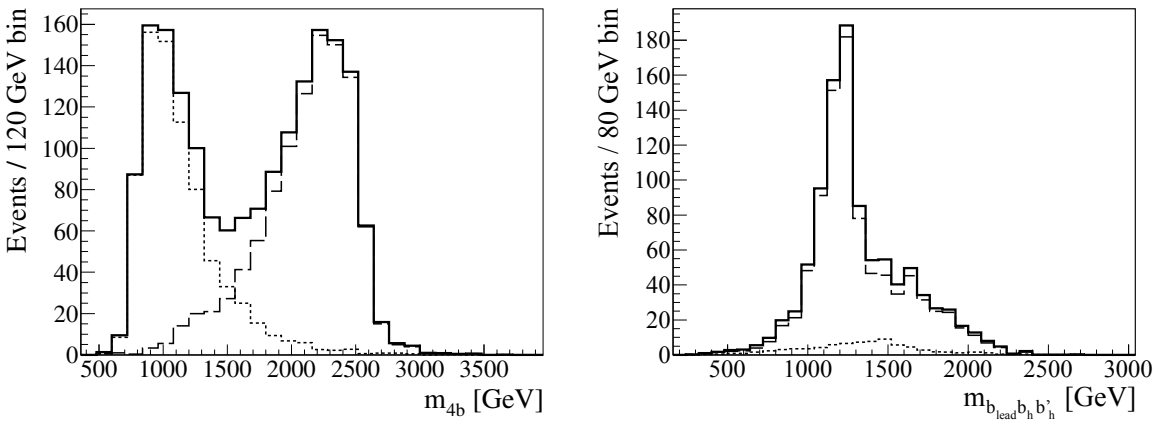

Figure 4.11: Plots of reconstructed events after the imposed cuts (see the text). The dashed, dotted and solid lines represent the signal, the background and the sum (data) respectively. Left: Reconstruction of G from the four leading b-tagged jets. Right: Reconstruction of B_h from the two jets reconstructing the Higgs plus the hardest among the remaining b-jets after the imposed cuts (see the text).

(right), for different values of the heavy gluon mass and for the two LHC configurations with LHC8 in the first figure and LHC14 in the second. In order to account for the finite statistics, in this case we use `SigCalc`, that takes $\tau \equiv \mathcal{L}_{\rm data}/\mathcal{L}_{\rm MC}$ as an input, where $\mathcal{L}_{\rm data}$ and $\mathcal{L}_{\rm MC}$ represent the actual and the generated luminosities respectively. The result given by `SigCalc` reduces to equation 3.6 in the limit $\tau \to \infty$. In this plot we show again the bounds derived from dijet searches [169], which are more constraining than multi-b searches for our model. As we see, despite the stringent bounds on the model from dijet searches, there are allowed regions in parameter space with heavy gluon masses in the $1.5 - 2.75$ TeV range that can be discovered with the LHC8 data. At the LHC14 masses up to 5 TeV can be constrained and up to 4.5 TeV discovered with 100 fb^{-1}.

Thus, as conclusions, the requirement of very stringent cuts on the p_T of the different b-tagged jets and a relaxation in the amount of E_T^{miss} requested can significantly reduce the background without sensibly affecting our signal. In this way, masses up to ~ 3 (2.75) TeV for the heavy gluon can be excluded (discovered) with current data at the LHC8. The bounds and discovery limits go up to ~ 5 and 4.5 TeV, respectively at the LHC14 with 100 fb^{-1} of integrated luminosity.

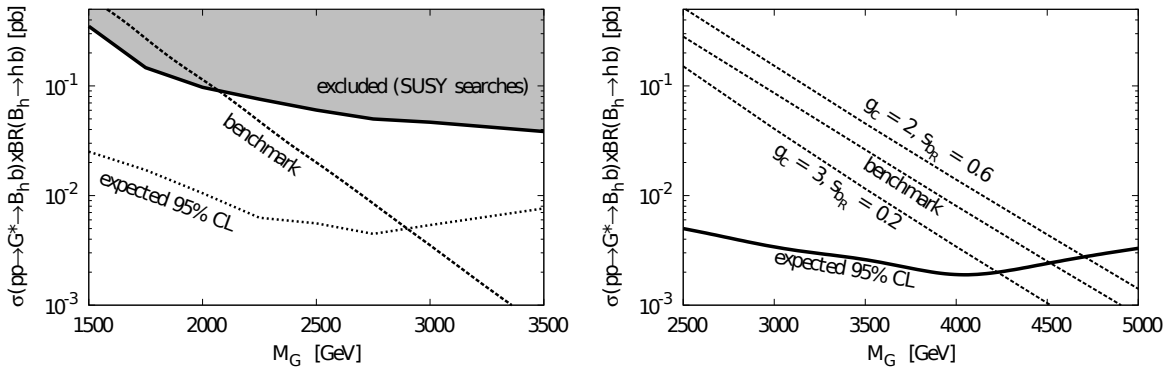

Figure 4.12: 95% C.L. exclusion bound on the $hb\bar{b}$ production cross section as a function of the heavy gluon mass for the LHC8 (left) and LHC14 (right) with 20 fb^{-1} and 100 fb^{-1} of integrated luminosity, respectively. The dashed lines correspond to the cross section in our model for different values of the input parameters.

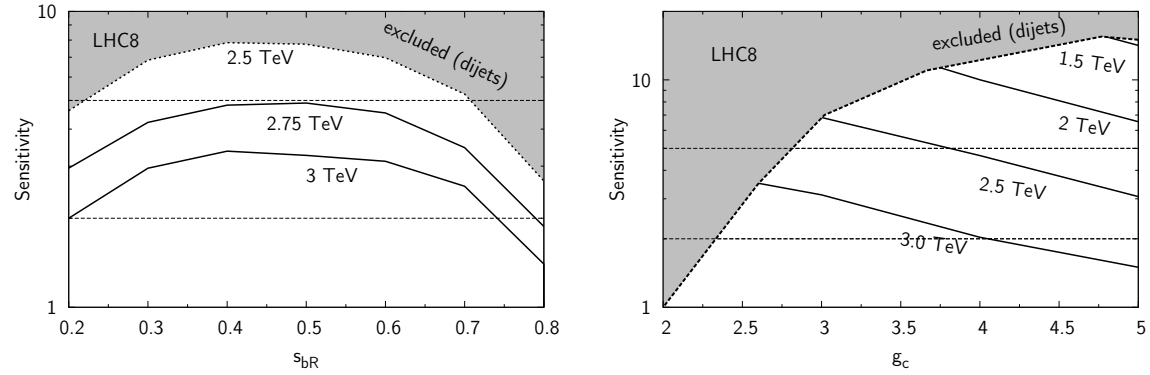

Figure 4.13: Sensitivity reach in the model as a function of s_{bR} (left) and g_c (right), for the LHC8 with 20 fb^{-1}. The bounds from current dijet searches are also shown.

4.7 Composite light quarks

We have argued before that, according to the partial compositeness setup (Section 4.3), light quarks are naturally mostly elementary and thus flavor-violating processes involving the first generations of quarks (which are very constrained) are suppressed by the small mixing angles. However, light quarks can be also strongly composite, and then interact strongly with the heavy fermions, if some new symmetry is enforced in the strong sector [190–193]. In the implementation of minimal flavor violation (MFV) in

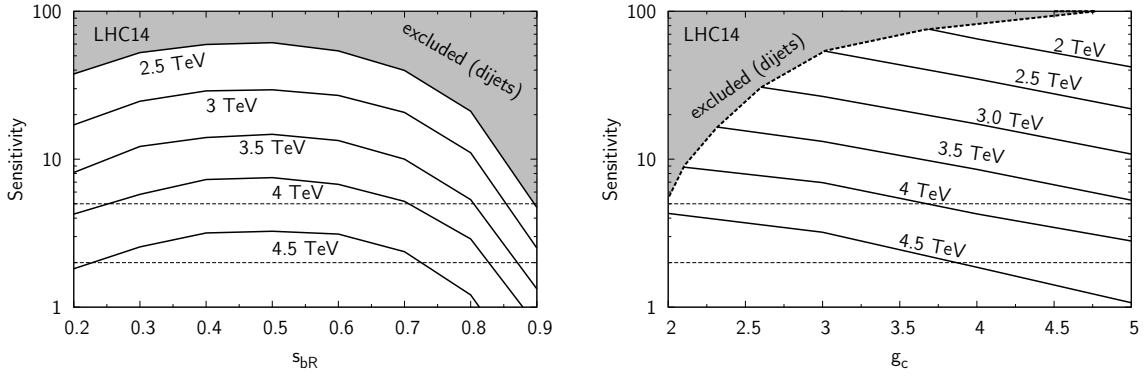

Figure 4.14: Sensitivity reach in the model as a function of s_{bR} (left) and g_c (right), for the LHC14 with 100 fb^{-1}.

CHMs [192, 194] this is guaranteed by imposing $\Delta_{L1} = \Delta_{L2} = 0$, so that LH light quarks are completely elementary. In that case we have, in particular, $M_{Q_{1/6}} = M_{Q_{7/6}} \equiv M$, where now $Q_{1/6}$ y $Q_{7/6}$ stand for the doublet resonances of the light quarks. Thus, we deal with two vector-like quarks $Q_{1/6} = (U, D)^T$ and $Q_{7/6} = (U_{5/3}, U_{2/3})$, degenerated in mass, with hypercharges 1/6 and 7/6 respectively, that couple with identical strength $\lambda_Q = Y_* \sin\phi_{uR}$ to the RH light up quarks. In the following, we disregard the down sector, as well as the physical singlet $\tilde{U}$. Given that u quarks are much more relevant than c quarks in processes mediated by quark anti-quark annihilation, hereafter we only consider that u_R is composite enough, and study its phenomenology. This model is known in the literature as the Degenerate Bidoublet model, and has been described in full detail in references [195, 196] (for an implementation in the lepton sector see references [197, 198]).

Let us denote the two charge 2/3 vector-like quarks present in the spectrum, U and $U_{2/3}$, by U_Z and U_h, respectively, and $U_{5/3}$ by X. After EWSB, all the observables can be parametrized in terms of two masses, that we take to be m_u, the SM up quark mass and the common mass $M \equiv m_{U_Z} = m_D = m_X$, and a mixing angle $s_R \equiv \sin\theta_R$ [18]. The relevant relations between all these parameters are given by the following set of

[18]Note that this angle has nothing to do with $\sin\phi_{uR}$. s_R refers to the mixing of u_R with the vector-like quarks after EWSB, while $\sin\phi_{uR}$ refers to the mass mixing term of u_R and $\tilde{U}$ coming from partial compositeness before EWSB. In terms of $\lambda_Q = Y_* \sin\phi_{uR}$, s_R is expressed as $s_R \sim -\sqrt{2}\lambda_Q v/M$.

equations:

$$m_{U_h} = Mc_L/c_R, \quad s_L = s_R m_u^2/M^2 \approx 0,$$
$$\kappa^R_{uU_Z} = \sqrt{2}\kappa^R_{uX} = \sqrt{2}\kappa^R_{uD} = s_R, \quad y^R_{uU_H} = s_R c_R \frac{m_{U_h}}{v}. \tag{4.40}$$

Here $\kappa^R_{uU_Z}$, κ^R_{uX} and κ^R_{uD} stand for the couplings of u_R, the heavy quarks and the gauge bosons when their interactions are written as

$$\frac{g}{\sqrt{2}} W^+_\mu \kappa_{uD} \overline{u_R} \gamma^\mu D_R + \frac{g}{\sqrt{2}} W^-_\mu \kappa_{uX} \overline{u_R} \gamma^\mu X_R + \frac{g}{2c_W} Z_\mu \kappa_{uU_Z} \overline{u_R} \gamma^\mu U_{Z,R} + \text{h.c.} \tag{4.41}$$

Similarly, $y^R_{uU_H}$ represents the Yukawa coupling between u_R, U_h and the Higgs boson. All other couplings are either vanishing or suppressed by powers of s_L and therefore negligible. From these couplings, it should be clear from the choice of notation that the only allowed decays for the charge 2/3 quarks are $U_Z \to Zu$ and $U_h \to hu$. Similarly, X and D can only have charged current decays.

4.7.1 Constraints

In order to study the phenomenology of this model (constraints and implications), there are two different approaches, depending on whether the heavy gluon is assumed to be present in the spectrum or not. Let us first concentrate in the second case. Note that the model enjoys a custodial symmetry protection of the SM quark gauge couplings, so that they only receive corrections proportional to powers of $|s_L| \lesssim 10^{-11}$ from the mixing with the new quarks. Thus, constraints on the S parameter [199] give the very mild bound [195] $|s_R| \lesssim 0.75$. Direct searches, however, result in the most stringent constraints for this model. Here we translate the constraints obtained in reference [200] to our model and the results are shown in Figure 4.15 (left). In reference [200] the bounds were obtained assuming only one type of quark at a time. In our model we have only one quark, U_Z, contributing to the neutral current channel, and therefore the experimental bound as given in reference [200] applies to our analysis as well. However for the charged current channel we have two quarks, X and D, contributing simultaneously whereas in reference [200] only one quark was considered. Hence in extracting the limits on the coupling we have to consider the case that both

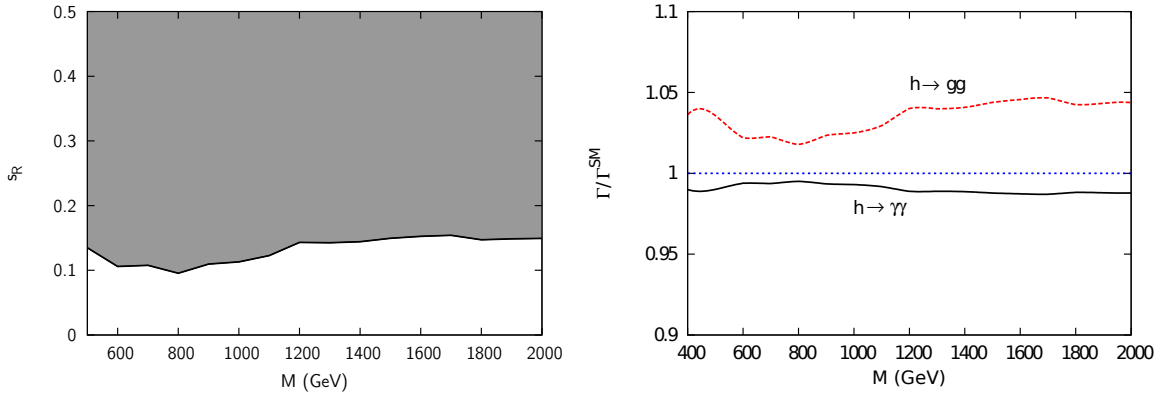

Figure 4.15: Left: Upper bound on the value of the mixing angle, s_R, as a function of the common heavy quark mass, M, for the degenerate bidoublet derived from direct searches [200]. Right: Maximum deviation of Higgs decay widths $\Gamma(h \to gg, \gamma\gamma)$ with respect to the SM in the degenerate bidoublet model when the bounds from direct searches (left panel) are taken into account.

quarks are simultaneously present [19]. The bound presented in Figure 4.15 (left) is the most stringent one of the charged and neutral current channels. These constraints are stringent enough that Higgs searches do not impose any further constraints. For instance, given the current bounds in Figure 4.15 (left), GF is enhanced with respect to the SM by less than 5% and the $h \to \gamma\gamma$ channel decreased by less than 2% as shown in Figure 4.15 (right). These direct constraints on s_R also imply that $m_{U_h} \approx M$ with an approximate precision of 1%, well within the experimental resolution. Thus, from now on we consider all four quarks to be degenerate.

If we consider that the heavy gluon is also present in the spectrum, we have to include the bounds we already considered in Section 4.5 too, namely dijet searches (that in this case becomes more important given that both the production of the heavy gluon and its decay into jets are enhanced) and $t\bar{t}$ searches. We include these constraints in the corresponding plots with the summary of the results of the phenomenology of this model when the heavy gluon is included.

[19] Although we have disregarded the interactions with $\tilde{U}$ in the present phenomenological study for it does not contribute to the Higgs channels, properly speaking we should include its contribution to these bounds. This, however, only slightly modify the values of s_R in Figure 4.15.

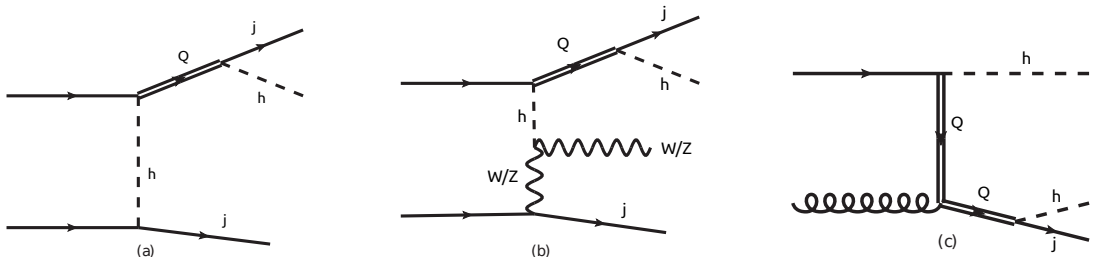

Figure 4.16: Sample diagrams for: (a) single production, (b) vector boson Higgs fusion and (c) associated production of U_h with subsequent decay into hu.

4.7.2 Collider signatures

As in the previous sections, we only concentrate in the relevant single production mechanisms of new quarks that involve at least one Higgs boson in the final state (see references [194, 195] for the discussion of non-Higgs mechanisms). Given current constraints from single production in the EW gauge boson channels we focus on the LHC running at its highest designed luminosity with $\sqrt{s} = 14$ TeV. Let us start considering the phenomenological collider implications of this model when the heavy gluon is assumed not to be in the spectrum. One important feature of the model is the fact that each of the heavy quarks couples to the u quark and only one gauge boson or the Higgs, *i.e.*, $\text{BR}(X \to uW^+) = \text{BR}(U_Z \to uZ) = \text{BR}(D \to uW^-) = \text{BR}(U_h \to uh) = 100\%$. This strongly restricts the number of relevant diagrams that contribute to Higgs production through the decay of the heavy quark U_h. The three mechanisms that we consider and their relevant features are: *(i) Single production:* $qq' \to jU_h \to jjh$. In this channel, the heavy quark U_h is produced in association with a single (forward) jet. Subsequent decay of the heavy quark to a jet and the Higgs boson leads to a final state of hjj as shown in Figure 4.16 (a). Single production is suppressed in our model by the up quark Yukawa coupling and is disregarded henceforth.

(ii) Vector boson Higgs fusion (VBHF) $qq' \to jVU_h \to jjVh$, where $V = W, Z$. In this channel, the heavy quark U_h is produced in association with a (forward) jet and an EW gauge boson. After the decay of the heavy quark we have a final state of $Vhjj$, where $V = W, Z$ gauge boson as shown in Figure 4.16 (b). The VBHF production mechanism is initiated by two valence quarks, involves unsuppressed couplings and has a longitudinal gauge boson enhancement. Thus, the corresponding cross section can

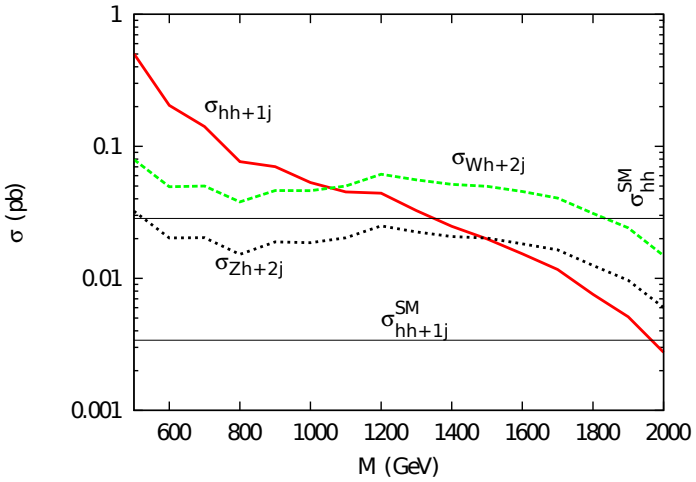

Figure 4.17: Cross sections for the associated production channel (labeled $hh + 1j$) and the VBHF channel (labeled $Wh + 2j$ or $Zh + 2j$) for s_R fixed to the current upper bound. For reference we also show the SM production cross section of two Higgs bosons and two Higgs bosons plus a hard jet with $p_T(j) > 100$ GeV.

be sizable and relatively insensitive to the mass of the heavy quark. This is shown in Figure 4.17 where the cross sections correspond to the currently allowed values of s_R. The presence of an EW gauge boson allows for a clean trigger using its leptonic decays thereby allowing the use of the dominant $b\bar{b}$ Higgs decay.

(iii) Associated Production: $qg \to hU_h \to jhh$. In this channel, the heavy quark U_h is produced in association with a Higgs boson and the subsequent decay of the heavy quark leads to a unique two Higgs plus a hard jet final state shown in Figure 4.16 (c). Double Higgs production has been studied as a way of measuring Higgs self-couplings [201–203] and anomalous Higgs couplings [204–206]. The presence of a hard jet from the decay of the heavy quark in our analysis enhances signal over background. Associated production is initiated by a valence quark and a gluon. Hence the cross sections can be quite large for small values of M but suffer a stronger suppression for larger values of the heavy quark mass, due to the steeply falling gluon PDFs. We show the cross section for this process in Figure 4.17 for the currently allowed values of s_R. For comparison we also show in Figure reffig:production the production cross section for $hh+X$ and $hh+j+X$ in the SM, with $p_T(j) \geq 100$ GeV, as computed in [202]. In the

Background	$\sigma(pb)$	Background	$\sigma(pb)$
$t\bar{t}$ semileptonic $+ 0 - 4j$	223	$W_{l\nu}WW + 0 - 2j$	0.14
$t\bar{t}$ fully leptonic $+ 0 - 4j$	54	$WWZ + 0 - 2j$	0.18
$W_{l\nu}b\bar{b} + 0 - 2j$	13	$W_{l\nu} + 1j,\ p_T^{j_h} > X$	178
$b\bar{b}b\bar{b} + 1j,\ p_T^{j_h} > X$	3.1	$t\bar{t}b\bar{b}$	0.9
$b\bar{b} + 3j$	515	$W_{l\nu}W + 0 - 2j$	49
$Z_{ll}/\gamma_{ll} + 1 - 4j$	1423	$WZ + 0 - 2j$	40
$Z_{ll}Z + 0 - 2j$	2.4	$Z_{ll}b\bar{b} + 0 - 2j$	4.5

Table 4.6: LO cross sections for the various background processes for $\sqrt{s} = 14$ TeV. In our notation $W_{l\nu}$ and Z_{ll} represent leptonic decays of the W and Z gauge bosons and $l = e, \mu, \tau$. The transverse momentum cut for the hardest jet (j_h) for W+jets background is $X = 130$ GeV. In the case of $b\bar{b}b\bar{b} + 1j$ we have $X = 150$ GeV. The explicit number of jets listed stands for the ones generated at the parton level and the rest of the jets are from initial and final state radiation. The first three are the main backgrounds to the VBHF channel and the next two are the main ones for the $b\bar{b}b\bar{b} + j$ associated production channel. The other background processes listed in the table have been considered in the analysis but become irrelevant after all the optimization cuts have been applied.

following we describe the analyses we propose to measure the VBHF and associated production mechanisms. In these analyses jets and leptons are defined as requiring $p_T^j > 30$ GeV, and $p_T^\ell > 20$ GeV. In Table 4.6 we show the relevant backgrounds for the analyses in this section with their corresponding cross sections at $\sqrt{s} = 14$ TeV.

In the VBHF channel, the heavy quark U_h is produced singly in association with a W or Z gauge boson and a jet leading to the final state $pp \to VU_hj \to Vhjj$, where $V = W, Z$. Of the two jets in the final state, the one coming from the heavy quark decay tends to be quite hard whereas the other one tends to be relatively forward. Furthermore the Higgs boson comes from the decay of a massive particle (U_h) and is typically quite boosted. These features can be used to enhance signal over backgrounds. Considering the leptonic decays of the gauge boson helps to reduce QCD backgrounds as well as provide a clean trigger. Hence we consider only the leading $h \to b\bar{b}$ decay. The final state is therefore $b\bar{b}jj\ell E_T^{miss}$ or $b\bar{b}jj\ell\ell$, for $V = W$ or Z gauge boson respectively. The latter process is potentially cleaner but suffers from reduced statistics. The cross section is of $\mathcal{O}$(fb) once the decay BRs of the Z and h are included. Thus, even a

M (GeV)	σ_s (fb)	ϵ_s	$\epsilon_{t\bar{t}}$	$\epsilon_{Wb\bar{b}}$
500	79	0.010	1.0×10^{-4}	1.4×10^{-4}
1000	46	0.040	4.7×10^{-5}	7.7×10^{-5}
1500	50	0.025	7.7×10^{-6}	1.4×10^{-5}

Table 4.7: Cross sections for the signal ($Whjj$) and efficiencies for signal and main backgrounds for different values of M. The corresponding background cross sections are listed in Table 4.6.

minimal set of cuts quickly reduces the number of events to just a few except for very large luminosities. For this reason we focus on the more promising charged current channel. For this channel we propose the following cuts: *(i)* exactly one charged lepton ℓ (e or μ) plus at least four jets j with exactly two b tags; *(ii)* $p_T(j_h) \geq 200$ GeV for the hardest jet that is not b-tagged; *(iii)* the two b-tagged jets have to reconstruct the Higgs mass, i.e., $|m_{bb} - m_h| \leq 30$ GeV; *(iv)* the Higgs is required to be boosted in the sense that $\Delta R(bb) \leq 1$. And finally *(v)*, we reconstruct the mass of the heavy quark requiring $|m_{bbj_h} - M| \leq 200$ GeV. We show in Table 4.7 the signal cross section and the total efficiencies for the signal and main backgrounds for different values of the heavy quark mass. All relevant background processes are considered but we only report the ones that are non-negligible after all the cuts in Table 4.7. In Figure 4.18 (left) we show the 2 and 5 σ sensitivity for the production cross section times BR for the $Whjj$ channel as a function of the heavy quark mass, M, for the LHC with $\sqrt{s} = 14$ TeV and an integrated luminosity of 300 fb^{-1}. For reference we also show the current (95% C.L.) upper bound (indicated by the dotted blue curve) imposed by the constraints on s_R.

In the associated production channel, the heavy quark, U_h, is produced in association with a Higgs boson as shown in Figure 4.16 (c). Subsequent decay of the heavy quark leads to the unique final state with two Higgs bosons and a hard jet: $pp \to hU_h \to hhj$. Double Higgs production has received some attention as a means of measuring the Higgs self-couplings in the SM, see for instance References [201–203]. In the case of the SM, this is a very difficult measurement at the LHC due to the very low cross section, $\sigma_{SM}(pp \to hh + X) = 28.4$ fb [202]. As shown in Figure 4.17 the double Higgs production cross section can be larger (by up to an order of magnitude for the lowest

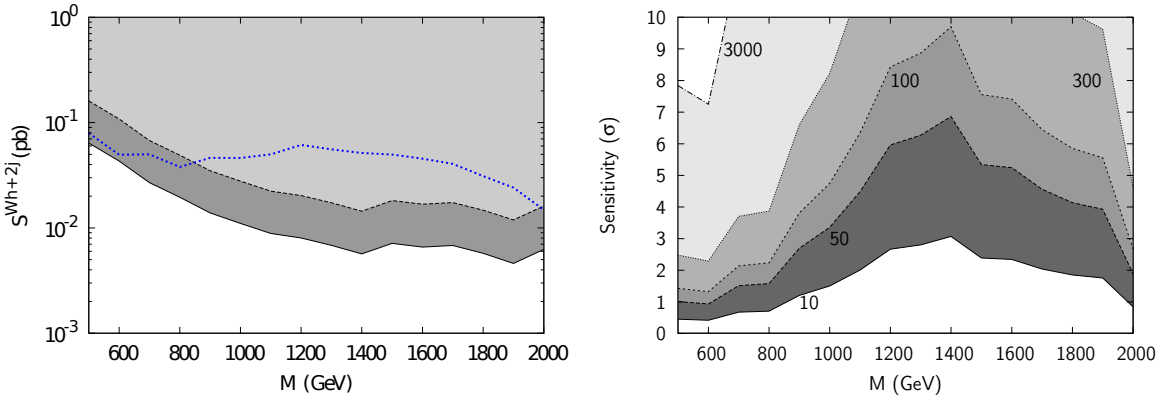

Figure 4.18: Left: 2 and 5 σ bounds (indicated by dark and light colored regions respectively) on the production cross section times BR for the $Whjj$ channel as a function of the heavy quark mass, M, for the LHC with $\sqrt{s} = 14$ TeV and an integrated luminosity of 300 fb^{-1}. For reference we also show the current (95% C.L.) upper bound (indicated by the dotted blue curve) in the context of the degenerate bidoublet model. Right: Contour plot of the luminosity required for a certain degree of C.L. as a function of the heavy quark mass with s_R fixed to the current limit.

masses) in our model for masses $M \lesssim 1.4$ TeV. Furthermore, the presence of a very hard jet from the decay of the heavy quark in our model provides better signal sensitivity over background. In fact, even for the lowest value of the masses considered, in over 90% of the signal events the hardest jet has $p_T(j_h) \geq 100$ GeV whereas in the SM the corresponding cross section goes down to $\sigma_{SM}(p \to hhj + X; p_T^j \geq 100 \text{ GeV}) = 3.2$ fb. Even without the extra hard jet it has been argued recently that the LHC can be sensitive to double Higgs production in models beyond the SM with anomalous Higgs couplings [204–206] with an enhancement factor with respect to the SM cross section similar to the one present in our model. Hence, our analysis, which probes the underlying structure of the degenerate bidoublet model, is competitive with the other double Higgs studies (which probe different theoretical aspects).

The presence of two Higgs bosons can lead to different final states based on the decay modes of the Higgs. We consider two scenarios: one where both Higgs bosons decay to $b\bar{b}$ and the other where one Higgs boson decays to $b\bar{b}$ and the other to a pair of photons. This gives rise to the final states $b\bar{b}b\bar{b}j$ and $b\bar{b}\gamma\gamma j$ respectively. We estimate the LHC reach for the associated production channel with these two final states.

The $b\bar{b}\gamma\gamma$ channel has been studied in detail in reference [201] in the context of

cut	ϵ_{800}	ϵ_{1600}	$\epsilon_{\text{irred.}}$
Equation (4.42)	0.14	0.087	0.00023
Equation (4.43)	0.76	0.7	0.13
Equation (4.44)	0.99	1	0.011

Table 4.8: Efficiencies for the signal (with $M = 800$ and 1600 GeV) and irreducible background in the $b\bar{b}\gamma\gamma$ channel for the various optimization cuts listed in equations (4.42) - (4.44).

the SM and in reference [205] in models with anomalous diHiggs couplings (like the ones present precisely in CHMs). The result is that the cross section is too small for a reasonable measurement in the SM but in some CHMs one can reach discovery in this channel for values of the cross section $\sigma(pp \to hh \to b\bar{b}\gamma\gamma) \gtrsim 6 \times \sigma(pp \to hh \to b\bar{b}\gamma\gamma)^{SM}$ [205]. In our model there are regions of parameter space in which the double Higgs production cross section is enhanced by an even larger factor with respect to the SM, even before taking into account the presence of a hard jet. In order to estimate the LHC reach we generate events for the signal and the irreducible background. We implement the following cuts as suggested in Reference [201]: *(i)* two b-tagged jets and two photons satisfying

$$\begin{aligned} &p_T(b) > 45 \text{ GeV}, \quad |\eta(b)| < 2.5, \quad \Delta R(b,b) > 0.4, \\ &p_T(\gamma) > 20 \text{ GeV}, \quad |\eta(\gamma)| < 2.5, \quad \Delta R(\gamma,\gamma) > 0.4, \\ &|m_{bb} - m_h| < 20 \text{ GeV}, \quad |m_{\gamma\gamma} - m_h| < 2.3 \text{ GeV}, \quad \Delta R(\gamma,b) > 0.4 \ . \end{aligned} \tag{4.42}$$

(ii) angular cuts:

$$\Delta R(b,\gamma) > 1.0, \quad \Delta R(\gamma,\gamma) < 2.0 \ . \tag{4.43}$$

(iii) finally we also impose an extra cut on the p_T of the hardest jet to further reduce the background:

$$p_T(j_h) > 100 \text{ GeV}. \tag{4.44}$$

The signal and irreducible background efficiencies for the cuts in equations (4.42) - (4.44) are shown in Table 4.8. Note that the cut on the p_T of the hard jet is rather conservative since a larger cut such as $p_T(j_h) > 300$ GeV reduces the background

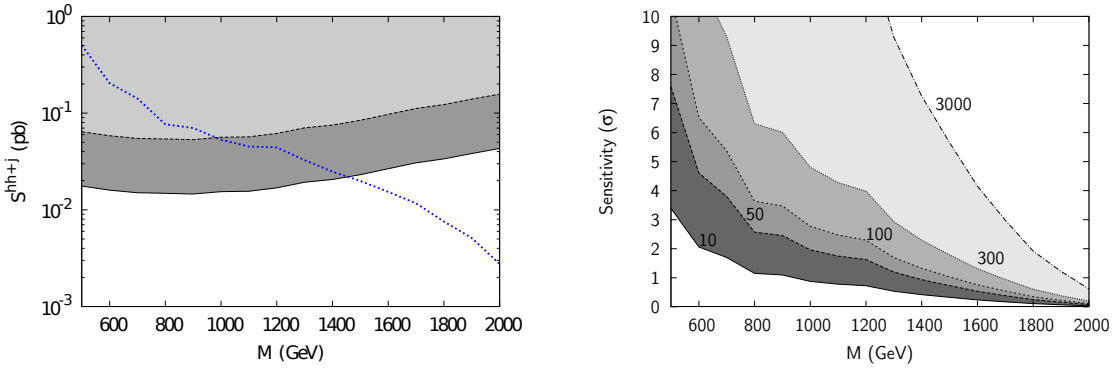

Figure 4.19: Same as Figure 4.18 but for the hhj channel with $b\bar{b}\gamma\gamma j$ final state.

significantly while preserving most of the signal. The cross section for the irreducible background after the cuts of equation (4.42) and equation (4.43) agree with those in references [201, 205] to within $\mathcal{O}(15\%)$. Given this agreement we use the efficiencies for the reducible (subleading) backgrounds from references [201, 205] and assume the same efficiency for the cut on the p_T of the hard jet as in the irreducible background. We use the resulting efficiencies to estimate the 2 and 5 σ reach for this channel at the LHC with $\sqrt{s} = 14$ TeV for 300 fb^{-1} of integrated luminosity and the results are shown in the left panel of Figure 4.19. For comparison the current bound in the model as obtained from single EW production is also shown as the blue dotted curve. In the figur panel of Figure 4.19 we show the C.L. as a function of the heavy quark mass for different values of total integrated luminosity when s_R is fixed to the current upper bound. We see that with an integrated luminosity of 300 fb^{-1} we can obtain a 2 (5) σ measurement up to 1.4 (1.0) TeV.

The $b\bar{b}b\bar{b}j$ channel (which turns out to be the channel with the largest BR), is *a priori* extremely challenging due to the immense QCD background [20]. A realistic determination of the feasibility of this multijet channel requires computing resources and data-driven methods that are beyond the scope of this analysis. Hence we can only get a rough estimate of the LHC reach for this channel. In this study we aim to

[20]Note that, although the topology of the final state is similar to that we studied in Section 4.6, the phase space regions are completely different. In particular, unlike this last one, the process we study in this section does not contain very hard b-tagged jets, and thus the copious production of MC events can not be easily performed.

point out the unique features of this final state that enhances signal sensitivity over the large backgrounds. These unique features include a very hard jet, four b quarks that reconstruct two Higgs bosons and the reconstructed heavy quark. We believe that our results are sufficiently promising to warrant a more detailed experimental study. We generate the following two background processes: the irreducible $b\bar{b}b\bar{b} + 1j$ and the $b\bar{b} + 3j$ backgrounds. The corresponding cross sections are shown in Table 4.6. The huge background reduction resulting from the requirement of four b-tagged jets (here we assume a fake tag rate of 1%) allows us to neglect pure multijet QCD backgrounds. We propose the following cuts: *(i)* at least five jets, four of which must be tagged as b-jets; *(ii)* $p_T(j_h) > 300$ GeV; and *(iii)* $|m_{jj} - m_h| < 50$ GeV (for both pairs of b-jets). The very large $b\bar{b} + 3j$ cross section (see Table 4.6) is greatly reduced due to the requirement of four b-tags, given the 1% mistag rate we consider. This huge reduction makes it very challenging to generate enough statistics to reasonably estimate the efficiency of the remaining cuts. In order to estimate this efficiency we do *not* impose the requirement of the four b-tags but rescaled the corresponding cross sections with the factors resulting from the b-tagging efficiency ($\epsilon_{4b}(bbbbj) \approx 0.25$) or mistagging rate ($\epsilon_{4b}(bbjjj) \approx 1.5 \times 10^{-4}$). The remaining cuts on the transverse momentum of the hard jet and the Higgs mass reconstruction are then implemented. The pairs of jets used to reconstruct the Higgs boson are selected from the four subleading jets, as in the signal the hardest jet is typically the one from the decay of U_h and is not a b quark. The two jets that reconstruct the Higgs mass closest to $m_h = 125$ GeV form the first pair while the remaining two jets reconstruct the other Higgs boson. Once the two Higgs candidates are selected we construct the invariant mass of one Higgs boson and the leading jet and require that at least one of these invariant masses is in the region $|m_{hj_h} - M| < 400$ GeV. We show the corresponding efficiencies after all cuts for the signal and the two backgrounds we consider in Table 4.9 and a summary of the results in Figure 4.20. Keeping in mind the inherent lack of precision in the estimation of the backgrounds for this process we see that this channel is potentially even more promising than the $b\bar{b}\gamma\gamma$ one. A 2 (5) σ sensitivity can be obtained for masses up to 1.7 (1.3) TeV with 300 fb^{-1} integrated luminosity.

Let us know consider the heavy gluon G to be present in the spectrum. This allows us to study the production of G and its decay into $\bar{u}U_h$, following by the subsequent

M (GeV)	σ_s (fb)	ϵ_s	ϵ_{4b+j}	ϵ_{2b+3j}	background events/100 fb^{-1}
500	125	0.033	0.0051	0.0029	456
1000	12.6	0.057	0.005	0.003	412
1500	5.6	0.03	0.0008	0.0005	71

Table 4.9: Cross sections for the signal ($b\bar{b}b\bar{b}j$ channel) and efficiencies for the signal and main backgrounds after all the cuts listed in the text for different values of heavy quark mass, M. The total number of background events with 100 fb^{-1} of integrated luminosity is also shown in the last column. The efficiency due to b-tagging as described in the text is not included in this table but it is used to compute the number of background events.

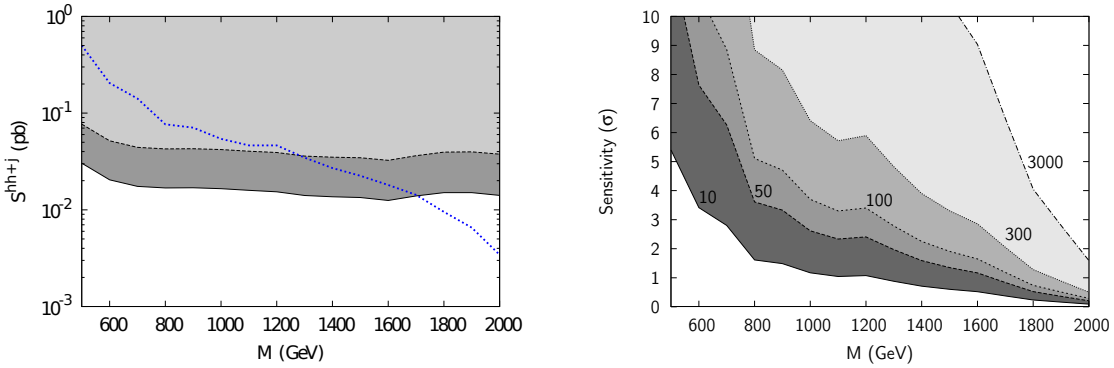

Figure 4.20: Same as Figure 4.18 but for the hhj channel with $b\bar{b}b\bar{b}j$ final state.

decay of U_h into hu. The Higgs is then produced in association with two jets. Due to the presence of the heavy gluon, the phenomenology of this channel can not be described just with the single parameter s_R. Thus, as in Section 4.5, we set $Y_* = 3$, $s_2 = 0.1$, $M_G = 2U_h$ and vary the parameters g_{*3}, M_G and $s_{uR} \equiv \sin\phi_{uR}$. The constraints on s_R are then translated to curves in this parameter space. The cross section for this processes for the choice $g_{*3} = 3$ and $s_{uR} = 0.6$ as a function of M_G is given in Figure 4.21. Even if the two extra jets are quite hard or forward, depending on whether we have an $s-$ or $t-$channel contribution, the signal is completely swamped by backgrounds if we consider the $h \to b\bar{b}$ decay channel. We are therefore forced to consider the $h \to WW^*$ channel. Even so, the relatively small cross sections and the huge W + jets background makes the dilepton mode the only one in which the signal can be realistically extracted

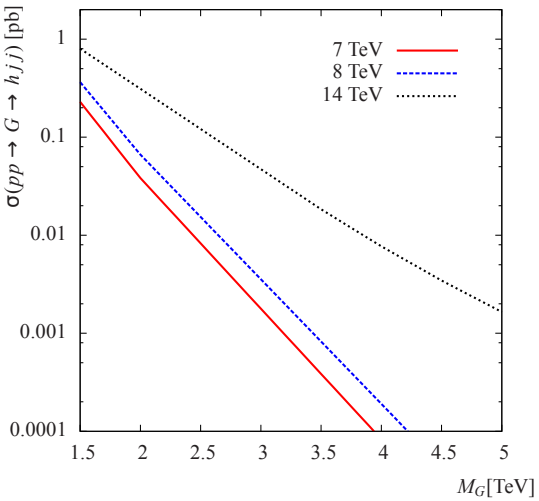

Figure 4.21: Left panel: $hj\bar{j}$ production cross section for $g_{*3} = 3$ and $s_{uR} = 0.6$ as a function of M_G mediated by a color octet vector resonance with decay into a fermionic resonance and a jet.

from the background. The penalty to pay is then the low cross sections and we are in all cases statistics limited. Due to this limitation, we only consider the high energy LHC phase (LHC14) for this channel. The process we are interested in is therefore

$$pp \to G \to U\bar{u} + \bar{U}u \to hu\bar{u} \to 2j + 2\ell + E_T^{miss}. \tag{4.45}$$

The main backgrounds are W + jets, Z + jets, WW + jets and $t\bar{t}$ + jets. The cuts we propose are: *(i)* at least two jets j; *(ii)* exactly two charged light leptons ℓ, both with $p_T(l) \geq 50$ GeV and $|\Delta\phi(\ell_1, \ell_2)| \leq 0.5$; *(iii)* a veto on b-tagged jets (no jet should be tagged as a b-jet); *(iv)* $p_T(j_1) > 400$ GeV, $p_T(j_2) > 200$ GeV ($j_{1,2}$ denote the two hardest jets); *(v)* a cut on the invariant mass of the two charged leptons 15 GeV $\leq m_{\ell\ell} \leq 70$ GeV; *(iv)* a cut on the transverse mass of the Higgs decay products $m_T(\ell, \ell, E_T^{miss}) < 120$ GeV, where the transverse mass is defined as

$$m_T = \sqrt{(E_T^{\ell\ell} + E_T^{miss})^2 - |\mathbf{p}_T^{\ell\ell} + \not{\mathbf{p}}_T|^2}, \tag{4.46}$$

with $E_T^{\ell\ell} = \sqrt{|\mathbf{p}_T^{\ell\ell}|^2 + m_{\ell\ell}^2}$, $|\not{\mathbf{p}}_T| = E_T^{miss}$, and $|\mathbf{p}_T^{\ell\ell}| = p_T^{\ell\ell}$. And *(vii)* a cut on $S_T >$ 1.5, 2.1 , 2.3 TeV for $M_G = 2,\ 2.5, \geq 3$ TeV. The effect of the cuts on the different backgrounds and our signal for $g_{*3} = 3$, $s_{uR} = 0.6$ and $M_G = 2$ TeV are described in

Cut	$\epsilon_{M_G=2\text{ TeV}}$	ϵ_W	$\epsilon_{t\bar{t}}$
$2 \leq n_j \leq 6$	99	76	96
$n_\ell = 2,\ p_T(\ell) \geq 50$ GeV, $\lvert\Delta\phi\rvert \leq 0.5$	28	0.0206	0.158
$n_b = 0$	95	86	22
$p_T(j_1) > 400$ GeV, $p_T(j_2) > 200$ GeV	79	31	4.8
$15 < m_{\ell\ell} < 70$ GeV	91	47	75
$m_T(\text{Higgs}) < 120$ GeV	62	19	17
S_T	97	98	97
Total	12	3.6×10^{-4}	2×10^{-4}

Table 4.10: Cut by cut efficiencies for the signal (with $g_{*3} = 3$, $s_{uR} = 0.6$ and $M_G = 2$ TeV) and the main backgrounds ($W+$ jets and $t\bar{t}$) in the hjj channel at $\sqrt{s} = 14$ TeV. All efficiencies are reported as percent.

M_G	$\epsilon_{M_G=2\text{ TeV}}$	ϵ_W	$\epsilon_{t\bar{t}}$	ϵ_{WW}
1.5	10.4	0.00148	0.00096	0.01
2	11.75	0.000361	0.0002	0
2.5	6.82	7.4×10^{-5}	1.57×10^{-5}	0
3	7.26	4.54×10^{-5}	0	0
3.5	8.15	4.54×10^{-5}	0	0

Table 4.11: Global efficiencies for the signal and main backgrounds as a function of the test mass in the hjj channel at $\sqrt{s} = 14$ TeV. All efficiencies are reported as per cent.

Table 4.10. The cuts completely kill the Z and WW backgrounds which are therefore not reported. The cut on S_T has no effect for this mass but is relevant for heavier masses. The global efficiencies for the signal and the main backgrounds as a function of the test mass are given in Table 4.11. The discovery and 95% bound contours for this channel as a function of (s_{uR}, M_G) and (g_{*3}, M_G) are given in Figure 4.22. Note that, even with $\sqrt{s} = 14$ TeV, more than 30 fb^{-1} of integrated luminosity are required for discovery in the allowed region of parameter space. With 100 fb^{-1}, masses up to $M_G \sim 3.3$ TeV can be discovered and up to $M_G \sim 3.5$ TeV excluded if no signal of NP is observed.

A last comment is in order. It has been shown [10, 207, 208] that the presence

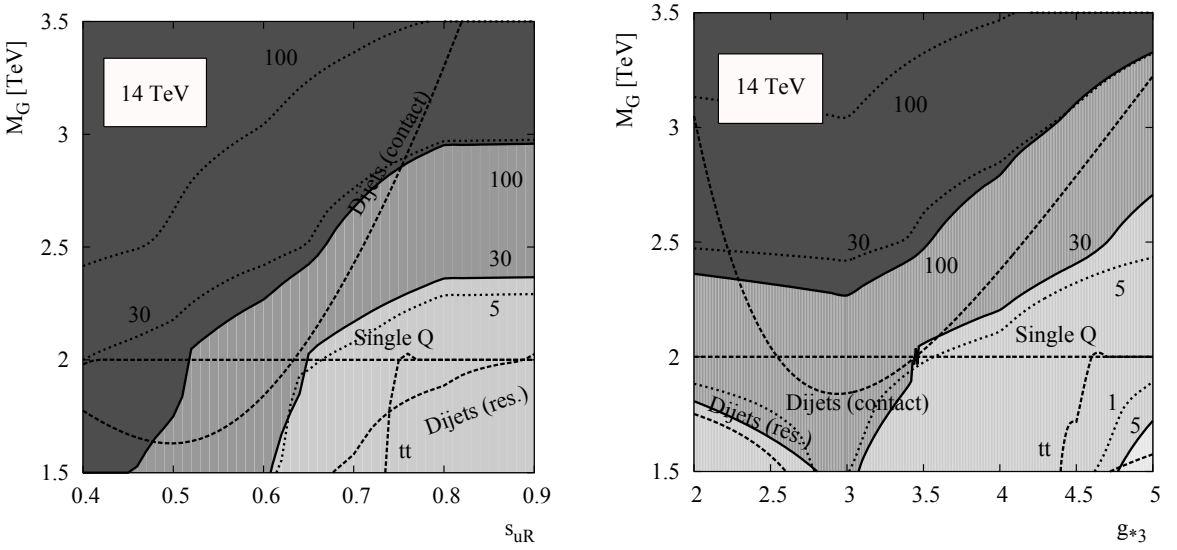

Figure 4.22: Contours of required luminosity for a 5 σ discovery (bands and solid lines) and 95% exclusion limits (dotted lines) as a function of s_{uR} and M_G (left column) and g_{*3} and M_G (right column) for $\sqrt{s} = 14$ TeV in the hjj channel. Current bounds are shown with dashed lines (the area below the dashed lines is excluded).

of heavy color octet resonances, that naturally arise in CHMs as we have repeatedly argued, can explain the observed $t\bar{t}$ forward-backward asymmetry ($A_{FB}^{t\bar{t}}$) at the Tevatron [209, 210]. Indeed, both Tevatron experiments, CDF and DØ, have observed an anomalously large $A_{FB}^{t\bar{t}}$ asymmetry in $t\bar{t}$ production, defined by

$$A_{FB}^{t\bar{t}} = \frac{N(\Delta y^{t\bar{t}} > 0) - N(\Delta y^{t\bar{t}} < 0)}{N(\Delta y^{t\bar{t}} > 0) + N(\Delta y^{t\bar{t}} < 0)}, \tag{4.47}$$

where $\Delta y^{t\bar{t}} \equiv y_t - y_{\bar{t}}$ and N is the total number of events satisfying the corresponding constraint. This asymmetry has been measured in semileptonic decays with the following result: $A_{FB}^{t\bar{t}}(\text{CDF}) = 0.164 \pm 0.047$ [209] and $A_{FB}^{t\bar{t}}(\text{D}\emptyset) = 0.196 \pm 0.065$ [210], to be compared with the SM NLO prediction with EW corrections included [211]: $A_{FB}^{t\bar{t}}(\text{SM}) = 0.088 \pm 0.006$. Although not statistically significant for a discovery, the observed excess is consistent among experiments. A puzzling aspect of the observed excess is that the large values of the measured asymmetries are not accompanied by any sizable deviation in other top observables, such as the total or differential $t\bar{t}$ production cross sections. This strongly constrains possible explanations of the anomalous $A_{FB}^{t\bar{t}}$.

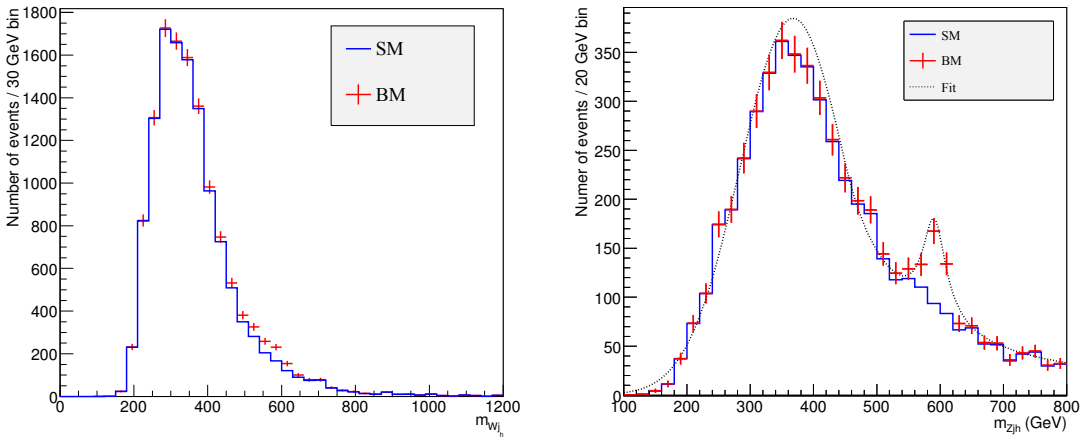

Figure 4.23: Left: Transverse mass for the Wj_h system in the Wjj analysis described in the text for the SM (solid blue) and the model with the heavy gluon (data points with statistical errors). (See reference [10] for the details.) Right: Result of the fit of the m_{Zj_h} distribution for the Zjj channel for the SM (solid blue), the model with the heavy gluon (data points with statistical errors) and the fit to both distributions (dotted black). Both plots are for the 7 TeV LHC with 4 fb^{-1}. In any case, j_h refers to the hardest jet.

However, it has been shown that an s–channel gluon resonance G of relatively low mass ($M_G \lesssim 1$ TeV) can explain the large value of the asymmetry consistently with all the other observations [10, 207, 208]. It needs to have small, close to axial couplings to the light quarks (thus light quarks have to be midly composite as in the case under study) together with a large coupling to the RH top quark. The key ingredient is in fact a large gluon width, provided by new decay modes of type $G \to Q\bar{q}, q\bar{Q}$, where q is a standard quark and Q a massive vector-like excitation [10]. Because this article is not strictly speaking part of this thesis, we refer to [10] for details and explain only briefly the main phenomenological LHC implications that can be pointed out from that study. These are mainly two: *(i)* the new fermionic resonances, produced through the decay of G, can be well looked for when they decay into non-Higgs channels (i.e., $pp \to G \to Q\bar{q}\,(q\bar{Q}) \to Vjj$, with $V = W, Z$). As an example, Figure 4.23 shows the heavy quark mass reconstruction in the Wjj (left) and Zjj channels. And *(ii)* two other observables, namely $A_{t\bar{t}}^C$ and $A_{\ell t}^C$, can drastically deviate from their values in the

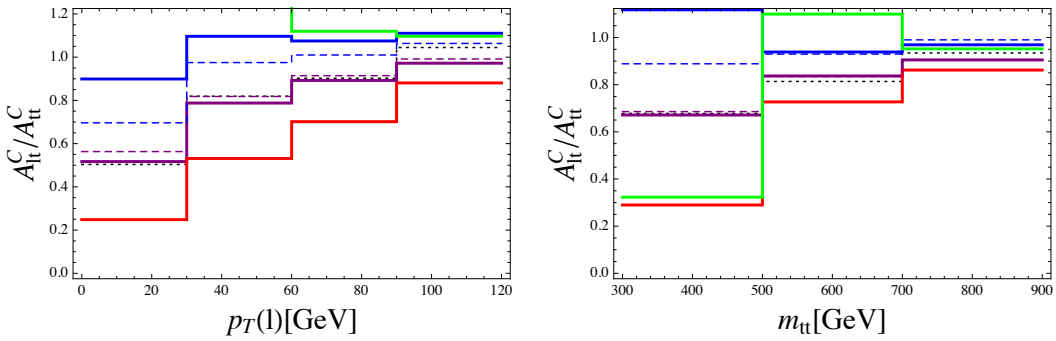

Figure 4.24: Distribution of the ratio $A^C_{\ell t}/A^C_{t\bar{t}}$ at the LHC as a function of p^ℓ_T (left) and $m_{t\bar{t}}$ (right) for the SM (dotted black), for six different heavy gluon models (lines solid blue, solid red, solid purple, dashed blue and dashed purple) and the Z' model of reference [212] (solid green). See reference [11] for the details.

SM. These observables are defined in semileptonic $t\bar{t}$ events by

$$A^C_{t\bar{t}} = \frac{N(\Delta|y|^{t\bar{t}} > 0) - N(\Delta|y|^{t\bar{t}} < 0)}{N(\Delta|y|^{t\bar{t}} > 0) + N(\Delta|y|^{t\bar{t}} < 0)} \tag{4.48}$$

and

$$A^C_{\ell t} = \frac{N(\Delta|y|^{t\ell} > 0) - N(\Delta|y|^{t\ell} < 0)}{N(\Delta|y|^{t\ell} > 0) + N(\Delta|y|^{t\ell} < 0)}, \tag{4.49}$$

where we define

$$\Delta|y|^{t\ell} \equiv \begin{cases} |y_{\ell^+}| - |y_{\bar{t}}|, & \text{for leptonic top decays} \\ |y_t| - |y_{\ell^-}|, & \text{for leptonic anti-top decays.} \end{cases} \tag{4.50}$$

In order not to exceed to much in this discussion, we only point out that the ratio of these observables is studied in different heavy models with heavy gluons (and other well-motivated models) in reference [11]. We show in Figure 4.24 this ratio for different scenarios beyond the SM (see reference [11] for details) and for the SM as a function of the p_T of both the lepton in the semileptonic decay and $m_{t\bar{t}}$. It is clear from the figure that the ratio of lepton-based and $t\bar{t}$ charge asymmetries can be a powerful discriminator of NP. This study have been performed for the LHC with $\sqrt{s} = 8$ TeV c.m.e. Nevertheless, the shape of the ratio of the asymmetries as function of p^ℓ_T or $m_{t\bar{t}}$ should be a particularly useful observable for the longer LHC run with an upgraded

energy $\sqrt{s} = 13/14$ TeV. Moreover, it is expected that the ratio of related asymmetries in the dileptonic $t\bar{t}$ channel has similar discriminating power.

4.8 A non-minimal composite Higgs model

In the previous pages we have seen that the MCHM can not only alleviate the problems related to the elementary nature of the Higgs boson, but also provide plausible explanations to the (slight) deviations that have been found both at the Tevatron and the LHC colliders. As an example, we have discussed the recent measurements of the $ht\bar{t}$ production cross section measured by the ATLAS and CMS experiments in Section 4.5.1 and the observed deviation of $A_{FB}^{t\bar{t}}$ and their implications at the LHC in the last section. However, there are other physical observations that can not be accommodated in the framework of the MCHM. The well-established evidence of DM [213] is a good example of this. In such a case, the MCHM can be extended to the non-MCHM $SO(6)/SO(5)$ [214], for which an extra pNGB, η, is present in the spectrum fulfilling the requirements of a weak-interacting massive particle (WIMP) if the SM fermions are embedded in appropriate representations of $SO(6)$ [215]. In this section, instead, we focus on a different observed discrepancy, namely the recent diphoton excess, which can be in fact a hint of an extended Higgs sector. Indeed, recent fits to a combination of ATLAS, CMS and Tevatron data on Higgs searches, seem to point to an excess in $h \to \gamma\gamma$ events by a factor of $\sim 1 - 1.5$ with respect to the SM prediction, while they agree pretty well in the rest of the channels [21]. Although the excess is not yet significant, it could mean an intriguing source of NP. For this reason, many groups have proposed explanations to this discrepancy, through the introduction of new uncolored (in order to not contribute to the GF channel) particles which, when running in the loops, can increase the $\Gamma(h \to \gamma\gamma)$ width, while keeping the rest of the channels invariant [198, 218–258]. In this way, the BR of the Higgs into diphotons can be easily increased up to the current measurement $\sim 1.2 \times \mathrm{BR}^{SM}$ without conflicting with the others channels. These new particles could be both uncolored scalars or leptons. In any case, the NP contribution is suppressed by the mass scale of the new particle running in the loop. Thus, the lighter these particles are, the larger the contribution is. This

[21] Actually, the excess is now present only in the ATLAS results [216]. In the first ATLAS [217] and CMS measurements [153], however, this excess was also pointed out.

requirement can be successfully achieved in the context of CHMs, given that the Higgs boson, as well as possible new scalar states, arise as a pNGB of a new strongly interacting sector and are therefore naturally light. However, we should consider non-MCHMs in order to get charged scalar states, like $SO(6)/SO(4)\times SO(2)$ 2HDM [259]. Spherical CHMs, based on $SO(n+1)/SO(n)$ can also explain this excess, whenever $n+1$ is such that possible anomalous representations appear. In that case, the Higgs boson can mix with the new extra singlet scalars which, although they are not charged, can still couple to pair of photons through $\eta F_{\mu\nu}F^{\mu\nu}$ interactions coming from anomalies in the strong sector [214, 260]. Here, however, we present a new CHM based on the symmetry breaking pattern of $SO(7)$ to G_2 [6]. In this case, an uncolored $SU(2)_L$ singlet charged scalar, $\kappa^\pm$, as well as a neutral singlet scalar, η, appear in the spectrum in addition to the SM Higgs doublet. As we show below, loops of $\kappa^\pm$ can substantially modify the h BR to photons, thus explaining the observed anomaly. This part of the text is then structured as follows. In Section 4.8.1 we introduce the group structure of the model and obtain the two-derivative scalar interactions described by the non-linear sigma model lagrangian. In Section 4.8.2 we also discuss the embedding of the SM fermions into representations of the whole group and construct the lagrangian quadratic in the fermion fields, in analogy to what we already did in Section 4.4 for the MCHM. Finally, in Section 4.8.4 we briefly discuss the constraints and phenomenological implications of this model at the LHC.

4.8.1 Scalar sector

The model is based on the symmetry breaking pattern $SO(7)/G_2$, which can be achieved through the VEV of a field Φ transforming in the spinor representation **8** of $SO(7)$. The 21 generators $J_{mn}=-J_{nm}$ of $SO(7)$ and the G_2 subgroup generators in this representation are detailed in Appendix D. The generators correspond to the sets F_i and M_i that are there explicitly shown. The rest of the generators, the set N_i, generate the coset manifold. They transform in the **7** representation of G_2, and decompose under the subgroup $SU(2)_L\times SU(2)_R$ into $(\mathbf{2},\mathbf{2})+(1,\mathbf{3})$. Some of the relevant commutation relations are $[F_i,F_j]=i\epsilon^{ijk}F_k$, $[M_i,M_j]=\frac{i}{\sqrt{3}}\epsilon^{ijk}M_k$, $[F_i,M_j]=0$, $[F_i,N_j]=0$, $[M_3,N_3]=0$, $[M_3,N^\pm]=\mp N^\pm$, $N^\pm=N_1\pm iN_2$, where $j=1,2,3$. All the $SO(7)$ generators of Appendix D are normalized according to $\mathrm{tr}(T_iT_j)=\delta_{ij}$ (note that the $SU(2)_R$ group is generated from $\sqrt{3}M_i$ rather than M_i alone). From these equations, we explicitly

see that $N_{1,2,3}$ are not charged under $SU(2)_L$ and we get their hypercharges. In fact, these generators transform in the $(\mathbf{1},\mathbf{3})$ representation mentioned above (and so do the corresponding NGBs), while the rest of them live in the $(\mathbf{2},\mathbf{2})$, giving rise to the Higgs doublet. Thus, the physical pNGB spectrum is composed of the Higgs boson h, a neutral scalar η and a singly charged scalar $\kappa^{\pm}$. Thus, according to the CCWZ formalism (see Section 4.2), the scalar lagrangian is described by a non-linear sigma model over $SO(7)/G_2$. Using the explicit expression of Π in Appendix D, we can write the lagrangian in terms of charge eigenstate fields up to order $\mathcal{O}(1/f^2)$ interactions:

$$\begin{aligned}\mathcal{L} = &\frac{1}{2}(\partial_\mu h)^2 + \frac{1}{2}(\partial_\mu \eta)^2 + (\partial_\mu \kappa)^2 + \frac{1}{2f^2}\left[\partial_\mu(\phi^\dagger\phi)\right]^2 + \frac{1}{2f^2}\eta^2(\partial_\mu\eta)^2 \\ &+ \frac{1}{2f^2}\partial_\mu(\phi^\dagger\phi)\partial^\mu\eta^2 + \frac{1}{2f^2}\left[\partial_\mu(\kappa^+\kappa^-)\right]^2 + \frac{1}{2f^2}\partial_\mu(\phi^\dagger\phi)\partial^\mu(\kappa^+\kappa^-) + \frac{1}{2f^2}\partial_\mu\eta^2\partial^\mu(\kappa^+\kappa^-),\end{aligned} \tag{4.51}$$

where, as before, $\phi^T = (\phi^+, \phi^0)$ and $\kappa^{\pm} = (k_1 \pm i k_2)/\sqrt{2}$.

4.8.2 Fermion spectrum

As in the case of the MCHM, in order to construct the effective lagrangian for the fermions, we extend the symmetry group to $SO(7)\times U(1)_X$ and embed the SM fermions in multiplets of this group [143], with the proper X charge. Two appropriate representations of the whole group $SO(7)$ are the fundamental $\mathbf{7}$ and the spinorial $\mathbf{8}$ representations. Under the unbroken subgroup G_2, the first one remains as $\mathbf{7}$ while the second decomposes as $1+\mathbf{7}$. We work in the latter scenario because, as we discuss later, the presence of a whole G_2 singlet is necessary to give a mass to the top quark. Under the custodial symmetry group $SU(2)_L\times SU(2)_R$, the $\mathbf{8}$ decomposes as $(1,1)+(\mathbf{2},\mathbf{2})+(1,\mathbf{3})$. The SM elementary fermions mix, therefore, with multiplets of $SO(7)$ with charges $\mathbf{8}_{2/3}$ and $\mathbf{8}_{-1/3}$. We pictorially [22] represent the $\mathbf{8}$ as

$$\mathbf{8}_{2/3} = \begin{bmatrix} (2,2) = (q, Q) \\ (1,3) = (X, t', b)^T \\ (1,1) = t \end{bmatrix}, \qquad \mathbf{8}_{-1/3} = \begin{bmatrix} (2,2) = (Q', q') \\ (1,3) = (t'', b'', Y)^T \\ (1,1) = b' \end{bmatrix}, \tag{4.52}$$

[22] Pictorially in the sense that we are not writing the generators of Appendix D in the canonical base of equation (4.52). Thus, for instance, in the base used for the generators, the custodial $(1,1)$ of the whole 8-dimensional space is not $(0,0,0,0,0,0,0,1)^T$ but rather $(0,1,0,1,0,-1,0,-1)^T$. Equations (4.53), (4.54) and (4.55) should then be clear in light of this consideration.

where the decomposition into irreducible representations of $SU(2)_L \times SU(2)_R$ is manifest. Let us discuss how the SM fields have to be divided among the different entries. For this purpose, in the following we consider that only the top and bottom quarks are composite enough and that is why we write t and b in the previous equation. In order to give a mass m_b to the bottom quark, both the LH components of the quarks along q'_L as well as the component of the bottom quark along b'_R should be different from zero. The component along q'_L, however, has to be small enough to protect the $Zb_L\bar{b}_L$ coupling [261], and then the component of b along b'_R should be near one to naturally get a non-negligible m_b. Thus, the component of the bottom quark along b_R can no longer be large. This, however, only affects the $\kappa^{\pm}$ decay width. b''_R can be fixed to zero without any conflict. On the other hand, the component of the top quark along t_R should be nearly one to allow a naturally large top mass, making the component along t'_R rather small. We choose a prescription consisting of two $\mathbf{8}_{2/3}$ fields, Q_L and T_R. The SM doublets can be embedded in the $(\mathbf{2},\mathbf{2})$ of Q_L, where the $Zb_L\bar{b}_L$ coupling becomes protected as mentioned above:

$$Q_L = \frac{1}{\sqrt{8}}(it_L - b_L, t_L - ib_L, -it_L - b_L, t_L + ib_L, it_L + b_L, t_L + ib_L, b_L - it_L, t_L - ib_L)^T. \quad (4.53)$$

The T_R field can contain the t_R singlet in both the $(1,1)$ and the neutral part of $(1,\mathbf{3})$, proportional to $\cos\theta$ and $\sin\theta$ respectively, and also a small component (parametrized by some parameter ϵ) of the b_R field in the same $(1,\mathbf{3})$:

$$T_R = \frac{1}{2}(s_\theta t_R, c_\theta t_R, -s_\theta t_R, c_\theta t_R, -s_\theta t_R, -c_\theta t_R, s_\theta t_R, -c_\theta t_R)^T + \epsilon B_R^T, \quad (4.54)$$

with

$$B_R = \frac{1}{\sqrt{8}}(ib_R, b_R, ib_R, -b_R, ib_R, b_R, ib_R, -b_R)^T. \quad (4.55)$$

Although the embedding of b_R in B_R does not give a mass to the bottom quark, ϵ has to be different from zero. Otherwise, $\kappa^{\pm}$ appears always in pairs and then becomes stable, giving rise to undesirable consequences [262–265]. The hypercharge Y of the different elementary fields is $Y = T_R^3 + Q_X$, where T_R^3 refers to the third generator of $SU(2)_R$. Note that, as we see below, whenever $\sin\theta$ is different from zero, a trilinear coupling for η is generated, allowing it to decay into pairs of fermions. The lagrangian for the

fermions and their interactions with the pNGBs can be written as

$$\begin{aligned}\mathcal{L}_{\text{eff}} =& \bar{T}_R \not{p} \left(\Pi^0_{t_R} + \tilde{\Pi}^1_{t_R} \Sigma^T \Sigma\right) T_R + \bar{Q}_L \not{p} \left(\Pi^0_{qL} + \Pi^1_{q_L} \Sigma^T \Sigma\right) Q_L \\ &+ \frac{1}{16} f \left(\tilde{M}_t \, \bar{Q}_L \Sigma^T \Sigma T_R + \text{h.c.}\right),\end{aligned} \tag{4.56}$$

where $\Sigma = \exp\left[-i\Pi(x)/f\right]\Sigma_0$, and $\Sigma_0 = (0,1,0,1,0,-1,0,-1)^T/2$ is the vacuum of Φ in the representation we are considering [266–268]. The explicit expression of $\Pi(x)$ in this case is given in Appendix D. After expanding this lagrangian up to $\mathcal{O}(1/f^2)$ we get, in the unitary gauge, the following effective lagrangian for the quarks:

$$\begin{aligned}\mathcal{L}_{\text{eff}} =& \, \bar{t}_R \not{p} \left(\Pi^0_{t_R} + \tilde{\Pi}^1_{t_R} \left[\cos^2\theta + \sin^2\theta \frac{\eta^2}{f^2} - \frac{c_\theta^2}{f^2}\left(h^2 + \eta^2 + 2\kappa^+\kappa^-\right) + 2\cos\theta \sin\theta \frac{\eta}{f}\right]\right) t_R \\ &+ \bar{t}_L \not{p} \left(\Pi^0_{q_L} + 2\Pi^1_{q_L} \frac{h^2}{f^2}\right) t_L + \Pi^0_{q_L} \bar{b}_L \not{p} b_L + \epsilon^2 \bar{b}_R \not{p} \left(\Pi^0_{t_R} + \frac{\tilde{\Pi}^1_{t_R}}{f^2} \kappa^+\kappa^-\right) b_R \\ &+ \left\{ \Pi^1_{t_R} \epsilon \cos\theta \bar{t}_R \not{p} \frac{\kappa^+}{f} \left(1 + \tan\theta \frac{\eta}{f}\right) b_R + \epsilon \frac{\tilde{M}_t}{\sqrt{2}} \bar{t}_L b_R h \frac{\kappa^+}{f} \right. \\ &\left. + \frac{\tilde{M}_t}{\sqrt{2}} \cos\theta \, \bar{t}_L t_R h \left[1 - \frac{1}{2f^2}\left(h^2 + \eta^2 + 2\kappa^+\kappa^-\right) + \tan\theta \, \frac{\eta}{f}\right] + \text{h.c.}\right\}.\end{aligned} \tag{4.57}$$

After EWSB, we obtain trilinear couplings of $\kappa^\pm$ to the fermions whenever ϵ is different from zero, that allows $\kappa^\pm$ to decay into SM particles. Similarly, if $\cos\theta = 1$ we get a symmetry $\eta \to -\eta$ that does not allow η to decay into pair of fermions [23]. Thus, hereafter we assume that $\epsilon \neq 0$ and $\cos\theta \neq 1$. Since the $\kappa^\pm$ are charged under T^3_R, they interact not only with the SM fermions through the lagrangian of equation (4.57), but also with the Z and γ bosons. These interactions are fixed by the gauge symmetry. They are given by the coupling of A_μ and Z_μ to the neutral current $J_\mu = i(\kappa^- \, partial_\mu \kappa^+ - \kappa^+ \partial_\mu \kappa^-)$.

Besides, as we already discussed in the MCHM, the Higgs interactions with the SM particles receive corrections of order $\xi = (v/f)^2$ [24]. In order to see that, note

[23] The $\eta \to -\eta$ symmetry is also present in the scalar lagrangian up to $\mathcal{O}(1/f^2)$, as can be directly probed regarding equation 4.51. Thus, if $\cos\theta = 1$, η provides a DM candidate [6]. This choice is, in fact, radiatively stable.

[24] In this case, $v = \langle h \rangle \sim 246$ GeV, because we are considering only up to $\mathcal{O}(1/f^2)$ interactions.

that the field h in the equations above is not written in the canonical way, since after EWSB we get new contributions to the Higgs field kinetic term coming from the $\mathcal{O}_H$ operator $\mathcal{O}_H = \frac{c_H}{2f^2}(\partial_\mu(\phi^\dagger\phi))^2$ typical of the strongly-interacting light Higgs (SILH) model [269], where the c_H parameter turns out to be $c_H = 1$ in this case. So, we should perform the following h field redefinition in order to get it canonically normalized: $h = \left[1 - \frac{\xi}{2} + \mathcal{O}(\xi^2)\right] h_{\text{phys}} + v$. Thus, the coupling of h to the gauge bosons W and Z and the fermions change. In our case, this change is the same as the MHCM5 one (see Section 4.4) at this order in the $1/f$ expansion.

4.8.3 The $h \to \gamma\gamma$ deviation

Once we have the fermionic lagrangian, we can compute the radiatively generated potential. We refer to [6] for the details, while here we concentrate only on the $\lambda_{h\kappa} h^2 \kappa^+ \kappa^-$ term that is generated as a part of this potential. It can be shown that negative values of $\lambda_{h\kappa}$ are allowed if one requires the EW VEV to be $\langle h \rangle = \sqrt{\mu_h^2/\lambda_h}$, $\langle \eta \rangle = \langle \kappa \rangle = 0$, being $-\mu_h^2$ and λ_h the quadratic and quartic Higgs terms respectively. And this is, in fact, what we need to increase the $\gamma\gamma$ rate. After EWSB, the term $\lambda_{h\kappa} h^2 \kappa^+ \kappa^-$ gives rise to the trilinear coupling $2\lambda_{h\kappa} v h \kappa^+ \kappa^-$. In general, the addition of a uncolored singly charged scalar particle S modifies the $\gamma\gamma$ width in the following way [246]:

$$\Gamma(h \to \gamma\gamma) = \frac{\alpha^2 m_h^2}{1024\pi^3} \left| \frac{g_{hWW}}{m_W^2} A_1(\tau_W) + \frac{8 g_{ht\bar{t}}}{3 m_t} A_{1/2}(\tau_t) + \frac{g_{hSS}}{m_S^2} A_0(\tau_S) \right|^2 , \tag{4.58}$$

when the only relevant SM considered contributions come from t and W loops. g_{hWW} and g_{htt} are the coupling constants of both W and t to the Higgs boson, which in the SM case become $g^2/2$ and $\lambda_t/\sqrt{2}$ respectively, while in CHMs they receive deviations of order ξ. m_S stands for the mass of the new scalar, $\tau_i \equiv 4m_i^2/m_h^2$ and A_1, A_0 and $A_{1/2}$ are defined as (see Appendix A of reference [246]):

$$\begin{aligned} A_0(x) &= -x^2 \left[x^{-1} - f(x^{-1})\right] , \\ A_1(x) &= -x^2 \left[2x^{-2} + 3x^{-1} + 3(2x^{-1} - 1) f(x^{-1})\right] , \\ A_{1/2}(x) &= 2x^2 \left[x^{-1} + (x^{-1} - 1) f(x^{-1})\right] , \end{aligned} \tag{4.59}$$

with $f(x) = \arcsin^2 \sqrt{x}$. In Figure 4.25 we show, for $\xi = 0$ (SM-like couplings), the $\Gamma/\Gamma^{SM}(h \to \gamma\gamma)$ as a function of both m_κ and $\lambda_{h\kappa}$. $\Gamma(h \to \gamma\gamma)$ is reduced by 10% for

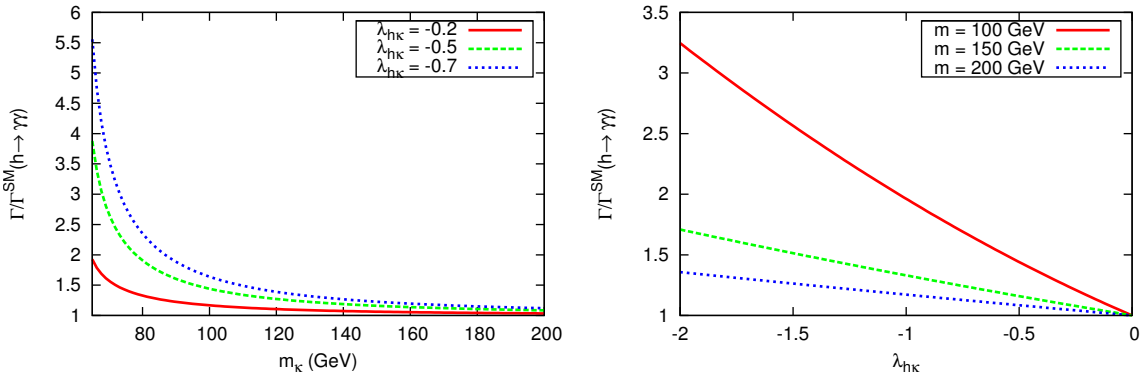

Figure 4.25: Left: $\Gamma/\Gamma^{SM}(h \to \gamma\gamma)$ in this model as a function of the mass of the new scalar $\kappa^{\pm}$ for different fixed $\lambda_{h\kappa}$ couplings. Right: $\Gamma/\Gamma^{SM}(h \to \gamma\gamma)$ as a function of $\lambda_{h\kappa}$ for different masses of $\kappa^{\pm}$. We are neglecting ξ corrections in any case, so that the couplings are SM-like.

$\xi \sim 0.25$, but then the other channels become also modified [269].

4.8.4 Constraints and collider implications

The phenomenology of $\kappa^{\pm}$ can be very different depending on its mass. For large masses, it can decay into $t\bar{b}(b\bar{t})$ pairs, and it can then been looked for at the LHC in the $t\bar{t}b\bar{b}$ final state coming from $\kappa^{+}\kappa^{-}$ production, since its production cross section is completely determined, up to ξ factors, by gauge interactions mediated by Z/γ (see Figure 4.26). These large masses, however, require a much larger coupling $\lambda_{h\kappa}$ in the term $h^2\kappa^{+}\kappa^{-}$ to explain the observed discrepancy in BR$(h \to \gamma\gamma)$. Moreover, searches of W' decaying to a top and a bottom quarks can impose important constraints on the mass of the $\kappa^{\pm}$ boson. The most important experimental constraints on these searches come from ATLAS [270], CMS [271], and also from CDF [272] and D0 experiments [273]. Both ATLAS and CMS put bounds on the mass of the W' near the 2 TeV for a $W'tb$ coupling $g' \sim g_w$. In our case, the amplitude for the production of $\kappa^{\pm}$ and decay into tb is proportional to $\xi \sim 0.1$, to be compared with $g_w^2 \sim 0.5$, and can still be very significant (unless the free coupling between $\kappa^{\pm}$ and the fermions is very small) depending on how the analyses affect the scalar signal compared to the vector one. For lower masses, where the $\gamma\gamma$ excess can be successfully explained, $\kappa^{\pm}$ can no longer decay into on-shell t and b quarks, and the decay through virtual heavy quarks is very small. Experiments

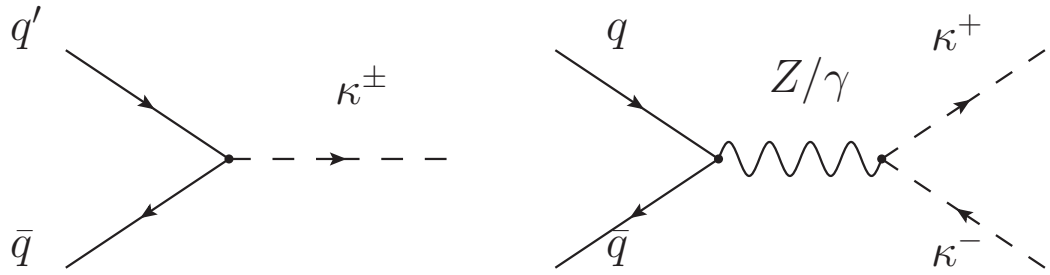

Figure 4.26: Main $\kappa^{\pm}$ production channels at the LHC. The coupling in the left plot is of order v/f and model-dependent, whereas the one in the diagram on the right panel is fixed by the gauge invariance.

at both LEP and LHC found limits on the mass $m_{H^{\pm}}$ of a charged SUSY-like scalar in the region 90 GeV $< m_{H^{\pm}} <$ 160 GeV, depending on its properties [43]. The decay into leptons and neutrinos is also strongly constrained by W' searches [274, 275], and the decay into jets [171, 276] is completely contaminated by the QCD background.

The η phenomenology is even more cumbersome, given that η is not charged under the SM gauge group. According to equation 4.57, η couples linearly to fermions but with a coupling suppressed by a factor $1/f$ through the operator $\mathcal{O} = \frac{cY}{f}\eta\bar{\psi}_L\phi\psi_R$ (other dimension 5 operators are equivalent to this one via the classical equations of motion), where Y is the fermion Yukawa coupling and c is expected to be order one. The main standard production mechanism for η is then GF but with a rate that is suppressed by a factor v^2/f^2 with respect to the SM Higgs GF production. Thus, for masses above twice the top mass, the GF production of η and its subsequent decay into $t\bar{t}$ is expected to be the main channel for the discovery of the singlet. However, for masses below $\sim$ 350 GeV [25], the main decay of η is into a $b\bar{b}$ final state, which suffers from a huge QCD background.

In this case, however, one can expect that a process similar to the one we have considered in Section 4.6, with the replacement of h with η,

$$pp \to G^* \to B_\eta \bar{b} + \bar{B}_\eta b \to \eta b\bar{b} \to 4b, \tag{4.60}$$

can provide the leading channel for the discovery of such a composite singlet.

[25] Remember that, due to their pNGB nature, composite scalars prefer to be light.

Chapter 5

Lepton number violating scalars

As we have argued in previous sections, the naturalness problem, as well as the puzzling quark mass hierarchy, can be alleviated if the Higgs boson is a composite state, whose dynamics is described by an extended scalar sector containing new effective interactions. We have then unraveled the phenomenological implications of such a scenario at the LHC. Nevertheless, not only these problems suggest that the minimal SM Higgs sector should be enlarged. The well-established neutrino masses [43], in fact, are the only clear experimental signal of physics beyond the SM so far, if we obviate the cosmological evidence of DM. And, as we assert below, they can be accommodated by an extended scalar sector involving LNV interactions.

Indeed, neutrinos are massless in the SM because they have no RH counterparts, ν_{Ri}, to form Dirac masses and LN is an accidental symmetry protecting them from acquire Majorana masses [277]. Hence, in order to describe neutrino masses, we have to add new degrees of freedom to the SM: either RH neutrinos with the corresponding Yukawa couplings giving Dirac masses to neutrinos after EWSB: $\mathcal{L}^{Y}_{m_\nu} = -y_{ij}\overline{L_{Li}}\nu_{Rj}\tilde{\phi} +$ h.c. $\rightarrow -y_{ij}(v/\sqrt{2})\overline{\nu_{Li}}\nu_{Rj} +$ h.c., with $v \sim 246$ GeV the Higgs VEV; or new (heavy) fields, which in particular may be also ν_{Ri}, with couplings violating LN explicitly or spontaneously and generating Majorana masses for the SM neutrinos at some given order in perturbation theory. In this case, once the heavy modes are integrated out, the model is described at low energy by an effective Lagrangian with extra higher-order operators, the one of lowest dimension being the Weinberg operator [278], $\mathcal{O}^{(5)} = (\overline{L^c_L}\tilde{\phi}^*)(\tilde{\phi}^\dagger L_L)$, parametrizing the neutrino Majorana masses: $\mathcal{L}^{(5)}_{m_\nu} = -c^{(5)}_{ij}\mathcal{O}^{(5)}_{ij}/\Lambda +$

h.c. $\to -(c_{ij}^{(5)} v^2/2\Lambda)\overline{\nu_{Li}^c}\nu_{Lj} + \text{h.c.}$, with Λ the scale of NP [1]. In such a case there are not new light degrees of freedom to start with; being the simplest realizations characterized at low energy by the very tiny LNV induced by the neutrino Majorana masses, $(m_\nu)_{ij} = c_{ij}^{(5)} v^2/\Lambda \sim 0.1$ eV, whose measurement is the purpose of the next generation of $0\nu\beta\beta$ experiments [279] [2].

However, the relevant question in the LHC era is whether LNV is at the LHC reach or not. This is to ask if there are new particles with masses $\Lambda \sim$ TeV (and then $c_{ij}^{(5)} \sim 10^{-11}$) with observable LNV signatures [282] [3]. There is a wide literature dealing with the simplest realizations of this scenario, which are referred to as *see-saw* mechanisms of type I, II and III and obtained extending the SM with RH neutrinos [75–79], a scalar triplet [80–85] and vector-like fermion triplets [86, 87], respectively, as we already commented in Section 2.4.2 .

In order to assert the violation of LN at the LHC it is enough to observe final states with non-zero LN, given that the LN of the initial state (pp) vanishes. This means in practice to observe events with an excess of leptons or anti-leptons. First, however, several general comments are worth to emphasize: (i) LNV is minuscule, and hence the production of LNV particles at the LHC must be very suppressed or their decay very slow. As in the former case these are not observable, they must transform non-trivially under the SM gauge symmetry and hence be produced with EW strength [4]. (ii) Thereby, LN must be violated in the decays of the new heavy particles, and thus they are required to have at least two dominant channels with different LN [5]. (iii) We

[1] Note that we are here using Λ instead of f for the scale of NP, to make clear that we are considering weakly-coupled physics now, rather than a new strong interaction.

[2] The leading contribution to $0\nu\beta\beta$ may come from other (higher-order) operators in very elaborated models [70–73, 280, 281].

[3] If the observed baryon asymmetry in the universe is originated from leptogenesis, LNV must be at work at some energy too [283].

[4] Obviously, singlets can be produced through mixing with non-singlet states, but this mechanism is in general suppressed by the corresponding mixing angles. An example is heavy neutrino production through mixing with SM leptons [284–286], which is suppressed because the corresponding mixing angles are bounded to be small by EWPD [287]. We in addition assume that new particles do not carry color charge.

[5] Majorana fermions are charge self-conjugated, so that if they decay into a final state with non-zero LN, they do also decay into the charge-conjugated state with opposite LN.

restrict ourselves to SM extensions with LNV in the scalar sector because, as stressed in 2.3, the discovery of the Higgs boson proves the fundamental character of the SM scalar sector at low energy which, however, remains the least known sector of the model and thus NP is likely related to it. In summary, the experimental observation of neutrino masses together with the outstanding LHC performance make the search for LNV scalars (eventually contributing to neutrino masses) especially timely.

Thus, in Section 5.1 we study the scalar multiplets that have renormalizable LNV interactions. We show that the only ones that are potentially observable at the LHC contain doubly-charged components like the *see-saw* of type II. Given that a fundamental renormalizable theory is likely far from the reach of the LHC, it is worth considering whether the particles of such a theory can give rise to similar LNV interactions mediated by doubly-charged scalars at a lower scale after integrating them out. That is to say, whether new scalar multiplets can have effective LNV interactions. In Section 5.2 we show that, in general, the larger their isospin, the higher the dimension of the operators parametrizing the heavy scalar decay and hence smaller their decay rate. This however does not play any crucial role, given that LNV interactions are highly suppressed by themselves, as we pointed out in (i). The production mechanisms for these particles are discussed in Section 5.3. The dominant mechanism for doubly-charged scalar pair and associated production is through the $s-$channel exchange of EW gauge bosons, while VBF contributions stay below 10% for the scalar masses of interest. On another front, the observation of LNV mediated by doubly-charged scalars requires the BR into two same-sign leptons to be comparable with the BR into gauge bosons. In simple models the region of parameter space allowed by this condition is small. In general, one of the two couplings is larger than the other and therefore the corresponding decay dominates, as we also discuss in Section 5.3. However, both decays can naturally have a similar rate in more elaborated models [70–74, 288–292].

In Sections 5.4 and 5.5 we describe the analyses performed by the ATLAS [293] and CMS [90] experiments, that we extend to estimate the current and future bounds on LNV processes mediated by doubly-charged scalars. In particular, we provide tables with the efficiencies for the reconstruction of the different decay modes, which allow us to derive the corresponding limits on doubly-charged scalar production for any set of BRs and hence model. Once LNV is observed the question is which its origin is. In

the case of the doubly-charged scalar production under consideration one would like to determine the type of multiplet the doubly-charged scalar belongs to. This can be done sampling appropriately the events with four and three isolated leptons, as we describe in detail in Section 5.6.

5.1 Renormalizable LNV interactions

If LN is violated in the scalar sector, new scalars coupling to leptons with non-vanishing LN must extend the SM. Indeed, the only renormalizable interactions involving scalars and leptons are given by Yukawa-like terms. The only lepton bilinears with non-vanishing LN available in the SM are $\overline{L_L^c} L_L$, $\overline{l_R^c} l_R$ and $\overline{L_L^c} l_R$, corresponding to the three different chirality pairings containing all of them the product of two same-sign charged leptons $l^- l^-$ [6]. In fact, we can restrict ourselves to the first two combinations because the operators involving the third one are not independent of those built with the first two: the third combination $\overline{L_L^c} l_R$ requires a γ_μ insertion because of the fermions' chirality, and hence the presence of a covariant derivative to ensure the operator is Lorentz invariant. Then, using integration by parts and the equations of motion, the corresponding operators can be seen to be equivalent to the ones involving $\overline{L_L^c} L_L$ and $\overline{l_R^c} l_R$. The two independent lepton bilinears can be coupled to build an $SU(2)_L$ triplet with hypercharge $Y = -1$, a singlet with $Y = -2$ or a singlet with $Y = -1$. (Of course, a flip on the sign of the hypercharge Y can be obtained in any case considering the charge-conjugated fields). This implies that the only LNV scalars that can be added in a renormalizable way to the minimal Higgs sector of the SM are an $SU(2)_L$ triplet $\Delta = (\Delta^{++}, \Delta^+, \Delta^0)^T$ with $Y = 1$ [80–85], a singlet κ^{++} with $Y = 2$ [70, 73, 294] and a singlet π^+ with $Y = 1$. The first two cases contain doubly-charged scalars [7], while the last one contains only a singly-charged scalar. The only dimension-four gauge invariant operators coupling κ^{++} and the doubly-charged component of Δ to a pair of same-sign charged leptons are given by

$$\mathcal{O}_\kappa = \overline{l_R^c} l_R \kappa^{++}; \qquad \mathcal{O}_\Delta = (\overline{\tilde{L}_L} \tau^a L_L) M_{ab}^\Delta \Delta^b, \quad \text{with } a, b = 1, 0, -1; \tag{5.1}$$

[6] Remember that charged leptons are denoted by $l(\ell)$ when tau leptons are (not) included.

[7] The first one is actually the *see-saw* of type II.

where, as we commented in Section 2, M^{Δ} is a three times three matrix with non-zero entries only for $a + b = 0$:

$$M^{\Delta}_{ab} = \begin{pmatrix} 0 & 0 & 1 \\ 0 & 1 & 0 \\ 1 & 0 & 0 \end{pmatrix}, \tag{5.2}$$

and τ^a are the Pauli matrices in the spherical basis, $A^{+1} = -\frac{1}{\sqrt{2}}(A_1 - iA_2), A^0 = A_3, A^{-1} = \frac{1}{\sqrt{2}}(A_1 + iA_2)$, times the Clebsch-Gordan coefficients $\mathrm{C}^{1\times 1\to 0}_{a,-a}$, up to a global factor and sign: $\tau^{\pm 1} = \pm(\sigma_1 \mp i\sigma_2)/2,\ \tau^0 = \sigma_3/\sqrt{2}$.

π^+ (resp. π^-) can eventually decay into $e^+\nu$ (resp. $e^-\overline{\nu}$), what in practice means that we are not able to distinguish its LNV interactions, given that we cannot differentiate between neutrinos and anti-neutrinos at the LHC for both manifest as E_T^{miss} in the detectors. Moreover, the observation of LNV at the LHC can be only established if the doubly-charged scalars decay also into SM boson pairs, giving rise to final states with vanishing LN. Otherwise, the coupling to same-sign charged leptons alone fixes the scalar LN equal to -2, but does not stand for LNV. Indeed, the only other possible two-body decay into SM particles of a doubly-charged scalar is into two W bosons, if we assume that the mass splitting between the different components of the multiplet is small and hence the mixing with heavier scalar multiplets and with the SM Higgs (otherwise, cascade decays within the multiplet, of EW strength, are overwhelming, and in addition the final fermions are softer and do not exhibit the resonant behavior in the same-sign dilepton channel). In the scalar triplet case the decay $\Delta^{\pm\pm} \to W^{\pm}W^{\pm}$ arises after the LN breaking by the (small) non-zero Δ^0 VEV. In the singlet case this coupling must appear through mixing with other (heavier) scalar multiplets with diboson couplings.

We know, however, that a fundamental renormalizable theory is likely at an energy scale much larger that those that are being (and will be) tested at the LHC. Thus, if some NP is observed at the LHC it will not be necessarily part of a renormalizable theory. Instead, new doubly-charged scalars at the TeV scale could be observable at the LHC if they decay into same-sign leptons through their mixing with any Δ^{++} or κ^{++} at a higher scale Λ, as it is schematically shown in Figure 5.1. The integration out of the scale Λ gives rise to a tower of effective operators mediating LNV decays, which are then suppressed by factors of Λ. Thus, we assume that there is a more fundamental

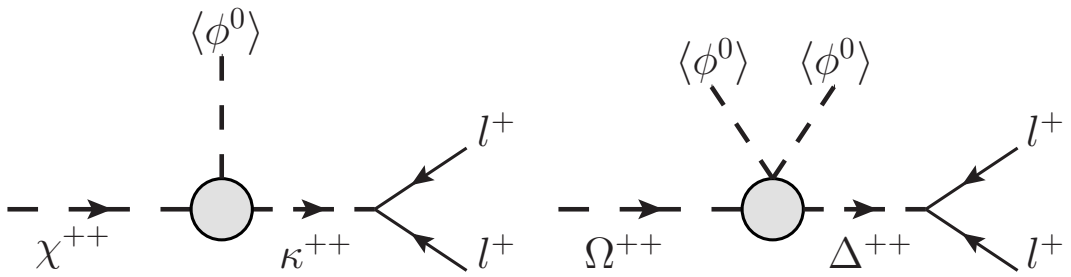

Figure 5.1: Left: Decay of the doubly-charged component of an $SU(2)_L$ doublet χ with $Y = 3/2$ into same-sign leptons through its mixing with a singlet κ^{++} with $Y = 2$ mediated by one Higgs field ϕ. Right: Decay of the doubly-charged component of an $SU(2)_L$ quintuplet Ω with $Y = 0$ into same-sign leptons through its mixing with the Δ^{++} component of a triplet with $Y = 1$ mediated by two Higgs fields.

theory reducing at lower energy to the SM plus an extra scalar multiplet H [8] near the TeV scale with LN= -2 and a doubly-charged component H^{++}. Hence, its isospin T and hypercharge Y must fulfill

$$T^{\mathrm{H}} \geq |T_3^{\mathrm{H}^{++}} = 2 - Y^{\mathrm{H}}|. \tag{5.3}$$

We extend the SM with an extra TeV scalar multiplet at a time, neglecting possible mixing effects with other heavier scalar multiplets (except to allow for the decay of the TeV scalar multiplet into gauge bosons as previously discussed). In the following section we describe the details of such scalars and their effective LNV interactions.

5.2 Effective LNV interactions

In general, for any pair of isospin and hypercharge assignments satisfying relation (5.3), there is a tower of gauge invariant operators with vanishing LN involving H, any of the two bilinears with LN = 2, $\overline{L_L^c} L_L$ or $\overline{l_R^c} l_R$, and an increasing number of Higgs doublets $\phi(\tilde{\phi})$. This reflects the fact that any $SU(2)_L \times U(1)_Y$ representation satisfying equation (5.3) can be obtained from the Clebsch-Gordan series of the product of a large enough

[8] In the text generic scalar multiplets are denoted by H and their doubly-charged component by $H^{\pm\pm}$.

number of fundamental representations $\phi(\tilde{\phi})$, with $T = 1/2$ and $Y = 1/2(-1/2)$ [8]. In particular, one can correlate the operators involving $\overline{\tilde{L}_L}\tau^a L_L$, with $T = 1$ and $Y = -1$, to those involving $\overline{l_R^c} l_R$, with $T = 0$ and $Y = -2$, contracting the former with $\phi^\dagger \tau^{-a} \tilde{\phi}$; and vice-versa multiplying by $\tilde{\phi}^\dagger \tau^a \phi$. In general, however, for any given H only the operators of lowest dimension matter because they are the ones formally giving the largest contributions to the dileptonic H^{++} decays after EWSB.

In the phenomenological studies, we restrict ourselves to scalars multiplets with at most doubly-charged components:

$$T^{\rm H} = T_3^{\rm H^{++}} \leq 2. \tag{5.4}$$

In fact, this exhausts the list of multiplets that can mix with κ^{++} and/or Δ trough the Higgs in a renormalizable way [9]. They are given by a doublet $\chi = (\chi^{++}, \chi^+)^T$ with $Y = 3/2$, a quadruplet $\Sigma = (\Sigma^{++}, \Sigma^+, \Sigma^0, \Sigma'^-)^T$ with $Y = 1/2$ and a quintuplet —which we assume to be real— $\Omega = (\Omega^{++}, \Omega^+, \Omega^0, \Omega^-, \Omega^{--})^T$ with $Y = 0$. The lowest order gauge invariant operators coupling the doubly-charged component of these multiplets to a pair of same-sign charged leptons after EWSB are of dimension five for χ and Σ, and six for Ω:

$$\begin{aligned}
&\mathcal{O}_\chi^{(1)} = \overline{l_R^c} l_R (\tilde{\phi}^\dagger \chi); \qquad \mathcal{O}_\chi^{(2)} = (\overline{\tilde{L}_L}\tau^a L_L) M^\chi_{ab} (\phi^\dagger \tau^b \chi), \quad \text{with } \ a, b = 1, 0, -1; \\
&\mathcal{O}_\Sigma = (\overline{\tilde{L}_L}\tau^a L_L) M^\Sigma_{c,ab} \phi^b \Sigma^c, \quad \text{with } \ a = 1, 0, -1, \ \ b = \pm\frac{1}{2}, \ \ c = \frac{3}{2}, \frac{1}{2}, -\frac{1}{2}, -\frac{3}{2}; \\
&\mathcal{O}_\Omega = (\overline{\tilde{L}_L}\tau^a L_L) M^\Omega_{c,ab} (\tilde{\phi}^\dagger \tau^b \phi) \Omega^c, \quad \text{with } \ a, b = 1, 0, -1, \ \ c = 2, 1, 0, -1, -2.
\end{aligned} \tag{5.5}$$

$M^{\rm H}$ are matrices with only non-zero entries for $a + b = 0$ in the case of χ and for $a + b + c = 0$ when $\rm H = \Sigma$ or Ω:

$$M^\chi_{ab} = \begin{pmatrix} 0 & 0 & 1 \\ 0 & -1 & 0 \\ 1 & 0 & 0 \end{pmatrix};$$

[9] Multiplets with higher charges can have striking signatures, $\rm H^{\pm\pm\pm} \to H^{\pm\pm} W^\pm \to \ell^\pm \ell^\pm W^\pm$, but the momenta of the final products are smaller and do not identify doubly-charged resonances in any case —what is required by current analyses, as we comment in Section 5.4—, although the total cross section is in general also larger for larger T (it also depends on T_3 and Y).

$$M^{\Sigma}_{\frac{3}{2},ab} = \begin{pmatrix} 0 & 0 \\ 0 & 0 \\ 0 & -1 \end{pmatrix}, \qquad M^{\Sigma}_{\frac{1}{2},ab} = \begin{pmatrix} 0 & 0 \\ 0 & -\sqrt{\frac{2}{3}} \\ \frac{1}{\sqrt{3}} & 0 \end{pmatrix}, \qquad M^{\Sigma}_{-c,-a-b} = -M^{\Sigma}_{c,ab} \; ;$$

$$M^{\Omega}_{2,ab} = \begin{pmatrix} 0 & 0 & 0 \\ 0 & 0 & 0 \\ 0 & 0 & 1 \end{pmatrix}, \qquad M^{\Omega}_{1,ab} = \begin{pmatrix} 0 & 0 & 0 \\ 0 & 0 & \frac{1}{\sqrt{2}} \\ 0 & \frac{1}{\sqrt{2}} & 0 \end{pmatrix}, \qquad M^{\Omega}_{0,ab} = \begin{pmatrix} 0 & 0 & \frac{1}{\sqrt{6}} \\ 0 & \sqrt{\frac{2}{3}} & 0 \\ \frac{1}{\sqrt{6}} & 0 & 0 \end{pmatrix},$$

$$M^{\Omega}_{-c,-a-b} = M^{\Omega}_{c,ab} \; . \tag{5.6}$$

In the case of the doublet χ, two more effective operators can be written: the one with the two lepton doublets coupled to form an $SU(2)_L$ singlet, given by the expression $(\overline{\tilde{L}_L} L_L)(\phi^\dagger \chi)$, and the operator given by $(\overline{\tilde{L}_L} \chi)(\phi^\dagger L_L)$. In the first case, however, the doubly-charged component χ^{++} couples to $\{\overline{e^c_L}\nu_L - \overline{\nu^c_L} e_L\}$ through the interchange of ϕ^-, rather than to a couple of same-sign leptons; while the second case can be related to the first operator and that of equation (5.5).

There can be also operators of the same order but, for instance, quadratic in the scalar fields. However, they are in general further suppressed. For example, in the quadruplet case the dimension-five operator $\mathcal{O}_{\Sigma\otimes\Sigma} = (\Sigma^\dagger O_a \Sigma)(\overline{\tilde{L}}_L \tau^a L_L)$ (where O_a are four-times-four matrices projecting the $\Sigma \otimes \Sigma$ product into the triplet representation) can also couple Σ^{++} to a pair of same-sign leptons once the neutral Σ component gets a VEV, $\langle \Sigma^0 \rangle$. However, this VEV has to be rather small ($\langle \Sigma^0 \rangle \sim$ few GeV) in order to satisfy, for instance, the constraint on the rho parameter ($\rho = 1.0004^{+0.0003}_{-0.0004}$ at the 95% C.L. [43]) [10]. This justifies neglecting the contribution of this operator.

The renormalizable interactions of κ^{++} and Δ with the leptons discussed in Section 5.1, as well as the previous effective interactions mediated by higher-isospin $SU(2)_L$ multiplets after EWSB, result in the following generic Yukawa interactions for the

[10] As can be derived from its generic expression (to lowest order in perturbation theory)

$$\rho = \frac{\sum_k \left[T_k(T_k+1) - Y_k^2\right] v_k^2}{\sum_k 2 Y_k^2 v_k^2},$$

where k labels the scalar multiplets in the model, and T_k, Y_k and v_k are the corresponding isospin, hypercharge and VEV, respectively.

Vertex	*Singlet*	*Doublet*	*Triplet*	*Quadruplet*	*Quintuplet*
α^L_{ij}	0	$-\frac{v}{\Lambda}c^{(2)}_{\chi ij}$	$-c_{\Delta ij}$	$\frac{v}{\Lambda}c_{\Sigma ij}$	$\frac{v^2}{\Lambda^2}c_{\Omega ij}$
α^R_{ij}	$c_{\kappa ij}$	$\frac{v}{\Lambda}c^{(1)}_{\chi ij}$	0	0	0
β_{ij}	0	$\frac{v}{\Lambda}\frac{c^{(2)}_{\chi ij}}{\sqrt{2}}$	$\frac{c_{\Delta ij}}{\sqrt{2}}$	$-\frac{v}{\Lambda}\frac{c_{\Sigma ij}}{\sqrt{3}}$	$-\frac{v^2}{\Lambda^2}\frac{c_{\Omega ij}}{2}$

Table 5.1: Scalar-Fermion-Fermion couplings for the different multiplet assignments in equation 5.7.

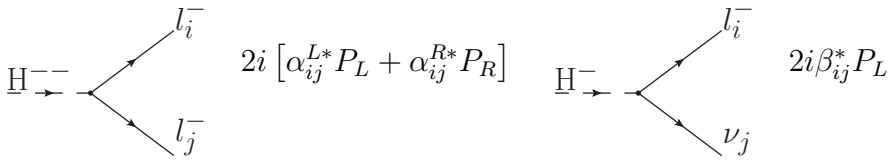

Table 5.2: Feynman diagrams and rules for Yukawa interactions. The arrows indicate the LN flow. α and β are shown in Table 5.1, and are in general symmetric, flavor-dependent and suppressed by powers of v/Λ. These diagrams mediate the decay of $H^{\pm\pm}$ and $H^{\pm}$ into dileptons.

singly- and the doubly-charged components:

$$\frac{c_{\mathrm{H}ij}}{\Lambda^{n_\mathrm{H}}}\mathcal{O}_{\mathrm{H}ij} \to \left(\alpha^L_{ij}\overline{l^c_{Li}}l_{Lj} + \alpha^R_{ij}\overline{l^c_{Ri}}l_{Rj}\right)\mathrm{H}^{++} + \beta_{ij}\left(\overline{\nu^c_{Li}}l_{Lj} + \overline{l^c_{Li}}\nu_{Lj}\right)\mathrm{H}^{+} + \cdots\,, \tag{5.7}$$

where the couplings α and β are in general symmetric, flavor-dependent and suppressed by powers of v/Λ, as shown in Table 5.1. Singly-charged scalar interactions are *a priori* related to doubly-charged ones, although in practice these relations only have phenomenological implications in quite specific models, as we argue later. The Feynman rules for these interactions are depicted in Figure 5.2. Note the importance of these equations, which means that the structure of any doubly-charged scalar decay into same-sign leptons is equivalent to that of the *see-saw* of type II (if we neglect the effects of different chiralities, that are not being studied in current experiments). This in particular implies that current searches, which concentrate on the triplet case, can also test NP scenarios without the need of any efficiency corrections (that typically

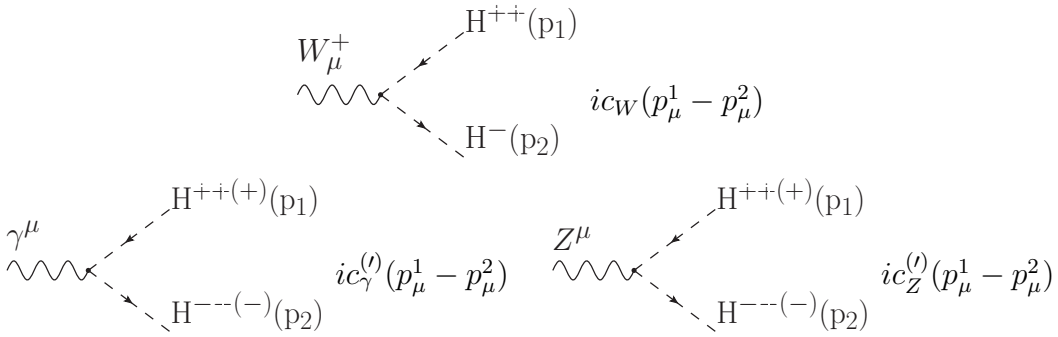

Figure 5.2: Feynman diagrams and rules for gauge trilinear interactions of doubly (c) and singly (c') charged scalars. The arrows indicate the LN flow; whereas the $\mathrm{H}^{++(+)}$ (p_1) and $\mathrm{H}^{--(-)}$ (p_2) momenta are leaving the vertex.

come from the presence of higher-order derivative interactions that potentially modify the kinematic distributions).

5.3 Production and decay

In order to study how H can be produced, let us note that these scalar multiplets, containing doubly-charged components, H^{++}, transform non-trivially under the EW gauge group and thus couple to γ, Z and W (except in the singlet case which only has neutral interactions). The explicit form of the gauge couplings is derived from the corresponding kinetic Lagrangian:

$$\mathcal{L}^K = (D^\mu \mathrm{H})^\dagger \, D_\mu \mathrm{H} \,, \tag{5.8}$$

where the action of the covariant derivative reads

$$\begin{aligned} D_\mu \mathrm{H} &= \left(\partial_\mu + igT_I W^I_\mu + ig' Y B_\mu\right) \mathrm{H} \\ &= \left[\partial_\mu + \frac{ig}{\sqrt{2}}\left(T^+ W^+_\mu + T^- W^-_\mu\right) + \frac{ig}{c_W}\left(T_3 - s^2_W Q\right) Z_\mu + ieQA_\mu\right] \mathrm{H} \,. \end{aligned} \tag{5.9}$$

Expanding $\mathcal{L}^K$ and reordering terms, the trilinear and quartic gauge couplings involved in the calculation of the pair and associated production of doubly-charged scalars can

Vertex	*Singlet*	*Doublet*	*Triplet*	*Quadruplet*	*Quintuplet*
c_W	0	$\frac{g}{\sqrt{2}}$	g	$\sqrt{\frac{3}{2}}g$	$\sqrt{2}g$
c_γ	$2e$	$2e$	$2e$	$2e$	$2e$
c_Z	$-2\frac{g}{c_W}s_W^2$	$\frac{g}{2c_W}\left(1-4s_W^2\right)$	$\frac{g}{c_W}\left(1-2s_W^2\right)$	$\frac{g}{2c_W}\left(3-4s_W^2\right)$	$\frac{2g}{c_W}\left(1-s_W^2\right)$
c'_γ	0	e	e	e	e
c'_Z	0	$-\frac{g}{2c_W}\left(1+2s_W^2\right)$	$-\frac{g}{c_W}s_W^2$	$\frac{g}{2c_W}\left(1-2s_W^2\right)$	$\frac{g}{c_W}\left(1-s_W^2\right)$

Table 5.3: Scalar-Scalar-Vector couplings for doubly (c) and singly (c') charged scalars.

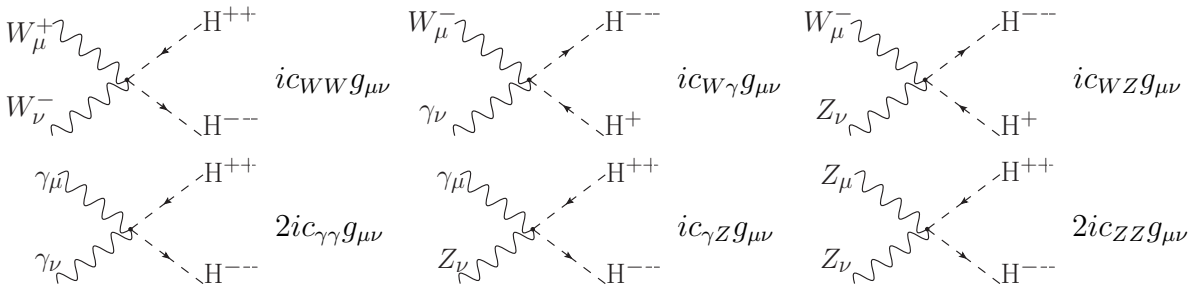

Figure 5.3: Feynman diagrams and rules for gauge quartic interactions of doubly and singly-charged scalars. The arrows indicate the LN flow.

be written

$$
\begin{aligned}
\mathcal{L}^K \to & \left\{ i\frac{g}{\sqrt{2}}\sqrt{(T-Y+2)(T+Y-1)}W_\mu^- \left[\mathrm{H}^{++}(\partial^\mu \mathrm{H}^-) - (\partial^\mu \mathrm{H}^{++})\mathrm{H}^-\right] \right. \\
& + i\left[2eA_\mu + \frac{g}{c_W}(2-Y-2s_W^2)Z_\mu\right]\mathrm{H}^{++}(\partial^\mu \mathrm{H}^{--}) \\
& \left. + i\left[eA_\mu + \frac{g}{c_W}(1-Y-s_W^2)Z_\mu\right]\mathrm{H}^{+}(\partial^\mu \mathrm{H}^{-}) + \mathrm{h.c.}\right\} \\
& + g^2\left[T(T+1)-(2-Y)^2\right]W_\mu^+ W^{-\mu}\mathrm{H}^{++}\mathrm{H}^{--} \\
& + \left\{\frac{g}{\sqrt{2}}\sqrt{(T-Y+2)(T+Y-1)}W_\mu^-\left[3eA^\mu + \frac{g}{c_W}(3-2Y-3s_W^2)Z^\mu\right]\mathrm{H}^{++}\mathrm{H}^{-} + \mathrm{h.c.}\right\} \\
& + \left[2eA_\mu + \frac{g}{c_W}(2-Y-2s_W^2)Z_\mu\right]\left[2eA^\mu + \frac{g}{c_W}(2-Y-2s_W^2)Z^\mu\right]\mathrm{H}^{++}\mathrm{H}^{--}\,.
\end{aligned}
\tag{5.10}
$$

These couplings depend on the type of multiplet, *i.e.*, on T and Y, the doubly-charged

$\mathcal{V}ertex$	*Singlet*	*Doublet*	*Triplet*	*Quadruplet*	*Quintuplet*
c_{WW}	0	$\frac{g^2}{2}$	g^2	$\frac{3g^2}{2}$	$2g^2$
$c_{W\gamma}$	0	$\frac{3}{\sqrt{2}}eg$	$3eg$	$3\sqrt{\frac{3}{2}}eg$	$3\sqrt{2}eg$
c_{WZ}	0	$\frac{-3g^2 s_W^2}{\sqrt{2}c_W}$	$\frac{g^2}{c_W}\left[1-3s_W^2\right]$	$\sqrt{\frac{3}{2}}\frac{g^2}{c_W}\left[2-3s_W^2\right]$	$\frac{3\sqrt{2}}{c_W}g^2\left[1-s_W^2\right]$
$c_{\gamma\gamma}$	$4e^2$	$4e^2$	$4e^2$	$4e^2$	$4e^2$
$c_{\gamma Z}$	$-8e^2\frac{s_W}{c_W}$	$\frac{2eg}{c_W}\left[1-4s_W^2\right]$	$\frac{4eg}{c_W}\left[1-2s_W^2\right]$	$\frac{2eg}{c_W}\left[3-4s_W^2\right]$	$\frac{8eg}{c_W}\left[1-s_W^2\right]$
c_{ZZ}	$4g^2\frac{s_W^4}{c_W^2}$	$\frac{g^2}{4c_W^2}\left[1-4s_W^2\right]^2$	$\frac{g^2}{c_W^2}\left[1-2s_W^2\right]^2$	$\frac{g^2}{4c_W^2}\left[3-4s_W^2\right]^2$	$\frac{4g^2}{c_W^2}\left[1-s_W^2\right]^2$

Table 5.4: Scalar-Scalar-Vector-Vector couplings for VBF doubly-charged pair and associated production.

scalar belongs to, as do the corresponding cross sections. In equation (5.10) we use equation (5.3) but omitting superindices for easy reading. The doubly (2) and singly (1) charges have been also made explicit. In Figures 5.2 and 5.3 and Tables 5.3 and 5.4 we gather the Feynman diagrams and rules (couplings) for the scalar multiplets satisfying equation (5.4). The first two lines describe the $s-$channel exchange of gauge bosons [8], whereas all of them enter in the calculation of the VBF contribution. Indeed, doubly-charged scalars are pair produced with EW strength through the $s-$channel exchange of photons and Z bosons, $pp \to \gamma^*/Z^* \to \mathrm{H}^{++}\mathrm{H}^{--}$. Similarly, its associated production with a singly-charged scalar proceeds through W exchange, $pp \to W^{\pm *} \to \mathrm{H}^{\pm\pm}\mathrm{H}^{\pm}$. Both cross sections depend on the quantum numbers of the scalar multiplet the doubly-charged scalar belongs to. In Figure 5.4 we plot them as a function of the doubly-charged scalar mass $m_{\mathrm{H}^{++}}$ for the five cases in Tables 5.3 and 5.4 and for $\sqrt{s} = 8$ TeV (cross sections for 7 TeV are only slightly reduced with respect to those of Figure 5.4). The corresponding cross sections for $\sqrt{s} = 14$ TeV are shown in Figure 5.5.

The two final states (i.e., pair and associated production) can be also produced through VBF but accompanied by two extra jets, $pp \to \mathrm{H}^{++}\mathrm{H}^{--}jj$, $\mathrm{H}^{\pm\pm}\mathrm{H}^{\mp}jj$. These processes are subleading as expected from gauge-coupling power counting. The con-

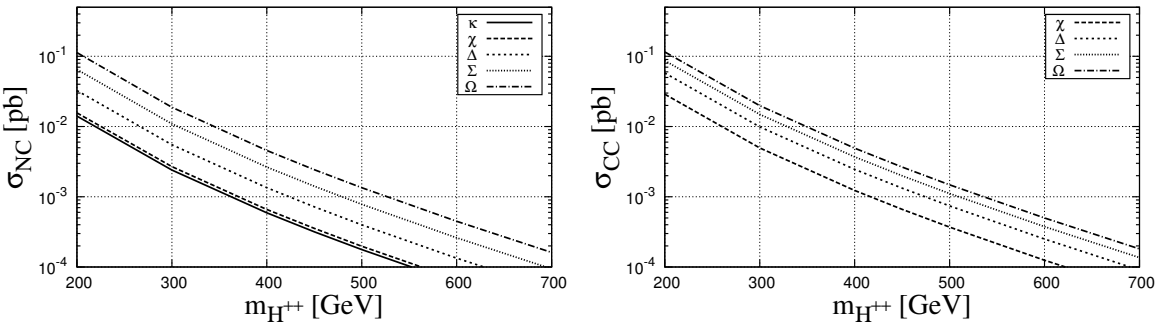

Figure 5.4: Doubly-charged scalar pair (left) and associated (right) production at the LHC for $\sqrt{s} = 8$ TeV, with scalars H belonging to a real quintuplet Ω, a quadruplet Σ, a triplet Δ, a doublet χ or a singlet κ with hypercharges 0, 1/2, 1, 3/2 and 2, respectively.

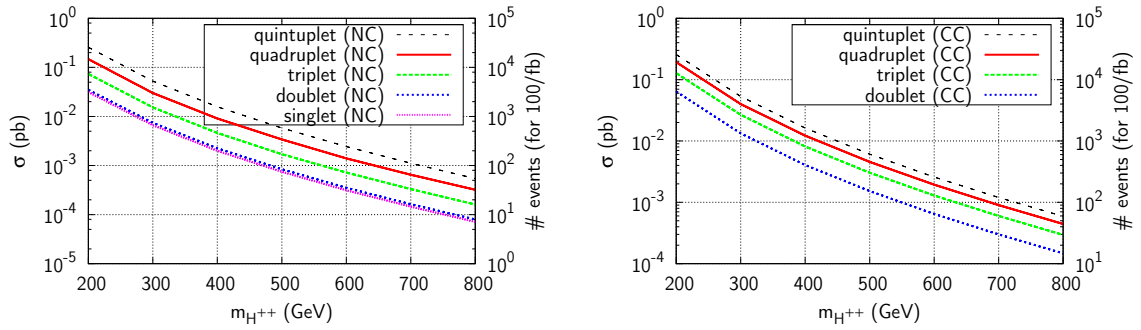

Figure 5.5: Same as Figure 5.4 but for $\sqrt{s} = 14$ TeV.

tributing diagrams are depicted in Figure 5.6. Although this mechanism is enhanced because the initial partons are both valence quarks, its size stays below 10% of the $s-$channel production, being almost negligible for low scalar masses. As an illustration, in Figure 5.7 we plot the ratio of the VBF to the $s-$channel production cross section for the same scalar multiplets and $\sqrt{s} = 8$ TeV [11]. As can be observed in the figure, VBF starts to be important only for large masses, when the valence quark PDFs are

[11]The ratio for pair production but including only the VBF of two photons, $\gamma\gamma \to H^{++}H^{--}$, is quite similar as previously shown in other articles. These partonic cross sections diverge when the photon is emitted collinearly and then are sensitive to the limit on the corresponding partonic transverse momentum. We assume as a conservative value $p_T^j > 10$ GeV throughout the paper.

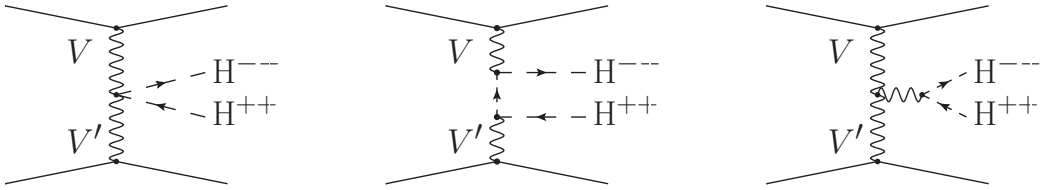

Figure 5.6: Feynman diagrams contributing to VBF doubly-charged scalar pair production.

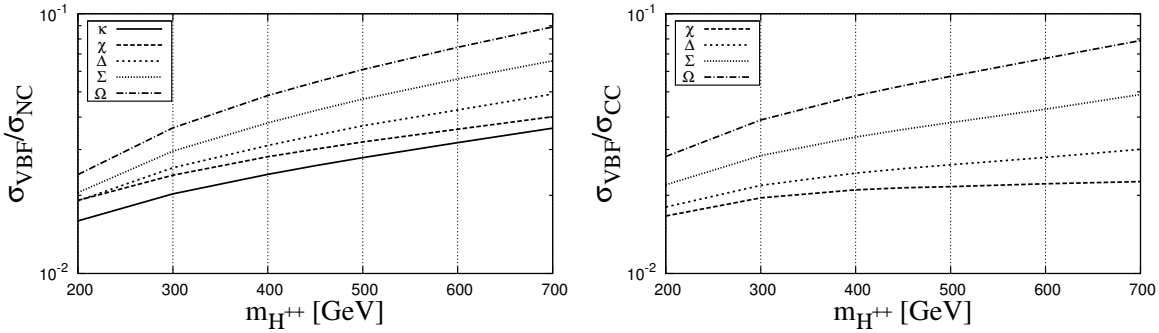

Figure 5.7: Ratio of the VBF to the pair (left) and associated (right) production cross sections as a function of the doubly-charged scalar mass for the same multiplets as in Figures 5.4 and 5.5 and $\sqrt{s} = 8$ TeV.

relatively large. At any rate, this production mechanism is always present and should be taken into account, although it is possible to separate the corresponding events by requiring two extra forward jets. (Collinear γ production can be calculated using the Weizsaecker-Williams approximation [295, 296], giving also similar contributions [297].)

Besides, there can be also NP contributions, although in general further suppressed. In one hand, contact interactions generated by (even) heavier particles after integrating them out, which arise naturally in the context, for instance, of non-minimal CHMs [214, 259], can be present. The corresponding operators, however, are at least of dimension six and hence suppressed by two powers of the heavier effective scale Λ. This means a suppression of the doubly-charged scalar production cross section at the LHC of the order of $(m_{\mathrm{H}^{++}}/\Lambda)^4$. Indeed, the contact interactions of lowest dimension must involve the gauge invariant contraction of two gluon field strength tensors $G^{\mu\nu}_a G^a_{\mu\nu}$ or a colorless quark bilinear $\bar{q}q'$. In the former case the EW singlet of lowest dimension involving at

least one scalar multiplet H with a doubly-charged component H^{++} is $H^\dagger H$. Thus, the corresponding lowest-order operator $G_a^{\mu\nu}G^a_{\mu\nu}H^\dagger H$ is of dimension six, being also the only one of this dimension and form. In addition, there are two possible types of quark bilinears depending on the fermion chirality: $\overline{q_{L(R)}}\gamma_\mu q'_{L(R)}$ and $\overline{q_{L(R)}}q'_{R(L)}$, where $q_R^{(\prime)} = u_R, d_R$. But there is no invariant product of any of them with only one scalar multiplet H coupling the quark bilinear to the H doubly-charged component in the unitary gauge, and hence contributing to doubly-charged scalar production at hadron colliders. Besides, the vector quark bilinear requires an additional covariant derivative to ensure that the operator is Lorentz invariant. In this case there is then only one invariant operator of lowest dimension involving two H multiplets and not suppressed by a small quark Yukawa coupling: $H^\dagger(D^\mu H)\overline{q_{L(R)}}\gamma_\mu q'_{L(R)}$. Other operators of dimension six with the covariant derivative acting on the quark fields can be shown to be suppressed by a small quark Yukawa coupling using the equations of motion; while the operator with the covariant derivative acting on the other scalar multiplet can be written as a combination of all the other operators integrating by parts.

The lowest order operators involving the other quark bilinear and two H multiplets are also of dimension six because they must involve at least a ϕ factor to render the operator invariant under isospin transformations. Thus, all such operators resemble $\overline{q}_L\phi u_R H^\dagger H$, being hence suppressed after EWSB by a $v/m_{H^{++}}$ factor relative to $H^\dagger(D^\mu H)\overline{q_{L(R)}}\gamma_\mu q'_{L(R)}$. Thus, the largest contribution (at least formally) coming from contact interactions results from the operators of this form which can be, for instance, obtained after integrating out a heavy Z'. But their contribution is in general suppressed far away from the heavy resonance by a $(m_{H^{++}}/\Lambda)^2$ factor (as it is the case for $G_a^{\mu\nu}G^a_{\mu\nu}H^\dagger H$, too).

On the other hand, possibly $s-$channel contributions are in addition suppressed by small far off-shell propagators [12]; while $t-$channel contributions are forbidden, since doubly-charged scalars do not have trilinear couplings to quark pairs.

In summary, although there can be a variety of production mechanisms, in general the main production cross sections are fixed by the scalar multiplet quantum numbers

[12]This is also the case for the Higgs s-channel exchange, whose rate is much smaller than the one from the exchange of gauge bosons, unless the effective Higgs coupling to doubly-charged scalars is unnaturally large (equal to λv with λ much larger than one).

in equation (5.10); and thus their measurement would allow to determine the total isospin and hypercharge of the scalar multiplet [8, 14]. In the signal simulations below we add the $s-$channel as well as the VBF production, multiplying the former by a K-factor equal to 1.25 in order to account for NLO corrections [298].

Concerning the decays of H, we emphasize that the Yukawa interactions described in equation (5.7), Table 5.1 and Figure 5.2 mediate the decay of $\mathrm{H}^{\pm\pm}$ and $\mathrm{H}^{\pm}$ into $l^{\pm}l^{\pm}$ and $l^{\pm}\nu_l(\overline{\nu_l})$ respectively. However, the quartic couplings of the scalar multiplets containing a neutral component H^0, *i.e.*, for $T^{\mathrm{H}} \geq |T_3^{\mathrm{H}^{++}} - 2|$, also mediate LNV doubly-charged scalar decays once the LN = 2 neutral component gets a VEV [13],

$$\mathcal{L}^K \to \frac{g^2}{2}\sqrt{(T+Y)(T+Y-1)(T-Y+2)(T-Y+1)}W_\mu^- W^{-\mu}\mathrm{H}^{++}\langle \mathrm{H}^0\rangle\,. \quad (5.11)$$

Moreover, as we have already stressed several times, multiplets without neutral components can also decay into W pairs by mixing with other multiplets with a neutral component developing a VEV, which may be expected in generic UV completions. In order to establish LNV both types of decays, $\mathrm{H}^{\pm\pm} \to l^{\pm}l^{\pm}, W^{\pm}W^{\pm}$, must be observed. Otherwise, the scalar LN could be just 2 in the former case or 0 in the latter one, but still conserved. In general, it makes sense to look for decays into lepton as well as into gauge boson pairs because, although the decay into vector bosons is proportional to a VEV (which turns out to be minuscule [14]), decays into same-sign charged lepton pairs are stringently constrained by current limits on lepton-flavor violation. In the case of the scalar triplet, for instance, $\Delta^{\pm\pm}$ can decay into lepton and boson pairs because it couples to two identical (neglecting family replication) lepton doublets (which defines its $|\mathrm{LN}| = 2$) and to gauge boson pairs (with LN = 0) if its neutral component gets a VEV, $\langle\Delta^0\rangle \neq 0$, breaking LN. If the Yukawa coupling is too large the triplet components always decay into two leptons, and if it is very small and $\langle\Delta^0\rangle$ large enough then their

[13] Similar arguments apply for the decay of $\mathrm{H}^{\pm}$ into $W^{\pm}Z$.

[14] Note that the small couplings can induce displaced vertices [299], although in any case the charged scalars always decay in the detector. For instance, in the *see-saw* of type II, if both channels have the same partial decay width, then the decay length is $\sim 10\mu$m. In general, for doubly-charged scalar masses heavier than few hundreds of GeV, $\left[\sum_{i,j=e,\mu,\tau}\Gamma(\Delta\to l_i l_j)\Gamma(\Delta\to WW)\right]^{-1} \approx 10^{-15}\left[\sum_{i=1,2,3} m_{\nu_i}^2\right]^{-1}\frac{m_W^4}{m_\Delta^4} > 10^5\frac{m_W^4}{m_\Delta^4}\mu\mathrm{m}^2$.

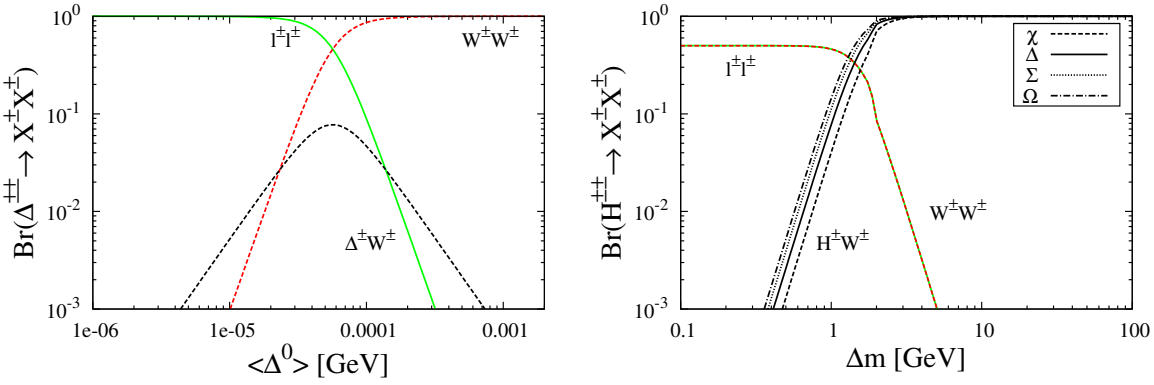

Figure 5.8: Left: Scalar BRs for the triplet Δ as a function of $\langle\Delta^0\rangle$ for $\sum_{i=1,2,3} m_{\nu_i}^2 = 0.1^2$ eV^2 and $m_{\Delta^{\pm\pm}} = 500$ GeV, and $\Delta m = 1$ GeV for the decay into $\Delta^{\pm}W^{\pm *} \to \Delta^{\pm}e^{\pm}\nu_e, \cdots$. Right: Scalar BRs for different H multiplets as a function of $\Delta m = m_{\mathrm{H}^{\pm\pm}} - m_{\mathrm{H}^{\pm}}$ for $m_{\mathrm{H}^{\pm\pm}} = 500$ GeV and $\Gamma(\mathrm{H}^{\pm\pm} \to l^{\pm}l^{\pm}) = \Gamma(\mathrm{H}^{\pm\pm} \to W^{\pm}W^{\pm})$ and the $\mathrm{H}W_{\mu}W^{\mu}$ coupling equal to $5.5 \times 10^{-5} g^2$ GeV.

decay is always into two gauge bosons. This is depicted in the left panel of Figure 5.8, where we plot the two-body BRs for the triplet doubly-charged scalar component as a function of $\langle\Delta^0\rangle$ [15]. As it is apparent, only near $\langle\Delta^0\rangle \approx 5.5 \times 10^{-5}$ GeV both decay rates are comparable and hence genuine LNV signals can be eventually observable at the LHC. However, in order to observe LNV at the LHC not only the two types of couplings involved in the process must be of the same order, but no other messenger decay can be much larger. This requirement further constrains the model, restricting the mixing of the new heavy multiplets with other scalars to small values [300], as it is confirmed by the curves in the right panel of Figure 5.8. There we plot the $\mathrm{H}^{\pm\pm} \to \mathrm{H}^{\pm}W^{\pm *}$ BR, which grows with the isospin T, for the different multiplets we are interested in [16], as a function of the mass splitting between contiguous components $\Delta m = m_{\mathrm{H}^{\pm\pm}} - m_{\mathrm{H}^{\pm}}$, which completely dominates for differences larger than the GeV. Thereby, it is clear

[15] This result can be trivially translated to any scalar multiplet if $\langle\Delta_0\rangle$ is changed by the effective diboson coupling properly normalized (i.e., divided by g^2).

[16] $\Gamma(\mathrm{H}^{\pm\pm} \to \mathrm{H}^{\pm}W^{\pm *} \to \mathrm{H}^{\pm}e^{\pm}\nu_e, \cdots) = n\frac{g^4 \mathrm{T}}{240\pi^3}\frac{\Delta m^5}{m_W^4}$ for small Δm, where n is the number of open lepton and quark channels (5 for $\Delta m < m_{\tau}, \cdots$) and T the total isospin (0 for κ, $\frac{1}{2}$ for χ, 1 for Δ, $\cdots$).

that observing LNV directly at the LHC carries serious difficulties. In the following we adopt the most optimistic approach (i.e., assuming that both decays into leptons and gauge bosons are similar and dominate over other decays) and consider how large can be the constraints that current LHC analyses impose.

5.4 Current constraints

CMS [90] and ATLAS [293] have provided limits on doubly-charged scalars decaying into same-sign e and μ pairs using samples with four and three isolated charged leptons for $\sqrt{s}$ =7 TeV, for the *see-saw* of type II model. CMS, besides, includes doubly-charged scalar decays into τ leptons. As we have commented previously, these searches can constrain the parameter space of not only the triplet case Δ, but also higher multiplets, as we describe in the next sections. Thus, in Section 5.4.1 we reproduce the analyses by CMS and obtain limits on the parameter space of the different H for 7 TeV. We also show how the bounds vary among the multiplets.

CMS has performed six different analyses using four and three isolated charged lepton samples, $\ell\ell\ell\ell$ and $\ell\ell\ell$, with $\ell = e, \mu$ (hadronic taus τ_h are also considered, although at least two of them must be same-sign electrons or muons). In any case the doubly-charged scalars (which are pair produced in the first three analyses while associated produced in the last three) are assumed to decay 100% of the time into $\ell^\pm\ell^\pm$, $\ell^\pm\tau^\pm$ and $\tau^\pm\tau^\pm$ in turn. The cuts and efficiencies are optimized for each case, and events are generated for different scalar masses. These analyses, however, are actually sensitive (i.e., they have large efficiencies) to more general processes, where the two produced scalars do not necessarily decay into the same final state. This includes, among others, LNV signals, for which we obtain the first LHC bounds in Section 5.4.2.

In this case, the MC simulations are performed implementing the relevant interactions in `MadGraph v5` using `FeynRules v1.6` [17], and `Delphes v3` is used for fast-detector simulation. Finaly, instead of `ROOT`, now we use `MadAnalysis v5` to perform the analyses.

[17] The `UFO` model can be found in http://cafpe.ugr.es/index.php/pages/other/software in the package LNV-Scalars_UFO.tar.gz.

5.4.1 Non-LNV processes

In Table 5.5 we collect the corresponding cuts and our estimates of the cumulative cut by cut efficiencies in the four leptons sample for a low (200 GeV) and a relatively large (500 GeV) scalar mass for illustration. As pointed out by CMS, the efficiencies slightly increase with the scalar mass. Among all the cuts, the mass window is the most effective one, implying a large reduction of the background. In the $\ell^\pm\tau^\pm\ell^\mp\tau^\mp$ and $\tau^\pm\tau^\pm\tau^\mp\tau^\mp$ analyses, tau decays into hadrons are also taken into account. Analogously, in Table 5.6 we gather the corresponding cuts and estimated cumulative efficiencies for the three charged lepton sample and doubly-charged scalar associated production. Similarly to the doubly-charged scalar, the singly-charged scalar $H^\pm$ is assumed to decay 100% of the time into $\ell^\pm\nu_\ell$, $\ell^\pm\nu_\tau(\tau^\pm\nu_\ell)$ and $\tau^\pm\nu_\tau$ in turn. In order to be conservative, we make use of the $\ell^\pm\tau^\pm\tau^\mp\nu_\ell$ efficiency also for $\ell^\pm\tau^\pm\ell^\mp\nu_\tau$, although the former is smaller due to the required extra tau BR into electrons and muons. As emphasized in the CMS analysis, the efficiencies for the three-lepton analyses are near a factor 2 smaller than for the corresponding four-lepton analyses. We also show in both Tables 5.5 and 5.6 the number of expected background events as well as the number of observed events as reported by CMS.

Using the estimated efficiencies for seven doubly-charged scalar masses, $m_{H^{\pm\pm}} =$ 200, 300, 400, 450, 500, 600 and 700 GeV, and the expected background and observed number of events, we can draw the corresponding exclusion plots as no event excess is observed. In Figure 5.9, from top to bottom, we plot the 95% C.L. limits (see Section 3.4 for the pertinent definitions) for the analyses in Tables 5.5 (left) and 5.6 (right) [18].

The bounds very much coincide with those reported by CMS for a doubly-charged scalar mediating the *see-saw* of type II, ranging from 400 to 200 GeV depending on the scalar decay mode. (What in particular implies that the efficiencies we use are consistent within the fast simulation algorithm uncertainties with those obtained by CMS.) However, if the doubly-charged scalar belongs to other type of multiplet, its cross sections vary and so the bounds on its mass. We superimpose in the plots the corresponding predictions for the five multiplets discussed before, increasing the limits with the cross section (total isospin). The most stringent bounds are then obtained for

[18] Exclusion limits for intermediate masses are obtained by splines interpolation.

Cuts		*Efficiencies*	
	$\ell^\pm\ell^\pm\ell^\mp\ell^\mp$		
Basic cuts	$p_T^{\ell_{1(2)}} > 20(10)$ GeV, $\lvert\eta^\ell\rvert < 2.5$	68	72
Total p_T	$\sum p_T^\ell > 0.6 m_{\mathrm{H}^{\pm\pm}} + 130$ GeV	99	100
Mass window	$m_{\ell^\pm\ell^\pm} \in [0.9 m_{\mathrm{H}^{\pm\pm}}, 1.1 m_{\mathrm{H}^{\pm\pm}}]$	92	89
Total		62	64
	$\ell^\pm\tau^\pm\ell^\mp\tau^\mp$		
Basic cuts	$p_T^{\ell_{1(2)}} > 20(10)$ GeV, $\lvert\eta^\ell\rvert < 2.5$	16	23
Total p_T	$\sum p_T^\ell > m_{\mathrm{H}^{\pm\pm}} + 100$ or > 400 GeV	82	99
Z veto	$\lvert m_{\ell^\pm\ell^\pm} - m_Z\rvert > 10$ GeV	85	92
Mass window	$m_{\ell^\pm\ell^\pm} \in [0.5 m_{\mathrm{H}^{\pm\pm}}, 1.1 m_{\mathrm{H}^{\pm\pm}}]$	81	66
Total		9.0	14
	$\tau^\pm\tau^\pm\tau^\mp\tau^\mp$		
Basic cuts	$p_T^{\ell_{1(2)}} > 20(10)$ GeV, $\lvert\eta^\ell\rvert < 2.5$	3.0	5.0
Total p_T	$\sum p_T^\ell > 120$ GeV	99	100
Z veto	$\lvert m_{\ell^\pm\ell^\pm} - m_Z\rvert > 50$ GeV	82	86
$\Delta\phi$	$\Delta\phi_{\ell^\pm\ell^\pm} < 2.5$	80	80
Total		2.0	3.5

Table 5.5: Applied cuts to the four isolated charged lepton sample $\ell\ell\ell\ell$, with two $\ell = e$ or μ and the other two e, μ or τ_h, and efficiency percentage for each successive cut for the final states $\ell^\pm\ell^\pm\ell^\mp\ell^\mp$, $\ell^\pm\tau^\pm\ell^\mp\tau^\mp$ and $\tau^\pm\tau^\pm\tau^\mp\tau^\mp$ and two representative scalar masses: 200 GeV (left) and 500 GeV (right). The basic transverse momentum cuts are imposed on the two leptons, electrons or muons, required by the trigger; whereas the transverse momentum sum is over the four charged leptons, as the generic pseudo-rapidity cut. In the three analyses no background events are expected and no event is observed for an integrated luminosity of 4.9 fb^{-1} at $\sqrt{s} = 7$ TeV.

Cuts		*Efficiencies*	
	$\ell^{\pm}\ell^{\pm}\ell^{\mp}\nu_{\ell}$		
Basic cuts	$p_T^{\ell_{1(2)}} > 20(10)$, $\lvert\eta^{\ell}\rvert < 2.5$	78	82
Total p_T	$\sum p_T^{\ell} > 1.1 m_{\mathrm{H}^{\pm\pm}} + 60$	84	87
Z veto	$\lvert m_{\ell^{\pm}\ell^{\pm}} - m_Z\rvert > 80$	59	90
$\Delta\phi$	$\Delta\phi_{\ell^{\pm}\ell^{\pm}} < m_{\mathrm{H}^{\pm\pm}}/600 + 1.95$	86	94
Mass window	$m_{\ell^{\pm}\ell^{\pm}} \in [0.9 m_{\mathrm{H}^{\pm\pm}}, 1.1 m_{\mathrm{H}^{\pm\pm}}]$	94	93
Total		31	56
Expected background		0.99	0.14
Observed events		2	1
	$\ell^{\pm}\tau^{\pm}\ell^{\mp}\nu_{\tau}(\tau^{\mp}\nu_{\ell})$		
Basic cuts	$p_T^{\ell_{1(2)}} > 20(10)$, $\lvert\eta^{\ell}\rvert < 2.5$	16	20
Total p_T	$\sum p_T^{\ell} > 0.85 m_{\mathrm{H}^{\pm\pm}} + 125$	38	48
Z veto	$\lvert m_{\ell^{\pm}\ell^{\pm}} - m_Z\rvert > 80$	85	93
E_T^{miss}	$E_T^{miss} > 20$	98	99
$\Delta\phi$	$\Delta\phi_{\ell^{\pm}\ell^{\pm}} < m_{\mathrm{H}^{\pm\pm}}/200 + 1.15$	83	100
Mass window	$m_{\ell^{\pm}\ell^{\pm}} \in [0.5 m_{\mathrm{H}^{\pm\pm}}, 1.1 m_{\mathrm{H}^{\pm\pm}}]$	91	89
Total		3.8	7.9
Expected background		1.51	0.18
Observed events		3	1
	$\tau^{\pm}\tau^{\pm}\tau^{\mp}\nu_{\tau}$		
Basic cuts	$p_T^{\ell_{1(2)}} > 20(10)$, $\lvert\eta^{\ell}\rvert < 2.5$	4.2	8.3
Total p_T	$\sum p_T^{\ell} > m_{\mathrm{H}^{\pm\pm}} - 10$ or > 200	55	91
Z veto	$\lvert m_{\ell^{\pm}\ell^{\pm}} - m_Z\rvert > 50$	80	85
E_T^{miss}	$E_T^{miss} > 40$	86	97
$\Delta\phi$	$\Delta\phi_{\ell^{\pm}\ell^{\pm}} < 2.1$	84	84
Mass window	$m_{\ell^{\pm}\ell^{\pm}} \in [0.5 m_{\mathrm{H}^{\pm\pm}} - 20, 1.1 m_{\mathrm{H}^{\pm\pm}}]$	76	42
Total		1.0	2.2
Expected background		1.51	0.18
Observed events		3	1

Table 5.6: Same as Table 5.5 but for the three isolated charged lepton sample.

	$m_{\mathrm{H}^{\pm\pm}}$						
$\epsilon_{ij}^{(4\ell)}$	200	300	400	450	500	600	700
$\ell\ell\ell\ell$	53	62	67	68	69	70	71
$\ell\ell\ell\tau$	23	27	30	31	32	32	33
$\ell\ell\tau\tau$	7.2	8.7	9.4	9.4	9.5	9.7	9.9
$\ell\ell WW$	0.6	1.1	1.3	1.3	1.4	1.4	1.5
$\ell\tau\ell\tau$	9.0	11	13	14	14	14	14
$\ell\tau\tau\tau$	2.0	2.6	3.3	3.4	3.4	3.4	3.7
$\ell\tau WW$	0.2	0.4	0.6	0.6	0.6	0.7	0.7
$\tau\tau\tau\tau$	0.3	0.5	0.6	0.7	0.7	0.7	0.7
$\tau\tau WW$	0.1	0.1	0.2	0.2	0.2	0.2	0.2
$WWWW$	< 0.1	< 0.1	< 0.1	< 0.1	< 0.1	< 0.1	< 0.1

Table 5.7: Efficiency percentages $\epsilon_{ij}^{(4\ell)}$ for different scalar masses (in GeV) and final modes ij for four-lepton analyses at $\sqrt{s} = 7$ TeV and the $\ell^{\pm}\tau^{\pm}\ell^{\mp}\tau^{\mp}$ cuts in Table 5.5. We omit the efficiencies for associated production processes because all of them are below $\sim 0.1\%$, as these final states do not pass the cuts imposed on the four-lepton sample.

the quintuplet, being typically ~ 150 GeV higher than for the triplet (*see-saw* of type II).

5.4.2 LNV processes

No dedicated searches for LNV signals are available for doubly-charged scalar production analyses up to now. However, the ATLAS and CMS searches for doubly-charged scalars using four- and three-lepton samples are also sensitive to other final states, including LNV processes. We in fact compute the efficiencies that such analyses have for the more general two-body decay processes (that is, for all the processes in which the two charged scalars can decay in any of their allowed two-body final states), and then use these efficiencies to bound LNV signals. This is actually a convenient way of giving a more complete information on the experimental bounds on NP, since the limits on new models can be thus estimated without performing new analyses. For instance, in the case at hand, just giving the bounds on the processes with the doubly-charged scalars decaying 100% of the time into $\ell^{\pm}\ell^{\pm}$ ($pp \to \mathrm{H}^{\pm\pm}\mathrm{H}^{\mp\mp} \to \ell^{\pm}\ell^{\pm}\ell^{\mp}\ell^{\mp}$) and into

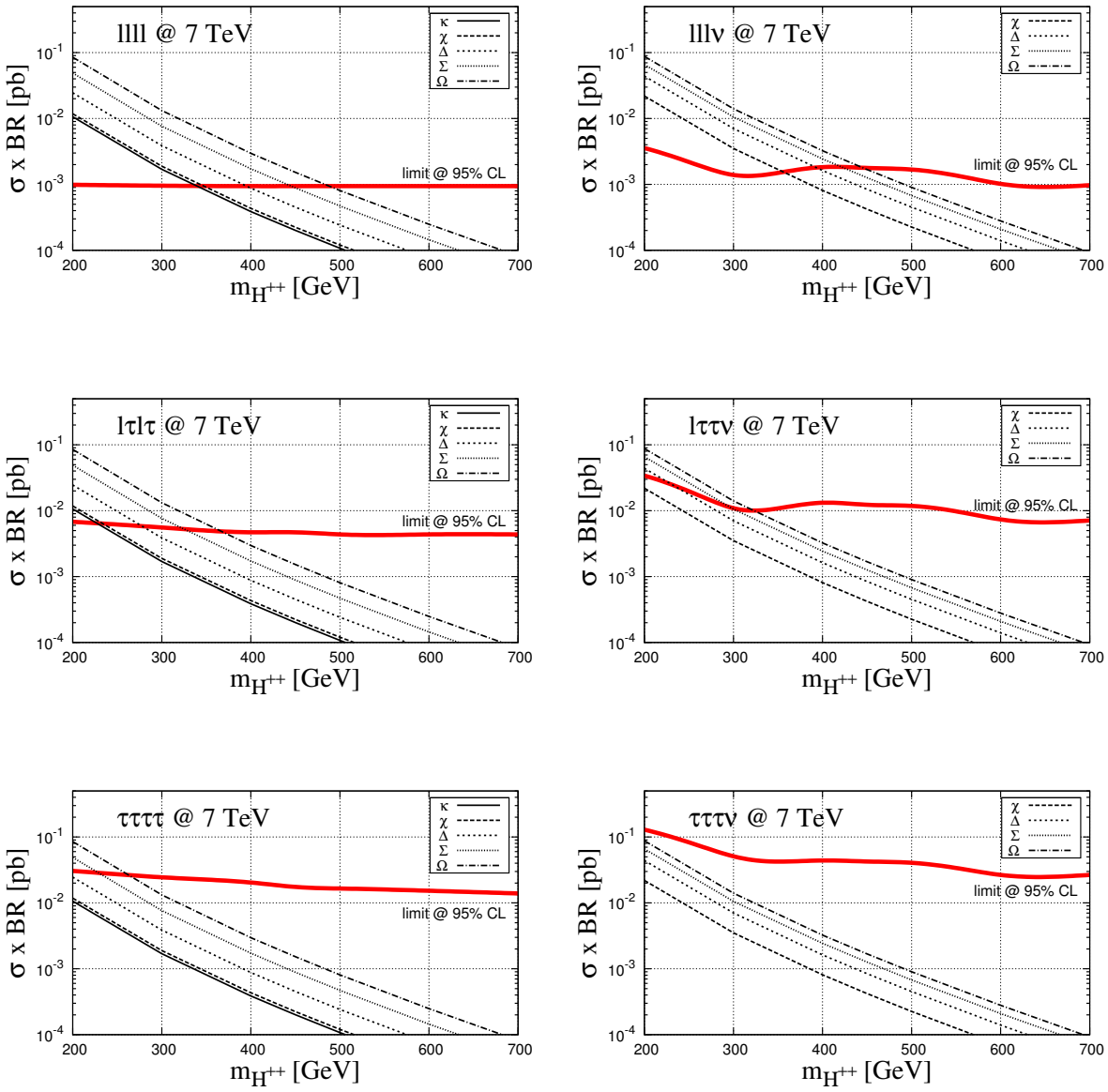

Figure 5.9: Estimated 95% C.L. limits on the final modes $\ell^\pm\ell^\pm\ell^\mp\ell^\mp$, $\ell^\pm\tau^\pm\ell^\mp\tau^\mp$, $\tau^\pm\tau^\pm\tau^\mp\tau^\mp$ (left column from top to bottom) and $\ell^\pm\ell^\pm\ell^\mp\nu_\ell$, $\ell^\pm\tau^\pm\ell^\mp\nu_\ell(\tau^\mp\nu_\tau)$, $\tau^\pm\tau^\pm\tau^\mp\nu_\tau$ (right column from top to bottom) as a function of the doubly-charged scalar mass H^{++} for $\sqrt{s} = 7$ TeV and $\mathcal{L}_{int} = 4.9$ fb^{-1} at LHC. There are superimposed the corresponding cross sections for the five scalar multiplets of lowest isospin and hypercharge containing a doubly-charged component, a singlet κ, a doublet χ, a triplet Δ, a quadruplet Σ and a quintuplet Ω.

	$m_{\mathrm{H}^{\pm\pm}}$						
$\epsilon_{ij}^{(3\ell)}$	200	300	400	450	500	600	700
$\ell\ell\ell\ell$	2.7	5.0	7.5	8.7	9.5	10	11
$\ell\ell\ell\tau$	17	25	31	33	34	34	35
$\ell\ell\tau\tau$	18	24	28	29	30	31	32
$\ell\ell WW$	6.9	13	17	18	19	20	21
$\ell\tau\ell\tau$	14	19	24	24	25	26	26
$\ell\tau\tau\tau$	4.9	6.9	8.6	8.6	9.0	9.2	9.3
$\ell\tau WW$	2.3	4.6	6.3	6.6	6.7	7.0	7.2
$\tau\tau\tau\tau$	0.8	1.2	1.4	1.4	1.4	1.6	1.6
$\tau\tau WW$	0.4	0.8	1.0	1.0	1.1	1.2	1.2
$WWWW$	< 0.1	0.3	0.4	0.4	0.5	0.5	0.5
$\ell\ell\ell\nu$	38	53	64	66	68	70	72
$\ell\ell\tau\nu$	18	26	31	33	34	35	36
$\ell\ell WZ$	5.0	8.5	11	12	13	13	14
$\ell\tau\ell\nu$	15	21	26	27	28	29	29
$\ell\tau\tau\nu$	3.8	5.4	7.4	7.6	7.9	8.4	8.5
$\ell\tau WZ$	1.6	2.9	3.9	4.0	4.1	4.5	4.5
$\tau\tau\ell\nu$	2.3	3.4	4.3	4.5	4.6	4.8	4.9
$\tau\tau\tau\nu$	0.4	0.6	0.7	0.8	0.8	0.8	0.9
$\tau\tau WZ$	0.2	0.4	0.6	0.6	0.6	0.6	0.7
$WW\ell\nu$	0.3	0.7	1.0	1.0	1.0	1.1	1.2
$WW\tau\nu$	0.1	0.2	0.3	0.4	0.4	0.4	0.4
$WWWZ$	< 0.1	0.1	0.1	0.2	0.2	0.2	0.2

Table 5.8: Efficiency percentages $\epsilon_{ij}^{(3\ell)}$ for different scalar masses (in GeV) and final modes ij for three-lepton analyses at $\sqrt{s} = 7$ TeV and the $\ell^{\pm}\tau^{\pm}\ell^{\mp}\nu_{\tau}(\tau^{\mp}\nu_{\ell})$ cuts in Table 5.6.

$\ell^{\pm}\tau^{\pm}$ ($pp \to \mathrm{H}^{\pm\pm}\mathrm{H}^{\mp\mp} \to \ell^{\pm}\tau^{\pm}\ell^{\mp}\tau^{\mp}$), in turn, one can estimate the corresponding limits on a model where the doubly-charged scalars decay half of the time into each of these two final states, but without being able to use the $\ell^{\pm}\ell^{\pm}\ell^{\mp}\tau^{\mp}$ events and hence half of the statistics. With this in mind, we collect the efficiencies for the four-lepton and three-lepton analyses in Tables 5.7 and 5.8, respectively, for all two-body decays of the doubly and singly-charged scalars, $\ell\ell, \ell\tau, \tau\tau, WW$ and $\ell\nu, \tau\nu, WZ$, and seven scalar masses, $m_{\mathrm{H}^{\pm\pm}} = 200$, 300, 400, 450, 500, 600 and 700 GeV.

As $H^{\pm\pm}$ ($H^{\pm}$) has 4 (3) different two-body decay modes, there are *a priori* $4\times 4 + 4\times 3 = 28$ final states and hence ϵ_{ij} efficiencies. But for pair production $\epsilon_{ij} = \epsilon_{ji}$, being then only 10 of the 16 efficiencies independent. In Table 5.7 we omit the $H^{\pm\pm}H^{\mp}$ decay modes because all their efficiencies are below $\sim 0.1\%$. For both analyses, the applied cuts are common to all final states, thus not optimized for the different modes but for the full set. Following CMS analyses for benchmark points we choose the cuts for $\ell^{\pm}\tau^{\pm}\ell^{\mp}\tau^{\mp}$ in Table 5.5 and for $\ell^{\pm}\tau^{\pm}\ell^{\mp}\nu_{\tau}(\tau^{\mp}\nu_{\ell})$ in Table 5.6 to calculate the efficiencies in Tables 5.7 and 5.8, respectively. They grow with the scalar mass because the cuts stay fixed. For example, electrons and muons are harder for larger scalar masses and thereby they satisfy more easily not only the basic cuts but also the cuts on $\sum p_T^{\ell}$ and on E_T^{miss}. The latter is particularly stringent for pair produced events because in this case the E_T^{miss} comes either from missed leptons or from E_T^{miss} measurement errors and, accordingly, it is relatively small. In addition, the E_T^{miss} and the total transverse momentum in the event are in general correlated. The Z veto, on another front, is also less restrictive for larger masses, in contrast with the mass window constraint for events involving tau leptons. Changes in parton shower and detector simulation inputs result in variations in the efficiencies of around $\sim 15\%$. This is the total uncertainty that has to be assumed for our estimates in Tables 5.7 and 5.8.

As already emphasized, we can make use of the these efficiencies in order to derive the corresponding bounds on LNV, given that no event excess has been observed neither in the four- nor in the three-lepton analysis. We restrict ourselves to the LNV final states $\ell\ell WW$ and $\ell\ell WZ$ because they have the largest efficiencies (see Tables 5.7 and 5.8), showing the results for the three-lepton analysis only for it is by far the most sensitive to LNV. For a given integrated luminosity $\mathcal{L}_{int}$, the number of signal events $N^{(3\ell)}_{\ell\ell WW(\ell\ell WZ)}$ is estimated multiplying $\mathcal{L}_{int}$ by the corresponding cross section, $\sigma_{NC(CC)}$ for doubly-charged scalar pair (associated) production, times the model BRs into $\ell\ell$ and WW (WZ) times the selection efficiency:

$$
\begin{aligned}
N^{(3\ell)}_{\ell\ell WW} &= \mathcal{L}_{int}\times\sigma_{NC}\times \mathrm{BR}(H^{\pm\pm}\to\ell^{\pm}\ell^{\pm})\times \mathrm{BR}(H^{\mp\mp}\to W^{\mp}W^{\mp})\times\epsilon^{(3\ell)}_{\ell\ell WW}\ ,\\
N^{(3\ell)}_{\ell\ell WZ} &= \mathcal{L}_{int}\times\sigma_{CC}\times \mathrm{BR}(H^{\pm\pm}\to\ell^{\pm}\ell^{\pm})\times \mathrm{BR}(H^{\mp}\to W^{\mp}Z)\times\epsilon^{(3\ell)}_{\ell\ell WZ}\ .
\end{aligned}
\tag{5.12}
$$

Making use of these expressions and the number of expected background events and observed events we can derive the exclusion plots for $\sigma_{NC(CC)}$ (see Section 3.4). In

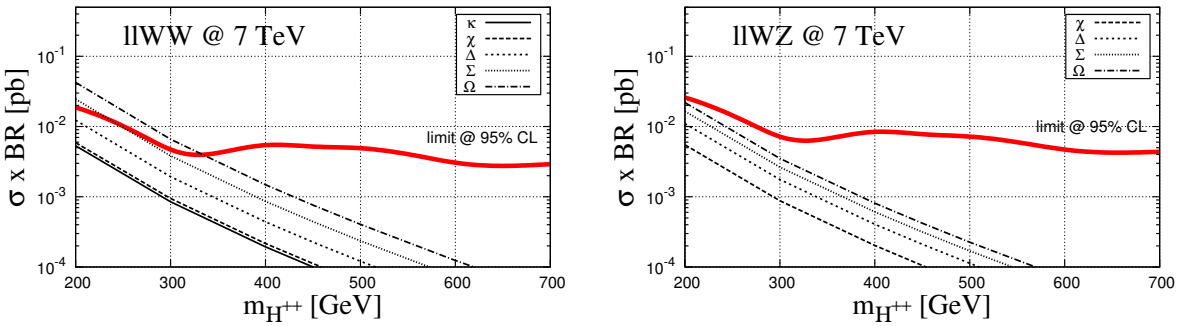

Figure 5.10: 95% C.L. limits on the LNV channels $pp \to \mathrm{H}^{\pm\pm}\mathrm{H}^{\mp\mp} \to \ell^{\pm}\ell^{\pm}W^{\mp}W^{\mp}$ (left) and $pp \to \mathrm{H}^{\pm\pm}\mathrm{H}^{\mp} \to \ell^{\pm}\ell^{\pm}W^{\mp}Z$ (right) as a function of the $\mathrm{H}^{\pm\pm}$ mass for $\sqrt{s} = 7$ TeV and $\mathcal{L}_{int} = 4.9$ fb^{-1} at the LHC. There are superimposed the corresponding cross sections for the five scalar multiplets of lowest isospin and hypercharge containing a doubly-charged component: the singlet κ, the doublet χ, the triplet Δ, the quadruplet Σ and the quintuplet Ω.

Figure 5.10 we plot the corresponding limits assuming that the heavy scalars have the same decay rate (50%) into light (first two families) lepton and gauge boson pairs. We superimpose the cross sections for the different doubly-charged multiplet assignments conveniently normalized by the assumed BRs: 1/2 for pair and 1/4 for associated production. The exclusion plot for $\ell\ell WW$ ($\ell\ell WZ$) is shown on the left (right). The number of expected background and observed events are the same as for the $\ell^{\pm}\tau^{\pm}\ell^{\mp}\nu_{\tau}(\tau^{\mp}\nu_{\ell})$ three-lepton analysis in Table 5.6.

As a conclusion of this section, we should emphasize several points: (*i*) the LHC in the current phase has in general no sensitivity to the LNV signals considered (this situation, as we discuss in the next section, is completely different for $\sqrt{s} = 8$ and $\sqrt{s} = 14$ TeV with a larger integrated luminosity). (*ii*) These estimates will be improved by the experimental collaborations when cuts and efficiencies are optimized for these searches. Indeed, note that we have used the only analyses sensitive to doubly-charged scalar production experimentally available up to now. Hence, more sophisticated analyses taking into account the specific topology of LNV processes have to be performed in order to extract all the possible information from future runs. A first attempt in this direction was already given in several works [8, 14]. (*iii*) LNV processes are in general rare and as previously indicated, only in special regions in parameter space they are relatively large with almost half of the events from doubly-charged scalar pair and as-

Process	σ[7 TeV] @ NLO (pb)	σ[8 TeV] @ NLO (pb)	σ[14 TeV] @ NLO (pb)
Drell-Yan	$(21 \pm 1) \times 10^2$	$(25 \pm 2) \times 10^2$	$(48 \pm 4) \times 10^2$
W^+W^-	41 ± 1	50 ± 2	107 ± 4
$W^\pm Z$	17 ± 1	21 ± 1	47 ± 2
ZZ	5.5 ± 0.2	6.6 ± 0.2	14.5 ± 0.4
$t\bar{t}$	141 ± 15	198 ± 20	766 ± 75

Table 5.9: Partonic cross sections for the main backgrounds considered in the analyses at NLO in QCD. They are calculated with `aMC@NLO` , using the 5 flavor scheme and the MC@NLO method [117] for matching with parton showers. Jet transverse momenta are in general required to be larger than 10 GeV; whereas Drell-Yan leptons must satisfy $p_T^l > 20$ GeV, $m_{l^+l^-} > 30$ GeV and $\Delta R_{l^+l^-} > 0.4$.

sociated production violating LN. This is what we assume to draw Figure 5.10. If the BRs are different we have to normalize the H cross sections accordingly to read the corresponding limit from the Figure. (*iv*) Relatively large LNV signals are natural in more elaborated models, as for example those with neutrino masses radiatively generated.

5.5 Future constraints

In this section we estimate the limits that can be obtained in experimental searches of doubly-charged scalars with the current collected data, 20 fb^{-1} at $\sqrt{s} = 8$ TeV and in a future larger run: $\sqrt{s} = 14$ TeV and 100 fb^{-1}. Given that no experimental information is still reported for these analyses, the expected bounds are set assuming that no departure from the SM is observed. In such a case, the number of expected observed events is equal to the number of predicted SM background events.

In order to estimate the number of background events at $\sqrt{s}$ =8 TeV, we proceed in the following way: since the signal efficiencies for $\sqrt{s} = 7$ and 8 TeV are similar (we find differences of at most $\sim 10\%$), we assume that this is also the case for the backgrounds and estimate them at 8 TeV scaling the CMS values in Table 5 of [90] by a factor of

$$\frac{\sigma_8}{\sigma_7} \times \frac{\mathcal{L}_8}{\mathcal{L}_7} \approx 1.2 \times 4.08 \,, \tag{5.13}$$

where the first number is the average of the ratios of the corresponding cross sections for

	$m_{\mathrm{H}^{\pm\pm}}$						
$\epsilon_{ij}^{(4\ell)}$	200	300	400	450	500	600	700
$\ell\ell\ell\ell$	54	62	66	68	69	69	70
$\ell\ell WW$	0.6	0.9	1.1	1.4	1.4	1.4	1.5
$WWWW$	< 0.1	< 0.1	< 0.1	< 0.1	< 0.1	< 0.1	< 0.1
$\ell\ell\ell\nu$	< 0.1	< 0.1	< 0.1	< 0.1	< 0.1	< 0.1	< 0.1
$\ell\ell WZ$	< 0.1	0.1	0.1	0.1	0.1	0.1	0.1
$WW\ell\nu$	< 0.1	< 0.1	< 0.1	< 0.1	< 0.1	< 0.1	< 0.1
$WWWZ$	< 0.1	< 0.1	< 0.1	< 0.1	< 0.1	< 0.1	< 0.1

Table 5.10: Efficiency percentages $\epsilon_{ij}^{(4\ell)}$ for different scalar masses (in GeV) and final modes ij for four-lepton analyses at $\sqrt{s} = 14$ TeV and the $\ell^{\pm}\tau^{\pm}\ell^{\mp}\tau^{\mp}$ cuts in Table 5.5.

the largest backgrounds in Table 5.9 (Drell-Yan, W^+W^-, $W^{\pm}Z$, ZZ and $t\bar{t}$ production), and the second one is the luminosity ratio 20/4.9. For the LHC run at 14 TeV we instead simulate the complete set of backgrounds in Table 5.9 for an integrated luminosity of 100 fb^{-1}. As well as in the case of 7 TeV, we can estimate the bounds on any particular

	$m_{\mathrm{H}^{\pm\pm}}$						
$\epsilon_{ij}^{(3\ell)}$	200	300	400	450	500	600	700
$\ell\ell\ell\ell$	3.9	6.9	10	11	12	13	14
$\ell\ell WW$	7.4	14	18	20	21	22	23
$WWWW$	< 0.1	0.3	0.4	0.5	0.6	0.7	0.7
$\ell\ell\ell\nu$	40	55	66	68	70	72	74
$\ell\ell WZ$	5.2	9.3	13	13	14	15	16
$WW\ell\nu$	0.3	0.8	1.0	1.1	1.1	1.2	1.3
$WWWZ$	< 0.1	0.2	0.2	0.3	0.2	0.3	0.3

Table 5.11: Efficiency percentages $\epsilon_{ij}^{(3\ell)}$ for different scalar masses (in GeV) and final modes ij for three-lepton analyses at $\sqrt{s} = 14$ TeV and the $\ell^{\pm}\tau^{\pm}\ell^{\mp}\nu_{\tau}(\tau^{\mp}\nu_{\ell})$ cuts in Table 5.8.

two-body decay process mediated by pair and associated production of doubly-charged scalars providing first the table of efficiencies for the different final states, assuming the

$\sqrt{s}$ (TeV), $\mathcal{L}_{\rm int}$(fb^{-1})	$\mathbf{Isospin}_{\rm hypercharge}$				
	$\mathbf{0}_2$	$\mathbf{\frac{1}{2}}_{\frac{3}{2}}$	$\mathbf{1}_1$	$\mathbf{\frac{1}{2}}_{\frac{3}{2}}$	$\mathbf{2}_0$
	$m_{H^{\pm\pm}}$ (GeV) bounds from $\ell^\pm\ell^\pm\ell^\mp\ell^\mp$				
7 , 4.9	340	350	395	450	490
8 , 20	480	490	550	610	665
14 , 100	900	915	1030	1140	1230

Table 5.12: Estimated limits on the cross section and on the corresponding scalar mass $m_{H^{\pm\pm}}$ (GeV) as a function of the multiplet if belongs to from LHC searches for doubly-charged scalars. We only consider the $\ell^\pm\ell^\pm\ell^\mp\ell^\mp$ analysis, and assume that $H^{\pm\pm} \to \ell^\pm\ell^\pm$ 100 % of the time.

same analyses as those already performed by CMS at 7 TeV and used in the previous section. For LHC at 8 TeV, as already emphasized, the corresponding table can not be distinguished from Table 5.8 within the fast simulation uncertainties. Thus, we stress that Table 5.8 also provides the 8 TeV information. In addition, as we learned from Table 5.8 that $\ell\ell\ell\ell$ and $\ell\ell WW$ (or $\ell\ell WZ$) final states result in the largest efficiencies for non-LNV and LNV processes respectively, we only provide reduced efficiency tables for LHC at $\sqrt{s} = 14$ TeV. These are shown in Table 5.10 and Table 5.11 for the four- and three-lepton analyses respectively.

5.5.1 Non-LNV processes

We briefly discuss the expected bounds for non-LNV signals mediated by doubly-charged scalars in the most promising channel, i.e., $\ell\ell\ell\ell$. We collect the expected limits for the different multiplets assignments in Table 5.12 for $\sqrt{s} = 8$ and 14 TeV. The results for $\sqrt{s} = 7$ TeV are also shown for comparison. We are again assuming a 100% BR of $H^{\pm\pm}$ into $\ell^\pm\ell^\pm$. We observe that the expected bounds at 8 TeV with $\mathcal{L}_{int} =$ 20 fb^{-1} range between $\sim$ 500 and 700 GeV depending on the scalar multiplet, while these limits can be up to $\sim$ 500 GeV larger at 14 TeV with an integrated luminosity of 100 fb^{-1}. In the next section we consider the bounds on LNV signals.

5.5.2 LNV processes

In order to establish the expected limits on LNV processes for $\sqrt{s} = 8$ and 14 TeV, we proceed as in Section 5.4, but using Table 5.8 for 8 TeV and Table 5.11 for 14 TeV. The number of expected and observed events for 8 TeV is computed following the principle we have commented at the beginning of this section. For 14 TeV, instead, we find a total of 42, 37, 18, 15, 9, 7 and 0 events for an integrated luminosity of 100 fb^{-1} and $m_{\mathrm{H}^{\pm\pm}} = 200$, 300, 400, 450, 500, 600 and 700 GeV, respectively, after the corresponding cuts. We draw these limits as a function of the mass of the doubly-charged scalar and for the different multiplets in Figure 5.11, for 8 TeV (top) and 14 TeV (bottom). As we already did for 7 TeV, we superimpose the cross sections for the different doubly-charged multiplet assignments conveniently normalized by the assumed BRs: 1/2 for pair and 1/4 for associated production. The exclusion plots for $\ell\ell WW$ ($\ell\ell WZ$) are shown on the left (right). Regarding these plots we note that, in future runs, masses of up to nearly the TeV can be excluded in LNV processes, what means a significant improvement with respect to the case of $\sqrt{s} = 7$ TeV.

5.6 Discovering LNV scalars

Doubly-charged scalars are predicted by many SM extensions and may show up at the LHC even if no LNV signal can be ever established at colliders. Therefore, a resonance in the same-sign charged dilepton channel can be detected and hence the question is whether the EW multiplet it belongs to can be determined. As stressed above, the production cross section depends on the total isospin and hypercharge but the number of observed events in each final state is also proportional to the corresponding BR. Then, a multi-sample analysis is mandatory. In Section 5.6.1 we explain how to measure the doubly-charged scalar pair production cross section. For the determination of the multiplet it belongs to it is also necessary to distinguish the doublet from the singlet, whose corresponding cross sections are similar, by the observation (or not) of charged-current processes. This is discussed in Section 5.6.2. We still assume that only two-body decays are sizable and the two-lepton channel $\mathrm{H}^{\pm\pm} \to \ell^\pm\ell^\pm$ is observable. We conclude that only with a relatively large statistics and a large enough $\mathrm{H}^{\pm\pm} \to \ell^\pm\ell^\pm$ BR it is possible to obtain a crucial test. For example, the production cross sections for the different multiplets stay apart by at least 3σ if $\mathrm{H}^{\pm\pm}$ only decays into $\ell^\pm\ell^\pm$ for $\sqrt{s} = 14$

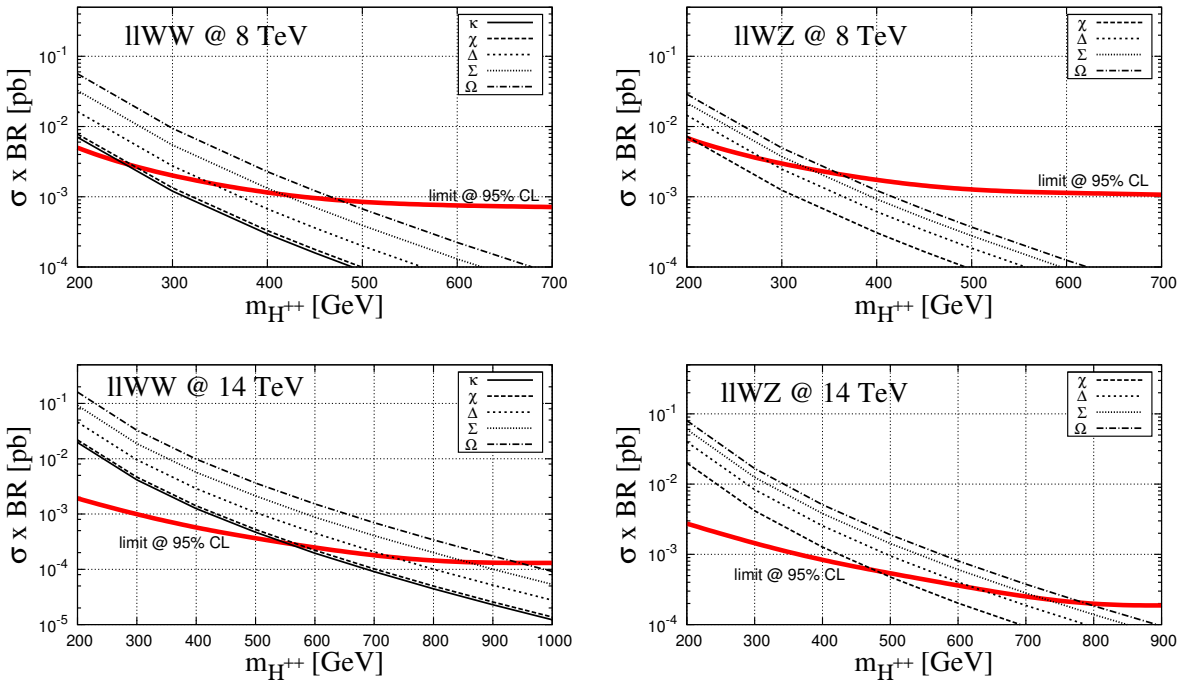

Figure 5.11: 95% C.L. limits on the LNV channels $pp \to \mathrm{H}^{\pm\pm}\mathrm{H}^{\mp\mp} \to \ell^{\pm}\ell^{\pm}W^{\mp}W^{\mp}$ (left) and $pp \to \mathrm{H}^{\pm\pm}\mathrm{H}^{\mp} \to \ell^{\pm}\ell^{\pm}W^{\mp}Z$ (right) as a function of the $\mathrm{H}^{\pm\pm}$ mass for $\sqrt{s} = 7$, 8 and 14 TeV and $\mathcal{L}_{int} = 4.9$, 20 and 100 fb^{-1} at LHC, respectively (from top to bottom). There are superimposed the corresponding cross sections for the five scalar multiplets of lowest isospin and hypercharge containing a doubly-charged component: the singlet κ, the doublet χ, the triplet Δ, the quadruplet Σ and the quintuplet Ω.

TeV and $\mathcal{L}_{\mathrm{int}} = 300$ fb^{-1}. However, if $\mathrm{H}^{\pm\pm}$ decays 50% of the time into $\ell^{\pm}\ell^{\pm}$ and $\ell^{\pm}\tau^{\pm}$, respectively, this integrated luminosity is not enough to separate the doublet from the triplet, and a longer run to accumulate 3000 fb^{-1} becomes necessary to distinguish the different cases.

5.6.1 Measurement of the cross section

We focus only on a large run with $\sqrt{s} = 14$ TeV, given that a large amount of statistic is necessary to properly measure the corresponding cross sections in the different channels. In Figure 5.5 we plotted the corresponding cross sections for the five cases listed in equations 5.1 and 5.5. It is important to note that since the hypercharge and the isospin are related by $T^{\mathrm{H}} + Y^{\mathrm{H}} = 2$ in these cases, it is enough to measure one of the

two production cross sections in order to discriminate among the different possibilities. Both, neutral and charged production grow with the isospin, but pair production provides a better discriminator because it has smaller backgrounds and a smaller number of channels that contribute to the final modes of interest [19]. Hence, in the following we concentrate on this case. Obviously, no particular channel allows the determination of the strength of the couplings involved in the production, but only their product by the corresponding BR. Hence, although the production cross sections are fixed by gauge symmetry, we have to rely on measuring several (preferably all) decay channels in order to estimate the total cross section, and determine which of the scalar multiplets is being produced. The proposed analysis is based on the refinement and extension of the searches discussed in the previous sections.

We focus only on four-leptons final states, either coming from the decay of $\mathrm{H}^{\pm\pm}$ into $\ell^\pm\ell^\pm$ or from its decay into ab, with $a, b = l^\pm, W^\pm$ and the subsequent decay of a and b into light leptons ℓ. Thus, the four charged lepton (ℓ) cross section for any given channel ab can be written $\sigma_{ab} = (2-\delta_{ab})\sigma z_a z_b$, where σ is the total scalar pair production cross section we want to measure and $z_{a,b}$ the corresponding BR. Thereby, the doubly-charged pair production cross section with both scalars decaying into two leptons of the first two families reads $\sigma z_{\ell\ell}^2$; whereas, for instance, the doubly-charged pair production cross section with one scalar decaying into two leptons of the first two families and the other to anything giving two charged leptons of the first two families, too, plus E_T^{miss} is written $\sigma_{\ell\ell\ell\ell E_T^{miss}} = \sigma_{\ell\ell\ell\ell} + 2\sum_{a=\ell\tau,\tau\tau,WW} \sigma z_{\ell\ell} z_a \mathrm{Br}(a \to \ell\ell + E_T^{miss})$. Hence, if we are able to reconstruct and estimate all $\sigma_{\ell\ell a} \equiv 2\sigma z_{\ell\ell} z_a, a \neq \ell\ell$, besides $\sigma_{\ell\ell\ell\ell}$, we can then evaluate

$$\sigma = \left(\sigma_{\ell\ell\ell\ell} + \frac{1}{2}\sum_{a\neq\ell\ell}\sigma_{\ell\ell a}\right)^2 / \sigma_{\ell\ell\ell\ell}\,. \tag{5.14}$$

In the following we argue that this is feasible, knowing that experimentalists can improve on the assumptions being made here, especially when using real data. We assume for illustration a heavy scalar mass $m_{\mathrm{H}^{\pm\pm}} = 500$ GeV [20], and proceed as follows. We select

[19] If we were considering three-leptons final states, both the $\ell\ell WW$ and $\ell\ell WZ$ decays enter in the computation, whose magnitudes are related by model-dependent relations.

[20] Note that present limits, showed in Figure 5.9, are much weakened when $\mathrm{H}^{\pm\pm}$ does not decay only into $\ell^\pm\ell^\pm$.

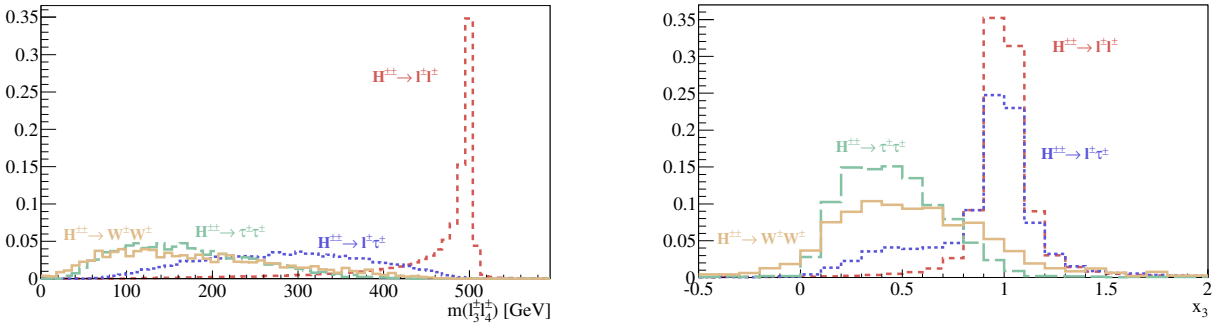

Figure 5.12: Left: Invariant mass of the two same-sign leptons that provides the poorest reconstruction of the $H^{\pm\pm}$ mass in doubly-charged scalar pair production for different decay modes. Right: Momentum fraction, x_3, of the most energetic lepton of the two which worst reconstruct the $H^{\pm\pm}$ mass in doubly-charged scalar pair production for different decay modes.

events with four charged leptons of the first two families with zero total electric charge, plus possibly E_T^{miss}, and require that at least one same-sign pair $\ell_1\ell_2$ reconstructs the scalar mass within ± 40 GeV. These events are then separated into three disjoint sets depending on the category associated to the other same-sign pair: $\ell\ell, \ell\tau$ and $\tau\tau + WW$. We denote by $\ell\ell$ those events resulting from the decay of the second doubly-charged scalar into two leptons of the first two families, and hence, those with the second same-sign lepton pair $\ell_3\ell_4$ also reconstructing the scalar mass within ± 40 GeV. For the remaining events we assume that ℓ_3 and ℓ_4 are products of semileptonic tau decays, and distribute the E_T^{miss} of the event between both tau leptons with the requirement that their momenta align along the momentum of the corresponding product charged-lepton momentum it decays to: $xp_\tau^\mu = p_\ell^\mu$, with $0 < x < 1$. Then, we identify the event with the second scalar decaying into a lepton of the first two families and a tau lepton, $\ell\tau$, as those fulfilling that the fraction momentum of the most energetic of the two leptons not reconstructing the scalar mass, which we name ℓ_3, (x_3) is larger than 0.8. The other events are classified as resulting from the decay of the second scalar into two tau leptons or two gauge bosons, $\tau\tau + WW$. Figure 5.12 proves the usefulness of the procedure. Indeed, the left panel of Figure 5.12 shows the same-sign dilepton invariant mass for the lepton pair which provides the poorest reconstruction of the doubly-charged scalar mass and for its four decay modes: $H^{\pm\pm} \to \ell_3^\pm\ell_4^\pm$,$H^{\pm\pm} \to \ell_3^\pm\tau^\pm \to \ell_3^\pm\ell_4^\pm\ E_T^{miss}$, $H^{\pm\pm} \to \tau^\pm\tau^\pm \to \ell_3^\pm\ell_4^\pm\ E_T^{miss}$, and $H^{\pm\pm} \to W^\pm W^\pm \to \ell_3^\pm\ell_4^\pm\ E_T^{miss}$. The separation of the

Variable	$\ell^\pm\ell^\pm\ell^\mp\ell^\mp$	$\ell^\pm\ell^\pm\ell^\mp\tau^\mp$	$\ell^\pm\ell^\pm\tau^\pm\tau^\pm(W^\pm W^\pm)$
# of leptons	4	4	4
$\lvert m_{\ell_1^\pm\ell_2^\pm} - m_{H^{\pm\pm}}\rvert$	≤ 40 GeV	≤ 40 GeV	≤ 40 GeV
$\lvert m_{\ell_3^\pm\ell_4^\pm} - m_{H^{\pm\pm}}\rvert$	≤ 40 GeV	≥ 40 GeV	≥ 40 GeV
E_T^{miss}	not applied	≥ 50 GeV	≥ 50 GeV
x_3	not applied	≥ 0.8	≤ 0.7

Table 5.13: Main applied cuts for the analyses used in the discrimination of the different multiplets.

first sample is obtained simply requiring $m_{\ell_3^\pm\ell_4^\pm}$ to be in between $m_{\mathrm{H}^{\pm\pm}} \pm 40$ GeV.

In the right panel we plot the momentum fraction assigned to the most energetic lepton of the second same-sign pair for the former four types of scalar decays. As can be observed, $x_3 \geq 0.8$ provides a rather clean separation of the first two decay modes from the last two. The different distributions reflect the fact that the leading lepton tends to be the one which is not a decay product of a τ or a W, and thus with $x_3 \sim 1$. In order to further reduce the contamination we also require $x_3 \leq 0.7$ for $\tau\tau + WW$ events. This discussion is summarized in Table 5.13, where the main cuts applied in this analysis are listed.

One last comment is in order: separating $\tau\tau$ and WW decays is rather inefficient (as shown in Figure 5.13 we can not rely on the invariant mass distribution of the reconstructed τs or Ws), so we have to keep both at the same time. This approach is justified by the fact that the efficiency ϵ for evaluating the cross sections of both types of processes is rather similar, allowing to treat both together consistently.

In order to measure the total pair production cross section using equation (5.14), we have to estimate the efficiency for each process. From our MC simulations we can calculate the efficiency for each subsample including the corresponding BRs, obtaining: $\epsilon_{\ell\ell\ell\ell} = 0.6, \epsilon_{\ell\ell\ell\tau} = 0.09$ and $\epsilon_{\ell\ell\tau\tau} \sim \epsilon_{\ell\ell WW} = 0.02$, respectively. Then, counting the number of events of each of the three subsets and dividing by the corresponding efficiency, we can measure the doubly-charged scalar pair production cross section, once the integrated luminosity $\mathcal{L}_{int}$ is known. If the statistics is low (either because the luminosity is small or because the BR into non-$\ell\ell$ states are large and then the efficiencies kill most

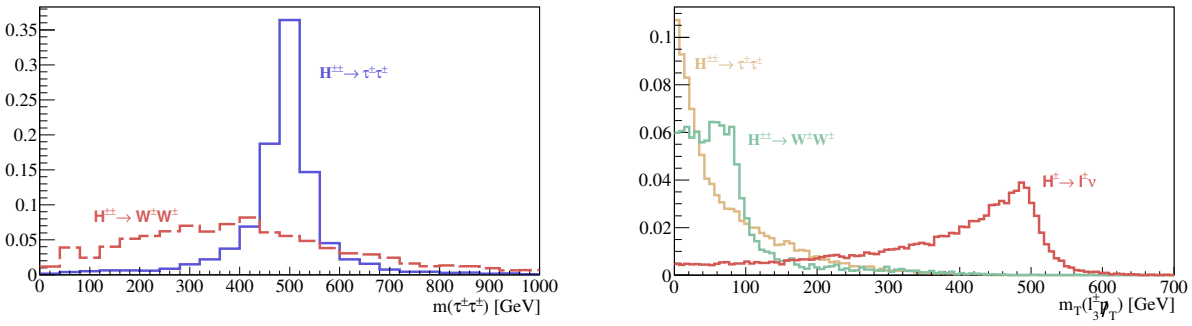

Figure 5.13: Left: Invariant mass distribution of the two reconstructed taus for both $\ell^\pm\ell^\pm W^\mp W^\mp$ and $\ell^\pm\ell^\pm\tau^\mp\tau^\mp$ decay channels in doubly-charged scalar pair production. Right: Transverse mass distribution of the opposite-sign lepton and the E_T^{miss} for several signals.

of the signal), the number of events entering equation 5.14 is small and then the relative error on the determination of σ is large. As an example, we illustrate in Table 5.14 four different cases: $(z_{\ell\ell}, z_{\ell\tau}, z_{\tau\tau} + z_{WW}) = (1,0,0), (1/2,1/2,0), (1/2,0,1/2), (1/3,1/3,1/3)$, [21] for each multiplet addition. Note that we specify in each case the total number of events passing the cuts in Table 5.13, $(\ell^\pm\ell^\pm)\ell^\mp\ell^\mp E_T^{miss}$, and also have both same-sign pairs reconstructing the doubly-charged scalar mass, $(\ell^\pm\ell^\pm)(\ell^\mp\ell^\mp)$.

5.6.2 Determination of the quantum numbers

Once the neutral cross section is determined, the different multiplets can be distinguished, excluding the singlet and the doublet which are essentially equivalent as their neutral cross sections are. In the left panel of Figure 5.14 we plot the statistical error for such a determination for several $H^{\pm\pm}$ BR assumptions and the five multiplet assignments T_Y discussed above.

The cross sections are correctly reproduced because they are an input, but what matters is with which precision can we measure them in order to distinguish between different multiplet assignments. We draw statistical errors including the effect of SM backgrounds for three different integrated luminosities: 100, 300 and 3000 fb^{-1}. (For

[21] In definite models as in the see-saw of type II, the Yukawa couplings giving neutrinos a mass are the same mediating the same-sign dileptonic scalar decay, and they are then constrained, but this is not so in general.

		(1, 0, 0)	$(\frac{1}{2}, \frac{1}{2}, 0)$	$(\frac{1}{2}, 0, \frac{1}{2})$	$(\frac{1}{3}, \frac{1}{3}, \frac{1}{3})$
Ω	$(l^{\pm}l^{\pm})l^{\mp}l^{\mp}E_T^{miss}$	1307 ± 38	501 ± 25	362 ± 22	238 ± 19
	$(l^{\pm}l^{\pm})(l^{\mp}l^{\mp})$	1046 ± 32	261 ± 16	261 ± 16	116 ± 11
Σ	$(l^{\pm}l^{\pm})l^{\mp}l^{\mp}E_T^{miss}$	765 ± 30	293 ± 20	212 ± 18	139 ± 16
	$(l^{\pm}l^{\pm})(l^{\mp}l^{\mp})$	612 ± 24	153 ± 12	153 ± 12	68 ± 8
Δ	$(l^{\pm}l^{\pm})l^{\mp}l^{\mp}E_T^{miss}$	383 ± 22	147 ± 16	106 ± 15	70 ± 13
	$(l^{\pm}l^{\pm})(l^{\mp}l^{\mp})$	306 ± 18	77 ± 9	77 ± 9	34 ± 6
χ	$(l^{\pm}l^{\pm})l^{\mp}l^{\mp}E_T^{miss}$	189 ± 17	73 ± 14	53 ± 13	35 ± 12
	$(l^{\pm}l^{\pm})(l^{\mp}l^{\mp})$	151 ± 12	38 ± 6	38 ± 6	17 ± 4
κ^{++}	$(l^{\pm}l^{\pm})l^{\mp}l^{\mp}E_T^{miss}$	168 ± 17	64 ± 13	47 ± 13	31 ± 12
	$(l^{\pm}l^{\pm})(l^{\mp}l^{\mp})$	135 ± 12	34 ± 6	34 ± 6	15 ± 4

Table 5.14: Number of expected signal events with four charged leptons, electrons or muons, at LHC with $\sqrt{s} = 14$ TeV and an integrated luminosity of 300 fb^{-1} for a doubly-charged scalar mass of 500 GeV belonging to an EW quintuplet, quadruplet, triplet, doublet or singlet with hypercharge 0, 1/2, 1, 3/2 and 2, respectively, and different BR $(z_{\ell\ell}, z_{\ell\tau}, z_{\tau\tau} + z_{WW})$ assumptions, after the cuts of Table 5.13. We also specify the number of events with the two same-sign pairs reconstructing both scalars. Only statistical errors are included.

example, we find ~ 50 background events for $\mathcal{L}_{int} = 300$ fb^{-1} with four charged leptons adding to zero total electric charge and a same-sign pair reconstructing the $H^{\pm\pm}$ mass within 40 GeV.) As in Table 5.14, we fix four definite sets of doubly-charged scalar BRs: $(z_{\ell\ell}, z_{l\tau}, z_{\tau\tau} + z_{WW}) = (1, 0, 0)$, $(1/2, 1/2, 0)$, $(1/2, 0, 1/2)$, $(1/3, 1/3, 1/3)$, being higher the precision with $z_{\ell\ell} > z_{\ell\tau} > z_{\tau\tau} + z_{WW}$. Concerning the discrimination of the singlet and the doublet, we have to rely on the associated production channel, given that this is absent in the first one. If there is a significant excess of events compatible with $H^{\pm\pm}H^{\mp}$, the singlet hypothesis is automatically ruled out. However, to establish whether this is the case must be carefully assessed because the observation of only three leptons in the final state does not uniquely characterize this (charged-current) process. For instance, pair produced doubly-charged scalars decaying into $\ell^{\pm}\ell^{\pm}\ell^{\mp}\tau^{\mp}$, $\ell^{\pm}\ell^{\pm}\tau^{\mp}\tau^{\mp}$ or $\ell^{\pm}\ell^{\pm}W^{\mp}W^{\mp}$ can also produce only three leptons if one τ or W decays hadronically. Therefore, we need to rely on extra variables in order to forbid these (neutral-current) contributions. Two discriminators appear to be most convenient: the E_T^{miss}, which is

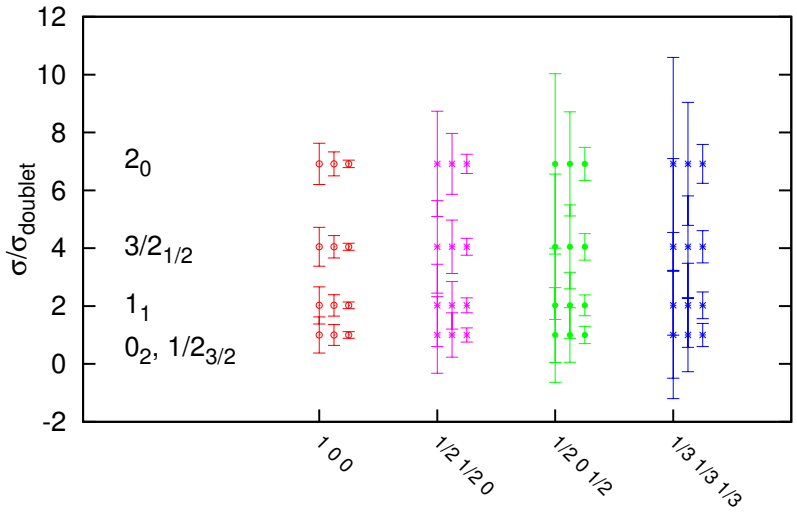

Figure 5.14: Uncertainty on the determination of $\sigma(pp \to \mathrm{H}^{++}\mathrm{H}^{--})$ for different $\mathrm{H}^{\pm\pm}$ BR assumptions at three different luminosities at the LHC: 100, 300 and 3000 fb^{-1}. The labels on the left stand for the doubly-charged scalar T_Y quantum numbers.

larger in single $\mathrm{H}^{\pm\pm}$ production than in $\ell^\pm\ell^\pm\ell^\mp\tau^\mp$ events with $\tau^\mp$ decaying hadronically, which allows to separate both contributions; and the transverse invariant mass of the opposite-sign lepton and the E_T^{miss}, $m_T(l_3^\pm E_T^{miss})$, which peaks near the $\mathrm{H}^\pm$ mass in the charged-current process, as shown in the right side of Figure 5.14. It is apparent from this figure that a cut on $m_T > 250$ GeV suppresses the neutral $\tau\tau$ and WW contributions quite efficiently.

A final comment concerns the experimental confirmation of LNV. A detailed analysis for such a purpose is not covered in the present text, although we propose the following guideline. If such a doubly-charged scalar is observed, one must attempt to separate $\tau\tau$ from WW events. This separation should make use of the invariant mass distribution in Figure 5.13: WW events are defined as those outside a wide enough interval around the $\mathrm{H}^{\pm\pm}$ mass. Reconstructed $\tau\tau$ events near the doubly-charged scalar mass are interpreted as genuine $\tau\tau$ decays. For the events left, and interpreted as WW decays, one must also check that the assignment is consistent with such an $\mathrm{H}^{\pm\pm}$ decay. One can also check the consistency with the excess of events resulting from the semileptonic decay of the WW pair, but this has additional backgrounds.

Chapter 6

Conclusions

The Standard Model of particle physics represents the triumph of our understanding of the properties and interactions of the elementary particles. In particular, with the discovery of the Higgs boson in 2013, the search for all the elementary particles predicted by the Standard Model has concluded. However, there are still intriguing open questions, both from the theoretical and experimental sides, that the Standard Model can not answer. Some of these questions are related to the mass of the elementary particles (and hence with the Higgs sector): why is the Higgs boson so light, if it is supposed to be an elementary particle? Why the mass of the elementary fermions are so different? And why neutrinos are massive, as evidenced by a large number of very different neutrino experiments, contrary to what the Standard Model asserts?

All these questions suggest that there should be physics beyond the Standard Model. Given that the Higgs sector is the source of most of these problems, and is the one from which we have the least experimental input, we have argued that new physics is likely related to the scalar sector. According to this, we have considered two important extensions of the Higgs sector that can give an answer to some of the open questions. These are composite Higgs models (which can explain why the Higgs boson is light in a natural way as well as the hierarchy in the fermion masses) and models with lepton number violating scalars (that can therefore account for the —Majorana— mass of the neutrinos). In both cases, new particles potentially observable at accelerators appear. We have mainly focused on the phenomenology of these particles at the LHC. In order to do that, we have first presented the relevant computational and statistical tools and

then we have discussed the phenomenology of these models in much detail.

Composite Higgs models assume the Higgs boson to be a bound state of a new strongly-interacting sector, with global symmetry group G spontaneously broken to H. The global symmetry is explicitly broken by the linear couplings between the composite and the elementary sectors (which mix the composite resonances with the fermions in the elementary sector). Then the Higgs boson arises as a pseudo Nambu-Goldstone boson. We have distinguished the phenomenological study of the new resonances (which can be either vector or fermionic) according to whether they interact mostly with the top quark t (Section 4.5), with the bottom quark b (Section 4.6) or with the light quarks q (Section 4.7). We have discussed [4, 5, 7, 10, 12, 15], in the minimal composite Higgs model, the production of an s-channel heavy gluon G and its subsequent decay through a quark ψ and its heavy partner Ψ, according to the process $pp \to G \to \psi\Psi \to h\psi\psi$, where h stands for the Higgs boson and $\psi = t, b$ or q depending on the case. The final states to which this process gives rise are, respectively, $ht\bar{t}$, $hb\bar{b}$ and $hq\bar{q}$. In the first two cases we can consider the main Higgs decay channel, that is $h \to b\bar{b}$, while in the third one we consider the decay into W bosons, $h \to W^{\pm *}W^{\mp}$. The detailed study of this process has allowed us to conclude that, even with the current experimental constraints, very large regions of the parameter space could be probed with the $\sqrt{s} = 7$ and 8 TeV LHC data. And even further when the LHC starts working at $\sqrt{s} = 14$ TeV.

In the $ht\bar{t}$ final state, the most stringent bounds come from ATLAS and CMS direct searches of fermionic resonances decaying into $t\bar{t}$, from dijets searches and, at a lesser extent, from Higgs measurements. With the analyses we have proposed, the $ht\bar{t}$ final state mediated by a heavy gluon of mass M_G can be discovered (excluded) with the current data for M_G of up to $\sim 2.5 - 2$ $(2.8 - 2.4)$ TeV, depending on the parameter space region. For $\sqrt{s} = 14$ TeV and an integrated luminosity of 100 fb^{-1}, these numbers are larger, being the discovery (exclusion) limit for this process at $M_G \sim 4.3$ (4.8) TeV.

In the $hb\bar{b}$ channel, the main experimental constraints are given by measurements in four b-jets final states, motivated mostly by SUSY searches, although dijets searches are also relevant. With the proposed analyses, the $hb\bar{b}$ final state mediated by a heavy gluon with mass M_G can be discovered (excluded) for $M_G \lesssim 1.5 - 2.7$ (3) TeV with the current data, and for $M_G \lesssim 4.5$ (5) TeV in a larger run with 14 TeV and 100 fb^{-1}.

In the $hq\bar{q}$ channel the most important bounds come from searches of single-produced

light quark resonances, although again dijets searches impose non-negligible constraints. The discovery of this final state mediated by a heavy gluon of mass M_G becomes unreachable with the 7 and 8 TeV data, and only for masses below ~ 3.3 (3.5) TeV could be discovered (excluded) at 14 TeV.

We also study the production of resonances of the up quark, U_h, not mediated by a heavy gluon. Two different channels are considered. First, the vector-boson-Higgs fusion channel, which leads to the $Vhjj$ final state (with $V = W, Z$). In this case, U_h masses of up to 1.8 (2) TeV can be discovered (excluded) depending on the region of the parameter space in LHC collisions at $\sqrt{s} = 14$ TeV and an integrated luminosity of 300 fb^{-1}. Second, the associated-production channel, $gq \to hU_h \to hjj$. In this channel the discovery and exclusion regions change depending on whether we consider the hh decay into $\gamma\gamma b\bar{b}$ or into $b\bar{b}b\bar{b}$. Again with $\sqrt{s} = 14$ TeV and 300 fb^{-1}, masses of up to 1 (1.4) TeV in the first case and up to 1.2 (1.6) in the second one can be discovered (excluded). In this section too, we argue that the $t\bar{t}$ asymmetry observed at the Tevatron can be also explained by the interference of a broad heavy gluon, provided it decays into a SM quark and its heavier composite partner ($\Psi\psi$) final state [10, 11].

We have also briefly introduced (Section 4.8) a new composite Higgs model based on the symmetry breaking pattern $SO(7) \to G_2$ [6]. We have seen that seven degrees of freedom arise in the scalar spectrum of this model, that transform as $(\mathbf{2}, \mathbf{2}) + (1, \mathbf{3})$ under the custodial symmetry group $SU(2)_L \times SU(2)_R$. Thus, they give rise to the Higgs doublet ϕ together with three additional singlets $\kappa^\pm$ and η with electric charges 0 and ± 1 respectively. We have seen that both the right- and the left-handed components of the top and bottom quarks can be embedded in two representations **8** of $SO(7)$, in such a way that: *(i)* the bottom (top) quark mass is naturally small (large); *(ii)* the $Z\overline{b_L}b_L$ coupling is protected; and *(iii)* $\kappa^\pm$ and η decay into Standard Model fermions. We have also outlined the phenomenological implications of this model. In particular, the Higgs decay into diphotons, wich becomes modified by loops of $\kappa^\pm$, in agreement with some recent measurements.

The phenomenology of lepton number violating scalars [9, 13] has been discussed in Sections 5.1 (for scalars with renormalizable couplings to the leptons) and 5.2 (for scalars with effective leptonic interactions). In this way, we have extended the *see-saw* model of type II and classified the scalar multiplets H which produce the same signals,

paying special attention to their lepton number violating decays: $pp \to H^{++}H^{--} \to \ell^{\pm}\ell^{\pm}W^{\mp}W^{\mp}$ and $pp \to H^{\pm\pm}H^{\mp} \to \ell^{\pm}\ell^{\pm}W^{\mp}Z$, not explicitly considered up to now. All those multiplets include doubly-charged scalars. We have discussed the main doubly-charged scalar production mechanisms and worked out the corresponding Feynman rules in detail, providing an `UFO` model for `MadGraph`. As a practical application we have reproduced the current searches for doubly-charged scalars performed by CMS and ATLAS at $\sqrt{s} = 7$ TeV. This has allowed us to provide an efficiency table for the different processes in which the charged scalars present two-body decays into Standard Model particles. Using this table for non lepton number violating processes we have obtained that current limits (Section 5.4) in the mass of these particles are of the order of 400 GeV for the triplet belonging to the *see-saw* model of type II (depending on the decay channel considered), going up to 500 GeV for the highest-spin multiplet (the quintuplet). For the first time, we obtain also limits for lepton number violating processes. Although current bounds are low (being always smaller than 300 GeV —see Section 5.4.2—), future analyses can exclude masses of the order of 1 TeV for $\sqrt{s} = 14$ TeV and 100 fb^{-1}. Finally, we have discussed how to measure the quantum numbers of H if it is experimentally observed in future collisions at the LHC [8, 14]. In order to do that, it is mandatory to count the number of events in some of the allowed decay channels that $H^{++}H^{--}$ and $H^{\pm\pm}H^{\mp}$ pairs can decay to (Section 5.6). As a result, we have found that the different scalar multiples can be distinguished at the 3 σ confidence level only with a large luminosity. For instance, if H decays only into $\ell^{\pm}\ell^{\pm}$ pairs, the required luminosity to discriminate between different multiplets stays around 300 fb^{-1} for $\sqrt{s} = 14$ TeV; while if H decays into $\ell^{\pm}\tau^{\pm}$ too, around 3000 fb^{-1} are necessary.

Note that for this study we have assumed the most optimistic scenario in order to estimate the LHC potential for these searches. We not only assume that doubly-charged scalars have similar decay rates into same-sign lepton and gauge bosons, but that cascade decays within the multiplet are negligible. Which requires that the scalar mixing is rather small. At any rate, it is worth to point out that in specific models (typically with radiatively-generated neutrino masses) this scenario naturally arises.

In summary, we have shown that the LHC has a unique potential to disentangle an extended Higgs sector, thereby providing essential information to address some of the most exciting mysteries of particle physics.

Conclusiones

El modelo estándar de la física de partículas ha supuesto un éxito sin precedentes en la comprensión de las propiedades de las partículas elementales y sus interacciones. En particular, con el descubrimiento del bosón de Higgs en 2013, la búsqueda de todas y cada una de las partículas predichas por el modelo estándar ha concluido. Sin embargo, todavía hoy existen cuestiones teóricas y experimentales de suma importancia a las que el modelo estándar no es capaz de dar respuesta. Algunas de las más destacadas están relacionadas con la masa de las partículas elementales (y, por lo tanto, con el sector de Higgs): ¿por qué el bosón de Higgs es tan ligero, siendo una partícula escalar elemental? ¿Por qué los fermiones tienen masas tan diferentes? Y ¿por qué los neutrinos tienen masa, como evidencia una vasta cantidad de experimentos, a diferencia de lo que afirma el modelo estándar?

Estas preguntas sugieren que ha de existir física más allá del modelo estándar. Por cuanto el sector de Higgs es la fuente principal de estas preguntas, y es asimismo el sector del que menos información experimental disponemos, hemos insistido en la física nueva ha de estar relacionada con el sector escalar. De acuerdo a esta observación, hemos considerado dos grandes extensiones del sector de Higgs que pueden dar respuesta a algunas de las preguntas abiertas: modelos de Higgs compuesto (que explican por qué el bosón de Higgs es tan ligero y por qué los fermiones tienen masas tan distintas) y modelos con escalares que violan número leptónico (que, por tanto, pueden explicar por qué los neutrinos tienen masa —de Majorana—). En ambos casos aparecen nuevas partículas que podrían producirse en aceleradores. Por su importancia actual, nos hemos centrado esencialmente en la fenomenología de estas partículas en el LHC. Para ello, hemos introducido primero las herramientas computacionales y estadísticas, y hemos discutido en detalle después la fenomenología de estos modelos.

En los modelos de Higgs compuesto se asume que el bosón de Higgs es un estado ligado de un nuevo sector fuertemente acoplado, con simetría global G espontáneamente rota a H. La simetría global está explćitamente rota por las interacciones lineales entre el sector compuesto y el sector elemental (que mezclan las resonancias de uno con las partículas del otro). El bosón de Higgs aparece así como un seudobosón de Nambu-Goldstone. Hemos distinguido el estudio de la fenomenología de las nuevas resonancias (fermiónicas y vectoriales) de acuerdo a si estas interaccionan más fuertemente con el quark *top* t (sección 4.5), con el *bottom* b (sección 4.6) o con los quarks ligeros q (sección 4.7). En los tres casos hemos estudiado en detalle [4, 5, 7, 10, 12, 15], en el modelo mínimo de Higgs compuesto, la producción de un gluón pesado G en canal s y su posterior desintegración vía un quark ψ y su correspondiente resonancia fermiónica Ψ, según el proceso $pp \to G \to \psi\Psi \to h\psi\psi$, siendo h el bosón de Higgs y $\psi = t, b, q$ según el caso considerado. Los estados finales a los que este proceso da lugar son, respectivamente, $ht\bar{t}$, $hb\bar{b}$ y $hq\bar{q}$. En los dos primeros podemos considerar la desintegración del bosón de Higgs en su canal principal, $b\bar{b}$. En el tercer caso consideramos $h \to W^{\pm *}W^{\mp}$. El estudio detallado de este proceso nos ha permitido concluir que, aun con las cotas experimentales actuales, podrían probarse regiones amplísimas del espacio de parámetros con los datos de que disponemos a $\sqrt{s} = 7$ y 8 TeV y, sobre todo, en un futuro próximo en el que el LHC funcione a $\sqrt{s} = 14$ TeV.

En el estado final $ht\bar{t}$, las cotas experimentales ms importantes vienen de bsquedas de resonancias fermiónicas en $t\bar{t}$, de búsquedas en pares de *jets* y, en menor medida, de medidas de las propiedades del bosón de Higgs. Con los análisis que hemos propuesto (sección 4.5.2), las resonancias del *top* producidas tras la desintegración de un gluón pesado G de masa M_G podrían descubrirse (excluirse) con los datos actuales para M_G de hasta $\sim 2.5 - 2$ $(2.8 - 2.4)$ TeV dependiendo de la región considerada del espacio de parámetros. Para $\sqrt{s} = 14$ TeV con una luminosidad integrada de 100 fb^{-1}, los límites crecen hasta $M_G \sim 4.3$ (4.8) TeV para el descubrimiento (la exclusión).

En el canal $hb\bar{b}$, las principales restricciones experimentales vienen de medidas en cuatro *jets* b, motivadas principalmente por búsquedas de SUSY, aunque las búsquedas en pares de *jets* son asimismo relevantes. Con los análisis propuestos, el canal $hb\bar{b}$ mediado por un gluón pesado de masa M_G podrá ser descubierto (excluido) para $M_G \lesssim 1.5 - 2.7$ (3) TeV con los datos actuales, y para $M_G \lesssim 4.5$ (5) TeV en una fase posterior

del LHC.

El canal $hq\bar{q}$ las cotas ms importantes vienen de búsquedas directas de resonancias de quarks ligeros, aunque de nuevo hay que tener en cuenta las búsquedas en pares de jets. El descubrimiento del estado final $hq\bar{q}$ mediado por un gluón pesado de masa M_G con los datos de LHC a 7 y 8 TeV serćasi imposible. No obstante, podría descubrirse (excluirse) para masas por debajo de $\sim$ 3.3 (3.5) TeV a 14 TeV. La producción de resonancias del quark *up* la estudiamos también en dos canales en los que no interviene un *gluón* pesado. En primer lugar, mediante fusión del Higgs con los bosones vectoriales, lo que da lugar al estado final $Vhjj$ (con $V = W, Z$). En tal caso, masas de U_h de hasta 1.8 (2) TeV podrían descubrirse (excluirse) dependiendo de la región del espacio de parámetros, en colisiones en el LHC a $\sqrt{s} = 14$ TeV con 300 fb^{-1} de luminosidad. Y en segundo lugar, ía producción asociada, $gq \to hU_h \to hjj$, en cuyo caso los límites son distintos dependiendo de si se considera la desintegración de hh en $\gamma\gamma b\bar{b}$ o en $b\bar{b}b\bar{b}$. As, con $\sqrt{s} = 14$ TeV y 300 fb^{-1} se podrían descubrir (excluir) masas de hasta 1 (1.4) TeV en el primer caso y de hasta 1.2 (1.6) en el segundo. En esa misma sección discutimos que, en regiones adecuadas del espacio de parámetros, la asimetría en $t\bar{t}$ observada en Tevatron también podría explicarse por la interferencia de un gluón pesado con una anchura grande debido a su desintegración en otras resonancias fermiónicas [10, 11].

También hemos introducido brevemente (sección 4.8) un nuevo modelo de Higgs compuesto basado en la rotura de simetría $SO(7) \to G_2$ [6]. Hemos visto que el sector escalar de este modelo está compuesto por siete grados de libertad, que transforman bajo la simetría custodial $SU(2)_L \times SU(2)_R$ como $(\mathbf{2}, \mathbf{2}) + (1, \mathbf{3})$, dando lugar al doblete de Higgs, ϕ, y a tres singletes $\kappa^{\pm}$ y η con cargas 0 y ± 1 respectivamente. Hemos visto cómo embeber las partes levórigas y dextrógiras de los quarks *top* y *bottom* en dos representaciones irreducibles **8** de $SO(7)$, de tal suerte que: *(i)* de forma natural, la masa del quark *bottom* (*top*) es pequeña (grande); *(ii)* el acoplamiento Zb_Lb_L está protegido; y *(iii)* $\kappa^{\pm}$ y η se desintegran en fermiones del modelo estándar. Hemos discutido someramente las consecuencias fenomenológicas de este modelo. En particular, la desintegración del Higgs en dos fotones, que se ve alterada por los *loops* de $\kappa^{\pm}$, de acuerdo con lo que sugieren algunas medidas recientes.

La fenomenología de los campos escalares que violan número leptónico [9, 13] la hemos discutido en las secciones 5.1 (aquellos cuyas interacciones con los leptones del

modelo estándar son renormalizables) y 5.2 (aquellos con interacciones efectivas con los leptones). De este modo, hemos extendido el modelo *see-saw* de tipo II y clasificado los multipletes escalares H que producen las mismas señales, prestando especial atención a los procesos que violan número leptónico: $pp \to \mathrm{H}^{++}\mathrm{H}^{--} \to \ell^{\pm}\ell^{\pm}\mathrm{W}^{\mp}\mathrm{W}^{\mp}$ y $pp \to \mathrm{H}^{\pm\pm}\mathrm{H}^{\mp} \to \ell^{\pm}\ell^{\pm}\mathrm{W}^{\mp}\mathrm{Z}$, los cuales no habían sido considerados explícitamente hasta la fecha. Todos estos multipletes contienen, pues, componentes escalares doblemente cargadas. La producción de estas y su consecuente desintegración las hemos estudiado en la sección 5.3. Asimismo, facilitamos las reglas de Feynman y el correspondiente modelo `UFO` para `MadGraph`. Con todo, hemos reproducido las búsquedas actuales de escalares doblemente cargados en ATLAS y CMS a $\sqrt{s} = 7$ TeV. Esto nos ha permitido construir una tabla de eficiencias para todos los procesos en los que los escalares cargados se desintegran en pares de partículas del modelo estándar. Utilizando esta tabla para procesos que no violan número leptónico, obtenemos que los límites actuales (sección 5.4) en la masa de estas partículas son del orden de 400 GeV para el triplete del *see-saw* de tipo II (dependiendo de el canal de desintegración considerado), y de hasta 500 GeV para el multiplete de mayor isospín (el quintuplete). Por primera vez, obtenemos también límites para procesos que violan número leptónico. Si bien las cotas actuales para la masa de los escalares que median estos procesos son pequeñas (menores de 300 GeV en cualquier caso —véase sección 5.4.2—), podrían llegar hasta cerca del TeV para $\sqrt{s} = 14$ TeV con una luminosidad de 100 fb^{-1}. Finalmente, hemos discutido cómo identificar los números cuánticos de H si este es observado experimentalmente en colisiones futuras en el LHC [8, 14]. La estrategia se basa en medir algunos de los distintos canales en los que los pares $\mathrm{H}^{++}\mathrm{H}^{--}$ y $\mathrm{H}^{\pm\pm}\mathrm{H}^{\mp}$ pueden desintegrarse (sección 5.6). Como resultado, encontramos que los multipletes escalares pueden distinguirse unos de otros (con una confianza de $3\,\sigma$) solo con suficiente luminosidad. Por ejemplo, si estos solo se desintegran en pares $\ell^{\pm}\ell^{\pm}$ se necesitarían 300 fb^{-1} a $\sqrt{s} = 14$ TeV; mientras que si se desintegran tanto en $\ell^{\pm}\ell^{\pm}$ como en $\ell^{\pm}\tau^{\pm}$ harían falta alrededor de 3000 fb^{-1}. Cabe destacar la relevancia de estos resultados para el estudio fenomenológico de modelos en los que as masas de los neutrinos se producen radiativamente.

En resumen, hemos mostrado que el LHC tiene una capacidad inigualable para desentrañar la física de un sector de Higgs no estándar. Y, por tanto, arrojar luz sobre algunos de los misterios más excitantes de la física de partículas actual.

Appendix A

SU(2) and the Pauli matrices

The $SU(2)$ group is the universal recovering of $SO(3)$ —the group of rotations in the three-dimensional vector space—. It has therefore dimension three. Its Lie algebra can then be expanded in terms of three operators that we label T_1, T_2 and T_3, independently of the explicit representation considered. The algebraic structure of $SU(2)$ can be defined through the commutation relations

$$[T_I, T_J] = i \sum_l \epsilon_{IJK} T_K, \tag{A.1}$$

where ϵ_{IJK} is the totally antisymmetric Levi-Civita tensor in three dimensions. In addition, two more operators, T^+ and T^-, are defined to be $T^\pm = T_1 \pm iT_2$. There is only one representation of $SU(2)$ for each dimension. The explicit matrix expressions of the first non-trivial representations are given below. For dimension two we have $T_I = 1/2\sigma_I$, being σ_I the Pauli matrices:

$$\sigma_1 = \begin{pmatrix} 0 & 1 \\ 1 & 0 \end{pmatrix}, \quad \sigma_2 = \begin{pmatrix} 0 & -i \\ i & 0 \end{pmatrix}, \quad \sigma_3 = \begin{pmatrix} 1 & 0 \\ 0 & -1 \end{pmatrix}. \tag{A.2}$$

For dimension three we have

$$T_1 = \frac{1}{\sqrt{2}} \begin{pmatrix} 0 & 1 & 0 \\ 1 & 0 & 1 \\ 0 & 1 & 0 \end{pmatrix}, \quad T_2 = \frac{i}{\sqrt{2}} \begin{pmatrix} 0 & -1 & 0 \\ 1 & 0 & -1 \\ 0 & 1 & 0 \end{pmatrix}, \quad T_3 = \begin{pmatrix} 1 & 0 & 0 \\ 0 & 0 & 0 \\ 0 & 0 & -1 \end{pmatrix}. \tag{A.3}$$

For dimension four we obtain

$$T_1 = \begin{pmatrix} 0 & \frac{\sqrt{3}}{2} & 0 & 0 \\ \frac{\sqrt{3}}{2} & 0 & 1 & 0 \\ 0 & 1 & 0 & \frac{\sqrt{3}}{2} \\ 0 & 0 & \frac{\sqrt{3}}{2} & 0 \end{pmatrix}, \quad T_2 = i \begin{pmatrix} 0 & -\frac{\sqrt{3}}{2} & 0 & 0 \\ \frac{\sqrt{3}}{2} & 0 & -1 & 0 \\ 0 & 1 & 0 & -\frac{\sqrt{3}}{2} \\ 0 & 0 & \frac{\sqrt{3}}{2} & 0 \end{pmatrix}, \tag{A.4}$$

$$T_3 = \begin{pmatrix} \frac{3}{2} & 0 & 0 & 0 \\ 0 & \frac{1}{2} & 0 & 0 \\ 0 & 0 & -\frac{1}{2} & 0 \\ 0 & 0 & 0 & -\frac{3}{2} \end{pmatrix};$$

while for dimension five we get

$$T_1 = \begin{pmatrix} 0 & 1 & 0 & 0 & 0 \\ 1 & 0 & \frac{\sqrt{6}}{2} & 0 & 0 \\ 0 & \frac{\sqrt{6}}{2} & 0 & \frac{\sqrt{6}}{2} & 0 \\ 0 & 0 & \frac{\sqrt{6}}{2} & 0 & 1 \\ 0 & 0 & 0 & 1 & 0 \end{pmatrix}, \quad T_2 = i \begin{pmatrix} 0 & -1 & 0 & 0 & 0 \\ 1 & 0 & -\frac{\sqrt{6}}{2} & 0 & 0 \\ 0 & \frac{\sqrt{6}}{2} & 0 & -\frac{\sqrt{6}}{2} & 0 \\ 0 & 0 & \frac{\sqrt{6}}{2} & 0 & -1 \\ 0 & 0 & 0 & 1 & 0 \end{pmatrix}, \tag{A.5}$$

$$T_3 = \begin{pmatrix} 2 & 0 & 0 & 0 & 0 \\ 0 & 1 & 0 & 0 & 0 \\ 0 & 0 & 0 & 0 & 0 \\ 0 & 0 & 0 & -1 & 0 \\ 0 & 0 & 0 & 0 & -2 \end{pmatrix}.$$

Appendix B

The non-linear sigma model and the Maurer-Cartan one-form

Typically in particle physics, and mainly in gauge theories, lagrangians are constructed out of fields taking values in linear spaces. In general, however, the introduction of target manifolds without any kind of vector structure is mandatory, giving rise to *non-linear sigma models*. This is the case, for instance, of the lagrangian describing the dynamics of a NGB coming from the symmetry breaking of G into H, in which the target manifold is the coset space G/H.

In the description of non-linear sigma models, a role of main importance is played by the *Maurer-Cartan one-form* over the group G. Let us call the Maurer-Cartan one-form over G as Ω. Ω is a one-form taking values in the Lie algebra of G, $\Omega : TG \to L(G)$, and thus a matrix of linear forms, defined in a point $g \in G$ as

$$\Omega_g^{ij} = \sum_k (g^{-1})^{ik} (dx^{kj})|_g, \tag{B.1}$$

where g^{ij} is the entry ij of the matrix defining the group element g, and x^{ij} are coordinate functions over G, $x^{ij} : G \to \mathbb{R}$ with $x^{ij}(g) = g^{ij}$. Given that physical fields are typically defined over the space-time $\mathcal{M}$, it is convenient to consider a section $\varphi : \mathcal{M} \to G$ of G, and pull-down Ω to the space-time by means of φ. That is:

$$(\varphi^* \Omega)_x^{ij} = \sum_\mu \sum_k \left(\varphi^{-1}(x)\right)^{ik} \frac{\partial}{\partial x^\mu} \varphi^{kj}(x) (dx^\mu)|_{\varphi(x)}, \tag{B.2}$$

i.e., a matrix of one-forms over $\mathcal{M}$, where now x^{ij} denote the usual coordinates on $\mathcal{M}$. This notation can be however a bit cumbersome. In order to get the standard notation, let us write $\varphi(x) = g(x)$, and forget the explicit dependence on x. Then,

$$(\varphi^*\Omega)^{ij} = \sum_\mu \sum_k (g^{-1})^{ik} \frac{\partial}{\partial x^\mu} g^{kj} dx^\mu. \tag{B.3}$$

Forgetting now the sums and the matrix components, and defining $\omega = \varphi^*\Omega$, we obtain

$$\omega = g^{-1}\partial_\mu g dx^\mu, \tag{B.4}$$

what is typically written as

$$\omega = g^{-1}dg. \tag{B.5}$$

Now, remember that every element of the group, $g \in G$, can be expressed as the exponential o some linear combination of generators in the Lie algebra of G:

$$g = \exp\left[i \sum h_a T^a\right] \tag{B.6}$$

for some real values h_a and a base T^a. In such a case, the Maurer-Cartan one form ω_μ can be written as

$$\omega_\mu = U^{-1}\partial_\mu U, \quad U = \exp\left[i \sum h_a(x) T^a\right]. \tag{B.7}$$

When dealing with coset manifolds G/H, we only consider the coset generators C_a instead of the whole set of generators T_a. Thus, we will usually work with the following objets:

$$\omega_\mu = U^{-1}\partial_\mu U, \quad U = \exp\left[i \sum h_a(x) C^a\right]. \tag{B.8}$$

Giving that ω takes values on the Lie algebra of G, it can be decomposed as the sum of two parts, one aligned along the broken generators C^a and the other along the unbroken ones T^a. These two parts are usually called d_μ and E_μ respectively. The Maurer-Cartan one-form can then be written as

$$\omega_\mu = U^{-1}\partial_\mu U = d^a_\mu T_a + E^a_\mu T_a = d_\mu + E_\mu. \tag{B.9}$$

d_μ will be the main object in the description of non-linear sigma models.

Appendix C

SO(5) and its SO(4) subgroup

The $SO(5)$ group is the group of rotations in the five-dimensional vector space. It has dimension ten, and thus its Lie algebra can be expanded by means of ten operators that we call J^{mn}, for $n > m$ and m running from 1 to 5. In its fundamental (i.e., five-dimensional) representation, the J^{mn} operators can be expressed in a convenient matrix form, with ij components given by

$$\mathrm{J}^{mn}_{ij} = -\frac{i}{\sqrt{2}}\left(\delta^m_i\delta^n_j - \delta^n_i\delta^m_j\right). \tag{C.1}$$

They are all normalized to $\mathrm{tr}(\mathrm{J}^{mn}\mathrm{J}^{lk}) = \delta^{ml}\delta^{nk}$. The $SO(4)$ group is maximally contained in $SO(5)$. Indeed, it is trivially expanded in terms of the the six operators $\mathrm{J}^{12}, \mathrm{J}^{13}, \mathrm{J}^{23}, \mathrm{J}^{24}$ and J^{34}. However, given that $SO(4)$ holds the well-known equality $SO(4) \simeq SU(2) \times SU(2)$, it is convenient to change the basis given by the previous operators to the one made of the operators

$$T^1_L = \frac{1}{\sqrt{2}}\left(\mathrm{J}^{14} + \mathrm{J}^{23}\right), \quad T^2_L = \frac{1}{\sqrt{2}}\left(\mathrm{J}^{24} - \mathrm{J}^{13}\right), \quad T^3_L = \frac{1}{\sqrt{2}}\left(\mathrm{J}^{12} + \mathrm{J}^{34}\right), \tag{C.2}$$

and

$$T^1_R = \frac{1}{\sqrt{2}}\left(\mathrm{J}^{23} - \mathrm{J}^{14}\right), \quad T^2_R = -\frac{1}{\sqrt{2}}\left(\mathrm{J}^{13} + \mathrm{J}^{24}\right), \quad T^3_R = \frac{1}{\sqrt{2}}\left(\mathrm{J}^{12} - \mathrm{J}^{34}\right). \tag{C.3}$$

Thus, the first three operators, T^I_L, expand the algebra of one $SU(2)$ that we call $SU(2)_L$, while the T^I_R expand $SU(2)_R$. The SM gauge group is trivially embedded in

$SO(4) \simeq SU(2)_L \times SU(2)_R$ once $U(1)_Y$ is identified with T^3_R. The rest of the operators, J^{m5}, expand the coset space $SO(5)/SO(4)$. We set by definition

$$C^m = \mathrm{J}^{m5}, \quad m = 1, 2, 3, 4. \tag{C.4}$$

The four C^m operators transform in the **4** (resp. the $(\mathbf{2} \times \mathbf{2})$) representation of $SO(4)$ (resp. $SU(2)_L \times SU(2)_R$), thus generating the quantum numbers of the SM Higgs boson. A vector in the **5** representation of $SO(5)$ transforms as

$$\mathbf{5} = \mathbf{4} + 1 = (\mathbf{2}, \mathbf{2}) + (1, 1) \tag{C.5}$$

under $SO(4)$ and $SU(2) \times SU(2)$ respectively [1]. Thus, in terms of its components along the custodial symmetry group, the five degrees of freedom of a field φ in the **5** representation of $SO(5)$ are expressed as

$$\varphi = \frac{1}{\sqrt{2}} \begin{pmatrix} \varphi_{--} - \varphi_{++} \\ -i(\varphi_{--} + i\varphi_{++}) \\ \varphi_{+-} + \varphi_{-+} \\ i(\varphi_{+-} - \varphi_{-+}) \\ \sqrt{2}\varphi_{00} \end{pmatrix}. \tag{C.6}$$

The indices s_1 and s_2 of $\varphi_{s_1 s_2}$ identify its charges under T^3_L and T^3_R. Thus, $s_1/2$ is the charge of $\varphi_{s_1 s_2}$ under T^3_L and $s_2/2$ is that under T^3_R. The $\sqrt{2}$ factors have been set to properly normalize φ. Finally, it is also worth noting that the commutator of two coset operators C^m and C^n has no components in the coset space. That is to say,

$$[C^m, C^n] = i \sum_l f^{mnl} C^l \tag{C.7}$$

for some structure functions f^{mnl}. In other words, the symmetry breaking pattern $SO(5)/SO(4)$ gives rise to a coset *symmetry space*.

---

[1] Indeed, a rotation in $SO(n)$ is always made around some vector $\vec{n}$. The vectors in the perpendicular plane to this vector rotate according to an $SO(n-1)$ transformation, while the vectors along $\vec{n}$ form a one-dimensional vector space that stays unchanged. This subspace is thus an invariant space. In the current representation, this vector space is the one expanded by the fifth component.

Appendix D

SO(7) and its G_2 subgroup

The generators of $SO(7)$ in its **8** representation can be constructed out of the seven γ matrices [267]: $\gamma_1 = i\sigma_2 \otimes i\sigma_2 \otimes i\sigma_2, \gamma_2 = \sigma_1 \otimes i\sigma_2 \otimes 1, \gamma_3 = i\sigma_2 \otimes 1, \gamma_4 = -i\sigma_2 \otimes 1 \otimes \sigma_3, \gamma_5 = 1 \otimes \sigma_1 \otimes i\sigma_2, \gamma_6 = -\sigma_3 \otimes i\sigma_2 \otimes 1$ and $\gamma_7 = -1 \otimes \sigma_3 \otimes i\sigma_2$, where σ_i represents the ith Pauli matrix. Out of them, we can construct the generators as $J_{mn} = -J_{nm} = -[J_m, J_n]/4$. The G_2 Lie algebra is then generated from the 14 generators F_i and M_i of the following set [266]:

$$
\begin{aligned}
F_1 &= -\frac{i}{2}(J_{24} - J_{51}), & M_1 &= \frac{i}{\sqrt{3}}(J_{24} + J_{51} - 2J_{73}), & N_1 &= \frac{i}{\sqrt{6}}(J_{24} + J_{51} + J_{73}),\\
F_2 &= \frac{i}{2}(J_{54} - J_{12}), & M_2 &= -\frac{i}{\sqrt{12}}(J_{54} + J_{12} - 2J_{67}), & N_2 &= \frac{i}{\sqrt{6}}(J_{54} + J_{12} + J_{67}),\\
F_3 &= -\frac{i}{2}(J_{14} - J_{25}), & M_3 &= \frac{i}{\sqrt{12}}(J_{14} + J_{25} - 2J_{36}), & N_3 &= \frac{i}{\sqrt{6}}(J_{14} + J_{25} + J_{36}),\\
F_4 &= -\frac{i}{2}(J_{16} - J_{43}), & M_4 &= \frac{i}{\sqrt{12}}(J_{16} + J_{43} - 2J_{72}), & N_4 &= \frac{i}{\sqrt{6}}(J_{16} + J_{43} + J_{72}),\\
F_5 &= -\frac{i}{2}(J_{46} - J_{31}), & M_5 &= \frac{i}{\sqrt{12}}(J_{46} + J_{31} - 2J_{57}), & N_5 &= \frac{i}{\sqrt{6}}(J_{46} + J_{31} + J_{57}),\\
F_6 &= -\frac{i}{2}(J_{35} - J_{62}), & M_6 &= \frac{i}{\sqrt{12}}(J_{35} + J_{62} - 2J_{71}), & N_6 &= \frac{i}{\sqrt{6}}(J_{35} + J_{62} + J_{71}),\\
F_7 &= \frac{i}{2}(J_{65} - J_{23}), & M_7 &= -\frac{i}{\sqrt{12}}(J_{65} + J_{23} - 2J_{47}), & N_7 &= \frac{i}{\sqrt{6}}(J_{65} + J_{23} + J_{47}).
\end{aligned}
$$

These are shown in Figure D.1. The coset manifold (represented by the red area in Figure D.1) and the relevant $SU(2)_L$ and $SU(2)_R$ groups (represented in gray) are also

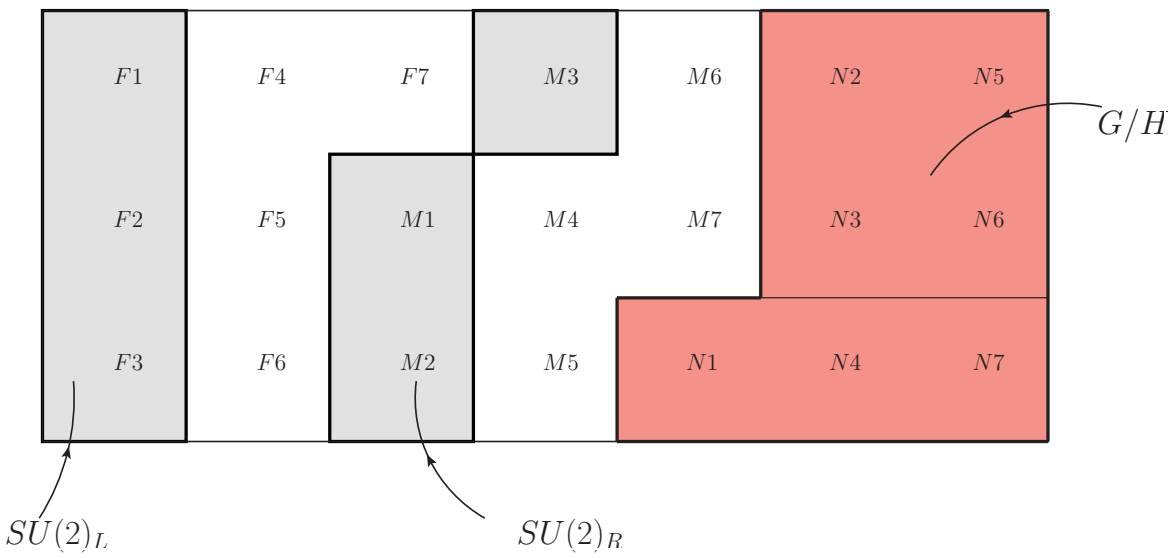

Figure D.1: Pictorial representation of the Lie algebra of $SO(7)$, and the embedding of its important subgroups $SU(2)_L \times SU(2)_R \subset G_2$.

shown.

The symmetry-breaking patter given by $SO(7) \to G_2$ provides seven new degrees of freedom. In order to describe the dynamics of these fields, we have to construct the Maurer-Cartan one-form of this manifold, and thus $U = \exp i\Pi$, where $\Pi = \sum C_a h^a$, C_a are the coset generators and h^a are the five pNGBs. The explicit expression of Π in the basis we are using is given by:

$$\Pi = \frac{2i}{3}\begin{pmatrix} 0 & \frac{k_2}{2} & -\frac{k_1}{2} & \frac{k_2+\eta}{2} & -\frac{h}{2} & -\frac{\eta}{2} & 0 & -\frac{k_2+\eta}{2} \\ -\frac{k_2}{2} & 0 & -\frac{k_2-\eta}{2} & \frac{k_1}{2} & \frac{\eta}{2} & -\frac{2\,k_1+h}{2} & -\frac{k_2+\eta}{2} & -h \\ \frac{k_1}{2} & \frac{k_2-\eta}{2} & 0 & \frac{k_2}{2} & 0 & -\frac{k_2-\eta}{2} & -\frac{h}{2} & \frac{\eta}{2} \\ -\frac{k_2+\eta}{2} & -\frac{k_1}{2} & -\frac{k_2}{2} & 0 & -\frac{k_2-\eta}{2} & -h & -\frac{\eta}{2} & \frac{2\,k_1-h}{2} \\ \frac{h}{2} & -\frac{\eta}{2} & 0 & \frac{k_2-\eta}{2} & 0 & -\frac{k_2}{2} & \frac{k_1}{2} & -\frac{k_2-\eta}{2} \\ \frac{\eta}{2} & \frac{2\,k_1+h}{2} & \frac{k_2-\eta}{2} & h & \frac{k_2}{2} & 0 & \frac{k_2+\eta}{2} & -\frac{k_1}{2} \\ 0 & \frac{k_2+\eta}{2} & \frac{h}{2} & \frac{\eta}{2} & -\frac{k_1}{2} & -\frac{k_2+\eta}{2} & 0 & -\frac{k_2}{2} \\ \frac{k_2+\eta}{2} & h & -\frac{\eta}{2} & -\frac{2\,k_1-h}{2} & \frac{k_2-\eta}{2} & \frac{k_1}{2} & \frac{k_2}{2} & 0 \end{pmatrix}. \quad \text{(D.1)}$$

Note that only the would-be physical degrees of freedom are explicitly written. The three degrees of freedom that, together with h form the Higgs doublets, are not shown.

List of Figures

List of Tables

Bibliography

[1] C. Csaki, C. Grojean, L. Pilo, and J. Terning, *Towards a realistic model of Higgsless electroweak symmetry breaking*, *Phys.Rev.Lett.* **92** (2004) 101802, [hep-ph/0308038].

[2] C. Csaki, C. Grojean, H. Murayama, L. Pilo, and J. Terning, *Gauge theories on an interval: Unitarity without a Higgs*, *Phys.Rev.* **D69** (2004) 055006, [hep-ph/0305237].

[3] A. Falkowski, C. Grojean, A. Kaminska, S. Pokorski, and A. Weiler, *If no Higgs then what?*, *JHEP* **1111** (2011) 028, [arXiv:1108.1183].

[4] A. Atre, M. Chala, and J. Santiago, *Searches for new vector like quarks: Higgs channels*, *JHEP* **1305** (2013) 099, [arXiv:1302.0270].

[5] A. Carmona, M. Chala, and J. Santiago, *New Higgs production mechanism in composite Higgs models*, *JHEP* **1207** (2012) 049, [arXiv:1205.2378].

[6] M. Chala, *$h \to \gamma\gamma$ excess and dark matter from composite Higgs models*, *JHEP* **1301** (2013) 122, [arXiv:1210.6208].

[7] M. Chala and J. Santiago, *$hb\bar{b}$ production in composite Higgs models*, *Phys.Rev.* **D88** (2013) 035010, [arXiv:1305.1940].

[8] F. del Aguila, M. Chala, A. Santamaria, and J. Wudka, *Discriminating between lepton number violating scalars using events with four and three charged leptons at the LHC*, *Phys.Lett.* **B725** (2013) 310–315, [arXiv:1305.3904].

[9] F. del Águila and M. Chala, *LHC bounds on lepton number violation mediated by doubly and singly-charged scalars*, *JHEP* **1403** (2014) 027, [arXiv:1311.1510].

[10] R. Barcelo, A. Carmona, M. Chala, M. Masip, and J. Santiago, *Single vectorlike quark production at the LHC*, *Nucl.Phys.* **B857** (2012) 172–184, [arXiv:1110.5914].

[11] A. Carmona, M. Chala, A. Falkowski, S. Khatibi, M. M. Najafabadi, et al., *From Tevatron's top and lepton-based asymmetries to the LHC*, arXiv:1401.2443.

[12] M. Chala and J. Santiago, *Physics of the interplay between the top quark and the Higgs boson*, *J.Phys.Conf.Ser.* **452** (2013) 012008, [arXiv:1303.0989].

[13] F. del Aguila, M. Chala, A. Santamaria, and J. Wudka, *Lepton number violation and scalar searches at the LHC*, *Acta Phys.Polon.* **B44** (2013) 2139–2148, [arXiv:1311.2950].

[14] F. del Aguila, M. Chala, A. Santamaria, and J. Wudka, *Distinguishing between lepton number violating scalars at the LHC*, *EPJ Web Conf.* **60** (2013) 17002, [arXiv:1307.0510].

[15] G. Brooijmans, B. Gripaios, F. Moortgat, J. Santiago, P. Skands, et al., *Les Houches 2011: Physics at TeV colliders new physics working group report*, arXiv:1203.1488.

[16] J. de Blas, M. Chala, and J. Santiago, *Global constraints on lepton-quark contact interactions*, *Phys.Rev.* **D88** (2013) 095011, [arXiv:1307.5068].

[17] S. L. Glashow, *Partial symmetries of weak interactions*, *Nucl.Phys.* **22** (1961) 579–588.

[18] P. W. Higgs, *Broken symmetries and the masses of gauge bosons*, *Phys.Rev.Lett.* **13** (1964) 508–509.

[19] F. Englert and R. Brout, *Broken symmetry and the mass of gauge vector mesons*, *Phys.Rev.Lett.* **13** (1964) 321–323.

[20] S. Weinberg, *A model of leptons*, *Phys.Rev.Lett.* **19** (1967) 1264–1266.

[21] M. Gell-Mann, *A schematic model of baryons and mesons*, *Phys.Lett.* **8** (1964) 214–215.

[22] G. Zweig, *An $SU(3)$ model for strong interaction symmetry and its breaking. version 1*, *CERN Document Server* (1964).

[23] M. Breidenbach, J. I. Friedman, H. W. Kendall, E. D. Bloom, D. H. Coward, et al., *Observed behavior of highly inelastic electron-proton scattering*, *Phys.Rev.Lett.* **23** (1969) 935–939.

[24] E. D. Bloom, D. H. Coward, H. C. DeStaebler, J. Drees, G. Miller, et al., *High-energy inelastic ep scattering at* 6 *degrees and* 10 *degrees*, *Phys.Rev.Lett.* **23** (1969) 930–934.

[25] M. L. Perl, G. S. Abrams, A. Boyarski, M. Breidenbach, D. Briggs, et al., *Evidence for anomalous lepton production in e^+e^- annihilation*, *Phys.Rev.Lett.* **35** (1975) 1489–1492.

[26] S. W. Herb, D. C. Hom, L. M. Lederman, J. C. Sens, H. D. Snyder, et al., *Observation of a dimuon resonance at* 9.5 *GeV in* 400 *GeV proton-nucleus collisions*, *Phys.Rev.Lett.* **39** (1977) 252–255.

[27] **PLUTO** Collaboration, C. Berger et al., *Jet analysis of the $\Upsilon(9.46)$ decay into charged hadrons*, *Phys.Lett.* **B82** (1979) 449.

[28] **TASSO** Collaboration, R. Brandelik et al., *Evidence for planar events in e^+e^- annihilation at high-energies*, *Phys.Lett.* **B86** (1979) 243.

[29] **UA2** Collaboration, M. Banner et al., *Observation of single isolated electrons of high transverse momentum in events with missing transverse energy at the CERN $\bar{p}p$ collider*, *Phys.Lett.* **B122** (1983) 476–485.

[30] **UA1** Collaboration, G. Arnison et al., *Experimental observation of isolated large transverse energy electrons with associated missing energy at $\sqrt{s} = 540$ GeV*, *Phys.Lett.* **B122** (1983) 103–116.

[31] **D0** Collaboration, S. Abachi et al., *Search for high mass top quark production in $p\bar{p}$ collisions at $\sqrt{s} = 1.8$ TeV*, *Phys.Rev.Lett.* **74** (1995) 2422–2426, [hep-ex/9411001].

[32] **CDF** Collaboration, F. Abe et al., *Observation of top quark production in $\bar{p}p$ collisions*, *Phys.Rev.Lett.* **74** (1995) 2626–2631, [hep-ex/9503002].

[33] **DONUT** Collaboration, K. Kodama et al., *Observation of tau neutrino interactions*, *Phys.Lett.* **B504** (2001) 218–224, [hep-ex/0012035].

[34] **ATLAS** Collaboration, G. Aad et al., *Observation of a new particle in the search for the Standard Model Higgs boson with the ATLAS detector at the LHC*, *Phys.Lett.* **B716** (2012) 1–29, [arXiv:1207.7214].

[35] **CMS** Collaboration, S. Chatrchyan et al., *Observation of a new boson at a mass of* 125 *GeV with the CMS experiment at the LHC*, *Phys.Lett.* **B716** (2012) 30–61, [arXiv:1207.7235].

[36] M. Baak, M. Goebel, J. Haller, A. Hoecker, D. Kennedy, et al., *The electroweak fit of the Standard Model after the discovery of a new boson at the LHC*, *Eur.Phys.J.* **C72** (2012) 2205, [arXiv:1209.2716].

[37] **ATLAS** Collaboration, *Updated coupling measurements of the Higgs boson with the ATLAS detector using up to* 25 fb^{-1} *of proton-proton collision data*, *CERN Document Server* (2014), no. ATLAS-CONF-2014-009.

[38] **CMS** Collaboration, S. Chatrchyan et al., *Search for the Standard Model Higgs boson produced in association with a w or a z boson and decaying to bottom quarks*, *Phys.Rev.* **D89** (2014) 012003, [arXiv:1310.3687].

[39] **CMS** Collaboration, S. Chatrchyan et al., *Evidence for the* 125 *GeV Higgs boson decaying to a pair of τ leptons*, arXiv:1401.5041.

[40] **CMS** Collaboration, S. Chatrchyan et al., *Measurement of Higgs boson production and properties in the ww decay channel with leptonic final states*, *JHEP* **1401** (2014) 096, [arXiv:1312.1129].

[41] **CMS** Collaboration, S. Chatrchyan et al., *Measurement of the properties of a Higgs boson in the four-lepton final state*, arXiv:1312.5353.

[42] **CMS** Collaboration, *Updated measurements of the Higgs boson at* 125 *GeV in the two photon decay channel*, *CERN Document Server* (2013), no. CMS-PAS-HIG-13-001.

[43] **Particle Data Group** Collaboration, J. Beringer et al., *Review of particle physics (rpp)*, *Phys.Rev.* **D86** (2012) 010001.

[44] T. Hambye, *Leptogenesis: beyond the minimal type I seesaw scenario*, *New J.Phys.* **14** (2012) 125014, [arXiv:1212.2888].

[45] J. Elias-Miro, J. R. Espinosa, G. F. Giudice, H. M. Lee, and A. Strumia, *Stabilization of the electroweak vacuum by a scalar threshold effect*, *JHEP* **1206** (2012) 031, [arXiv:1203.0237].

[46] J. Elias-Miro, J. R. Espinosa, G. F. Giudice, G. Isidori, A. Riotto, et al., *Higgs mass implications on the stability of the electroweak vacuum*, *Phys.Lett.* **B709** (2012) 222–228, [arXiv:1112.3022].

[47] A. de Gouvea, D. Hernandez, and T. M. P. Tait, *Criteria for natural hierarchies*, arXiv:1402.2658.

[48] B. T. Cleveland, T. Daily, J. Davis, Raymond, J. R. Distel, K. Lande, et al., *Measurement of the solar electron neutrino flux with the homestake chlorine detector*, *Astrophys.J.* **496** (1998) 505–526.

[49] **GALLEX** Collaboration, W. Hampel et al., *Gallex solar neutrino observations: Results for gallex iv*, *Phys.Lett.* **B447** (1999) 127–133.

[50] **GNO** Collaboration, M. Altmann et al., *Complete results for five years of GNO solar neutrino observations*, *Phys.Lett.* **B616** (2005) 174–190, [hep-ex/0504037].

[51] **SAGE** Collaboration, J. N. Abdurashitov et al., *Solar neutrino flux measurements by the soviet-american gallium experiment (SAGE) for half the 22 year solar cycle*, *J.Exp.Theor.Phys.* **95** (2002) 181–193, [astro-ph/0204245].

[52] **Super-Kamiokande** Collaboration, J. Hosaka et al., *Solar neutrino measurements in super-Kamiokande-I*, *Phys.Rev.* **D73** (2006) 112001, [hep-ex/0508053].

[53] **Super-Kamiokande** Collaboration, K. Abe et al., *Solar neutrino results in super-Kamiokande-III*, *Phys.Rev.* **D83** (2011) 052010, [arXiv:1010.0118].

[54] R. Becker-Szendy, C. B. Bratton, D. Casper, S. T. Dye, W. Gajewski, et al., *The electron-neutrino and muon-neutrino content of the atmospheric flux*, *Phys.Rev.* **D46** (1992) 3720–3724.

[55] **Super-Kamiokande** Collaboration, Y. Ashie et al., *A measurement of atmospheric neutrino oscillation parameters by super-Kamiokande I*, *Phys.Rev.* **D71** (2005) 112005, [hep-ex/0501064].

[56] **CALTECH-SIN-TUM** Collaboration, G. Zacek et al., *Neutrino oscillation experiments at the Gosgen nuclear power reactor*, *Phys.Rev.* **D34** (1986) 2621–2636.

[57] **CHOOZ** Collaboration, M. Apollonio et al., *Limits on neutrino oscillations from the chooz experiment*, *Phys.Lett.* **B466** (1999) 415–430, [hep-ex/9907037].

[58] F. Boehm, J. Busenitz, B. Cook, G. Gratta, H. Henrikson, et al., *Final results from the palo verde neutrino oscillation experiment*, *Phys.Rev.* **D64** (2001) 112001, [hep-ex/0107009].

[59] **KamLAND** Collaboration, A. Gando et al., *Constraints on θ_{13} from a three-flavor oscillation analysis of reactor antineutrinos at KamLAND*, *Phys.Rev.* **D83** (2011) 052002, [arXiv:1009.4771].

[60] **K2K** Collaboration, M. H. Ahn et al., *Measurement of neutrino oscillation by the K2K experiment*, *Phys.Rev.* **D74** (2006) 072003, [hep-ex/0606032].

[61] **MINOS** Collaboration, P. Adamson et al., *Improved search for muon-neutrino to electron-neutrino oscillations in MINOS*, *Phys.Rev.Lett.* **107** (2011) 181802, [arXiv:1108.0015].

[62] **T2K** Collaboration, K. Abe et al., *Indication of electron neutrino appearance from an accelerator-produced off-axis muon neutrino beam*, *Phys.Rev.Lett.* **107** (2011) 041801, [arXiv:1106.2822].

[63] D. B. Kaplan and H. Georgi, $SU(2) \times U(1)$ *breaking by vacuum misalignment*, *Phys.Lett.* **B136** (1984) 183.

[64] D. B. Kaplan, H. Georgi, and S. Dimopoulos, *Composite Higgs scalars*, *Phys.Lett.* **B136** (1984) 187.

[65] S. Dimopoulos and J. Preskill, *Massless composites with massive constituents*, *Nucl.Phys.* **B199** (1982) 206.

[66] D. B. Kaplan, *Flavor at ssc energies: A new mechanism for dynamically generated fermion masses*, *Nucl.Phys.* **B365** (1991) 259–278.

[67] M. S. Carena, E. Ponton, J. Santiago, and C. E. M. Wagner, *Light Kaluza Klein states in Randall-Sundrum models with custodial* $SU(2)$, *Nucl.Phys.* **B759** (2006) 202–227, [hep-ph/0607106].

[68] K. Agashe and R. Contino, *The minimal composite Higgs model and electroweak precision tests*, *Nucl.Phys.* **B742** (2006) 59–85, [hep-ph/0510164].

[69] M. S. Carena, E. Ponton, J. Santiago, and C. E. M. Wagner, *Electroweak constraints on warped models with custodial symmetry*, *Phys.Rev.* **D76** (2007) 035006, [hep-ph/0701055].

[70] F. del Aguila, A. Aparici, S. Bhattacharya, A. Santamaria, and J. Wudka, *A realistic model of neutrino masses with a large neutrinoless double beta decay rate*, *JHEP* **1205** (2012) 133, [arXiv:1111.6960].

[71] F. del Aguila, A. Aparici, S. Bhattacharya, A. Santamaria, and J. Wudka, *Effective lagrangian approach to neutrinoless double beta decay and neutrino masses*, *JHEP* **1206** (2012) 146, [arXiv:1204.5986].

[72] F. del Águila, A. Aparici, S. Bhattacharya, A. Santamaria, and J. Wudka, *Neutrinoless double* β *decay with small neutrino masses*, *PoS* **Corfu2012** (2013) 028, [arXiv:1305.4900].

[73] M. Gustafsson, J. M. No, and M. A. Rivera, *Predictive model for radiatively induced neutrino masses and mixings with dark matter*, *Phys.Rev.Lett.* **110** (2013) 211802, [arXiv:1212.4806].

[74] K. S. Babu, S. Nandi, and Z. Tavartkiladze, *New mechanism for neutrino mass generation and triply charged Higgs bosons at the LHC*, *Phys.Rev.* **D80** (2009) 071702, [arXiv:0905.2710].

[75] P. Minkowski, $\mu \to e\gamma$ *at a rate of one out of* 1*-billion muon decays?*, *Phys.Lett.* **B67** (1977) 421.

[76] T. Yanagida, *Horizontal symmetry and masses of neutrinos*, *Conf.Proc.* **C7902131** (1979) 95–99.

[77] M. Gell-Mann, P. Ramond, and R. Slansky, *Complex spinors and unified theories*, *Conf.Proc.* **C790927** (1979) 315–321, [arXiv:1306.4669].

[78] S. L. Glashow, *The future of elementary particle physics*, *NATO Adv.Study Inst.Ser.B Phys.* **59** (1980) 687.

[79] R. N. Mohapatra and G. Senjanovic, *Neutrino mass and spontaneous parity violation*, *Phys.Rev.Lett.* **44** (1980) 912.

[80] J. Schechter and J. W. F. Valle, *Neutrino masses in* $SU(2) \times U(1)$ *theories*, *Phys.Rev.* **D22** (1980) 2227.

[81] M. Magg and C. Wetterich, *Neutrino mass problem and gauge hierarchy*, *Phys.Lett.* **B94** (1980) 61.

[82] T. P. Cheng and L.-F. Li, *Neutrino masses, mixings and oscillations in* $SU(2) \times U(1)$ *models of electroweak interactions*, *Phys.Rev.* **D22** (1980) 2860.

[83] G. B. Gelmini and M. Roncadelli, *Left-handed neutrino mass scale and spontaneously broken lepton number*, *Phys.Lett.* **B99** (1981) 411.

[84] G. Lazarides, Q. Shafi, and C. Wetterich, *Proton lifetime and fermion masses in an* $SO(10)$ *model*, *Nucl.Phys.* **B181** (1981) 287–300.

[85] R. N. Mohapatra and G. Senjanovic, *Neutrino masses and mixings in gauge models with spontaneous parity violation*, *Phys.Rev.* **D23** (1981) 165.

[86] R. Foot, H. Lew, X. G. He, and G. C. Joshi, *Seesaw neutrino masses induced by a triplet of leptons*, *Z.Phys.* **C44** (1989) 441.

[87] E. Ma, *Pathways to naturally small neutrino masses*, *Phys.Rev.Lett.* **81** (1998) 1171–1174, [hep-ph/9805219].

[88] F. del Aguila and J. A. Aguilar-Saavedra, *Distinguishing seesaw models at LHC with multi-lepton signals*, *Nucl.Phys.* **B813** (2009) 22–90, [arXiv:0808.2468].

[89] **ATLAS** Collaboration, G. Aad et al., *Search for high-mass resonances decaying to dilepton final states in pp collisions at $\sqrt{s} = 7$ TeV with the ATLAS detector*, *JHEP* **1211** (2012) 138, [arXiv:1209.2535].

[90] **CMS** Collaboration, S. Chatrchyan et al., *A search for a doubly-charged Higgs boson in pp collisions at $\sqrt{s} = 7$ TeV*, *Eur.Phys.J.* **C72** (2012) 2189, [arXiv:1207.2666].

[91] M. Perelstein, *Introduction to collider physics*, arXiv:1002.0274.

[92] M. L. Mangano and S. J. Parke, *Multiparton amplitudes in gauge theories*, *Phys.Rept.* **200** (1991) 301–367, [hep-th/0509223].

[93] N. F. da Silva Fernandes de Castro, *Study of the wtb vertex structure at the ATLAS experiment*, *CERN Document Server* (2008), no. CERN-THESIS-2012-305.

[94] M. Benedikt, P. Collier, V. Mertens, J. Poole, and K. Schindl, *LHC design report. 3. the LHC injector chain*, *CERN Document Server* (2004), no. CERN-2004-003-V-3.

[95] O. Buning, P. Collier, P. Lebrun, S. Myers, R. Ostojic, et al., *LHC design report. 2. the LHC infrastructure and general services*, *CERN Document Server* (2004), no. CERN-2004-003-V-2.

[96] O. S. Bruning, P. Collier, P. Lebrun, S. Myers, R. Ostojic, et al., *LHC design report. 1. the LHC main ring*, *CERN Document Server* (2004), no. CERN-2004-003-V-1.

[97] E. Halkiadakis, *Proceedings for tasi 2009 summer school on 'physics of the large and the small': Introduction to the LHC experiments*, arXiv:1004.5564.

[98] **ATLAS** Collaboration, *ATLAS: Detector and physics performance technical design report. volume 1*, *CERN ATLAS Server* (1999).

[99] **ATLAS** Collaboration, *ATLAS: Detector and physics performance technical design report. volume 2*, *CERN ATLAS Server* (1999).

[100] **CMS** Collaboration, G. L. Bayatian et al., *Cms technical design report, volumes I, II and III: Physics performance*, *J.Phys.* **G34** (2007) 995–1579.

[101] G. P. Salam, *Towards jetography*, *Eur.Phys.J.* **C67** (2010) 637–686, [arXiv:0906.1833].

[102] G. C. Blazey, J. R. Dittmann, S. D. Ellis, V. D. Elvira, K. Frame, et al., *Run II jet physics*, hep-ex/0005012.

[103] S. Catani, Y. L. Dokshitzer, M. H. Seymour, and B. R. Webber, *Longitudinally invariant k_t clustering algorithms for hadron hadron collisions*, *Nucl.Phys.* **B406** (1993) 187–224.

[104] S. D. Ellis and D. E. Soper, *Successive combination jet algorithm for hadron collisions*, *Phys.Rev.* **D48** (1993) 3160–3166, [hep-ph/9305266].

[105] M. Cacciari, G. P. Salam, and G. Soyez, *The anti-k_t jet clustering algorithm*, *JHEP* **0804** (2008) 063, [arXiv:0802.1189].

[106] T. Gleisberg, S. Hoeche, F. Krauss, M. Schonherr, S. Schumann, et al., *Event generation with sherpa 1.1*, *JHEP* **0902** (2009) 007, [arXiv:0811.4622].

[107] M. L. Mangano, M. Moretti, F. Piccinini, R. Pittau, and A. D. Polosa, *Alpgen, a generator for hard multiparton processes in hadronic collisions*, *JHEP* **0307** (2003) 001, [hep-ph/0206293].

[108] A. Cafarella, C. G. Papadopoulos, and M. Worek, *Helac-phegas: A generator for all parton level processes*, *Comput.Phys.Commun.* **180** (2009) 1941–1955, [arXiv:0710.2427].

[109] F. Caravaglios, M. L. Mangano, M. Moretti, and R. Pittau, *A new approach to multijet calculations in hadron collisions*, *Nucl.Phys.* **B539** (1999) 215–232, [hep-ph/9807570].

[110] F. J. Dyson, *The S matrix in quantum electrodynamics*, *Phys.Rev.* **75** (1949) 1736–1755.

[111] J. S. Schwinger, *On the Green's functions of quantized fields. 2.*, *Proc.Nat.Acad.Sci.* **37** (1951) 455–459.

[112] J. S. Schwinger, *On the Green's functions of quantized fields. 1.*, *Proc.Nat.Acad.Sci.* **37** (1951) 452–455.

[113] B. R. Webber, *Monte Carlo simulation of hard hadronic processes*, *Ann.Rev.Nucl.Part.Sci.* **36** (1986) 253–286.

[114] T. Sjostrand, S. Mrenna, and P. Z. Skands, *Pythia 6.4 physics and manual*, *JHEP* **0605** (2006) 026, [hep-ph/0603175].

[115] M. Bahr, S. Gieseke, M. A. Gigg, D. Grellscheid, K. Hamilton, et al., *Herwig++ physics and manual*, *Eur.Phys.J.* **C58** (2008) 639–707, [arXiv:0803.0883].

[116] F. E. Paige, S. D. Proto, H. Baer, and X. Tata, *Isajet 7.40: A Monte Carlo event generator for pp, $\bar{p}p$, and e^+e^- reactions*, hep-ph/9810440.

[117] S. Frixione and B. R. Webber, *Matching NLO QCD computations and parton shower simulations*, *JHEP* **0206** (2002) 029, [hep-ph/0204244].

[118] S. Catani, F. Krauss, R. Kuhn, and B. R. Webber, *QCD matrix elements + parton showers*, *JHEP* **0111** (2001) 063, [hep-ph/0109231].

[119] F. Krauss, *Matrix elements and parton showers in hadronic interactions*, *JHEP* **0208** (2002) 015, [hep-ph/0205283].

[120] S. Hoeche, F. Krauss, N. Lavesson, L. Lonnblad, M. Mangano, et al., *Matching parton showers and matrix elements*, hep-ph/0602031.

[121] J. Conway, R. Culbertson, R. Demina, B. Kilminster, M. Kruse, et al., *Pgs 4*, *www.physics.ucdavis.edu/∼conway/research/software/pgs/pgs4-general.htm* (2012).

[122] S. Ovyn, X. Rouby, and V. Lemaitre, *Delphes, a framework for fast simulation of a generic collider experiment*, arXiv:0903.2225.

[123] J. Alwall, A. Ballestrero, P. Bartalini, S. Belov, E. Boos, et al., *A standard format for Les Houches event files*, *Comput.Phys.Commun.* **176** (2007) 300–304, [hep-ph/0609017].

[124] R. Brun and F. Rademakers, *ROOT: An object oriented data analysis framework*, *Nucl.Instrum.Meth.* **A389** (1997) 81–86.

[125] J. Alwall, P. Demin, S. de Visscher, R. Frederix, M. Herquet, et al., *Madgraph/Madevent v4: The new web generation*, *JHEP* **0709** (2007) 028, [arXiv:0706.2334].

[126] F. Hubaut, E. Monnier, P. Pralavorio, K. Smolek, and V. Simak, *ATLAS sensitivity to top quark and w boson polarization in $t\bar{t}$ events*, *Eur.Phys.J.* **C44S2** (2005) 13–33, [hep-ex/0508061].

[127] S. Kretzer, H. L. Lai, F. I. Olness, and W. K. Tung, *CTEQ6 parton distributions with heavy quark mass effects*, *Phys.Rev.* **D69** (2004) 114005, [hep-ph/0307022].

[128] M. Cacciari, G. P. Salam, and G. Soyez, *Fastjet user manual*, *Eur.Phys.J.* **C72** (2012) 1896, [arXiv:1111.6097].

[129] A. L. Read, *Presentation of search results: The CL_s technique*, *J.Phys.* **G28** (2002) 2693–2704.

[130] G. Cowan, *Sigcalc, a program for calculating discovery significance using profile likelihood*, *www.pp.rhul.ac.uk/cowan/stat/sigcalc/* (2011).

[131] L. Susskind, *Dynamics of spontaneous symmetry breaking in the Weinberg-Salam theory*, *Phys.Rev.* **D20** (1979) 2619–2625.

[132] E. Farhi and L. Susskind, *Technicolor*, *Phys.Rept.* **74** (1981) 277.

[133] S. Weinberg, *Implications of dynamical symmetry breaking: An addendum*, *Phys.Rev.* **D19** (1979) 1277–1280.

[134] N. Arkani-Hamed, A. G. Cohen, T. Gregoire, and J. G. Wacker, *Phenomenology of electroweak symmetry breaking from theory space*, *JHEP* **0208** (2002) 020, [hep-ph/0202089].

[135] N. Arkani-Hamed, A. G. Cohen, and H. Georgi, *Electroweak symmetry breaking from dimensional deconstruction*, *Phys.Lett.* **B513** (2001) 232–240, [hep-ph/0105239].

[136] N. Vignaroli, *Phenomenology of heavy fermion and vector resonances in composite Higgs models*, arXiv:1112.0218.

[137] R. Contino, *The Higgs as a composite Nambu-Goldstone boson*, arXiv:1005.4269.

[138] R. Contino, D. Marzocca, D. Pappadopulo, and R. Rattazzi, *On the effect of resonances in composite Higgs phenomenology*, *JHEP* **1110** (2011) 081, [arXiv:1109.1570].

[139] **ATLAS** Collaboration, *A general search for new phenomena with the ATLAS detector in pp collisions at* $\sqrt{s} = 8$ *TeV*, *CERN Document Server* (2014), no. ATLAS-CONF-2014-006.

[140] E. Witten, *Some inequalities among hadron masses*, *Phys.Rev.Lett.* **51** (1983) 2351.

[141] J. Callan, Curtis G., S. R. Coleman, J. Wess, and B. Zumino, *Structure of phenomenological lagrangians. 2.*, *Phys.Rev.* **177** (1969) 2247–2250.

[142] S. R. Coleman, J. Wess, and B. Zumino, *Structure of phenomenological lagrangians. 1.*, *Phys.Rev.* **177** (1969) 2239–2247.

[143] K. Agashe, R. Contino, and A. Pomarol, *The minimal composite Higgs model*, *Nucl.Phys.* **B719** (2005) 165–187, [hep-ph/0412089].

[144] R. Contino, L. Da Rold, and A. Pomarol, *Light custodians in natural composite Higgs models*, *Phys.Rev.* **D75** (2007) 055014, [hep-ph/0612048].

[145] G. Panico, M. Safari, and M. Serone, *Simple and realistic composite Higgs models in flat extra dimensions*, *JHEP* **1102** (2011) 103, [arXiv:1012.2875].

[146] A. Pomarol and F. Riva, *The composite Higgs and light resonance connection*, *JHEP* **1208** (2012) 135, [arXiv:1205.6434].

[147] G. Panico, M. Redi, A. Tesi, and A. Wulzer, *On the tuning and the mass of the composite Higgs*, *JHEP* **1303** (2013) 051, [arXiv:1210.7114].

[148] D. Pappadopulo, A. Thamm, and R. Torre, *A minimally tuned composite Higgs model from an extra dimension*, *JHEP* **1307** (2013) 058, [arXiv:1303.3062].

[149] S. R. Coleman and E. J. Weinberg, *Radiative corrections as the origin of spontaneous symmetry breaking*, *Phys.Rev.* **D7** (1973) 1888–1910.

[150] R. Jackiw, *Functional evaluation of the effective potential*, *Phys.Rev.* **D9** (1974) 1686.

[151] J. R. Espinosa, C. Grojean, and M. Muhlleitner, *Composite Higgs under LHC experimental scrutiny*, *EPJ Web Conf.* **28** (2012) 08004, [arXiv:1202.1286].

[152] J. R. Espinosa, C. Grojean, and M. Muhlleitner, *Composite Higgs search at the LHC*, *JHEP* **1005** (2010) 065, [arXiv:1003.3251].

[153] **CMS** Collaboration, *Combination of Standard Model Higgs boson searches and measurements of the properties of the new boson with a mass near* 125 *GeV*, *CERN Document Server* (2012), no. CMS-PAS-HIG-12-045.

[154] S. Weinberg, *Precise relations between the spectra of vector and axial vector mesons*, *Phys.Rev.Lett.* **18** (1967) 507–509.

[155] D. Marzocca, M. Serone, and J. Shu, *General composite Higgs models*, *JHEP* **1208** (2012) 013, [arXiv:1205.0770].

[156] G. 't Hooft, *A two-dimensional model for mesons*, *Nucl.Phys.* **B75** (1974) 461.

[157] G. 't Hooft, *A planar diagram theory for strong interactions*, *Nucl.Phys.* **B72** (1974) 461.

[158] O. Matsedonskyi, G. Panico, and A. Wulzer, *Light top partners for a light composite Higgs*, *JHEP* **1301** (2013) 164, [arXiv:1204.6333].

[159] M. Redi and A. Tesi, *Implications of a light Higgs in composite models*, *JHEP* **1210** (2012) 166, [arXiv:1205.0232].

[160] M. Bando, T. Kugo, S. Uehara, K. Yamawaki, and T. Yanagida, *Is the ρ meson a dynamical gauge boson of hidden local symmetry?*, *Phys. Rev. Lett.* **54** (Mar, 1985) 1215–1218.

[161] A. De Simone, O. Matsedonskyi, R. Rattazzi, and A. Wulzer, *A first top partner hunter's guide*, *JHEP* **1304** (2013) 004, [arXiv:1211.5663].

[162] G. Panico and A. Wulzer, *The discrete composite Higgs model*, *JHEP* **1109** (2011) 135, [arXiv:1106.2719].

[163] S. De Curtis, M. Redi, and A. Tesi, *The 4d composite Higgs*, *JHEP* **1204** (2012) 042, [arXiv:1110.1613].

[164] C. Bini, R. Contino, and N. Vignaroli, *Heavy-light decay topologies as a new strategy to discover a heavy gluon*, *JHEP* **1201** (2012) 157, [arXiv:1110.6058].

[165] R. Contino and G. Servant, *Discovering the top partners at the LHC using same-sign dilepton final states*, *JHEP* **0806** (2008) 026, [arXiv:0801.1679].

[166] J. A. Aguilar-Saavedra, *Identifying top partners at LHC*, *JHEP* **0911** (2009) 030, [arXiv:0907.3155].

[167] G. Azuelos, K. Benslama, D. Costanzo, G. Couture, J. E. Garcia, et al., *Exploring little Higgs models with ATLAS at the LHC*, *Eur.Phys.J.* **C39S2** (2005) 13–24, [hep-ph/0402037].

[168] N. Vignaroli, *Discovering the composite Higgs through the decay of a heavy fermion*, *JHEP* **1207** (2012) 158, [arXiv:1204.0468].

[169] O. Domenech, A. Pomarol, and J. Serra, *Probing the SM with dijets at the LHC*, *Phys.Rev.* **D85** (2012) 074030, [arXiv:1201.6510].

[170] **CMS** Collaboration, S. Chatrchyan et al., *Search for quark compositeness in dijet angular distributions from pp collisions at* $\sqrt{s} = 7$ *TeV*, *JHEP* **1205** (2012) 055, [arXiv:1202.5535].

[171] **ATLAS** Collaboration, G. Aad et al., *Search for new physics in the dijet mass distribution using* 1 fb^{-1} *of pp collision data at* $\sqrt{s} = 7$ *TeV collected by the ATLAS detector*, *Phys.Lett.* **B708** (2012) 37–54, [arXiv:1108.6311].

[172] **CMS** Collaboration, *A search for resonances in semileptonic top pair production*, *CERN Document Server* (2012), no. CMS-PAS-TOP-11-009.

[173] **ATLAS** Collaboration, *A search for* $t\bar{t}$ *resonances in the dilepton channel in* 1.04 fb^{-1} *of pp collisions at* $\sqrt{s} = 7$ *TeV with the ATLAS experiment*, arXiv:1111.6933.

[174] **ATLAS** Collaboration, *A search for* $t\bar{t}$ *resonances in the lepton plus jets channel using* 2.05 fb^{-1} *of pp collisions at* $\sqrt{s} = 7$ *TeV*, *CERN Document Server* (2012), no. ATLAS-CONF-2012-029.

[175] D. Carmi, A. Falkowski, E. Kuflik, and T. Volansky, *Interpreting LHC Higgs results from natural new physics perspective*, *JHEP* **1207** (2012) 136, [arXiv:1202.3144].

[176] A. Azatov, R. Contino, and J. Galloway, *Model-independent bounds on a light Higgs*, *JHEP* **1204** (2012) 127, [arXiv:1202.3415].

[177] J. R. Espinosa, C. Grojean, M. Muhlleitner, and M. Trott, *Fingerprinting Higgs suspects at the LHC*, *JHEP* **1205** (2012) 097, [arXiv:1202.3697].

[178] P. P. Giardino, K. Kannike, M. Raidal, and A. Strumia, *Reconstructing Higgs boson properties from the LHC and Tevatron data*, *JHEP* **1206** (2012) 117, [arXiv:1203.4254].

[179] **CMS** Collaboration, S. Chatrchyan et al., *Search for the Standard Model Higgs boson produced in association with a top-quark pair in pp collisions at the LHC*, *JHEP* **1305** (2013) 145, [arXiv:1303.0763].

[180] **ATLAS** Collaboration, *Search for anomalous production of events with same-sign dileptons and b jets in* 14.3 fb^{-1} *of pp collisions at* $\sqrt{s} = 8$ *TeV with the ATLAS detector*, *CERN Document Server* (2013), no. ATLAS-CONF-2013-051.

[181] **CMS** Collaboration, *https://twiki.cern.ch/twiki/bin/view/cmspublic/tevscalethexpphysics*, *CERN CMS Server* (2013).

[182] J. L. Diaz-Cruz, H.-J. He, T. M. P. Tait, and C. P. Yuan, *Higgs bosons with large bottom yukawa coupling at Tevatron and LHC*, *Phys.Rev.Lett.* **80** (1998) 4641–4644, [hep-ph/9802294].

[183] J. Dai, J. F. Gunion, and R. Vega, *LHC detection of neutral MSSM Higgs bosons via* $gg \to b\bar{b}h \to b\bar{b}b\bar{b}$, *Phys.Lett.* **B345** (1995) 29–35, [hep-ph/9403362].

[184] M. S. Carena, S. Mrenna, and C. E. M. Wagner, *MSSM Higgs boson phenomenology at the Tevatron collider*, *Phys.Rev.* **D60** (1999) 075010, [hep-ph/9808312].

[185] C. Balazs, J. L. Diaz-Cruz, H. J. He, T. M. P. Tait, and C. P. Yuan, *Probing Higgs bosons with large bottom yukawa coupling at hadron colliders*, *Phys.Rev.* **D59** (1999) 055016, [hep-ph/9807349].

[186] **CMS** Collaboration, S. Chatrchyan et al., *Search for supersymmetry in hadronic final states with missing transverse energy using the variables* α_t *and b-quark multiplicity in pp collisions at* $\sqrt{s} = 8$ *TeV*, *Eur.Phys.J.* **C73** (2013) 2568, [arXiv:1303.2985].

[187] **CMS** Collaboration, S. Chatrchyan et al., *Search for gluino mediated bottom- and top-squark production in multijet final states in pp collisions at 8 TeV*, *Phys.Lett.* **B725** (2013) 243–270, [arXiv:1305.2390].

[188] N. Greiner, A. Guffanti, J.-P. Guillet, T. Reiter, and J. Reuter, *NLO QCD corrections to 4 b-quark production*, *PoS* **DIS2010** (2010) 156, [arXiv:1006.5339].

[189] G. Bevilacqua, M. Czakon, M. Krämer, M. Kubocz, and M. Worek, *Quantifying quark mass effects at the LHC: A study of $pp \to b\bar{b}b\bar{b} + x$ at next-to-leading order*, *JHEP* **1307** (2013) 095, [arXiv:1304.6860].

[190] C. Csaki, A. Falkowski, and A. Weiler, *A simple flavor protection for RS*, *Phys.Rev.* **D80** (2009) 016001, [arXiv:0806.3757].

[191] C. Csaki, A. Falkowski, and A. Weiler, *The flavor of the composite pseudo-Goldstone Higgs*, *JHEP* **0809** (2008) 008, [arXiv:0804.1954].

[192] M. Redi and A. Weiler, *Flavor and CP invariant composite Higgs models*, *JHEP* **1111** (2011) 108, [arXiv:1106.6357].

[193] C. Csaki, G. Perez, Z. Surujon, and A. Weiler, *Flavor alignment via shining in RS*, *Phys.Rev.* **D81** (2010) 075025, [arXiv:0907.0474].

[194] M. Redi, V. Sanz, M. de Vries, and A. Weiler, *Strong signatures of right-handed compositeness*, *JHEP* **1308** (2013) 008, [arXiv:1305.3818].

[195] A. Atre, G. Azuelos, M. Carena, T. Han, E. Ozcan, et al., *Model-independent searches for new quarks at the LHC*, *JHEP* **1108** (2011) 080, [arXiv:1102.1987].

[196] A. Atre, M. Carena, T. Han, and J. Santiago, *Heavy quarks above the top at the Tevatron*, *Phys.Rev.* **D79** (2009) 054018, [arXiv:0806.3966].

[197] F. del Aguila, A. Carmona, and J. Santiago, *Tau custodian searches at the LHC*, *Phys.Lett.* **B695** (2011) 449–453, [arXiv:1007.4206].

[198] A. Carmona and F. Goertz, *Custodial leptons and Higgs decays*, *JHEP* **1304** (2013) 163, [arXiv:1301.5856].

[199] M. E. Peskin and T. Takeuchi, *A new constraint on a strongly interacting Higgs sector*, *Phys.Rev.Lett.* **65** (1990) 964–967.

[200] **ATLAS** Collaboration, *Search for single production of vector-like quarks coupling to light generations in* 4.64 fb^{-1} *of data at* $\sqrt{s} = 7$ *TeV*, *CERN Document Server* (2012), no. ATLAS-CONF-2012-137.

[201] U. Baur, T. Plehn, and D. L. Rainwater, *Probing the Higgs selfcoupling at hadron colliders using rare decays*, *Phys.Rev.* **D69** (2004) 053004, [hep-ph/0310056].

[202] M. J. Dolan, C. Englert, and M. Spannowsky, *Higgs self-coupling measurements at the LHC*, *JHEP* **1210** (2012) 112, [arXiv:1206.5001].

[203] F. Goertz, A. Papaefstathiou, L. L. Yang, and J. Zurita, *Higgs boson self-coupling measurements using ratios of cross sections*, *JHEP* **1306** (2013) 016, [arXiv:1301.3492].

[204] R. Grober and M. Muhlleitner, *Composite Higgs boson pair production at the LHC*, *JHEP* **1106** (2011) 020, [arXiv:1012.1562].

[205] R. Contino, M. Ghezzi, M. Moretti, G. Panico, F. Piccinini, et al., *Anomalous couplings in double Higgs production*, *JHEP* **1208** (2012) 154, [arXiv:1205.5444].

[206] M. J. Dolan, C. Englert, and M. Spannowsky, *New physics in LHC Higgs boson pair production*, *Phys.Rev.* **D87** (2013) 055002, [arXiv:1210.8166].

[207] R. Barcelo, A. Carmona, M. Masip, and J. Santiago, *Stealth gluons at hadron colliders*, *Phys.Lett.* **B707** (2012) 88–91, [arXiv:1106.4054].

[208] R. Barcelo, A. Carmona, M. Masip, and J. Santiago, *Gluon excitations in* $t\bar{t}$ *production at hadron colliders*, *Phys.Rev.* **D84** (2011) 014024, [arXiv:1105.3333].

[209] **CDF** Collaboration, T. Aaltonen et al., *Measurement of the top quark forward-backward production asymmetry and its dependence on event kinematic properties*, *Phys.Rev.* **D87** (2013) 092002, [arXiv:1211.1003].

[210] **D0** Collaboration, V. M. Abazov et al., *Forward-backward asymmetry in top quark-antiquark production*, *Phys.Rev.* **D84** (2011) 112005, [arXiv:1107.4995].

[211] W. Bernreuther and Z.-G. Si, *Top quark and leptonic charge asymmetries for the Tevatron and LHC*, *Phys.Rev.* **D86** (2012) 034026, [arXiv:1205.6580].

[212] J. Drobnak, A. L. Kagan, J. F. Kamenik, G. Perez, and J. Zupan, *Forward Tevatron tops and backward LHC tops with associates*, *Phys.Rev.* **D86** (2012) 094040, [arXiv:1209.4872].

[213] **Planck** Collaboration, P. A. R. Ade et al., *Planck 2013 results. XVI. cosmological parameters*, arXiv:1303.5076.

[214] B. Gripaios, A. Pomarol, F. Riva, and J. Serra, *Beyond the minimal composite Higgs model*, *JHEP* **0904** (2009) 070, [arXiv:0902.1483].

[215] M. Frigerio, A. Pomarol, F. Riva, and A. Urbano, *Composite scalar dark matter*, *JHEP* **1207** (2012) 015, [arXiv:1204.2808].

[216] **ATLAS** Collaboration, *Measurements of the properties of the Higgs-like boson in the two photon decay channel with the ATLAS detector using* 25 fb^{-1} *of proton-proton collision data*, *CERN Document Server* (2013), no. ATLAS-CONF-2013-012.

[217] **ATLAS** Collaboration, *Coupling properties of the new Higgs-like boson observed with the ATLAS detector at the LHC*, *CERN Document Server* (2012), no. ATLAS-CONF-2012-127.

[218] A. Djouadi, *Squark effects on Higgs boson production and decay at the LHC*, *Phys.Lett.* **B435** (1998) 101–108, [hep-ph/9806315].

[219] F. J. Petriello, *Kaluza-Klein effects on Higgs physics in universal extra dimensions*, *JHEP* **0205** (2002) 003, [hep-ph/0204067].

[220] T. Han, H. E. Logan, B. McElrath, and L.-T. Wang, *Loop induced decays of the little Higgs:* $h \to gg$, $\gamma\gamma$, *Phys.Lett.* **B563** (2003) 191–202, [hep-ph/0302188].

[221] C.-R. Chen, K. Tobe, and C. P. Yuan, *Higgs boson production and decay in little Higgs models with t-parity*, *Phys.Lett.* **B640** (2006) 263–271, [hep-ph/0602211].

[222] R. Dermisek and I. Low, *Probing the stop sector and the sanity of the MSSM with the Higgs boson at the LHC*, *Phys.Rev.* **D77** (2008) 035012, [hep-ph/0701235].

[223] I. Low and S. Shalgar, *Implications of the Higgs discovery in the MSSM golden region*, *JHEP* **0904** (2009) 091, [arXiv:0901.0266].

[224] I. Low, R. Rattazzi, and A. Vichi, *Theoretical constraints on the Higgs effective couplings*, *JHEP* **1004** (2010) 126, [arXiv:0907.5413].

[225] G. Cacciapaglia, A. Deandrea, and J. Llodra-Perez, *Higgs $\to$ gamma gamma beyond the Standard Model*, *JHEP* **0906** (2009) 054, [arXiv:0901.0927].

[226] S. Casagrande, F. Goertz, U. Haisch, M. Neubert, and T. Pfoh, *The custodial Randall-Sundrum model: From precision tests to Higgs physics*, *JHEP* **1009** (2010) 014, [arXiv:1005.4315].

[227] K. Cheung and T.-C. Yuan, *Could the excess seen at $124-126$ GeV be due to the Randall-Sundrum radion?*, *Phys.Rev.Lett.* **108** (2012) 141602, [arXiv:1112.4146].

[228] M. Carena, S. Gori, N. R. Shah, and C. E. M. Wagner, *A 125 GeV SM-like Higgs in the MSSM and the $\gamma\gamma$ rate*, *JHEP* **1203** (2012) 014, [arXiv:1112.3336].

[229] J. Cao, Z. Heng, T. Liu, and J. M. Yang, *Di-photon Higgs signal at the LHC: A comparative study for different supersymmetric models*, *Phys.Lett.* **B703** (2011) 462–468, [arXiv:1103.0631].

[230] B. Batell, S. Gori, and L.-T. Wang, *Exploring the Higgs portal with 10/fb at the LHC*, *JHEP* **1206** (2012) 172, [arXiv:1112.5180].

[231] A. Arvanitaki and G. Villadoro, *A non Standard Model Higgs at the LHC as a sign of naturalness*, *JHEP* **1202** (2012) 144, [arXiv:1112.4835].

[232] V. Barger, M. Ishida, and W.-Y. Keung, *Total width of 125 GeV Higgs boson*, *Phys.Rev.Lett.* **108** (2012) 261801, [arXiv:1203.3456].

[233] N. Arkani-Hamed, K. Blum, R. T. D'Agnolo, and J. Fan, 2 : 1 *for naturalness at the LHC?*, *JHEP* **1301** (2013) 149, [arXiv:1207.4482].

[234] A. Arhrib, R. Benbrik, and C.-H. Chen, $h \to \gamma\gamma$ *in the complex two Higgs doublet model*, arXiv:1205.5536.

[235] A. Alves, E. Ramirez Barreto, A. G. Dias, C. A. de S. Pires, F. S. Queiroz, et al., *Probing* $3-3-1$ *models in diphoton Higgs boson decay*, *Phys.Rev.* **D84** (2011) 115004, [arXiv:1109.0238].

[236] H. M. Lee, M. Park, and W.-I. Park, *Axion-mediated dark matter and Higgs diphoton signal*, *JHEP* **1212** (2012) 037, [arXiv:1209.1955].

[237] J. Kearney, A. Pierce, and N. Weiner, *Vectorlike fermions and Higgs couplings*, *Phys.Rev.* **D86** (2012) 113005, [arXiv:1207.7062].

[238] S. Kanemura and K. Yagyu, *Radiative corrections to electroweak parameters in the Higgs triplet model and implication with the recent Higgs boson searches*, *Phys.Rev.* **D85** (2012) 115009, [arXiv:1201.6287].

[239] A. Joglekar, P. Schwaller, and C. E. M. Wagner, *Dark matter and enhanced Higgs to di-photon rate from vector-like leptons*, *JHEP* **1212** (2012) 064, [arXiv:1207.4235].

[240] I. Dorsner, S. Fajfer, A. Greljo, and J. F. Kamenik, *Higgs uncovering light scalar remnants of high scale matter unification*, *JHEP* **1211** (2012) 130, [arXiv:1208.1266].

[241] L. G. Almeida, E. Bertuzzo, P. A. N. Machado, and R. Z. Funchal, *Does* $h \to \gamma\gamma$ *taste like vanilla new physics?*, *JHEP* **1211** (2012) 085, [arXiv:1207.5254].

[242] P. Draper and D. McKeen, *Diphotons from tetraphotons in the decay of a* 125 *GeV Higgs at the LHC*, *Phys.Rev.* **D85** (2012) 115023, [arXiv:1204.1061].

[243] A. G. Akeroyd and S. Moretti, *Enhancement of h to gamma gamma from doubly charged scalars in the Higgs triplet model*, *Phys.Rev.* **D86** (2012) 035015, [arXiv:1206.0535].

[244] S. Dawson and E. Furlan, *A Higgs conundrum with vector fermions*, *Phys.Rev.* **D86** (2012) 015021, [arXiv:1205.4733].

[245] N. D. Christensen, T. Han, and S. Su, *MSSM Higgs bosons at the LHC*, *Phys.Rev.* **D85** (2012) 115018, [arXiv:1203.3207].

[246] M. Carena, I. Low, and C. E. M. Wagner, *Implications of a modified Higgs to diphoton decay width*, *JHEP* **1208** (2012) 060, [arXiv:1206.1082].

[247] A. Delgado, G. Nardini, and M. Quiros, *Large diphoton Higgs rates from supersymmetric triplets*, *Phys.Rev.* **D86** (2012) 115010, [arXiv:1207.6596].

[248] E. J. Chun, H. M. Lee, and P. Sharma, *Vacuum stability, perturbativity, ewpd and Higgs-to-diphoton rate in type II seesaw models*, *JHEP* **1211** (2012) 106, [arXiv:1209.1303].

[249] M. Carena, S. Gori, I. Low, N. R. Shah, and C. E. M. Wagner, *Vacuum stability and Higgs diphoton decays in the MSSM*, *JHEP* **1302** (2013) 114, [arXiv:1211.6136].

[250] M. Berg, I. Buchberger, D. M. Ghilencea, and C. Petersson, *Higgs diphoton rate enhancement from supersymmetric physics beyond the MSSM*, *Phys.Rev.* **D88** (2013) 025017, [arXiv:1212.5009].

[251] G.-N. Li, G. Guo, B. Ren, Y.-J. Zheng, and X.-G. He, *Lepton number violation and $h \to \gamma\gamma$ in a radiative inverse seesaw dark matter model*, *JHEP* **1304** (2013) 026, [arXiv:1212.5528].

[252] E. O. Iltan, *Higgs to diphoton decay rate and the antisymmetric tensor unparticle mediation*, *Acta Phys.Polon.* **B44** (2013) 1287–1295, [arXiv:1212.5695].

[253] X.-F. Han, L. Wang, J. M. Yang, and J. Zhu, *Little Higgs theory confronted with the LHC Higgs data*, *Phys.Rev.* **D87** (2013) 055004, [arXiv:1301.0090].

[254] J. Cao, L. Wu, P. Wu, and J. M. Yang, *The z+photon and diphoton decays of the Higgs boson as a joint probe of low energy SUSY models*, *JHEP* **1309** (2013) 043, [arXiv:1301.4641].

[255] W.-Z. Feng and P. Nath, *Higgs diphoton rate and mass enhancement with vectorlike leptons and the scale of supersymmetry*, *Phys.Rev.* **D87** (2013) 075018, [arXiv:1303.0289].

[256] N. Maru and N. Okada, *Diphoton decay excess and* 125 *GeV Higgs boson in gauge-Higgs unification*, *Phys.Rev.* **D87** (2013) 095019, [arXiv:1303.5810].

[257] M. Badziak, M. Olechowski, and S. Pokorski, *Light staus and enhanced Higgs diphoton rate with non-universal gaugino masses and $SO(10)$ yukawa unification*, *JHEP* **1310** (2013) 088, [arXiv:1307.7999].

[258] K. Schmidt-Hoberg, F. Staub, and M. W. Winkler, *Enhanced diphoton rates at fermi and the LHC*, *JHEP* **1301** (2013) 124, [arXiv:1211.2835].

[259] J. Mrazek, A. Pomarol, R. Rattazzi, M. Redi, J. Serra, et al., *The other natural two Higgs doublet model*, *Nucl.Phys.* **B853** (2011) 1–48, [arXiv:1105.5403].

[260] M. Montull and F. Riva, *Higgs discovery: the beginning or the end of natural ewsb?*, *JHEP* **11** (2012) 018, [arXiv:1207.1716].

[261] K. Agashe, R. Contino, L. Da Rold, and A. Pomarol, *A custodial symmetry for $zb\bar{b}$*, *Phys.Lett.* **B641** (2006) 62–66, [hep-ph/0605341].

[262] A. De Rujula, S. L. Glashow, and U. Sarid, *Charged dark matter*, *Nucl.Phys.* **B333** (1990) 173.

[263] S. Dimopoulos, D. Eichler, R. Esmailzadeh, and G. D. Starkman, *Getting a charge out of dark matter*, *Phys.Rev.* **D41** (1990) 2388.

[264] R. S. Chivukula, A. G. Cohen, S. Dimopoulos, and T. P. Walker, *Bounds on halo particle interactions from interstellar calorimetry*, *Phys.Rev.Lett.* **65** (1990) 957–959.

[265] A. Gould, B. T. Draine, R. W. Romani, and S. Nussinov, *Neutron stars: Graveyard of charged dark matter*, *Phys.Lett.* **B238** (1990) 337.

[266] M. Gunaydin and F. Gursey, *Quark structure and octonions*, *J.Math.Phys.* **14** (1973) 1651–1667.

[267] J. M. Evans, *Supersymmetry algebras and lorentz invariance for $d = 10$ superyang-mills*, *Phys.Lett.* **B334** (1994) 105–112, [hep-th/9404190].

[268] M. Gunaydin and S. V. Ketov, *Seven sphere and the exceptional $n = 7$ and $n = 8$ superconformal algebras*, *Nucl.Phys.* **B467** (1996) 215–246, [hep-th/9601072].

[269] G. F. Giudice, C. Grojean, A. Pomarol, and R. Rattazzi, *The strongly-interacting light Higgs*, *JHEP* **0706** (2007) 045, [hep-ph/0703164].

[270] **ATLAS** Collaboration, *Search for $w' \to t\bar{b}$ in proton-proton collisions at a centre-of-mass energy of $\sqrt{s} = 8$ TeV with the ATLAS detector*, .

[271] **CMS** Collaboration, S. Chatrchyan et al., *Search for a w' boson decaying to a bottom quark and a top quark in pp collisions at $\sqrt{s} = 7$ TeV*, *Phys.Lett.* **B718** (2013) 1229–1251, [arXiv:1208.0956].

[272] **CDF** Collaboration, D. Acosta et al., *Search for a w' boson decaying to a top and bottom quark pair in 1.8 TeV $p\bar{p}$ collisions*, *Phys.Rev.Lett.* **90** (2003) 081802, [hep-ex/0209030].

[273] **D0** Collaboration, V. M. Abazov et al., *Search for w' boson resonances decaying to a top quark and a bottom quark*, *Phys.Rev.Lett.* **100** (2008) 211803, [arXiv:0803.3256].

[274] **CMS** Collaboration, S. Chatrchyan et al., *Search for leptonic decays of w' bosons in pp collisions at $\sqrt{s} = 7$ TeV*, *JHEP* **1208** (2012) 023, [arXiv:1204.4764].

[275] **CMS** Collaboration, S. Chatrchyan et al., *Search for new physics in final states with a lepton and missing transverse energy in pp collisions at the LHC*, *Phys.Rev.* **D87** (2013) 072005, [arXiv:1302.2812].

[276] **CMS** Collaboration, S. Chatrchyan et al., *Search for resonances in the dijet mass spectrum from $\sqrt{s} = 7$ TeV pp collisions at CMS*, *Phys.Lett.* **B704** (2011) 123–142, [arXiv:1107.4771].

[277] R. N. Mohapatra and P. B. Pal, *Massive neutrinos in physics and astrophysics. second edition*, *World Sci.Lect.Notes Phys.* **60** (1998) 1–397.

[278] S. Weinberg, *Baryon and lepton nonconserving processes*, *Phys.Rev.Lett.* **43** (1979) 1566–1570.

[279] W. H. Furry, *On transition probabilities in double beta-disintegration*, *Phys.Rev.* **56** (1939) 1184–1193.

[280] A. de Gouvea and J. Jenkins, *A survey of lepton number violation via effective operators*, *Phys.Rev.* **D77** (2008) 013008, [arXiv:0708.1344].

[281] R. Franceschini and R. N. Mohapatra, *Radiatively induced type II seesaw and vector-like 5/3 charge quarks*, arXiv:1306.6108.

[282] W.-Y. Keung and G. Senjanovic, *Majorana neutrinos and the production of the right-handed charged gauge boson*, *Phys.Rev.Lett.* **50** (1983) 1427.

[283] M. Fukugita and T. Yanagida, *Baryogenesis without grand unification*, *Phys.Lett.* **B174** (1986) 45.

[284] T. Han and B. Zhang, *Signatures for majorana neutrinos at hadron colliders*, *Phys.Rev.Lett.* **97** (2006) 171804, [hep-ph/0604064].

[285] F. del Aguila, J. A. Aguilar-Saavedra, and R. Pittau, *Heavy neutrino signals at large hadron colliders*, *JHEP* **0710** (2007) 047, [hep-ph/0703261].

[286] A. Atre, T. Han, S. Pascoli, and B. Zhang, *The search for heavy majorana neutrinos*, *JHEP* **0905** (2009) 030, [arXiv:0901.3589].

[287] F. del Aguila, J. de Blas, and M. Perez-Victoria, *Effects of new leptons in electroweak precision data*, *Phys.Rev.* **D78** (2008) 013010, [arXiv:0803.4008].

[288] J. Schechter and J. W. F. Valle, *Neutrinoless double beta decay in $SU(2) \times U(1)$ theories*, *Phys.Rev.* **D25** (1982) 2951.

[289] K. S. Babu and C. N. Leung, *Classification of effective neutrino mass operators*, *Nucl.Phys.* **B619** (2001) 667–689, [hep-ph/0106054].

[290] K.-w. Choi, K. S. Jeong, and W. Y. Song, *Operator analysis of neutrinoless double beta decay*, *Phys.Rev.* **D66** (2002) 093007, [hep-ph/0207180].

[291] J. Engel and P. Vogel, *Effective operators for double beta decay*, *Phys.Rev.* **C69** (2004) 034304, [nucl-th/0311072].

[292] G. Bambhaniya, J. Chakrabortty, S. Goswami, and P. Konar, *Generation of neutrino mass from new physics at TeV scale and multi-lepton signatures at the LHC*, *Phys.Rev.* **D88** (2013) 075006, [arXiv:1305.2795].

[293] **ATLAS** Collaboration, *Search for doubly-charged Higgs bosons in like-sign dilepton final states at $\sqrt{s} = 7$ TeV with the ATLAS detector*, *Eur.Phys.J.* **C72** (2012) 2244, [arXiv:1210.5070].

[294] K. S. Babu, *Model of 'calculable' majorana neutrino masses*, *Phys.Lett.* **B203** (1988) 132.

[295] E. J. Williams, *Nature of the high-energy particles of penetrating radiation and status of ionization and radiation formulae*, *Phys.Rev.* **45** (1934) 729–730.

[296] C. F. von Weizsacker, *Radiation emitted in collisions of very fast electrons*, *Z.Phys.* **88** (1934) 612–625.

[297] T. Han, B. Mukhopadhyaya, Z. Si, and K. Wang, *Pair production of doubly-charged scalars: Neutrino mass constraints and signals at the LHC*, *Phys.Rev.* **D76** (2007) 075013, [arXiv:0706.0441].

[298] M. Muhlleitner and M. Spira, *A note on doubly charged Higgs pair production at hadron colliders*, *Phys.Rev.* **D68** (2003) 117701, [hep-ph/0305288].

[299] R. Franceschini, T. Hambye, and A. Strumia, *Type-III see-saw at LHC*, *Phys.Rev.* **D78** (2008) 033002, [arXiv:0805.1613].

[300] P. Fileviez Perez, T. Han, G.-y. Huang, T. Li, and K. Wang, *Neutrino masses and the cern LHC: Testing type II seesaw*, *Phys.Rev.* **D78** (2008) 015018, [arXiv:0805.3536].